AWARD NUMBER: W81XWH-15-1-0717

TITLE: Tumor-Associated Neutrophils in Human Lung Cancer

PRINCIPAL INVESTIGATOR: Evgeniy Eruslanov

CONTRACTING ORGANIZATION: Trustees of the University of Pennsylvania
Philadelphia, PA 19104

REPORT DATE: October 2016

TYPE OF REPORT: Annual

PREPARED FOR: U.S. Army Medical Research and Materiel Command
Fort Detrick, Maryland 21702-5012

REPORT DOCUMENTATION PAGE

Form Approved
OMB No. 0704-0188

1. REPORT DATE	2. REPORT TYPE	3. DATES COVERED
October 2016	Annual	30 Sep 2015 - 29 Sep 2016

4. TITLE AND SUBTITLE:

Tumor-Associated Neutrophils in Human Lung Cancer

5a. CONTRACT NUMBER

5b. GRANT NUMBER
W81XWH-15-1-0717

5c. PROGRAM ELEMENT NUMBER

6. AUTHOR(S): Evgeniy Eruslanov

E-Mail: evgeniy.eruslanov@uphs.upenn.edu

5d. PROJECT NUMBER

5e. TASK NUMBER

5f. WORK UNIT NUMBER

7. PERFORMING ORGANIZATION NAME(S) AND ADDRESS(ES)
Trustees of the University of
Pennsylvania
Philadelphia, PA 19104-6205

8. PERFORMING ORGANIZATION REPORT NUMBER

9. SPONSORING / MONITORING AGENCY NAME(S) AND ADDRESS(ES)

U.S. Army Medical Research and Materiel Command
Fort Detrick, Maryland 21702-5012

10. SPONSOR/MONITOR'S ACRONYM(S)

11. SPONSOR/MONITOR'S REPORT NUMBER(S)

12. DISTRIBUTION / AVAILABILITY STATEMENT

Approved for Public Release; Distribution Unlimited

13. SUPPLEMENTARY NOTES

14. ABSTRACT: The role of tumor-associated neutrophils (TANs) in cancer progression remains unclear and has only been recently investigated in murine tumor models. However, there are limited data about the TANs in human tumor. The goal of this study is to provide a phenotypic and functional characterization of TANs in lung cancer patients. We have identified two major subsets of TANs in lung tumors: "canonical" TANs that express classic neutrophil markers and "APC-like hybrid" TANs that display a combination of canonical neutrophil markers and markers of antigen-presenting cells. In this study we have performed analysis of key inflammatory factors secreted by canonical and hybrid neutrophils. We have also performed whole human genome RNA expression profiles of these neutrophil subsets. We found that the APC-like hybrid neutrophils are superior to canonical neutrophils in their ability to trigger and support T cell responses in direct cell-cell interactions. This property of hybrid neutrophils may provide new opportunities to boost the efficacy of vaccines based on cytotoxic T lymphocyte induction. Our study for the first time provide a comprehensive functional characterization of TAN subsets in lung cancer patients and bridge the knowledge gap between prior data from murine studies to the human scenario.

15. SUBJECT TERMS: human lung cancer, human tumor microenvironment, phenotype and function of tumor-associated neutrophils and their subsets, tumoricidal neutrophils, tumor inflammation, anti-tumor neutrophils, anti-tumor innate immune response, anti-tumor adaptive immune response, neutrophil and T cell interaction.

16. SECURITY CLASSIFICATION OF: U			17. LIMITATION OF ABSTRACT	18. NUMBER OF PAGES	19a. NAME OF RESPONSIBLE PERSON
a. REPORT	b. ABSTRACT	c. THIS PAGE			19b. TELEPHONE NUMBER *(include area code)*
Unclassified	Unclassified	Unclassified	Unclassified	114	USAMRMC

Table of Contents

Page

INTRODUCTION

Subject: Lung cancer is the most common cause of cancer death amongst Veterans in the United States. Despite advances in therapeutic strategies, patients with lung cancer have a poor prognosis and the overall survival rate is less than 20% for all stages. Immunotherapy represents an attractive approach in the treatment of lung cancer; however previous cancer vaccines have been unsuccessful, likely due to the failure to address the influence of the tumor microenvironment. To date, the characterization of the human lung tumor microenvironment is still in its infancy and the functional cross-talk between immune and tumor cells in humans remains largely unexplored. Tumor-recruited myeloid cells represent a significant portion of inflammatory cells in the tumor microenvironment and influence nearly all steps of tumor progression. Among these cells, TANs represent a predominant cell type. The role of tumor-associated neutrophils (TANs) in cancer progression remains unclear and has only been recently investigated in murine models. However, virtually nothing is known about the phenotype and function of TANs in lung human tumors. Our study for the first time provide a comprehensive functional characterization of tumor-infiltrating neutrophil subsets in early-stage lung cancer patients and will bridge the knowledge gap between prior data from murine studies to the human scenario. We study a large cohort of veterans that were diagnosed with lung cancer in the Philadelphia VA Medical Center.

Purpose and scope of the research We have identified two major sub-populations of TANs in freshly isolated tumors from Non-Small Cell Lung Cancer (NSCLC) patients with Stage I-II. One subset of "canonical" TANs expressed classic neutrophil markers $CD11b^{+}Arg1^{+}MPO^{+}CD66b^{+}CD15^{hi}$. A second subset of TANs displayed a combination of canonical neutrophil markers plus markers ($CD14^{+}HLA\text{-}DR^{+}CCR7^{+}CD86^{+}$) normally expressed on antigen-presenting cells (APC). We termed this unique neutrophil population "APC-like hybrid TANs". The purpose of this proposal is to determine the specific roles of these distinct subsets of tumor-associated neutrophils in human lung cancers and to develop novel approaches to boost anti-tumor immunity. Specifically, (1) investigate the inflammatory profile of canonical and hybrid TANs, (2) investigate the effects of canonical and hybrid TANs on T cell responses and on the maturation and function of dendritic cells, and (3) define the cytotoxic phenotype of canonical and hybrid neutrophils and the mechanisms by which these neutrophils inhibit tumor growth.

KEYWORDS

human lung cancer, human tumor microenvironment, tumor-associated neutrophils, tumoricidal neutrophils, tumor inflammation, anti-tumor neutrophils, anti-tumor innate immune response. anti-tumor adaptive immune response, neutrophil and T cell interaction.

ACCOMPLISHMENTS

There were no significant changes in the project. We have performed all experiments according to plan proposed in the original proposal and approved SOW.

What were the major goals of the project?
The goal of this proposal is to determine the specific role of distinct subsets of tumor-associated neutrophils (TAN) in non-small cell lung cancer. Specifically:
Aim 1 goal: Investigate the inflammatory profile of canonical and hybrid TANs, (timeline 1-12 months).
Aim 2 goal: Investigate the effects of canonical and hybrid TANs on T cell responses and on the maturation and function of dendritic cells, (timeline 1-18 months).
Aim 3 goal: Define the cytotoxic phenotype of canonical and hybrid neutrophils and the mechanisms by which these neutrophils inhibit tumor growth, (timeline 12-24 months).

What was accomplished under these goals?

Aim 1. This aim is largely completed

Specific objectives: The cytokines and chemokines produced by TAN subsets within the lung tumor are critical in mediating their effects on the tumor microenvironment. The purpose of this Aim was to characterize the inflammatory profile of canonical and hybrid TANs. Using transcriptomics and protein-based approaches we aimed to quantify key secreted inflammatory cytokines, chemokines, and growth factors secreted by canonical and hybrid TANs.

Major activities: We have been able to isolate TANs and TAN subsets using flow cytometry sorting. Given that frequency of hybrid TANs in tissue is extremely low, the number of these sorted cells was relatively small to perform good quality multi-analyte analysis and whole human genome RNA expression profiles. We used these sorted hybrid TANs for functional assays proposed in Aim 2. To obtain larger numbers of cells for these studies, we took advantage of our BM neutrophil model described in our original proposal. In this aim we have justified the use of this new model of bone marrow-derived canonical and hybrid neutrophils to comprehensively investigate the rare subset of hybrid TANs. Using this model we have performed analysis of key inflammatory factors secreted by canonical and hybrid neutrophils. We have also performed whole human genome RNA expression profiles of these neutrophil subsets. See all details below.

The result were presented at the following meetings:

- The Society For Leukocyte Biology's 49th Annual Meeting and "Neutrophil 2016": Neutrophils and Other Leukocytes, University of Verona, Verona, Italy, September 15-17, 2016, **Invited Speaker**.
- Regulatory Myeloid Suppressor Cells Conference, Philadelphia, The Wistar Institute, June 16-19, 2016 **Invited Speaker**.
- Immunology School "Regulation of Lung Inflammation", Moscow, Russia, May11-13, 2016. **Invited Speaker**.
- AACR annual meeting: The function of tumor microenvironment in cancer. San Diego, Jan 7, 2016, **poster presentation**

Please see official invitations from Scientific Organizing Committee of these conferences in appendices

Significant results and outcomes: To obtain sufficient numbers of hybrid and canonical neutrophils cells for this study we have identified conditions in which the immature bone marrow granulocytes could be differentiated into cells that phenotypically and functionally recapitulate canonical TANs or TAN hybrid cells. Briefly, we obtained a highly enriched population of immature human bone marrow neutrophils (BMNs) from discarded rib fragments that were removed from patients during lung cancer surgery. CD15 bead isolated BMNs expressed the myeloid/granulocytic specific markers CD11b, CD66b, CD15, Arg1, and myeloperoxidase

(MPO) and were mostly "band"-like immature neutrophils in appearance (Fig. 1B). Of note, the purified BMNs were HLA-DR and CD14 negative cells and not contaminated with macrophages/monocytes. Importantly, unlike blood and tumor neutrophils, about 40% of these BMNs could survive in cell culture for up to 1 week and dramatically increased their viability in the presence of TCM (Fig. 1A). We collected tumor-conditioned media (TCM) from digested tumors which contained ≥ 15% of hybrid TANs among all TANs (termed hybrid-inducing TCM). We exposed purified BMNs to hybrid-inducing TCM and after 7 days of incubation we observed the formation of a cell subset that retained all granulocytic markers and acquired the same phenotype as the tumor-derived hybrid TANs (HLA-DR$^+$CD14$^+$CD86$^+$CD206$^+$CCR7$^+$) (Fig1. B-D). TCM collected from digested tumors where we did not find hybrid TANs was used to differentiate immature BMN into canonical neutrophils. For more details see our published paper (Singhal et al., Cancer Cell, 2016).

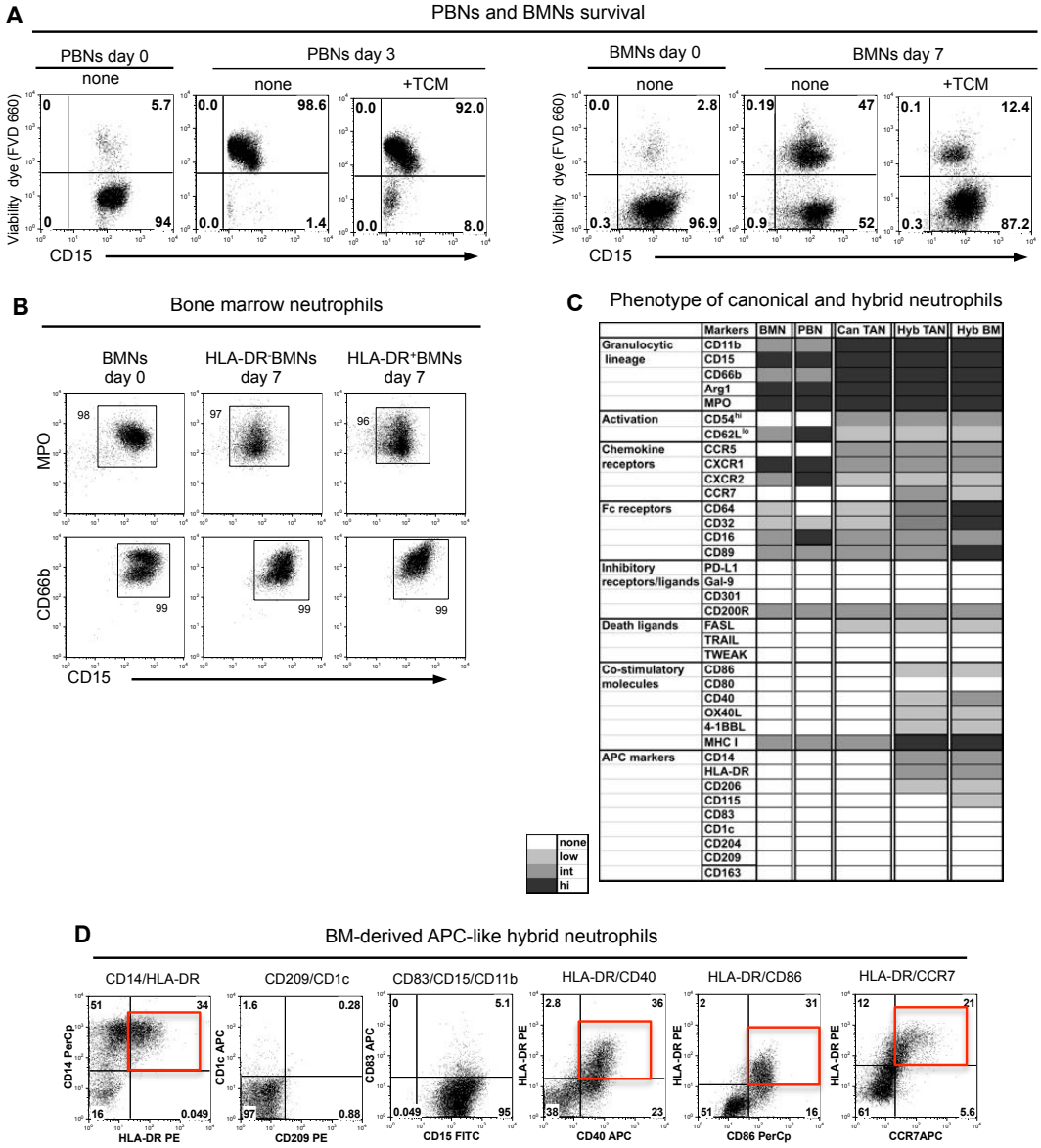

Figure 1.
The differentiation of bone marrow immature neutrophils into canonical and hybrid neutrophils.
(A) Fixable Viability Dye eFluor® 660 (FVD 660) was used to discriminate viable neutrophils in cell culture. Representative dot plots from 1 of 6 experiments are shown. (B) BMNs were isolated by CD15-conjugated magnetic beads. Flow cytometric analysis of the expression of MPO, CD66b, and CD15 markers on freshly isolated BMNs (day 0) and BMNs cultured with (HLA-DR$^+$ BMNs) or without hybrid-inducing TCM (HLA-DR$^-$ BMNs) for 7 days. (C) Heat map comparing the phenotypes of BMNs, PBNs, canonical TANs (Can TAN), hybrid TANs (Hyb TAN) and BM-derived hybrid neutrophils (Hyb BM). (D) Flow cytometric analysis of the expression of indicated APC markers on BM-derived hybrid neutrophils (red boxes), Expression of APC markers was analyzed by flow cytometry on gated CD11b$^+$CD15^{hi}CD66b$^+$ BMNs.

Next, we investigated whether the BM-derived hybrid neutrophils also functionally resemble hybrid TANs in their ability to stimulate T cell responses. For this purpose we differentiated immature BMNs into activated canonical and hybrid neutrophils and co-cultured them with autologous PBMCs stimulated with plate-bound anti-CD3 Abs. Similar to canonical and hybrid TANs, both subsets of BM derived neutrophils were able to augment the expression of activation markers CD25 and CD69 on stimulated T cells to the same level.

However, HLA-DR$^+$ hybrid neutrophils exerted a significantly stronger stimulatory effect ($p<0.02$) on T cell proliferation and IFN-γ production than the canonical neutrophils (Fig. 2A and 2B). Therefore, BM derived hybrid and canonical neutrophils differentiated with different TCMs completely recapitulate the phenotype of hybrid and canonical TANs as well as their functions. These data demonstrate the resemblance between BM-derived and tumor-derived hybrid neutrophils, and justify the use of this model to investigate additional functions of this rare subset of TANs. For more details see our published paper (Singhal et al., Cancer Cell, 2016).

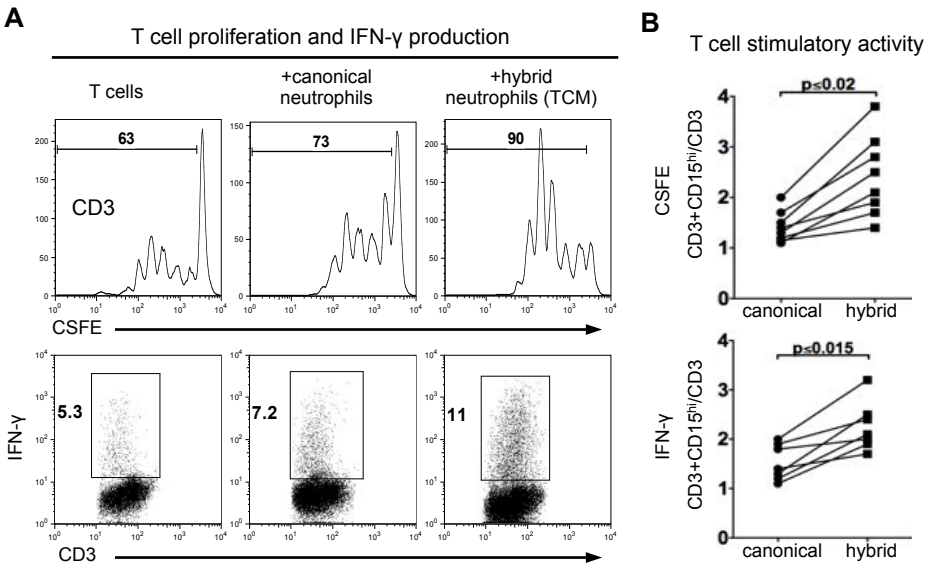

Figure 2. BM-derived hybrid neutrophils are able to stimulate T cell responses. (A) The proliferation and IFN-γ production of anti-CD3 Abs stimulated autologous T cells in the presence of BM-derived canonical and hybrid neutrophils differentiated with hybrid-inducing TCM. T cell proliferation was measured in CFSE dilution assay. IFN-γ production was measured intracellular by flow cytometry. (B) Summary results of autologous T cell proliferation (top graph) and IFN-γ production (bottom graph) in the presence of canonical and hybrid neutrophils. Data are presented as a ratio (CD3 cells+CD15^{hi})/(CD3) (n = 8,Wilcoxon matched-pairs rank test).

The differentiation of BMNs into HLA-DR$^+$CD14$^+$ APC-like hybrid BMNs after exposure to hybrid-inducing TCM was donor-dependent and varied from 20% to 80% of the initial BMN population (Fig.1D). To obtain pure population of hybrid neutrophils, we sort these cells by flow cytometry based on CD15$^+$CD66b$^+$HLA-DR$^+$CD14$^+$ phenotype (Fig. 3A, red box, HLA-DR$^+$CD14$^+$ Double Positive, DP) whereas canonical neutrophils were sorted as CD15$^+$CD66b$^+$HLA-DR$^-$CD14$^-$ cells (Fig. 3A, green box, Double Negative, DN)

In some experiments we enriched hybrid neutrophils using magnetic beads coated with anti-CD14 Abs. We incubated these sorted hybrid and canonical neutrophils in the cell culture DME/F-12 1:1 media (HyClone,

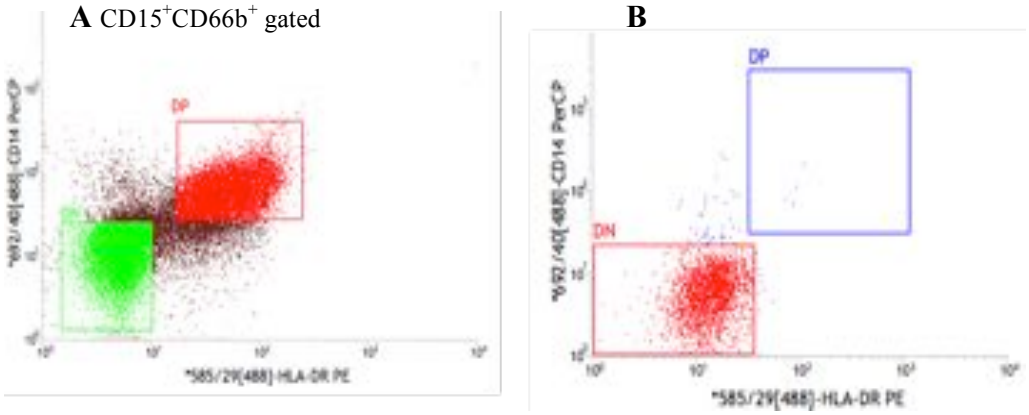

Figure 3. **Flow cytometry assisted cell-sorting strategy.** (A) Populations were sorted from a heterogeneous pool of BM CD15$^+$ cells cultured in the presence of hybrid inducing TCM or IFN-g and GM-CSF. The plot shows a representative sample of gating strategy. (B) Verification of sort purity was performed on the DN population to preserve DP sample. Sort purity ranged from 90 to 97%.

Thermo Scientific) supplemented with 2.5 mM L-glutamine, 15mM HEPES Buffer, 10% of Embryonic Stem

(ES) Cell Screened FBS (U.S.) (Thermo Scientific™ HyClone™), Penicillin (100U/ml) and Streptomycin (100 µg/mL). Twenty-four hours later, cell culture supernatants were collected, filtered and stored at -80 C°. To quantify key secreted inflammatory cytokines, chemokines, and growth factors secreted, we used multi-analyte analysis (Luminex® Assays) of the supernatants. Samples from at least 5 patients were studied. We summarized the results using a "heat map" format (Fig. 4). Consistent with our hypothesis, hybrid BM neutrophils produced more pro-inflammatory cytokines (i.e. IL-8, MCP-1, MIP-1α and MIP-1β) than canonical BM neutrophils.

Figure 4. Cytokine/chemokine profile of hybrid BM neutrophils

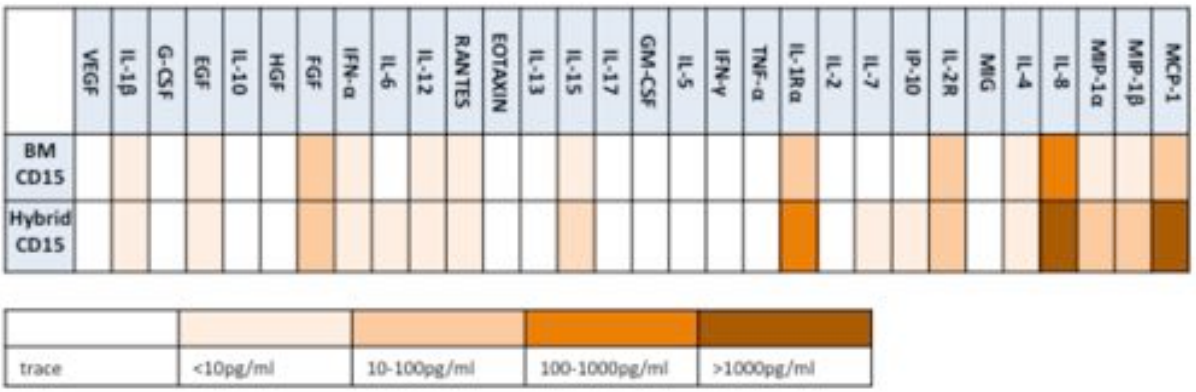

To more fully characterize these cells in a non-biased fashion and to allow us to look at many other pathways, the same subsets of cells were flow sorted and immediately placed into RNAlater® Stabilization Solution. mRNA were isolated using the Qiagen RNAeasy micro kit from sorted HLA-DR^{+}CD14^{+} Double Positive (DP) hybrid and HLA-DR^{-}CD14^{-} Double Negative (DN) canonical neutrophils. Whole human genome RNA expression profiles have been performed using RNA next generation sequencing (Penn Molecular Profiling Facility).

Data are provided in two forms. One set pooled the subtypes submitted (i.e. all HLA-DR^{+}CD14^{+} Double Positive DPs hybrid cells, all HLA-DR^{-}CD14^{-} Double Negative DNs canonical cells, all non-treated) from multiple patients. The other analysis took into account differences in baseline expression that occurred for the same gene across multiple subjects. Results were provided showing fold change as log2 test group/control group as well as a False Discovery Rate from p-values using the Benjamini-Hochberg correction. An analysis of the quality of the reads shows that the intra-sample variability was low, suggesting similar gene clusters are induced within treatment groups (Fig.5). Yet several gene clusters are differentially expressed between DN and DP, indicating unique profile of factors is induced in each subset that can be identified and studied for links to fate decision and cell function (Fig.5). In order to perform a cursory analysis of our results, we sought to compare fold change in RNA as measured in the RNAseq experiment to our previously published data showing the surface expression of various immune markers on either CD15+ cells, hybrid cells isolated within the tumor, and hybrid cells generated in vitro. We observed a strong correlation between gene expression and our previous published surface protein data. For instance, in agreement with flow cytometry data, we observed that RNA coding for surface proteins such as HLA-DR, CD14, CD40, and CD86 all are upregulated approximately 4 to 60-fold in DP hybrid cells than DN canonical cells. Conversely, Arg1 and CXCR1 are more highly expressed in the un-treated DN group compared with the TCM DP group. These initial findings impart confidence that future analysis of any transcriptional differences between each subset will yield meaningful targets.

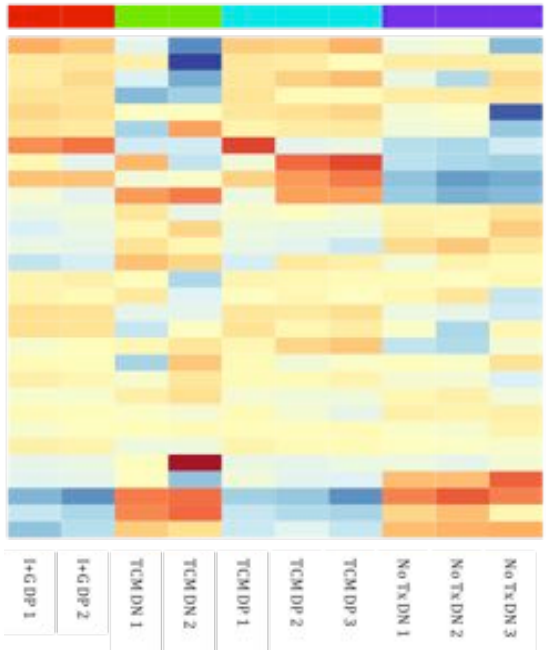

Figure 5. K-means heatmap of RNAseq data indicating intra-condition consistency.
Hybrid neutrophils were differentiated from BM CD15 immature neutrophils in the presence of hybrid inducing TCM (TCM DP) or IFN-g and GM-CSF (I+G DP) and flow sorted as HLA-DR^{+}CD14^{+} Double Positive (DP) cells. Canonical neutrophils were sorted as HLA-DR^{-}CD14^{-} Double Negative (DN) cells. Non treated BM CD15 neutrophils (NoTxDN) were served as a control. Hybrid and canonical neutropihls were obtained at least from three patients. Heatmap indicates that changes between conditions are consistent across samples. For example, the gene expression within clusters across samples of the I+G DP are similar color, while gene expression across treatment groups differs significantly in certain areas.

Next, we plan to work with members of the Institute for Biomedical Informatics (IBI) at the Perelman School of Medicine at the University of Pennsylvania. The staff will be able to perform top-level analysis of our data and provide information on differential gene expression, any alternative splice variations of critical genes, and quantification of gene and transcript levels. Furthermore, biostatisticians will perform gene-annotation enrichment analysis, functional annotation clustering, gene-disease association, and translational targets. The wealth of information will provide key genes that can be manipulated to test whether or not specific proteins are necessary and sufficient for maturation from CD15 precursors to hybrid neutrophils.

Aim 2. This aim is largely completed

Specific objectives: Goal of this aim was to evaluate the interaction of canonical and hybrid TANs with T cells in patients with NSCLC. Specifically, investigate the effects of TAN subsets on the antigen non-specific and specific T cell responses. Given that hybrid TANs exhibit many of the essential features of professional antigen presenting cells, we hypothesized that this hybrid TAN subset can trigger and augment T cell responses as compared to canonical TANs. Understanding the role of TANs in regulating T cell responses in cancer patients is particularly important because cytotoxic T lymphocytes are the chief effector cells mediating antigen-driven anti-tumor immunity.

Major activities: We studied the effect of TAN subsets on effector T cell responses using autologous T cells isolated from peripheral blood mononuclear cells (PBMC) of cancer patients and new model of human TCR-transfected CD8 cells (Ly95 effectors) that recognizes a HLA-A*02-restricted peptide of human cancer testis NY-ESO-1. TAN subsets were isolated by flow cytometry cell sorting based on phenotype of canonical and hybrid neutrophils (see a gating strategy in figure 6). Given that hybrid TAN subset is very rare in tumor, in some experiments we used hybrid neutrophils differentiated form bone marrow progenitors as described in aim1. To determine effect of TAN subsets on antigen-nonspecific T cell responses, sorted TAN subsets were co-cultured with autologous PBMCs that had been stimulated with plate-bound anti-CD3 Abs. To determine effect of TANs on antigen-specific memory T cell responses we co-cultured autologous T cells with TAN subsets that had been pulsed with mixtures of overlapping peptides designed to stimulate T cells with a broad array of HLA types. In addition, we also determined effect of TAN subsets on tumor-specific effector T cell responses. For this purpose, we co-cultured neutrophil subsets with Ly95 effectors stimulated with genetically modified A549 human lung adenocarcinoma cell line expressing the tumor NY-ESO-1 protein in the context of HLA-A*02. To determine whether APC-like hybrid neutrophils could directly trigger NY-ESO-1 specific response of Ly95 cells, we pulsed HLA-A*02 BM-derived canonical and hybrid neutrophils with the NY-ESO-1 peptide and then co-cultured the exposed neutrophils with Ly95 T cells. We evaluated T cell response by

measuring (i) proliferation (CFSE and BrdU assays), (ii) production of IFN-g (intracellular and ELISPOT asays), and (iii) activation (CD45RO, CD25, CD62L, and CD69).
I was invited several times to be a speaker and present these results at the following conferences:

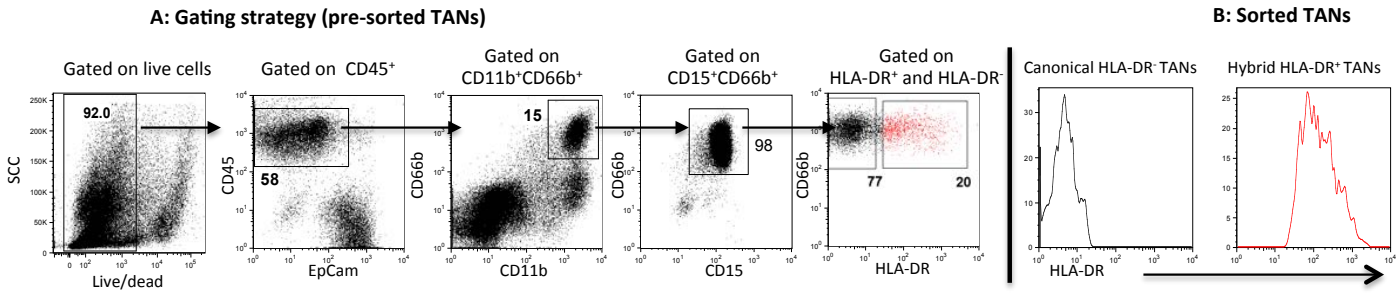

Figure 6. Gating strategy for sorting of canonical HLA-DR$^-$ and hybrid HLA-DR$^+$ TANs by flow cytometry. (A) A single cell suspension was obtained from freshly harvested tumor, stained for indicated markers and sorted based on the phenotype of canonical (CD11b$^+$CD66b$^+$CD15^{hi}HLA-DR$^-$) and hybrid (CD11b$^+$CD66b$^+$CD15^{hi}HLA-DR$^+$) TANs. The purity of sorted subsets is shown on hystograms

1. Inflammation, Immunity and Cancer: The Society For Leukocyte Biology's 49th Annual Meeting and "Neutrophil 2016": Neutrophils and Other Leukocytes, University of Verona, Verona, Italy, September 15-17, 2016, **Invited Speaker**.
2. Regulatory Myeloid Suppressor Cells Conference, Philadelphia, The Wistar Institute, June 16-19, 2016 **Invited Speaker**.
3. Immunology School "Regulation of Lung Inflammation", Moscow, Russia, May11-13, 2016. **Invited Speaker**.

Please see official invitations from Scientific Organizing Committee of these conferences in appendices

Significant results and outcomes:

Aim 2.1 (Investigate the effects of TAN subpopulations on T cell responses). This aim is completed.

We have rigorously tested our hypothesis and proved it correct. Our team has published these results in the following journals:

1. Journal of Clinical Investigation: Eruslanov EB, et al., Tumor-associated neutrophils stimulate T cell responses in early-stage human lung cancer. 2014 Dec;124(12):5466-80. doi: 10.1172/JCI77053. Epub 2014 Nov 10.
2. Cancer Cell: Singhal S, … Albelda S. and Eruslanov E. Origin and Role of a Subset of Tumor-Associated Neutrophils with Antigen Presenting Cell Features in Early-Stage Human Lung Cancer. Cancer Cell, 2016, Jul 11;30 (1):120-35)
3. Clinical Cancer Research (Moon E, Ranganathan R, Eruslanov E … and Albelda S. Blockade of Programmed Death 1 Augments the Ability of Human T cells Engineered to Target NY-ESO-1 to Control Tumor Growth after Adoptive Transfer. Clinical Cancer Research; 2016 Jan 15;22 (2):436-47).

We found that the APC-like hybrid neutrophils are superior to canonical neutrophils in their ability to: (1) stimulate antigen non-specific autologous T cell responses induced by plate-bound anti-CD3 antibodies, (2) directly stimulate antigen-specific autologous memory T cell responses and (3) augment NY-ESO-1 specific effector T cell responses by providing a co-stimulatory signals through the OX40L, 4-1BBL CD86, CD54 molecules in direct cell-cell contact.

For the proposed experiments we isolated TAN subsets from tumor digest by flow cytometry cell sorting and mixed them with activated autologous T cells isolated from PBMC. We found that both subsets of neutrophils

were able to augment the expression of activation markers CD25 and CD69 on CD3 stimulated T cells to the same level. However, HLA-DR$^+$ hybrid TANs exerted a significantly stronger stimulatory effect on T cell proliferation than canonical TANs (Fig.7A). Specifically, each sorted TAN subset was co-cultured with autologous CFSE-labeled PBMCs that had been stimulated with plate-bound anti-CD3 Abs. We found that the proliferation of CD4 and CD8 cells after 4 days of stimulation was markedly augmented ($p<0.03$) after exposure to HLA-DR$^+$ hybrid TANs versus the HLA-DR$^-$ canonical TANs (Fig.7A). We next determined whether APC-like hybrid TANs could trigger and sustain antigen-specific T-cell responses. We co-cultured autologous T cells with TAN subsets that had been pulsed with peptides from commercially available peptide pools that contained mixtures of overlapping peptides. Each peptide pool corresponded to a defined HLA class I or II restricted T-cell epitopes from Cytomegalovirus, Epstein-Barr virus, Influenza virus or Clostridium tetani designed to stimulate T cells with a broad array of HLA types. As shown in Figure 7B, the HLA-DR$^+$ hybrid TANs efficiently triggered memory CD8 and CD4 T cell responses to HLA class I and II restricted T cell epitopes, respectively. Canonical TANs and PBNs induced only weak CD8 T cell responses and did not trigger CD4 T cell responses. Together, these data demonstrate that HLA-DR$^+$ hybrid TANs are able to function as efficient APCs and dramatically augment T cell response.

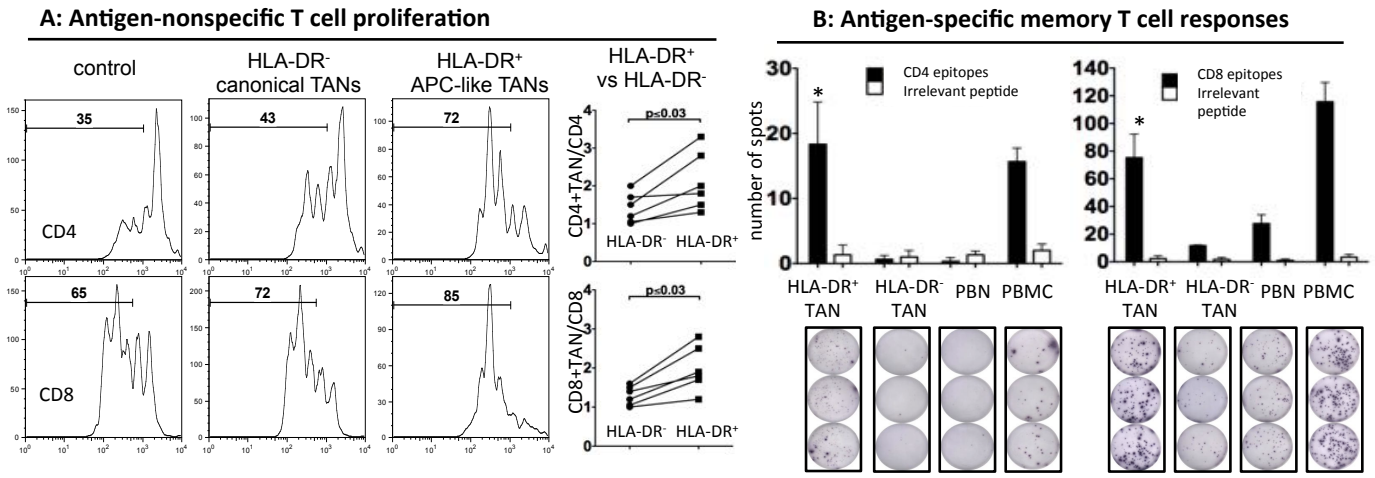

Figure 7. The effect of canonical and hybrid TANs on T cell responses. (A) The proliferation of autologous CFSE-labeled PBMC stimulated with plate-bound anti-CD3 Abs in the presence of hybrid HLA-DR$^+$ or canonical HLA-DR$^-$ TANs. The T cell proliferation was measured in CFSE dilution assay. T cell stimulatory activity was defined as the ratio CFSE^{lo} (T cells+TANs) / CFSE^{lo} (T cells) (n=6, Wilcoxon matched-pairs rank test). (B) Autologous virus-specific memory T cell responses in the presence of APC-like hybrid HLA-DR$^+$ or canonical HLA-DR$^-$ TANs. IFN-γ-ELISPOT assay (mean ± SEM, n=3, *p ≤ 0.01 canonical vs. hybrid, Mann-Whitney test).

Next, we evaluated the effect of canonical and hybrid neutrophils on anti-tumor effector T cells using a newly developed *in vitro* model. We transduced human T cells with a high-affinity transgenic T cell receptor (TCR) called Ly95 that recognizes an HLA-A*0201-restricted peptide sequence in the human cancer testis antigen, NY-ESO-1. As target cells, we used genetically modified A549 human lung adenocarcinoma cell line expressing the NY-ESO-1 protein in the context of HLA-A*0201 (A549A2-NY-ESO-1 cells). Co-culturing of Ly95 T cells (TCR Vb13.1$^+$CD8$^+$) with A549A2-NY-ESO-1 (A2/ESO A549) tumor cells resulted in robust production of IFN-γ and Granzyme B in Ly95 T cells (Fig.8A). When we added BM-derived hybrid neutrophils into this system, the production of IFN-γ and Granzyme B in Ly95 T cells was markedly elevated (Fig.8A and 8B). Of note, the addition of the hybrid neutrophils into Ly95 T cells co-cultured with control A549 cells did not induce the production of these factors, indicating that hybrid neutrophil-mediated stimulation of Ly95 cells was NY-ESO-1-specific and not the result of allostimulation (data not shown). As a follow-up, using a transwell assay system, we found that HLA-DR$^+$ hybrid BMNs induced the stimulation of IFN-γ production by Ly95 T cells only when the cells were in direct contact. Since hybrid BMNs are characterized by increased expression of co-stimulatory molecules OX40L, 4-1BBL CD86, CD54 (, we co-cultured Ly95 T cells activated with A549 A2-NY-ESO-1 tumor cells and with hybrid BMNs in the presence of blocking Abs to these up-regulated co-

stimulatory molecules. Figure 8A shows a representative experiment where the stimulatory effect of hybrid neutrophils was partially abrogated in the presence of anti-CD54, 4-1BBL, OX-40L, and CD86 blocking Abs.
Next we asked whether APC-like hybrid neutrophils could directly trigger NY-ESO-1 specific response of Ly95 cells. Given that Ly95 cells specifically recognizes HLA-A*02-restricted peptide of NY-ESO-1, we pulsed HLA-A*02^{+}BM-derived canonical and hybrid neutrophils with the NY-ESO-1 (157-165, SLLMWITQV) peptide and then co-cultured the exposed neutrophils with Ly95 T cells for 24 hours. We found that hybrid

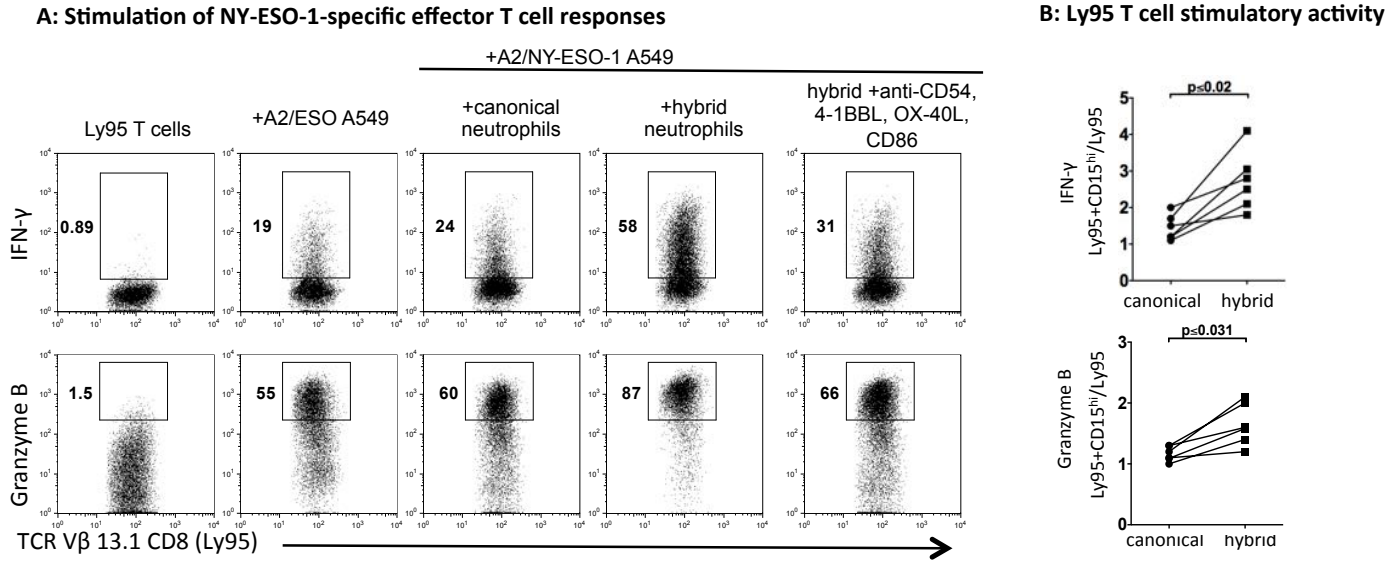

Figure 8. APC-like hybrid neutrophils are able to stimulate NY-ESO specific effector T cell responses. A) NY-ESO-specific Ly95 cells (TCR Vβ13.1^{+}CD8^{+}) were stimulated with A549 tumor cell line expressing NY-ESO-1 in the context of HLA-A*02 (A2/NY-ESO-1 A549) in the presence of BM-derived canonical and hybrid neutrophils. In some experiments anti-CD54, 4-1BBL, OX-40L, and CD86 blocking Abs were added to this system. Intracellular IFN-γ and Granzyme B production was measured by flow cytometry.(B) Cumulative results showing the Ly95 cell stimulatory activity of canonical and hybrid neutrophils. Stimulatory activity was defined as a ratio (Ly95 cells+A549-NY-ESO+BMN)/(Ly95cells+A549-NY-ESO) (n=6,Wilcoxon matched-pairs rank test).

HLA-A*02^{+}HLA-DR^{+} hybrid neutrophils preloaded with the peptide were able to present this peptide and trigger IFN-γ production in Ly95 T cells more effectively than peptide-loaded canonical neutrophils (Fig.9). These data show that hybrid neutrophils can trigger and significantly augment the activation of antigen-specific effector T cells.

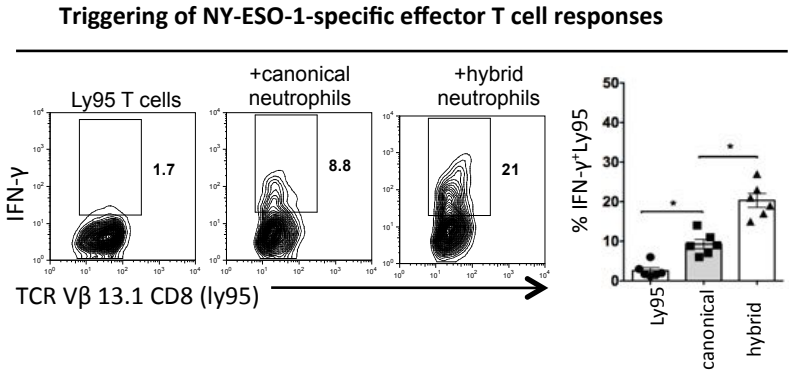

Figure 9. APC-like hybrid neutrophils are able to trigger NY-ESO specific effector T cell responses HLA-A02^{+} canonical or hybrid neutrophils were pulsed with synthetic NY-ESO-1 peptide and co-cultured with Ly95 cells for 24 hrs. Intracellular IFN-γ was assessed by flow cytometry, (mean ± SEM, n = 6, *p ≤ 0.01,Wilcoxon matched-pairs rank test)

Conclusions: The concept of neutrophil diversity and plasticity has begun to emerge in a variety of inflammatory disorders and murine tumor models; however, to date there has been no convincing evidence showing that specialized neutrophil subpopulations with different functions exist in human cancers. Thus, we provide the first evidence of two subsets of TANs in human lung cancer. All TANs have an activated phenotype and could support (rather than inhibit) T cell functions to some degree. However, we identified a subset of TAN in early-stage lung tumors that can undergo a unique differentiation process resulting in formation of

specialized subset of APC-like hybrid neutrophils. These hybrid TANs had enhanced ability to trigger and support T cell responses in direct cell-cell interactions. This property of hybrid neutrophils may provide new opportunities to boost the efficacy of vaccines based on cytotoxic T lymphocyte induction.

Aim 2.2: Determine the effects of TAN subpopulations on the maturation and function of dendritic cells.

Activities, results and outcomes: We have not started to work on these aims yet but plan to do it in the second year.

Aim 3: Define the cytotoxic phenotype of canonical and hybrid neutrophils and the mechanisms by which these neutrophils inhibit tumor growth.

Activities, results and outcomes: We have not started to work on these aims yet but plan to do it in the second year.

What opportunities for training and professional development has the project provided?

During the first year I have followed to my career development plan. Specifically,
1. I have learned new research skills and expanded my research scope by taking the following:

- courses in advanced molecular immunology provided by Institute of Immunology at University of Pennsylvania
- research seminars in lung cancer that are sponsored through the Lung Cancer Translational Center of Excellence at University of Pennsylvania
- several grant writing seminars for junior faculty offered at University of Pennsylvania
- several scientific paper writing seminars for junior faculty offered at University of Pennsylvania
- weekly research seminars in immunology sponsored by the Penn Institute of Immunology and Penn Transplant Institute

2. I meet on a weekly basis with my mentor Dr. Albelda to monitor my scientific progress and ensure my career milestones are being met. Dr. Albelda has been granting me the necessary rigor of the scientific approach and oversight to succeed.

3. I participated in major immunology and cancer biology conferences sponsored by American Association for Cancer Research (AACR), American Association of Immunologists (AAI) and Society For Leukocyte Biology (SLB). As recognition of my research, I was invited several times to be a speaker and present results at the following conferences:

- E. Eruslanov. Tumor-Associated Neutrophils in Human Lung Cancer. Inflammation, Immunity and Cancer: The Society For Leukocyte Biology's 49th Annual Meeting and "Neutrophil 2016": Neutrophils and Other Leukocytes, University of Verona, Verona, Italy, September 15-17, 2016, **Invited Speaker**.
- E. Eruslanov. Origin and Role of a Subset of Tumor-Associated Neutrophils with Antigen Presenting Cell Features in Early-Stage Human Lung Cancer. Regulatory Myeloid Suppressor Cells Conference, Philadelphia, The Wistar Institute, June 16-19, 2016 **Invited Speaker**.
- E. Eruslanov. Origin and Role of a Subset of Tumor-Associated Neutrophils with Antigen Presenting Cell Features (Hybrid TANs) in Early-Stage Human Lung Cancer. Immunology School "Regulation of Lung Inflammation", Moscow, Russia, May11-13, 2016. **Invited Speaker**.
- Eruslanov, P Bhojnagarwala, J Quatromoni, S O'Brien, E Moon, T Stephen, A Rao, A Garfall, W Hancock, J Conejo-Garcia, C Deshpande, M Feldman, S Singhal and S Albelda. The origin and role of

APC-like hybrid tumor-associated neutrophils in early-stage human lung cancer. AACR annual meeting: The function of tumor microenvironment in cancer. San Diego, Jan 7, 2016, **poster presentation**

Please see official invitations from Scientific Organizing Committee of these conferences in appendices.

Therefore, this career development award enables me to develop new research skills, knowledge and collaborations that dramatically advances my career as researcher of the human tumor microenvironment.

How were the results disseminated to communities of interest?

"Nothing to Report."

What do you plan to do during the next reporting period to accomplish the goals?

We will follow to our plans, approaches, and goals that I specified for each aim in the original proposal.

Aim 1: Investigate the inflammatory profile of canonical and hybrid TANs, (timeline 1-12 months). This aim is largely completed.

Our primary analysis correlating RNAseq data to flow cytometry data has provided confidence that in-depth analysis will reveal valid transcritpional targets for interrogation. During the next year we plan to work with members of the Institute for Biomedical Informatics (IBI) at the Perelman School of Medicine at the University of Pennsylvania. The staff will be able to perform top-level analysis of our data and provide information on differential gene expression, any alternative splice variations of critical genes, and quantification of gene and transcript levels. Furthermore, biostatisticians will perform gene-annotation enrichment analysis, functional annotation clustering, gene-disease association, and translational targets to define the unique features of hybrid neutrophils.

Aim 2: Investigate the effects of canonical and hybrid TANs on T cell responses and on the maturation and function of dendritic cells, (timeline 1-18 months).

Aim 2.1: Investigate the effects of TAN subpopulations on T cell responses. This aim is completed.
Aim 2.2: Determine the effects of TAN subpopulations on the maturation and function of dendritic cells.

We plan to start this aim 2.2 in the next reporting period with performing experiments as originally described in the proposal. The role of TANs in cross-talk with dendritic cells (DCs) in the tumor microenvironment has been unexplored. Thus, the goal of this subAim will be to determine whether TANs “license” DCs towards immunogenic or tolerogenic cells. We hypothesize that hybrid TANs promote the maturation of immunogenic DCs. To prove our hypothesis we will co-culture monocyte-derived DCs (MoDCs) with unsorted TANs, canonical TANs, or hybrid TANs. The following characteristics of DCs will be examined after being exposed to different subsets of neutrophils: (i) Maturation: To study the maturation of MoDCs, DCs will be stimulated with LPS and co-cultured with or without different types of neutrophils. Twenty-four hours later, the phenotypic maturation of MoDCs will be evaluated by measuring the surface markers indicative of DC-maturation (CD40, CD86, CD80, HLA-DR, CCR7, CD83) and DC-tolerogenicity (PD-L1, ILT3, IDO). We will analyze the effects of neutrophils on cytokine production by MoDCs during their maturation. The cytokines IL-6, IL-10, IL-12, TNF-a, and TGF-b1 will be detected by intracellular staining in LPS-stimulated $CD209^{+}$ MoDCs exposed to different types of neutrophils. (ii) Allostimulation: The effect of neutrophils on the allostimulatory ability of MoDCs will be quantified by performing mixed lymphocyte response (MLR) studies. MoDCs will mature in the presence or absence of LPS and each type of TAN (canonical, or tri-hybrid TANs). Twenty-four hours later, neutrophils will be removed using CD15 beads and each group of mature DCs will be added to allogeneic T cells. Proliferation of CD4 and CD8 cells in an MLR will be quantified by CFSE dilution at day 5. Controls will consist of cultures with untreated immature DCs or LPS-matured DCs. The T cell type will be characterized by flow cytometry: Treg ($CD4^{+}CD25^{+}Foxp3^{+}$), Th1 ($CD4^{+}$IFN-ã$^{+}$), Th2 ($CD4^{+}$IL-4^{+}), or Th17 (IL-17^{+}).

Aim 3: Define the cytotoxic phenotype of canonical and hybrid neutrophils and the mechanisms by which these neutrophils inhibit tumor growth, (timeline 12-24 months).

.

We plan to start this aim in the next reporting period. We will perform experiments according to our original plan described in the proposal. Goal of this aim is to evaluate tumorocidal activity of canonical and hybrid neutrophils. First we will evaluate spontaneous cytotxic activity against tumor cells of the various subtypes of neutrophils (blood, BM neutrophils, BM-derived hybrid cells, canonical TANs, and hybrid TANs). For this purpose we will use GFP-expressing tumor cell lines (lung carcinoma cells A549 and H460) as a target. These lines will be incubated with the neutrophils for 24 hours, at which time all floating cells will be removed. Cytotoxicity will be calculated the remaining cell-associated GFP fluorescence of adherent tumor cells cultured with neutrophils to control wells (tumor cells without neutrophils). We will test whether priming of neutrophils can augment cytotoxic activity of neutrophil subsets. We will also determine the contribution of TAN subsets to Ab-dependent cellular cytotoxicity by mixing them with tumor cells pre-treated with cetuximab (anti-EGFR Abs). If we see differences in cytotoxicity, follow-up studies will characterize the mechanisms of TAN-induced cell killing among the different subtypes. To determine the role of ROS dependent mechanisms, inhibitors of the NADPH oxidase complex will be added to cytotoxicity assay. To characterize the possible role of superoxide anion O_2^-', hydrogen peroxide, or hypochlorous acid (HOCl) in TAN-mediated killing, cytotoxic assays will be performed in the presence of their specific inhibitors: superoxide dismutase (SOD), catalase, and taurine, respectively. It is also possible that alternative non-oxidative pathways and other neutrophil cellular products are involved in tumor cell lysis. This can be explored by using inhibitors of different serine proteinases, peptide defensins, granzyme B, and perforins. We can also use antibodies that block possible death receptor/death receptor ligands including anti-TRAIL and anti-FASL antibodies. To determine whether the generation of reactive nitrogen intermediates by activated neutrophils is involved in neutrophil-mediated tumor cell killing, the nitric oxide synthase inhibitor L-NMMA will be added to the cytotoxic assay.

In addition we will develop and optimize our in vitro flow cytometry based approach to carefully evaluate and quantify cytotoxic activity of BM-derived canonical and hybrid neutrophils against tumor cells opsonized with tumor-specific therapeutic antibody. Tumoricidal activity of neutrophils may depend on the size of tumor cell and the level of expression of surface tumor antigen. To address these points in our model, we will use large size with high level of expression of $EGFR^{hi}$ A431 tumor cell line and large size with low level of expression of $EGFR^{lo}$ A549 tumor cell line. These tumor cell lines will be opsonized with anti-EGFR monoclonal humanized antibodies (cetuximab) that are actively used in clinic. Also, we will use small size Daudi tumor cell line opsonized with anti-CD20 Abs (rituximab). In addition to our established cytotoxic assay based on cell-associated GFP fluorescence of target cells, we will develop flow cytometry based assay to identify if antibody-dependent phagocytosis (ADP) is involved in the elimination of opsonized target cells by hybrid neutrophils. Specifically, we will label tumor cells with red-fluorescent dye PKH26 (Sigma) and co-cutlure them with BM-derived canonical and hybrid neutrophils in the presence of cetuximab or rituximab. $Fc_\gamma R$-bearing monocyte-derived macrophages and blood NK cells will be used in this assay as a positive control for ADP and ADCC, respectively. At the end of incubation cells will be collected and stained with FITC-Abs specific for neutrophil marker CD66b and with a viability dye FVD eFluor® 660. Phagocytosed PKH tumor cells will be identified as both PKH^+ and $CD66b^+$ cells by flow cytometry. Direct tumor cell death will be calculated as a percent of $PKH^+FVD660^+$ $CD66b^-$cells that were not phagocyted. We will determine the role of ROS- or RNI-dependent mechanisms by adding specific inhibitors to cytotoxicity assay.

Once we have established the mechanisms of hybrid neutrophil cytotoxicity triggered by tumor-specific Abs in vitro, we will start to explore the clinical potential of hybrid cells generated from BM to mediate ADCC in vivo. We will inject 5 million human neutrophils intratumorally into established human lung cancer cell line-derived tumors ($100mm^3$A549 lung cancer xenografts) growing in NSG mice and subsequently measure tumor volume. In addition, we will characterize the ability of different neutrophil subsets to induce ADCC using the anti-EGFR mAb cetuximab.

IMPACT

What was the impact on the development of the principal discipline(s) of the project?
To date, the characterization of the human lung tumor microenvironment is still in its infancy and the functional cross-talk between immune and tumor cells in humans remains largely unexplored. A better understanding of the interaction between cancer cells and the lung microenvironment may allow tumor immunologists to develop novel strategies to improve anti-tumor immune responses. Tumor-recruited myeloid cells represent a significant portion of inflammatory cells in the tumor microenvironment and influence nearly all steps of tumor progression. Among the different types of myeloid cells, tumor-associated macrophages (TAMs) have been the best characterized and are generally considered pro-tumoral in murine tumor models. The role of tumor-associated neutrophils (TANs) in cancer progression remains unclear and has only been recently investigated in murine models. Characterization of human TANs is even less well-developed. Numerous findings in murine model systems suggest a predominantly pro-tumoral role for neutrophils in cancer development. However, there are crucial species differences in the evolution of tumors, genetic diversity, immune and inflammatory response, and intrinsic biology of neutrophils that we postulate have a profound impact on tumor development and the function of neutrophils in mouse tumors versus human. A crucial difference is that the majority of mouse tumor models lack the prolonged initial phases of multistage tumor evolution present in humans, such as elimination and equilibrium phases, where anti-tumoral mechanisms are activated. It is a sobering fact that the majority of cancer immune therapies that work well in mice fail to provide similar efficacy in humans; the average rate of successful translation from animal models to clinical cancer trials is less than 8% (2). Thus, there is a continuing need to develop new and innovative approaches to characterize granulocytes in human cancers and to characterize the variety of their functions in the human tumor microenvironment.

Our study generates new knowledge about human TANs and exerts a sustained influence on the field. Therefore, this work is a first-of-its kind and will important ramifications for patients with lung cancer. Specifically, we for the first time provided the detailed phenotypic and functional characteristics TAN and their subsets in human early-stage cancer. We provide the first evidence of two subsets of TANs in human lung cancer. All TANs had an activated phenotype and could support (rather than inhibit) T cell functions to some degree. In contrast to mouse tumor models, our data demonstrate that in patients with early stage lung cancer, TANs do not significantly contribute to the inhibition of T cell responses. In fact, the TANs isolated from a vast majority of small size early stages tumors were actually able to stimulate T cell response to varying degrees. We identified a subset of TAN in early-stage lung tumors that can undergo a unique differentiation process resulting in formation of specialized subset of APC-like hybrid neutrophils. These hybrid TANs had enhanced ability to trigger and support anti-tumor T cell responses in direct cell-cell interactions. This property of hybrid neutrophils may provide new opportunities to boost the efficacy of vaccines based on cytotoxic T lymphocyte induction. Understanding the role of TANs in regulating T cell responses is particularly important because cytotoxic T lymphocytes are the primary effector cells mediating antigen-driven anti-tumor immunity.

These results have been published in JCI, Cancer Cell and Clinical Cancer Research. In addition these results have been presented at a major cancer immunology conferences organized by AACR and AAI (please see details in PRODUCTS). This knowledge will allow us to develop different therapeutic strategies to regulate the function of TANs depending on tumor stage in human. Understanding how to direct and maintain the human TANs towards anti-tumor effector cells will open new therapeutic options in the future design of active immunotherapy to potentially boost natural or vaccine-induced anti-tumor immunity.

What was the impact on other disciplines?
Nothing to Report
What was the impact on technology transfer?
Nothing to Report
What was the impact on society beyond science and technology?
Nothing to Report

CHANGES/PROBLEMS

There were no changes and problems during this reporting period
"Nothing to Report"

PRODUCTS

Publications, conference papers, and presentations

Journal publications (please see these papers in appendices):

1. **Eruslanov E** (corresponding author), Bhojnagarwala P, Quatromoni J, Stephen T, Ranganathan A, Deshpande C, Akimova T, Vachani A, Litzky L, Hancock W, Conejo-Garcia J, Feldman M, Albelda S, and Singhal S. Tumor-associated neutrophils stimulate T cell responses in early-stage human lung cancer. **The Journal of Clinical Investigation**, 2014, Dec 1; 124(12): 5466-80, highlighted as a featured paper.
2. Singhal S, Bhojnagarwala P, O'Brien S, Moon E, Garfall A, Rao A,. Quatromoni J, Stephen T, Litzky L, Deshpande D, Feldman M, Hancock W, Conejo-Garcia J, Albelda S, and **Eruslanov E.** Origin and Role of a Subset of Tumor-Associated Neutrophils with Antigen Presenting Cell Features in Early-Stage Human Lung Cancer. **Cancer Cell**, 2016, Jul 11;30(1):120-35. doi: 10.1016/j.ccell.2016.06.001
3. Moon E, Ranganathan R, **Eruslanov E**, Kim S, Newick K, O'Brien S, Lo A, Liu X, Zhao Y, and Albelda S. Blockade of Programmed Death 1 Augments the Ability of Human T cells Engineered to Target NY-ESO-1 to Control Tumor Growth after Adoptive Transfer. **Clinical Cancer Research**; 2016 Jan 15;22(2):436-47. doi: 10.1158/1078-0432.CCR-15-1070.
4. T Condamine, G. Dominguez, Je-In Youn, A. Kossenkov, S Mony, KAlicea-Torres, E Tcyganov, A Hashimoto, Y Nefedova, C Lin, S Partlova, A Garfall, D. Vogl, X Xu, S Knight, G Malietzis, G Han Lee, **E Eruslanov**, S Albelda, X Wang, J Mehta, M Bewtra, A Rustgi, N Hockstein, R Witt, G Masters, B Nam, D Smirnov, M Sepulveda and D Gabrilovich. Lectin-type oxidized LDL receptor-1 distinguishes population of human polymorphonuclear myeloid-derived suppressor cells in cancer patients. **Science Immunology**. 5 August 2016, DOI: 10.1126/sciimmunol.aaf8943
5. Svoronos N, Perales-Puchalt A, Allegrezza MJ, Rutkowski MR, Payne KK, Tesone AJ, Nguyen JM, Curiel TJ, Cadungog MG, Singhal S, **Eruslanov EB**, Zhang P, Tchou J, Zhang R, Conejo-Garcia JR. Tumor Cell-Independent Estrogen Signaling Drives Disease Progression through Mobilization of Myeloid-Derived Supressor Cells. **Cancer Discovery**. 2016 Sep 30. pii: CD-16-0502. PubMed PMID: 27694385, in press.

Books or other non-periodical, one-time publications.
Nothing to Report

Other publications, conference papers, and presentations.

Conference presentations:

1. **E. Eruslanov**. Tumor-Associated Neutrophils in Human Lung Cancer. Inflammation, Immunity and Cancer: The Society For Leukocyte Biology's 49th Annual Meeting and "Neutrophil 2016": Neutrophils and Other Leukocytes, University of Verona, Verona, Italy, September 15-17, 2016, Invited Speaker.*
2. **E. Eruslanov**, Origin and Role of a Subset of Tumor-Associated Neutrophils with Antigen Presenting Cell Features in Early-Stage Human Lung Cancer. Regulatory Myeloid Suppressor Cells Conference, Philadelphia, The Wistar Institute, June 16-19, 2016 Invited Speaker.*
3. **E. Eruslanov,** Origin and Role of a Subset of Tumor-Associated Neutrophils with Antigen Presenting Cell Features (Hybrid TANs) in Early-Stage Human Lung Cancer. Immunology School "Regulation of Lung Inflammation", Moscow, Russia, May11-13, 2016. Invited Speaker.*
4. **E. Eruslanov**, P Bhojnagarwala, J Quatromoni, S O'Brien, E Moon, T Stephen, A Rao, A Garfall, W Hancock, J Conejo-Garcia, C Deshpande, M Feldman, S Singhal and S Albelda. The origin and role of APC-like hybrid tumor-associated neutrophils in early-stage human lung cancer. AACR annual meeting: The function of tumor microenvironment in cancer. San Diego, Jan 7, 2016, poster presentation*

(*) presentation produced a manuscript.

Website(s) or other Internet site(s)

Penn Medicine News Site:

- *http://www.uphs.upenn.edu/news/News_Releases/2016/07/eruslanov/*

Technologies or techniques
Nothing to Report

Inventions, patent applications, and/or licenses
Nothing to Report

Other Products
Nothing to Report

PARTICIPANTS & OTHER COLLABORATING ORGANIZATIONS

What individuals have worked on the project?

Name:	Evgeniy Eruslanov
Project Role:	PI
Researcher Identifier Penn ID	14731836
Nearest person month worked:	5
Contribution to Project:	Dr. Eruslanov has performed some experiments, and is responsible for supervising the overall conduct of the project, planning and coordinating experiments, analyzing and interpreting data, and writing results and progress reports.
Funding Support:	DoD LC140199

Name:	Michael Annunziata
Project Role:	Research Specialist
Researcher Identifier Penn ID	54294537
Nearest person month worked:	6
Contribution to Project:	Michael obtained and prepared the tumor tissues for analysis. He has also performed flow cytometry, cell culturing and functional assays.
Funding Support:	DoD LC140199

Has there been a change in the active other support of the PD/PI(s) or senior/key personnel since the last reporting period?

"Nothing to Report."

What other organizations were involved as partners?

"Nothing to Report."

SPECIAL REPORTING REQUIREMENTS

COLLABORATIVE AWARDS:

"Nothing to Report."

QUAD CHARTS:

"Nothing to Report."

.

APPENDICES

Please cite this article in press as: Singhal et al., Origin and Role of a Subset of Tumor-Associated Neutrophils with Antigen-Presenting Cell Features in Early-Stage Human Lung Cancer, Cancer Cell (2016), http://dx.doi.org/10.1016/j.ccell.2016.06.001

Cancer Cell
Article

Origin and Role of a Subset of Tumor-Associated Neutrophils with Antigen-Presenting Cell Features in Early-Stage Human Lung Cancer

Sunil Singhal,[1,5] Pratik S. Bhojnagarwala,[1] Shaun O'Brien,[2] Edmund K. Moon,[2] Alfred L. Garfall,[3] Abhishek S. Rao,[1] Jon G. Quatromoni,[1] Tom Li Stephen,[6] Leslie Litzky,[4] Charuhas Deshpande,[4] Michael D. Feldman,[4] Wayne W. Hancock,[4,7] Jose R. Conejo-Garcia,[6] Steven M. Albelda,[2] and Evgeniy B. Eruslanov[1,*]
[1]Division of Thoracic Surgery, Department of Surgery
[2]Division of Pulmonary, Allergy, and Critical Care
[3]Division of Hematology/Oncology, Department of Medicine
[4]Department of Pathology and Laboratory Medicine
Perelman School of Medicine at the University of Pennsylvania, Philadelphia, PA 19104, USA
[5]Division of Thoracic Surgery, Department of Surgery, Philadelphia VA Medical Center, Philadelphia, PA 19104, USA
[6]Tumor Microenvironment and Metastasis Program, The Wistar Institute, Philadelphia, PA 19104, USA
[7]Department of Pathology and Laboratory Medicine, Children's Hospital of Philadelphia, Philadelphia, PA 19104, USA
*Correspondence: evgeniy.eruslanov@uphs.upenn.edu
http://dx.doi.org/10.1016/j.ccell.2016.06.001

SUMMARY

Based on studies in mouse tumor models, granulocytes appear to play a tumor-promoting role. However, there are limited data about the phenotype and function of tumor-associated neutrophils (TANs) in humans. Here, we identify a subset of TANs that exhibited characteristics of both neutrophils and antigen-presenting cells (APCs) in early-stage human lung cancer. These APC-like "hybrid neutrophils," which originate from $CD11b^{+}CD15^{hi}CD10^{-}CD16^{low}$ immature progenitors, are able to cross-present antigens, as well as trigger and augment anti-tumor T cell responses. Interferon-γ and granulocyte-macrophage colony-stimulating factor are requisite factors in the tumor that, working through the Ikaros transcription factor, synergistically exert their APC-promoting effects on the progenitors. Overall, these data demonstrate the existence of a specialized TAN subset with anti-tumor capabilities in human cancer.

INTRODUCTION

Tumor-associated inflammation contributes to cancer development and progression and is often associated with a high degree of inflammatory cell infiltration (Grivennikov et al., 2010). Tumor-associated neutrophils (TANs) represent a significant portion of tumor-infiltrating cells and accumulate in many types of cancers, including lung cancer (Carus et al., 2013; Ilie et al., 2012). Although the role of TANs in tumor development is beginning to be investigated in murine models, it remains largely unexplored in humans.

In murine studies, it appears that TANs can exert both pro-tumor and anti-tumor effects (Brandau, 2013; Fridlender et al., 2009). Numerous studies have shown that neutrophils can promote tumor progression by degrading matrix, immunosculpting, stimulating tumor cell proliferation, increasing metastasis, and enhancing angiogenesis (Houghton, 2010; Piccard et al., 2012). However, they can also exert anti-tumor functions such as inducing tumor cell death via their powerful antimicrobial killing machinery (Dallegri and Ottonello, 1992; van Egmond and Bakema, 2013) and by producing factors to recruit and activate cells of the innate and adaptive immune system (Mantovani et al., 2011). Given these varying effects of mouse TANs on tumor growth, the paradigm of anti-tumor "N1 neutrophils" versus pro-tumor "N2 neutrophils" was proposed (Fridlender et al.,

Significance

Tumor-associated neutrophils (TANs) represent a significant fraction of the inflammatory cells in the tumor microenvironment; however, the contribution of these cells in inhibiting or promoting tumor expansion in humans remains unclear. Although the concept of neutrophil phenotypic and functional diversity has emerged in murine tumor models, it is unknown whether TAN subsets with different functions exist in humans. Here, we provide evidence that early-stage lung tumors can induce the formation of a unique subset of TANs that can trigger and support anti-tumor T cell responses. These findings demonstrate the potential anti-tumor role of TANs in early-stage cancer and may provide opportunities to boost the anti-tumor efficacy of cytotoxic T lymphocytes.

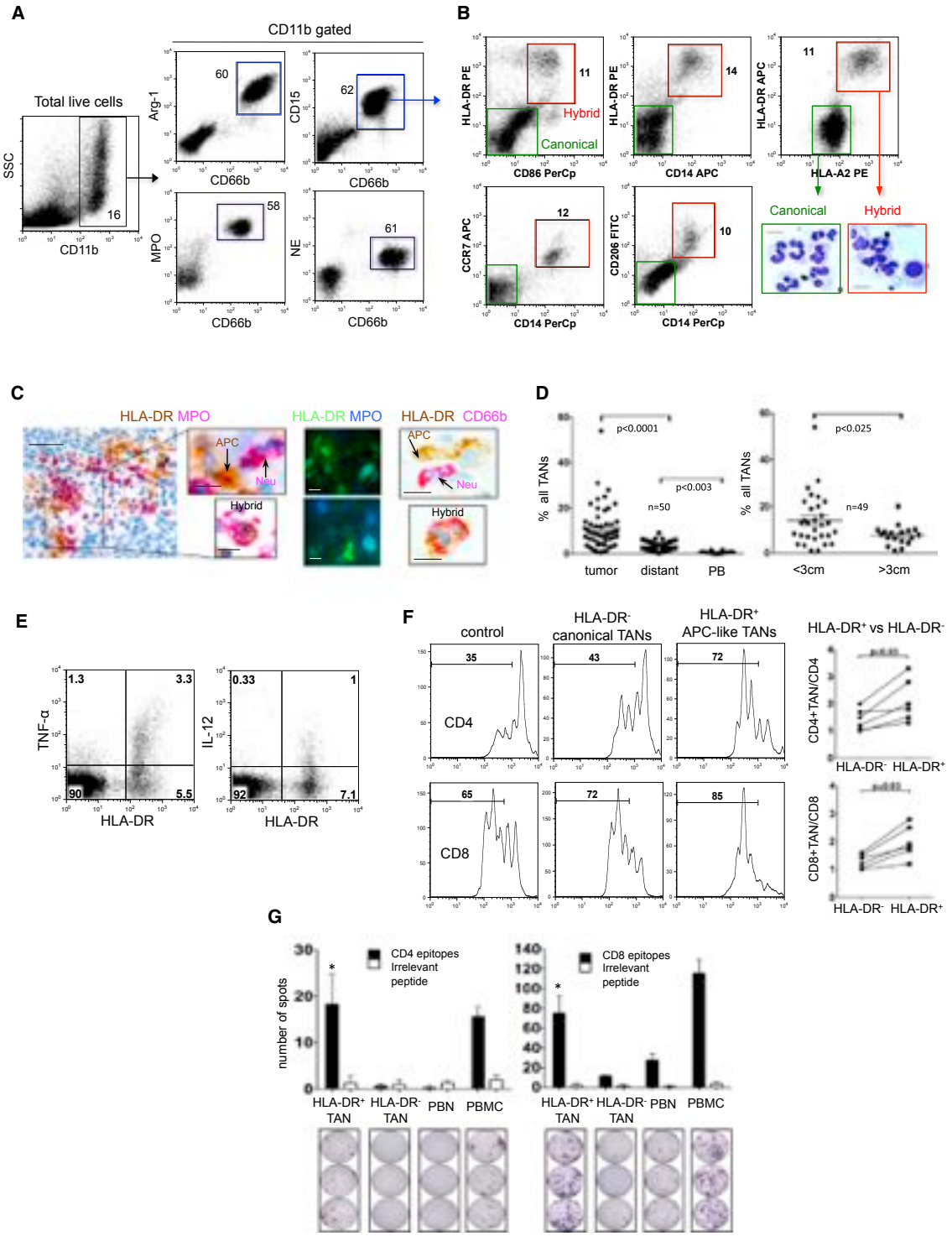

Figure 1. A Subset of TANs with Hybrid Characteristics of Neutrophils and APCs

(A) A single-cell suspension was obtained from fresh tumor and the expression of the indicated granulocytic markers was analyzed by flow cytometry on gated live CD11b cells. Total TANs are shown in blue boxes.

(legend continued on next page)

2009). However, most of these data were derived from mouse models that use tumor cell lines adapted to grow rapidly in vivo and have thus already undergone cancer immunoediting (Schreiber et al., 2011). These models are also characterized by high tumor burden, minimal matrix, and rapid tumor growth. Because these features are dissimilar to human cancers that evolve slowly over time, the role of tumor-infiltrating myeloid cells in human cancers may not be the same and the function of human TANs, particularly in the early stages of tumor development, remains largely unexplored.

Understanding the role of TANs in the regulation of the T cell response in cancer patients is important because the cytotoxic T lymphocytes are the major effector cells mediating antigen-driven anti-tumor immunity. We recently demonstrated that early-stage lung cancers are highly infiltrated with activated neutrophils and that these TANs exhibit heterogeneous expression of T cell co-stimulatory molecules (Eruslanov et al., 2014). In contrast to the data from murine studies, TANs isolated from vast majority of small early-stage tumors were not immunosuppressive, but in fact stimulated T cell responses (Eruslanov et al., 2014). Interestingly, the T cell activation property of TANs became less prominent with disease progression, consistent with the emerging concept of an immunogenic "switch" from anti-tumor to pro-tumor phenotype (Granot and Fridlender, 2015).

As part of our phenotypic analysis of early-stage lung cancer TANs (Eruslanov et al., 2014), we identified a subset of cells exhibiting the hybrid phenotype of both neutrophils and antigen-presenting cells (APCs). We hypothesized that early-stage tumors, where the immunosuppressive environment might not be fully developed, can drive recruited granulocytes to further differentiate into a specialized cell subset with strong T cell stimulatory activity. The purpose of this study was to characterize the phenotype, function, and origin of these hybrid cells in lung cancer patients.

RESULTS

Early-Stage Human Lung Cancers Accumulate a Neutrophil Subset with a Composite Phenotype of Granulocytes and APCs

Since TANs in patients with early-stage lung cancer have the ability to heterogeneously express some T cell co-stimulatory molecules (Eruslanov et al., 2014), we postulated that there might be a subset of TANs with characteristics of APCs. We thus analyzed the expression of APC surface markers on neutrophils from three locations: lung cancer tissue, adjacent (within the same lobe) lung parenchyma (termed "distant tissue"), and peripheral blood (Figure S1A). We performed phenotypic analysis of 50 random patients with stage I–II non-small cell lung cancer (NSCLC). Detailed characteristics of all patients involved in this study are shown in Table S1. Fresh tissue was digested using defined conditions that minimize enzyme-induced ex vivo effects on the viability, premature activation, phenotype, and function of neutrophils (Quatromoni et al., 2015). Previously, we performed extensive phenotypic analysis of neutrophils in NSCLC and characterized TANs as $CD11b^{+}CD15^{hi}CD66b^{+}MPO^{+}Arg1^{+}CD16^{int}IL\text{-}5R\alpha^{-}$ cells (Eruslanov et al., 2014). Importantly, all $CD66b^{+}CD11b^{+}$ cells also expressed the other neutrophil/myeloid cell markers CD15, MPO (myeloperoxidase), Arg-1 (arginase-1), and NE (neutrophil elastase) at very high levels (Figure 1A, blue boxes) and thus could be segregated from other $CD15^{lo}MPO^{lo}NE^{lo}Arg\text{-}1^{-}$ non-granulocytic $CD11b^{+}$ myeloid cells. Since there was a high concordance among the selected neutrophil markers, for our studies we defined TANs as $CD15^{hi}CD66b^{+}CD11b^{+}$ cells. Our analysis revealed that the majority of neutrophils from lung tumors, which we term "canonical TANs," expressed only these classic neutrophil markers (Figures 1A and S1A). However, we also identified TANs with surface expression of additional markers normally expressed on APCs, specifically human leukocyte antigen (HLA)-DR, CD14, CD206, CD86, and CCR7 (Figures S1B–S1F). These receptors were completely absent in peripheral blood neutrophils (PBNs). The "distant tissue" neutrophils also expressed these APC markers, albeit at much lower levels in comparison with TANs.

Further analysis revealed that the APC markers ($CD14^{+}HLA\text{-}DR^{+}HLA\text{-}ABC^{hi}CCR7^{+}CD86^{+}CD206^{+}$) were co-expressed on a unique subset of $CD11b^{+}CD66b^{+}CD15^{hi}$ TANs (Figure 1B), exhibiting a composite phenotype of canonical neutrophils and APCs. We termed this subset "APC-like hybrid TANs." This population of hybrid TANs expressed some markers of the APC phenotype (e.g., CD14, HLA-DR, CCR7, CD86, and CD206) but lacked other defining markers of "professional APC" such as CD209, CD204, CD83, CD163, CD1c, and CCR6 (data not shown). Of note, the expression of CD206, CCR7, and CD86 varied, whereas there was a consistent co-expression of HLA-DR and CD14 on hybrid TANs. Cytospins prepared from flow-sorted $HLA\text{-}DR^{-}$ canonical and $HLA\text{-}DR^{+}$ hybrid TANs revealed that some of the hybrid TANs had round and oval nuclear shapes in comparison with the classic nuclear segmentation of canonical TANs (Figure 1B). Histological review of lung tumors also revealed "double-positive" $MPO^{+}HLA\text{-}DR^{+}$ and $CD66b^{+}HLA\text{-}DR^{+}$ TANs that were scattered throughout lung tumors

(B) Flow cytometric analysis of the expression of APC markers on gated $CD11b^{+}CD15^{hi}CD66b^{+}$ TANs. The representative cytomorphology of canonical (green boxes) and APC-like hybrid TANs (red boxes) in NSCLC. Scale bar, 10 μm.

(C) The presence of APC-like hybrid TANs in tumor detected by immunohistochemistry and immunofluorescence double staining. Scale bar, 50 μm (left image) and 10 μm (other images).

(D) The frequency of APC-like hybrid neutrophils in tumors, distant lung tissue, and peripheral blood (PB) (right graph) and in tumors of different sizes (left graph) (line represents mean ± SEM, n = 50, one-way ANOVA test and unpaired t test). APC-like hybrid TANs were defined as live $HLA\text{-}DR^{+}CD11b^{+}CD15^{hi}CD66b^{+}$ cells.

(E) Intracellular TNF-α and IL-12 production by $HLA\text{-}DR^{+}$ hybrid or $HLA\text{-}DR^{-}$ canonical TANs after stimulation with LPS. TANs were gated on $CD11b^{+}CD15^{hi}CD66b^{+}$ cells. Representative results from one of five experiments are shown.

(F) The proliferation of autologous CFSE-labeled PBMC stimulated with plate-bound anti-CD3 Abs in the presence of hybrid $HLA\text{-}DR^{+}$ or canonical $HLA\text{-}DR^{-}$ TANs. T cell stimulatory activity was defined as the ratio $CFSE^{lo}$ (T cells + TANs)/$CFSE^{lo}$ (T cells) (n = 6, Wilcoxon matched-pairs rank test).

(G) Autologous virus-specific memory T cell responses in the presence of APC-like hybrid $HLA\text{-}DR^{+}$ or canonical $HLA\text{-}DR^{-}$ TANs. IFN-γ-ELISPOT assay (mean ± SEM, n = 3, $^{*}p \leq 0.01$ canonical versus hybrid, Mann-Whitney test).

See also Figure S1.

(Figure 1C). Additionally, we detected a small, but clearly distinguishable population of HLA-DR$^+$CD15^{hi}CD66b$^+$CD11b$^+$ cells in the draining lymph nodes of several lung cancer patients (Figure S1G).

The frequency of this identified subset of TANs varied from 0.5% to 25% among all TANs (Figure 1D) and from 0.1% to 4.3% among all cells in tumor digests (Figure S1H). The hybrid population was significantly higher in patients with adenocarcinoma compared with patients with squamous cell carcinoma (Figure S1I). There were no significant associations between the frequency of APC-like TANs and tumor stage or smoking history (Figures S1J and S1K). Interestingly, we found a significantly smaller percentage of HLA-DR$^+$ hybrid neutrophils among TANs in large tumors (diameter >3 cm) versus the small tumors (diameter <3 cm) (Figures 1D and S1L). Thus, the hybrid population appears to decline as tumors enlarge, and is completely absent in tumors greater than 5–7 cm in diameter. Together, these data demonstrate that neutrophils in some early-stage lung tumors undergo unique phenotypic changes, yielding a subset of TANs with composite characteristics of neutrophils and APC.

APC-like Hybrid TANs Stimulate and Support T Cell Responses

Previously, we showed that TANs isolated from small, early-stage lung tumors were able to stimulate antigen non-specific T cell responses (Eruslanov et al., 2014). Having identified these APC-like TANs, we hypothesized that this subset may be primarily responsible for stimulating T cell responses in these early-stage lung tumors.

We first evaluated the functional activity of APC-like TANs to ensure that these activated cells were not "exhausted" or hypofunctional. TANs were thus isolated from tumors and stimulated with lipopolysaccharide (LPS). After LPS stimulation, HLA-DR$^+$ hybrid TANs produced much more tumor necrosis factor α (TNF-α) and interleukin-12 (IL-12) when compared with HLA-DR$^-$ canonical TANs (Figure 1E). Furthermore, HLA-DR$^+$ hybrid TANs phagocytosed *Escherichia coli* bioparticles more efficiently than HLA-DR$^-$ canonical TANs (Figure S1M). These data demonstrate that APC-like hybrid TANs are fully functional and, in fact, perform major functions such as cytokine production and phagocytosis superior to canonical TANs.

To determine the effect of APC-like hybrid TANs on T cell responses, we isolated TAN subsets by flow cytometry cell sorting (Figures S1N and S1O). Each sorted TAN subset was co-cultured with autologous carboxyfluorescein succinimidyl ester (CFSE)-labeled peripheral blood mononuclear cells (PBMCs) that had been stimulated with plate-bound anti-CD3 antibodies (Abs) (Figure 1F). We observed that the proliferation of CD4 and CD8 cells after 4 days of stimulation was markedly augmented after exposure to HLA-DR$^+$ hybrid TANs versus the HLA-DR$^-$ canonical TANs (Figure 1F).

We next determined whether APC-like hybrid TANs could trigger and sustain antigen-specific T cell responses. Therefore, we co-cultured autologous T cells with TAN subsets that had been pulsed with mixtures of overlapping peptides from commercially available peptide pools. Each peptide pool corresponded to defined HLA class I or II restricted T cell epitopes from cytomegalovirus, Epstein-Barr virus, influenza virus, or *Clostridium tetani* designed to stimulate T cells with a broad array of HLA types. As shown in Figure 1G, the HLA-DR$^+$ hybrid TANs efficiently triggered memory CD8 and CD4 T cell responses to HLA class I and II restricted T cell epitopes, respectively. Canonical TANs and PBNs induced only weak CD8 T cell responses and did not trigger CD4 T cell responses. Together, these data demonstrate that HLA-DR$^+$ hybrid TANs are able to function as efficient APCs.

Long-Lived Immature Neutrophils Recapitulate the Phenotype of APC-like Hybrid TANs in the Presence of Tumor-Derived Factors

Given the potential anti-tumor activity of APC-like TANs due to their strong stimulatory effect on T cell responses, we investigated the mechanisms by which these cells could originate and expand in the human tumor microenvironment.

We collected tumor-conditioned media (TCM) from digested lung cancers that contained $\geq$15% of hybrid TANs among all TANs (termed hybrid-inducing TCM). We exposed purified PBNs to hybrid-inducing TCM and found that PBNs did not differentiate into the HLA-DR$^+$CD14$^+$ neutrophils (data not shown) and died within 3 days (Figure 2A). To determine whether more immature neutrophils with a higher degree of plasticity differentiate into APC-like hybrid neutrophils, we obtained a highly enriched population of immature human bone marrow neutrophils (BMNs). Isolated BMNs expressed the myeloid/granulocytic specific markers CD11b, CD66b, CD15, Arg-1, NE, and MPO and were mostly "band"-like immature neutrophils in appearance (Figures 2B and S2A). Of note, the purified BMNs did not express HLA-DR and CD14 and were not contaminated with macrophages and monocytes (Figure S2A). Unlike blood neutrophils, about 40% of these BMNs could survive in cell culture for up to 1 week and their viability was dramatically increased in the presence of TCM (Figures 2A, 2C, and S2B). Thus, BMNs with a prolonged lifespan in vitro provided us with large quantities of cells that could be used to model the origins and differentiation process of neutrophils in the tumor microenvironment.

After 7 days of incubation of BMNs with hybrid-inducing TCMs, we observed the formation of a cell subset that retained all its granulocytic markers (Figures 2B and 2D) and acquired the same phenotype as the tumor-derived hybrid TANs (HLA-DR$^+$CD14$^+$CD86$^+$CD206$^+$CCR7$^+$) (Figure 2E). Similar to hybrid TANs, most of the BMNs also changed their nuclear shape from band-like to oval when they converted into hybrid BMNs (Figure 2B). A detailed phenotypic comparison of PBNs, BMNs, and bone marrow (BM)- and tumor-derived hybrid neutrophils is summarized in Figure 2D. The differentiation of BMNs into HLA-DR$^+$CD14$^+$ APC-like hybrid BMNs after exposure to hybrid-inducing TCM was donor dependent and varied from 20% to 80% of the initial BMN population (Figure S2C). BMNs began to upregulate CD14 within 24 hr of co-culturing with hybrid-inducing TCM, while the expression of HLA-DR, CD86, CCR7, and CD206 markers did not appear until day 4 (Figure S2D). This suggests that these late APC markers are synthesized de novo.

Similar to hybrid TANs, differentiated hybrid BMNs acquired only the partial phenotype of dendritic cells (DC) and macrophages (Mph) (HLA-DR$^+$CD14$^+$CD86$^+$CD206$^+$) (Figures 2E–2G). The hybrid subset of BMNs and TANs differed from BM-derived DC and Mph by absence of CD1c, CD83, CD163, and CD209

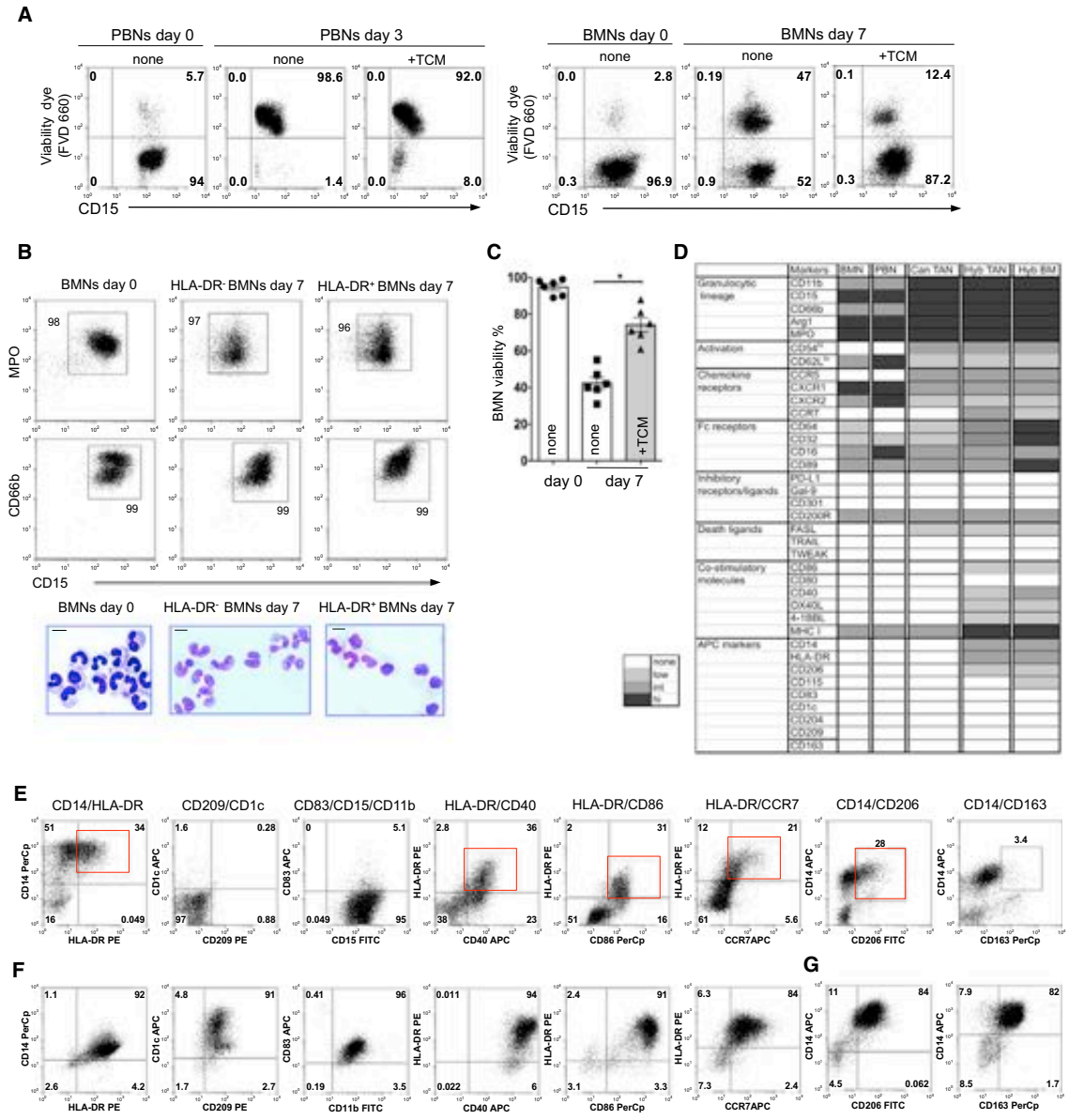

Figure 2. Tumor-Derived Factors Differentiate Long-Lived Immature BMNs into a Hybrid Subset with a Partial Phenotype of Dendritic Cells and Macrophages

(A) Fixable viability dye eFluor 660 (FVD 660) was used to discriminate viable neutrophils in cell culture. Representative dot plots from one of six experiments are shown.

(B) Flow cytometric analysis of the expression of MPO, CD66b, and CD15 markers on freshly isolated BMNs (day 0) and BMNs cultured with (HLA-DR$^+$ BMNs) or without hybrid-inducing TCM (HLA-DR$^-$ BMNs) for 7 days. Cytospins show the cytomorphology of these BMNs. Scale bar, 10 μm.

(C) Survival of BMNs in the cell culture in the presence or absence of TCM. Viability dye FVD 660 was used to discriminate viable BMNs in cell culture (mean ± SEM, n = 6, *p ≤ 0.01, Wilcoxon matched-pairs rank test).

(D) Heatmap comparing the phenotypes of BMNs, PBNs, canonical TANs (Can TAN), hybrid TANs (Hyb TAN), and BM-derived hybrid neutrophils (Hyb BM).

(E–G) Flow cytometric analysis of the expression of indicated APC markers on BM-derived hybrid neutrophils (E) (red boxes), dendritic cells (F), and macrophages (G). Expression of APC markers was analyzed by flow cytometry on gated CD11b$^+$CD15^{hi}CD66b$^+$ BMNs.

See also Figure S2.

markers, and low expression of CD40, CD86, CD115, and CCR7 (Figures 2D–2G). The level of the transcription factor IRF8, which regulates monocyte/DC lineage commitment (Yanez et al., 2015), was not dramatically changed in hybrid BMNs and was much lower than the amount detected in BM-derived Mph and DC (Figure S2E).

We next asked whether the differentiated APC-like hybrid BMNs could proliferate in the presence of hybrid-inducing TCM and thus represent a self-maintained population of neutrophils. A bromodeoxyuridine (BrdU) incorporation assay revealed that within 24 hr of treatment with hybrid-inducing TCM, 10%–15% of BMNs begin to synthesize DNA in vitro (Figure S2F). As the differentiation process progressed, a small proportion of HLA-DR$^-$ BMNs continued to incorporate BrdU up to day 8, whereas the differentiated HLA-DR$^+$ neutrophils lost proliferative potential (Figure S2F).

Given that the frequency of hybrid TANs was reduced in large tumors (Figure 1D), we hypothesized that hypoxia, which is strongly associated with the tumor progression, may negatively regulate the formation of hybrid neutrophils. Thus, BMNs were cultured in the presence of hybrid-inducing TCM for 6 days under normoxic (5% CO_2 and 21% O_2) and hypoxic (5% CO_2 and 5% O_2) cell culture conditions. We also cultured BMNs in the presence of hybrid-inducing TCM and cobalt chloride, an agent that induces hypoxia-inducible factor 1α (HIF-1α), the main transcriptional factor activated in hypoxic conditions (Dai et al., 2012). We found that the development of hybrid CD14$^+$HLA-DR$^+$ neutrophils was profoundly inhibited under these hypoxic and hypoxia-simulating conditions (Figure 3A).

IFN-γ and GM-CSF Are Requisite Factors in the Tumor Microenvironment for the Development of Hybrid Neutrophils

To determine the particular tumor-specific factors that promote the formation of hybrid TANs, we screened primary TCMs collected from 20 consecutive lung cancer patients, and categorized the TCMs based on their ability to induce: (1) the full phenotype of hybrid cells (CD14$^+$HLA-DR$^+$CD11b$^+$CD66b$^+$CD15^{hi}) (Figure 3B, example TCM #41); (2) the partial phenotype of hybrid cells (CD14$^+$HLA-DR$^-$CD11b$^+$CD66b$^+$CD15^{hi}) (Figure 3B, example TCM #63); or (3) no phenotypic changes (Figure 3B, example TCM #58). We evaluated each TCM using a multiplex cytokine/chemokine bead assay and found that those TCMs that induced CD14$^+$HLA-DR$^+$ hybrid cells had increased amounts of granulocyte-colony stimulating factor (G-CSF), IL-6, IL-15, granulocyte-macrophage colony-stimulating factor (GM-CSF), interferon-γ (IFN-γ), macrophage inflammatory protein-1α (MIP-1α), TNF-α, monocyte chemoattractant protein-1 (MCP-1), and monokine induced by IFN-γ (MIG) compared with TCMs that did not induce hybrid cells. When we tested the ability of each of these factors (at the low concentrations found in the TCMs) to induce the CD14$^+$HLA-DR$^+$ hybrid phenotype in BMNs, we found that only IFN-γ and GM-CSF were able to induce the phenotype, although in a relatively low percentage of cells (Figures 3B and S3A). However, we observed that these factors worked in a synergistic manner: when combined at very low concentrations of 50 pg/ml of each factor, they induced expression of APC markers in a large proportion (>40%) of the cells in a donor-dependent fashion (Figures 3B and S3A). The addition of neutralizing monoclonal antibodies for either IFN-γ or GM-CSF completely inhibited the formation of BM hybrid cells in the presence of hybrid-inducing TCM (Figure 3C), thereby confirming that both IFN-γ and GM-CSF play a key role in the induction process. Interestingly, incubation of BMNs with a low dose of GM-CSF (50 pg/ml) and increasing concentrations of IFN-γ (from 50 pg/ml to 20 ng/ml) resulted in the expansion of CD14$^+$HLA-DR$^+$ BMNs from 40% to 96% among all BMNs (Figure 3D, upper panel). However, the treatment of BMNs with IFN-γ at a concentration of more than 1 ng/ml gradually induced the expression of PD-L1 on the HLA-DR$^+$ BMNs (Figure 3D, lower panel), resulting in the formation of hybrid neutrophils with T cell suppressive activity (described in detail below).

We next analyzed the frequency of APC-like TANs in the tumor digests, and, in parallel, measured the concentration of IFN-γ and GM-CSF in the supernatants collected from digested autologous tumor cell cultures. Figures 3E and 3F demonstrate that the levels of IFN-γ and GM-CSF were statistically higher in tumors where there was a high proportion of hybrid TANs (>10% of all TANs). However, the generation of hybrid neutrophils in vivo is most likely more complex and not solely due to IFN-γ and GM-CSF levels, because the absolute levels of IFN-γ and GM-CSF in the TCM did not necessarily correlate with the frequency of hybrid neutrophils (>10% of all TANs) in each tumor as shown in Figures 3E and 3F. Also, when we exposed BMNs from the same donor to different hybrid-inducing TCMs containing variable concentrations of IFN-γ and GM-CSF, we were also unable to observe a clear relationship between absolute levels of GM-CSF and IFN-γ and the degree of hybrid neutrophil formation (Figure S3B). These data suggest that there is a requisite threshold level of GM-CSF and IFN-γ, and additional tumor-derived factors may contribute to the process of hybrid neutrophil differentiation.

CD11b$^+$CD15^{hi}CD10$^-$CD16$^{int/low}$ Progenitors Give Rise to APC-like Hybrid Neutrophils

The low frequency of APC-like hybrid TANs along with high heterogeneity in their accumulation in cancer patients suggested that there might be precursor cells that could differentiate into this unique subset of neutrophils under specific favorable conditions in some tumors. Therefore, we sought to determine whether the ability of long-lived immature BMNs to develop hybrid neutrophils is either shared by all immature subsets or limited to a specific differentiation stage.

To address this question, we used the combined expression of the CD11b, CD15, CD10, CD49d, and CD16 to distinguish the different maturational states of BMNs (Elghetany, 2002). As expected, we found that CD11b$^+$CD15^{hi} BMNs consist of a heterogeneous combination of mature CD16^{hi}CD10$^+$CD49d$^-$ cells, immature CD16^{int}CD10$^-$CD49d$^-$ band cells, and CD16$^{low/-}$CD10$^-$CD49d$^+$ metamyelocytes/myelocytes (Figure 4A; expression of CD49d is not shown). Of note, all mature and immature BMNs express CD66b but at slightly different levels (Figure S4A). The detailed phenotype of neutrophils at different maturation stages is summarized in Figure S4B. We isolated BMNs at different stages of maturation by flow cytometry sorting based on these phenotypes. Cytomorphology confirmed that each population was associated with distinct maturation stages (Figure 4B). These sorted subsets of BMNs were cultured in the presence of low concentration of IFN-γ (50 pg/ml) and GM-CSF (50 pg/ml) for 6 days, after which the resulting CD11b$^+$CD15^{hi}CD66b$^+$ neutrophil populations were analyzed for surface expression of CD14 and HLA-DR (Figure 4C). Our data revealed that CD14$^+$HLA-DR$^+$ hybrid neutrophils could be generated from all immature stages of neutrophils except the terminally differentiated, mature, segmented neutrophils. However, the

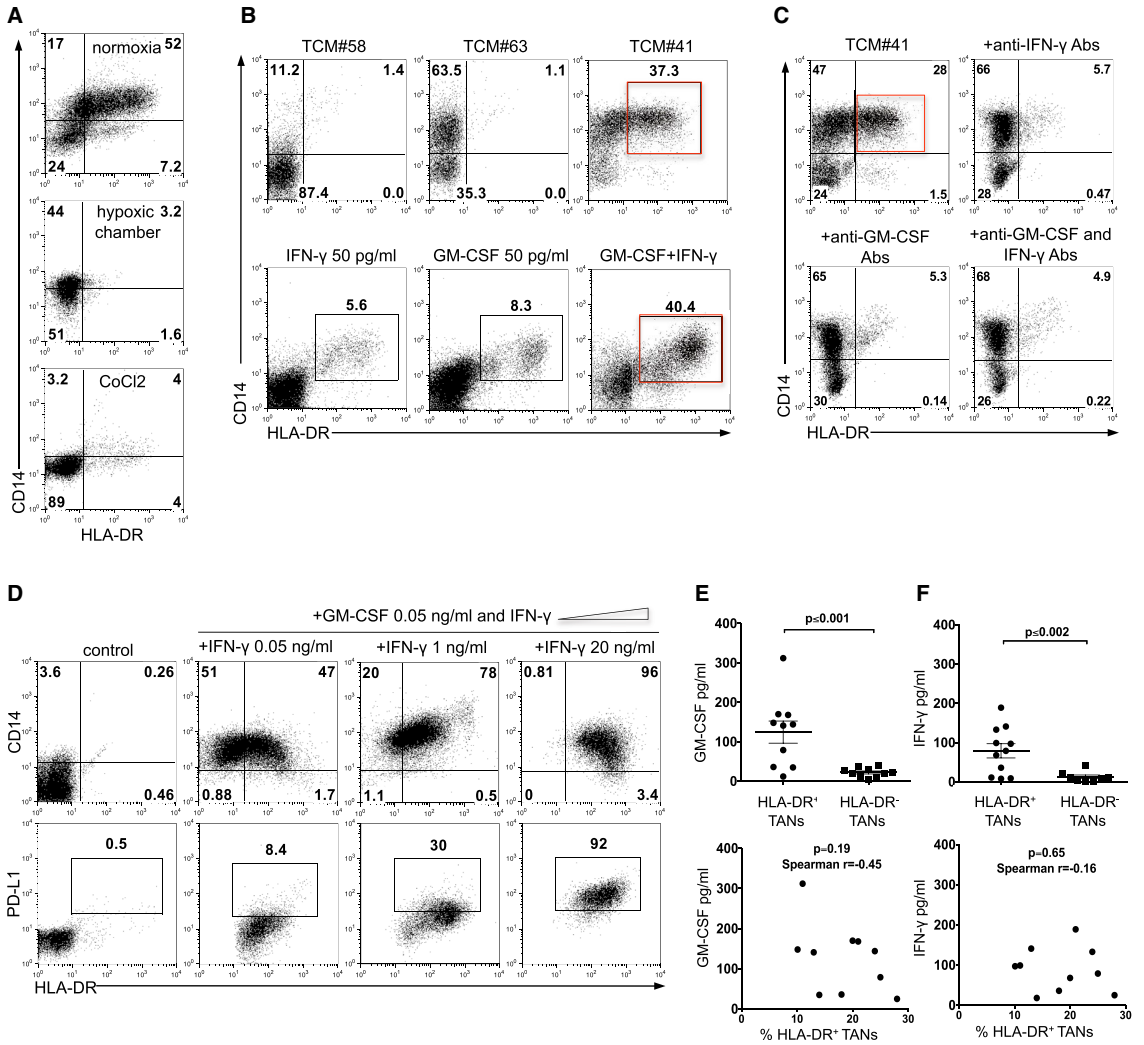

Figure 3. Tumor-Derived IFN-γ and GM-SCF Synergistically Differentiate Immature Neutrophils into a Subset of APC-like Hybrid Neutrophils

(A) Flow cytometric analysis of CD14 and HLA-DR expression on gated live CD11b$^+$CD15^{hi}CD66b$^+$ BMNs cultured in the presence of hybrid-inducing TCM under normoxic and hypoxic cell culture conditions.

(B) Flow cytometric analysis of CD14 and HLA-DR expression on gated live CD11b$^+$CD15^{hi}CD66b$^+$ BMNs cultured in the presence of different TCMs (upper panel) or with IFN-γ and/or GM-CSF (lower panel).

(C) The effect of IFN-γ and GM-CSF blocking Abs (5 μg/ml) in blunting the formation of HLA-DR$^+$CD14$^+$ hybrid neutrophils in vitro (red box).

(D) The expression of CD14 and HLA-DR markers on live CD11b$^+$CD15^{hi}CD66b$^+$ BMNs (upper panel) and PD-L1 on gated HLA-DR$^+$CD14$^+$ hybrid neutrophils (lower panel) differentiated with GM-CSF (50 pg/ml) and increasing doses of IFN-γ in vitro.

(E and F) Levels of IFN-γ (E) and GM-CSF (F) in supernatants collected from the cell culture of small-sized tumor digests where APC-like hybrid TANs were or were not previously detected (set-off was >10% among all TANs) (line represents mean ± SEM, n = 10, Mann-Whitney test for unpaired data). Lower panels represent the correlation between the absolute levels of IFN-γ and GM-CSF in the TCM, with the frequency of hybrid neutrophils in each tumor shown in the upper graphs. Non-parametric Spearman test was used to determine the degree of correlation.

Representative dot plots from one of five experiments are shown in (A–D). See also Figure S3.

level of HLA-DR expression on these hybrid neutrophils was affected by the degree of immaturity of the neutrophils prior to exposure to IFN-γ and GM-CSF: the more mature CD15^{hi}CD10$^-$CD16^{int} band cells gave rise to hybrid neutrophils, with the highest expression of HLA-DR on the surface when compared with hybrid neutrophils differentiated from CD15^{hi}CD10$^-$CD16$^{-/lo}$ myelocytes and metamyelocytes/early bands (Figure 4C). Interestingly, the majority of the neutrophils differentiated from CD15^{hi}CD10$^-$CD16^{int} band cells were able to change their nuclear contour from band-like to oval when compared with neutrophils differentiated from CD15^{hi}CD10$^-$CD16$^{-/lo}$ myelocytes and metamyelocytes/early bands (Figure 4D).

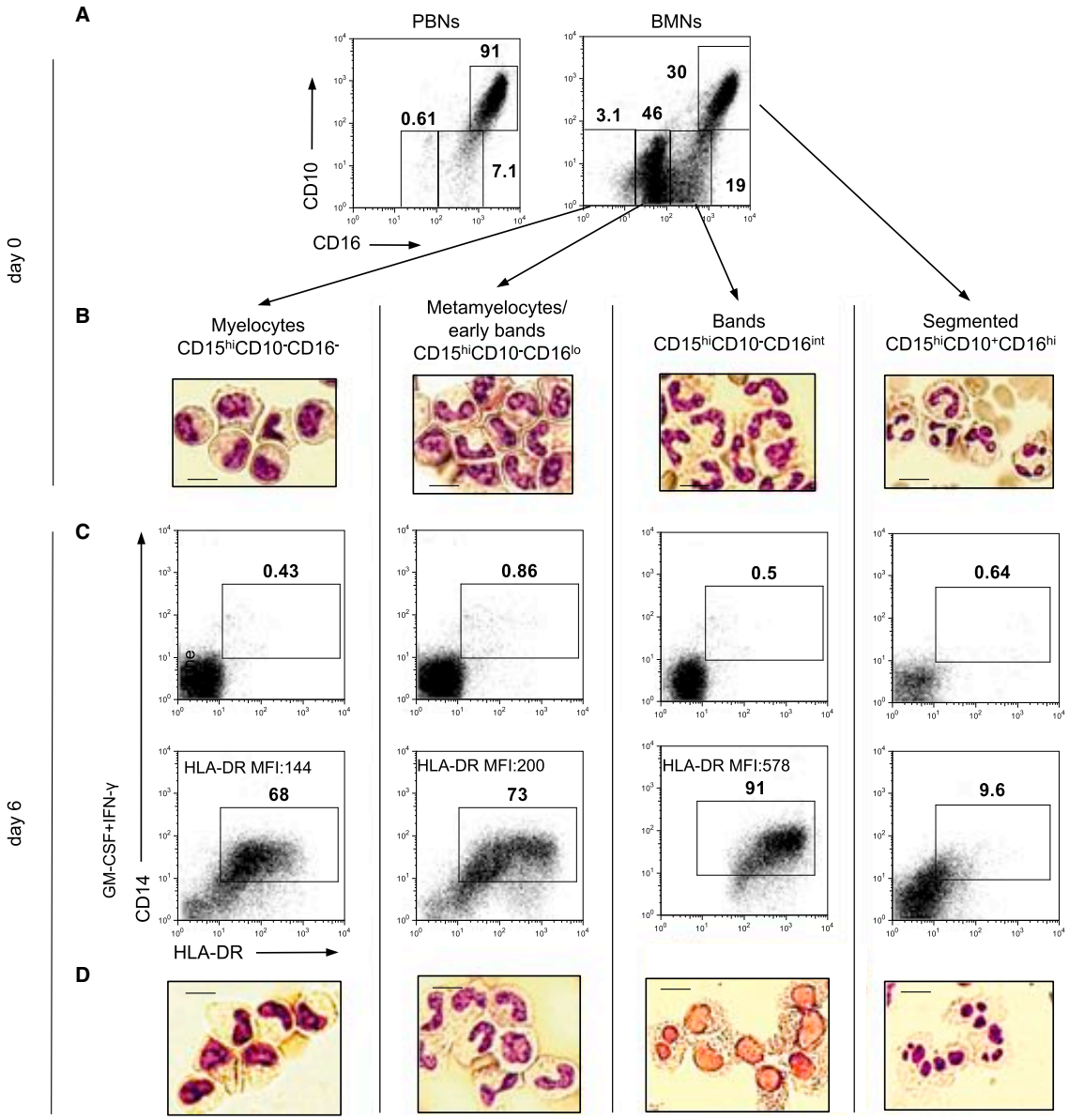

Figure 4. APC-like Hybrid Neutrophils Originate from CD11b$^+$CD15^{hi}CD66b$^+$CD10$^-$CD16$^{lo/int}$ Progenitors

(A) Flow cytometric analysis of the expression of CD10 and CD16 on gated live CD11b$^+$CD15^{hi}CD66b$^+$ neutrophils isolated from peripheral blood (PBNs) and bone marrow (BMNs) of cancer patients.

(B) Cytospins were made from sorted BMNs at different stages of maturation and stained with the Hema3 Stat Pack Kit (Wright-Giemsa-like stain).

(C) Sorted BMNs at different stages of maturation were differentiated in the presence of IFN-γ (50 pg/ml) and GM-CSF (50 pg/ml) in vitro. Expression of HLA-DR and CD14 markers was analyzed by flow cytometry on CD11b$^+$CD15^{hi}CD66b$^+$ BMNs.

(D) Cytomorphology of APC-like HLA-DR$^+$ hybrid neutrophils differentiated from the sorted populations of BMNs at different stages of maturation.

Representative results from one of four experiments are shown in (A–D). Scale bar, 10 μm. See also Figure S4.

Importantly, the circulating blood CD16$^{int/lo}$CD10$^-$ immature neutrophils that could potentially traffic into tumors were also able to differentiate into hybrid neutrophils in the presence of hybrid-inducing TCM or IFN-γ and GM-CSF (Figure S4C).

Ikaros Negatively Regulates the Development of APC-like Hybrid Neutrophils

Murine models have shown that the transcription factor Ikaros is involved in the control of neutrophil differentiation by silencing specific pathways in common precursors that allow

for macrophage-monocyte development (Dumortier et al., 2003; Papathanasiou et al., 2003). Given that hybrid neutrophils exhibit some characteristics of monocytic lineage cells, but can be differentiated from granulocyte-committed precursors, we hypothesized that the hybrid-inducing ability of TCM may be due to two possible synergistic effects on granulocyte progenitor cells: (1) premature downregulation of Ikaros, thus allowing some degree of monocyte differentiation to occur; and (2) the provision of the appropriate macrophage stimulating factors (i.e., GM-CSF) to activate the monocyte differentiation pathways.

We measured the level of Ikaros expression in BMNs at different stages of maturation and found that Ikaros was upregulated in all immature neutrophils (bands and metamyelocytes), with lower levels in mature BMNs and PBNs (Figure 5A). The analysis of BMNs treated with hybrid-inducing TCM revealed that the Ikaros level was lower in HLA-DR$^+$ hybrid BMNs compared with HLA-DR$^-$ canonical BMNs (Figure 5B). Thus hybrid-inducing TCM induced premature downregulation of Ikaros in HLA-DR$^+$ hybrid BMNs. We next cultured BMNs with hybrid-inducing TCM in the presence or absence of the drug lenalidomide, which causes proteasomal degradation of the human Ikaros proteins (Kronke et al., 2014). The addition of lenalidomide to TCM-treated BM neutrophils dramatically facilitated the development of HLA-DR$^+$CD14$^+$ hybrid neutrophils (Figure 5C). Together, these data suggest that Ikaros negatively regulates this process in the presence of tumor-derived factors.

We then measured the level of Ikaros in BMN progenitors incubated with or without low-dose IFN-γ and/or GM-CSF at days 1, 3, and 5. Downregulation of Ikaros was only observed when both IFN-γ and GM-CSF were present for at least 5 days, confirming their synergistic effect in this process (Figure 5D). Next, we downregulated Ikaros in BMNs by adding lenalidomide and cultured these cells with either IFN-γ or GM-CSF. The incubation of BMNs with the combination of GM-CSF and lenalidomide, but not IFN-γ and lenalidomide, resulted in efficient development of HLA-DR$^+$CD14$^+$ hybrid cells (80%–90% among all BMNs) (Figure 5D). These data confirm the hypothesis that the premature downregulation of Ikaros in concert with the macrophage stimulatory factor GM-CSF are requisite for the development of hybrid neutrophils from neutrophil progenitors.

BM-Derived Hybrid Neutrophils Recapitulate the Function of APC-like Hybrid TANs

Next, we investigated whether the BM-derived hybrid neutrophils also functionally resemble hybrid TANs in their ability to stimulate T cell responses. For this purpose, we differentiated immature BMNs into activated canonical and hybrid neutrophils (Figure S5A) and co-cultured them with autologous PBMCs stimulated with plate-bound anti-CD3 Abs. We found that both subsets of neutrophils augmented the expression of activation markers CD25 and CD69 on stimulated T cells to the same degree (Figure S5B). However, HLA-DR$^+$ hybrid neutrophils exerted a significantly stronger stimulatory effect on T cell proliferation and IFN-γ production than the canonical neutrophils (Figures 6A and 6B). The BM-derived hybrid neutrophils differentiated with low doses of IFN-γ and GM-CSF also recapitulated the T cell stimulatory activity of hybrid TANs (Figure 6A). However, as described above, the treatment of BMNs with a low dose of GM-CSF and IFN-γ at concentrations more than 1 ng/ml gradually induced the expression of PD-L1 on the HLA-DR$^+$ BMNs (Figure 3D, lower panel). When we co-cultured these PD-L1$^+$HLA-DR$^+$ BMNs with autologous PBMCs stimulated with anti-CD3 Abs, we found marked suppression of T cell proliferation (Figure 6C, upper panel), which was substantially inhibited by PD-L1 blocking Abs (Figure 6C, lower panel). Thus, high doses of IFN-γ can convert the T cell stimulatory HLA-DR$^+$ BMNs into a suppressive population via upregulation of PD-L1. These results demonstrate some functional plasticity in the APC-like neutrophils.

To determine whether the hybrid neutrophils are able to induce the proliferation of allogeneic T cells in a mixed-lymphocyte reaction, we co-cultured BM-derived hybrid and canonical neutrophils with allogeneic T cells purified from the peripheral blood of healthy donors. BrdU incorporation assays revealed that hybrid neutrophils, but not canonical neutrophils, were able to initiate the allogeneic proliferation of both CD4 and CD8 cells (Figure 6D). In addition, similar to hybrid TANs, BM-derived hybrid neutrophils pulsed with a peptide pool of viral antigens were able to initiate the autologous memory CD8 and CD4 cell response more efficiently than canonical neutrophils (Figure S5C). These data demonstrate the functional resemblance between BM-derived and tumor-derived hybrid neutrophils, and justify the use of this model to investigate additional functions of this rare subset of TANs.

APC-like Hybrid Neutrophils Stimulate and Augment Anti-Tumor Effector T Cell Responses

Next, we evaluated the effect of canonical and hybrid neutrophils on anti-tumor effector T cells using a newly developed in vitro model. We transduced human T cells with a high-affinity transgenic T cell receptor (TCR) called Ly95 that recognizes an HLA-A*0201-restricted peptide sequence in the human cancer testis antigen, NY-ESO-1 (Moon et al., 2016). As target cells, we used a genetically modified A549 human lung adenocarcinoma cell line expressing the NY-ESO-1 protein in the context of HLA-A*0201 (A549 A2-NY-ESO-1 cells) (Moon et al., 2016). Co-culturing of Ly95 T cells with A549 A2-NY-ESO-1 tumor cells resulted in robust production of IFN-γ and Granzyme B in Ly95 T cells (Figure 7A). When we added BM-derived hybrid neutrophils into this system, the production of IFN-γ and Granzyme B in Ly95 T cells was markedly elevated (Figures 7A and 7B) and increased compared with canonical neutrophils. Of note, the addition of the hybrid neutrophils into Ly95 T cells co-cultured with control A549 cells did not induce the production of these factors, indicating that hybrid neutrophil-mediated stimulation of Ly95 cells was NY-ESO-1 specific and not the result of allostimulation (data not shown).

Using a transwell assay system, we found that HLA-DR$^+$ hybrid BMNs induced the stimulation of IFN-γ production by Ly95 T cells only when the cells were in direct contact (Figure S5D). Since hybrid BMNs are characterized by increased expression of co-stimulatory molecules OX40L, 4-1BBL CD86, and CD54 (Figures 2D, 2E, and S2D), we co-cultured Ly95 T cells with A549 A2-NY-ESO-1 tumor cells and with hybrid BMNs in the presence of blocking Abs to these upregulated co-stimulatory molecules. Figure 7A shows a representative experiment in which the stimulatory effect of hybrid neutrophils

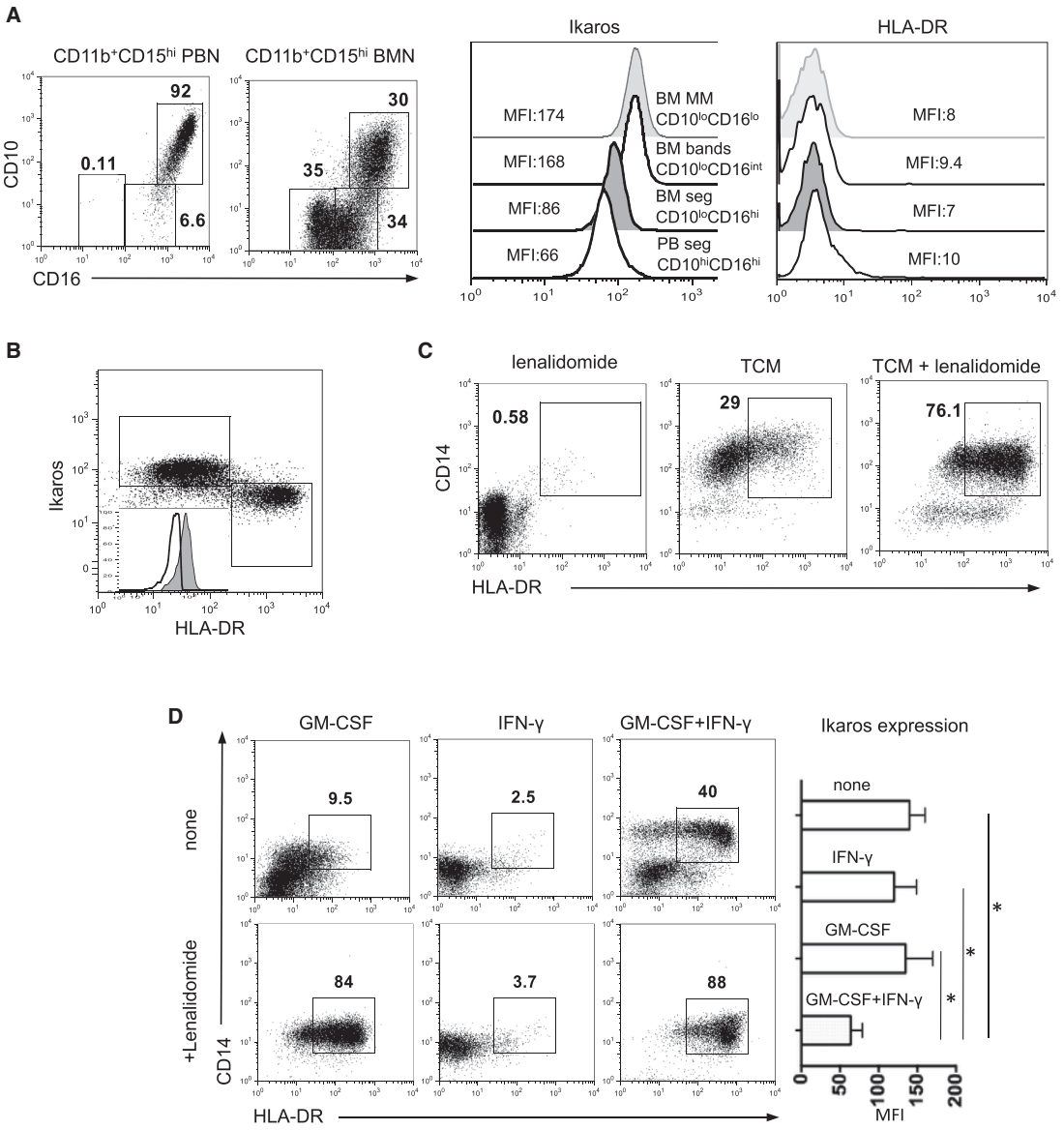

Figure 5. Transcription Factor Ikaros Negatively Regulates the Differentiation of Hybrid Neutrophils

(A) Flow cytometric analysis of the level of Ikaros and HLA-DR expression in PBNs and BMNs at different stages of maturation. Results are shown as mean fluorescence intensity (MFI).

(B) Flow cytometric analysis of the level of Ikaros expression in the HLA-DR$^+$ hybrid and HLA-DR$^-$ canonical CD11b$^+$CD15^{hi}CD66b$^+$ BMNs.

(C) Flow cytometric analysis of CD14 and HLA-DR expression on gated live CD11b$^+$CD15^{hi}CD66b$^+$ BMNs cultured in the presence of lenalidomide (10 μM) and hybrid-inducing TCM (30% v/v) for 6 days.

(D) The effect of IFN-γ (50 pg/ml) and GM-CSF (50 pg/ml) on the formation of HLA-DR$^+$CD14$^+$ hybrid neutrophils in the absence (upper panel) or presence (lower panel) of lenalidomide (10 μM) in vitro. The level of Ikaros expression (MFI) in BMNs treated with IFN-γ (50 pg/ml) and GM-CSF (50 pg/ml) for 5 days is shown (mean ± SEM, n = 3, *p ≤ 0.01, Wilcoxon matched-pairs rank test).

Representative dot plots from one of six experiments are shown in (A–D).

was partially abrogated in the presence of anti-CD54, 4-1BBL, OX-40L, and CD86 blocking Abs (Figure 7A).

Next we asked whether APC-like hybrid neutrophils could directly trigger NY-ESO-1 specific response of Ly95 cells. Given that Ly95 cells specifically recognize the HLA-A*02-restricted peptide of NY-ESO-1, we pulsed HLA-A*02$^+$ BM-derived canonical and hybrid neutrophils with the NY-ESO-1 (157–165, SLLMWITQV) peptide and then co-cultured the exposed neutrophils with Ly95 T cells for 24 hr. We found that hybrid HLA-A*02$^+$HLA-DR$^+$ hybrid neutrophils preloaded with the peptide

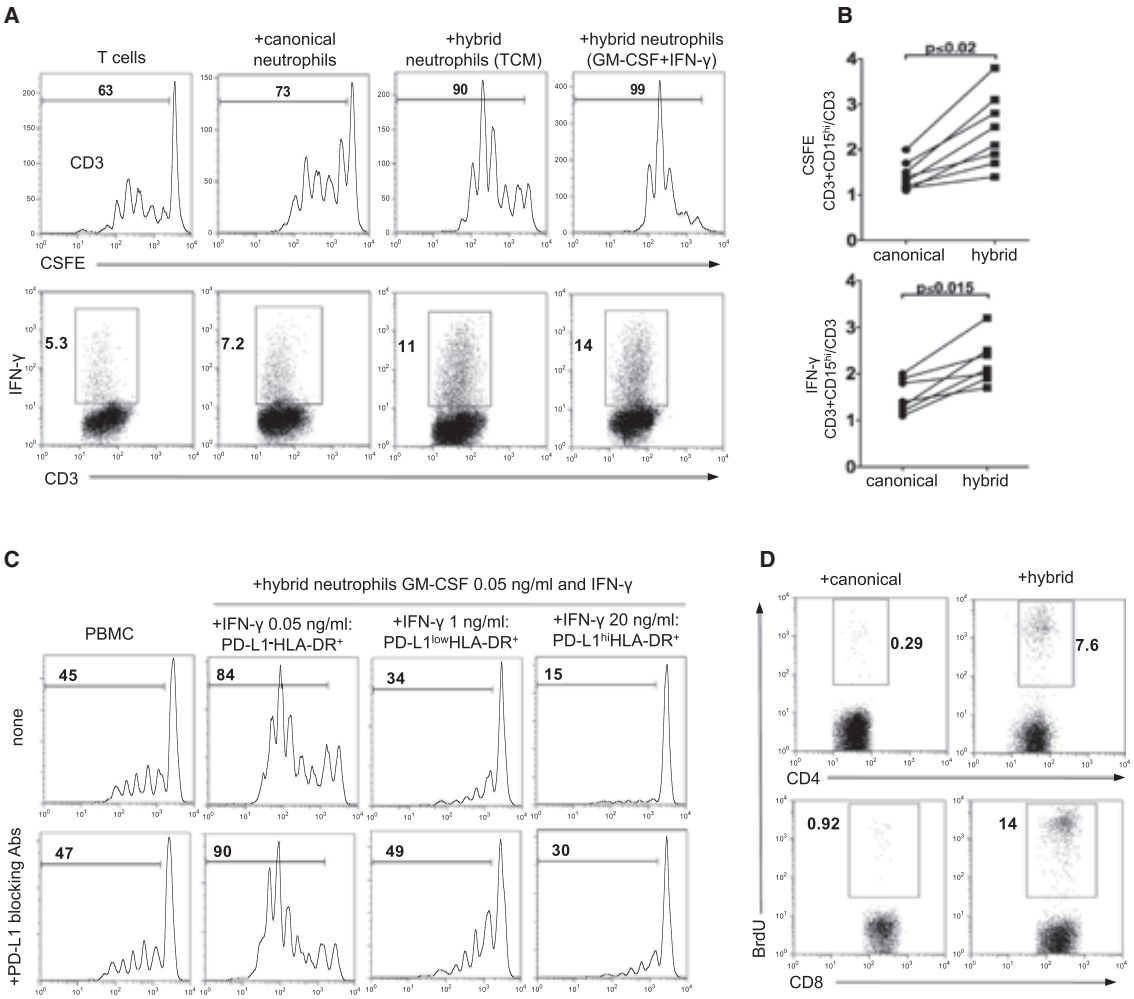

Figure 6. APC-like Hybrid Neutrophils Stimulate Antigen-Nonspecific T Cell Responses

(A) The proliferation and IFN-γ production of anti-CD3 Abs stimulated autologous T cells in the presence of BM-derived canonical and hybrid neutrophils differentiated with hybrid-inducing TCM or IFN-γ (50 pg/ml) and GM-CSF (50 pg/ml).

(B) Summary results of autologous T cell proliferation (upper graph) and IFN-γ production (lower graph) in the presence of canonical and hybrid neutrophils. Data are presented as a ratio (CD3 cells + $CD15^{hi}$)/(CD3) (n = 8, Wilcoxon matched-pairs rank test).

(C) The proliferation of CFSE-labeled autologous PBMCs cultured with hybrid BMNs with different level of PD-L1 expression in the presence (lower panel) or absence PD-L1 blocking Abs (5 μg/ml) (upper panel). $PD\text{-}L1^{-/lo/hi}HLA\text{-}DR^{+}$ hybrid neutrophils were differentiated with GM-CSF (50 pg/ml) and increasing doses of IFN-γ.

(D) The proliferation of allogeneic T cells from healthy donors in the presence of APC-like hybrid neutrophils in a mixed-lymphocyte reaction.

Representative results from one of six experiments are shown in (C) and (D). See also Figure S5.

triggered IFN-γ production in Ly95 T cells more effectively than peptide-loaded canonical neutrophils (Figure 7C). These data demonstrate that hybrid neutrophils can trigger and significantly augment the activation of antigen-specific effector T cells.

APC-like Hybrid Neutrophils Are Able to Cross-Present Tumor Antigens

The assays described above evaluated the ability of the TANs to present antigenic peptides, but did not address the ability of hybrid neutrophils to process antigens, as the high-affinity major histocompatibility (MHC) class I binding peptides could bind directly to the surface MHC class I and do not require uptake and processing. We therefore performed experiments with DQ ovalbumin (DQ-OVA) and demonstrated that hybrid neutrophils were able to take up and process ovalbumin to a higher degree than canonical neutrophils (Figure 7D). To evaluate whether hybrid neutrophils are able to present extracellular protein to effector CD8 cells (cross-presentation), we preloaded HLA-A*02-positive BM-derived hybrid and canonical neutrophils with full-length NY-ESO-1 protein and mixed them with Ly95 cells for 24 hr (Figure 7E). We found that these canonical and hybrid neutrophils were not sufficient to trigger Ly95 T cell response.

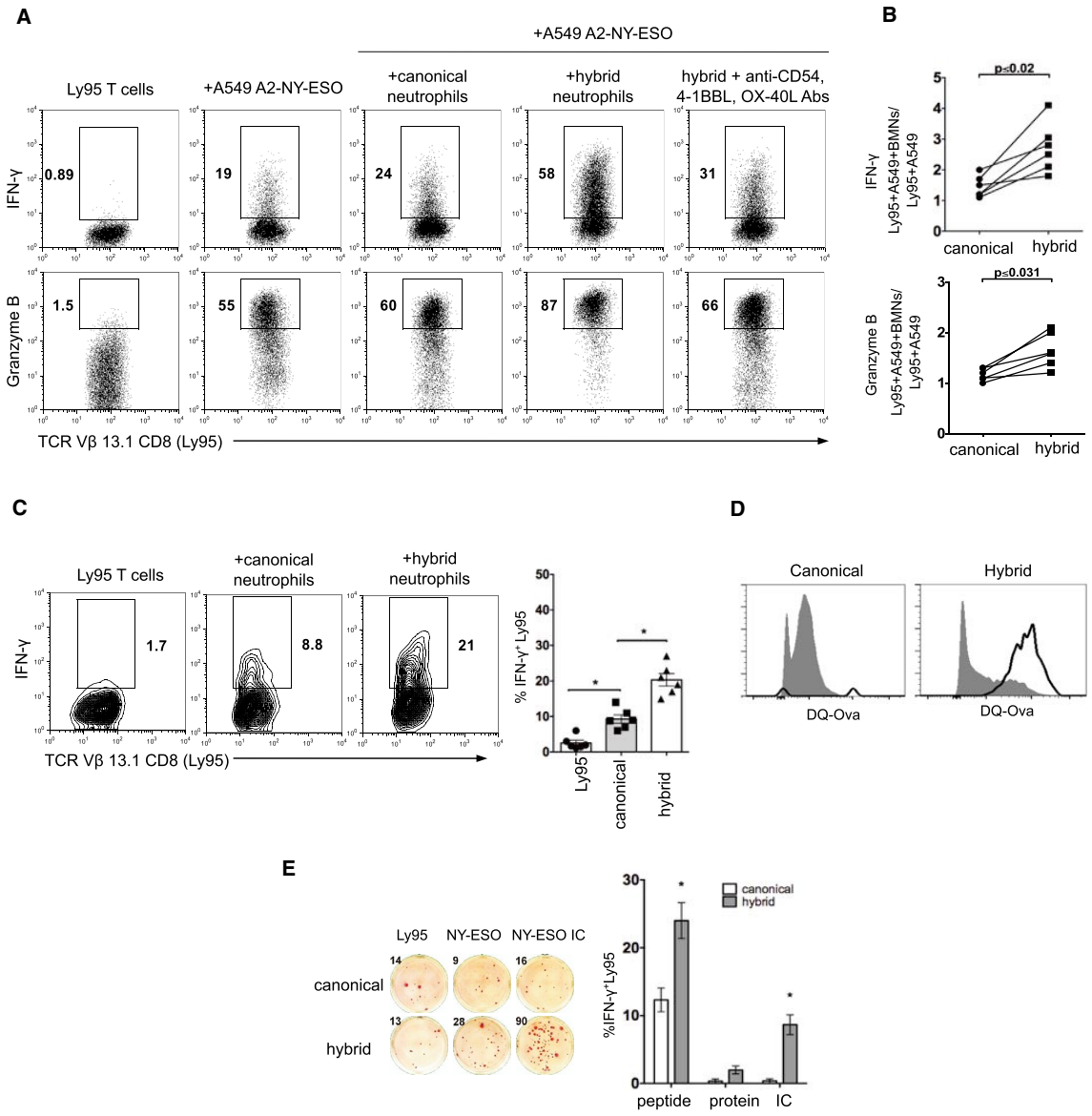

Figure 7. APC-like Hybrid Neutrophils Are Able to Trigger and Stimulate NY-ESO-Specific Effector T Cell Responses

(A) NY-ESO-specific Ly95 cells (TCR Vβ13.1$^+$CD8$^+$) were stimulated with A549 tumor cell line expressing NY-ESO-1 in the context of HLA-A*02 (A2/NY-ESO-1 A549) in the presence of BM-derived canonical and hybrid neutrophils. Intracellular IFN-γ and Granzyme B production was measured by flow cytometry.

(B) Cumulative results showing the Ly95 cell stimulatory activity of canonical and hybrid neutrophils. Stimulatory activity was defined as a ratio (Ly95 cells + A549-NY-ESO + BMN)/(Ly95 cells + A549-NY-ESO) (n = 6, Wilcoxon matched-pairs rank test).

(C) HLA-A02$^+$ canonical or hybrid neutrophils were pulsed with synthetic NY-ESO-1 peptide and co-cultured with Ly95 cells for 24 hr. Intracellular IFN-γ was assessed by flow cytometry (mean ± SEM, n = 6, *p ≤ 0.01, Wilcoxon matched-pairs rank test).

(D) DQ-OVA uptake and processing by BM-derived canonical or hybrid neutrophils (open histograms). Cells incubated at 4°C served as controls (shaded histograms).

(E) Cross-presentation of NY-ESO-1 epitopes to Ly95 cells by HLA-A02$^+$ canonical or hybrid neutrophils preloaded with NY-ESO-1 protein, NY-ESO-1 peptide, or NY-ESO-immune complex (IC). IFN-γ ELISpot (mean ± SEM, n = 6, *p ≤ 0.01 canonical versus hybrid, Wilcoxon matched-pairs rank test).

Ly95 T cells mixed with control, unloaded neutrophils generated a low background of IFN-γ-positive spots due to endogenous activity of Ly95 cells from the prior CD3 stimulation required for expansion of these cells after TCR transduction (Figure 7E).

Next, we sought to employ the Fc receptors (FcγR) that are highly expressed on hybrid neutrophils (Figure 2D) and deliver the NY-ESO-1 protein as an immunoglobulin G (IgG)-immune complex to trigger the more efficient FcγR-mediated antigen

uptake and presentation. For this purpose, we pre-exposed the neutrophil subsets to NY-ESO-1 immune complexes formed by incubating the NY-ESO-1 protein with anti-NY-ESO-1 monoclonal Abs and mixed them with Ly95 cells for 24 hr. Under these conditions, we observed that hybrid neutrophils, but not canonical neutrophils, were able to cross-present NY-ESO epitopes and induce low-level, but NY-ESO-specific, production of IFN-γ by Ly95 T cells (Figure 7E). These data demonstrate that hybrid neutrophils have the ability to take up and cross-present exogenous tumor antigens, at least under the conditions used here.

DISCUSSION

We identified a subset of TANs that exhibited the hybrid phenotypic and functional characteristics of neutrophils and APCs. These APC-like hybrid TANs were superior to canonical TANs in their ability to induce and stimulate anti-tumor T cell responses. We identified the progenitors of APC-like hybrid TANs, along with the tumor-derived and transcriptional factors responsible for the development of these cells. Thus, our findings demonstrate that the early-stage lung tumor microenvironment can drive neutrophils to differentiate into a cell subset with enhanced anti-tumor capabilities.

It has been previously recognized that neutrophils can acquire characteristics of "professional APCs" under certain non-cancerous physiological and pathological conditions (Ashtekar and Saha, 2003). Specifically, neutrophils have been reported to upregulate MHC class II molecules and co-stimulatory molecules, such as CD80 and CD86, in response to inflammatory cytokines and during autoimmune pathology or inflammatory diseases (Iking-Konert et al., 2005; Wagner et al., 2006). There have also been several reports demonstrating the ability of neutrophils to present viral and bacterial antigens to T cells, provide accessory signals for T cell activation, and prime antigen-specific Th1 and Th17 cells (Abi Abdallah et al., 2011; Radsak et al., 2000; Tvinnereim et al., 2004). Little is known, however, about factors that trigger the formation and origin of these cells, and the precise functional capacities they possess, especially in humans. Moreover, the detailed phenotype and function of these APC-like neutrophils have not yet been reported and studied in cancer patients. The cells most similar to hybrid TANs appear to be those recently identified by Geng et al. (2013) and Matsushima et al. (2013), who described the ability of a subset of murine neutrophils to acquire markers of dendritic cells (CD11c, MHC II, CD80, and CD86) and termed these cells "neutrophil-DC hybrids." However, the phenotype of these neutrophil-DC hybrids is somewhat different from APC-like hybrid TANs that exhibit a partial phenotype of DC (MHC class II, CD86, CCR7) along with a partial phenotype of monocytes/macrophages (CD14, CD206, $CD64^{hi}$, $CD32^{hi}$), and lacked other defining markers of dendritic cells and macrophages such as CD209, CD204, CD83, CD80, CD1c, CD163, and CCR6.

Over the last decade there has been an increasing focus on the interactions between inflammatory myeloid cells and T cells within the tumor microenvironment. In this study, we identified a specialized neutrophil subpopulation enabling augmentation of both antigen non-specific and tumor-specific T cell responses by providing co-stimulatory signals through the OX40L, 4-1BBL CD86, and CD54 molecules. Our data are concordant with previous studies showing that activated granulocytes can provide accessory signals for T cell activation (Radsak et al., 2000). We also found evidence for functional plasticity in the generation of APC-like neutrophils in terms of regulation of T cell response. Differentiation of immature neutrophils with low doses of IFN-γ resulted in highly immunostimulatory cells; however, high doses of IFN-γ resulted in formation of $PD\text{-}L1^{hi}$ hybrid neutrophils that profoundly suppressed T cell responses. This dichotomous in vitro effect of neutrophils on T cell response may suggest an important role of hybrid neutrophils in the regulation of the normal physiological inflammatory processes, whereby T cell stimulation needs to be followed by suppression to resolve an inflammatory process.

One of the key functional findings of our study was that APC-like hybrid TANs acquired new functions compared with canonical TANs and were able to take up, degrade, and cross-present tumor antigens. Cross-presentation was triggered in hybrid neutrophils when NY-ESO-1 protein was delivered as an IgG-immune complex; however, this cross-presentation occurred at a relatively low level. These data suggest that the hybrid neutrophils can take up and process antigens by means of the high-affinity IgG receptors FcγRI and FcγRII, which are highly expressed on hybrid neutrophils compared with canonical neutrophils. These hybrid neutrophils may "regurgitate" processed peptide outside of the cell (Potter and Harding, 2001) and thus facilitate the antigen uptake and processing by other professional APCs. Our data are consistent with previous studies showing the critical role of FcγR in enhancing the cross-presentation of NY-ESO-1 by professional APCs (Nagata et al., 2002).

The ability of human neutrophils to express some APC markers in vitro after stimulation with inflammatory factors such as macrophage CSF, IFN-γ, GM-CSF, TNF-α, IL-3, IL-1β, and IL-4 was discovered over a decade ago (Gosselin et al., 1993; Reinisch et al., 1996; Oehler et al., 1998). For example, the combination of GM-CSF, IL-4, and TNF-α induced the expression of MHC II, CD40, CD86, CD1a, CD1b, and CD1c, whereas the combination of GM-CSF, TNF-α, and IFN-γ triggered MHC II, CD80, CD83, and CD86 expression by human neutrophils (Iking-Konert et al., 2001; Oehler et al., 1998). Moreover, it has been reported that neutrophils could even be reprogrammed and transdifferentiated into macrophages and DC after co-culture with multiple cytokines in vitro (Araki et al., 2004; Iking-Konert et al., 2005; Koffel et al., 2014). It should be noted, however, that high (generally non-physiologic) concentrations of inflammatory factors (ranging from 1 to 100 ng/ml) were used in all these previous studies to induce the upregulation of APC markers, and differentiation could even be observed in mature end-stage neutrophils. It seems unlikely that neutrophils would encounter these artificial conditions in vivo and it has been unknown whether these factors are required and sufficient for the generation of APC-like neutrophils in vivo. We found that the tumors containing an increased number of hybrid TANs secreted many of the inflammatory factors described above at very low concentrations when compared with tumors without hybrid TANs. When tested, however, only IFN-γ and GM-CSF at the low

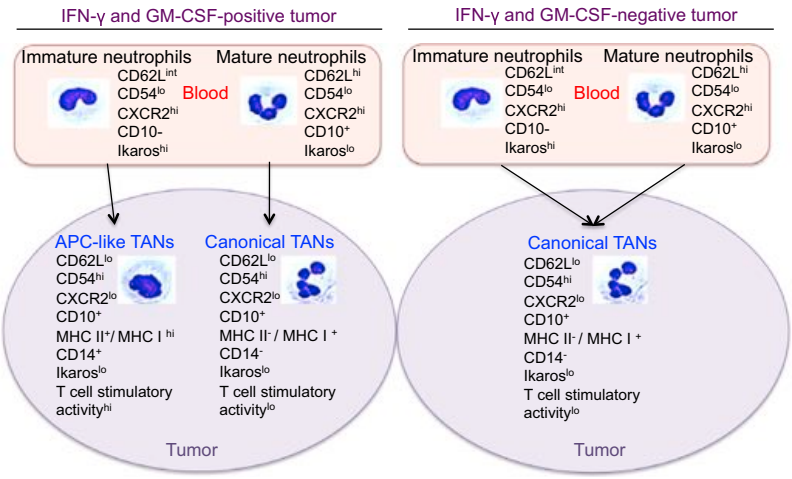

Figure 8. Schematic Model of Neutrophil Differentiation in Early-Stage Human Lung Cancer

concentrations found in TCM were able to synergistically induce hybrid neutrophils. The development of APC-like neutrophils occurred over a 5-day time period and required the synthesis of APC receptors de novo in the long-lived $CD10^{-}CD16^{low/int}$ immature neutrophils, suggesting that hybrid neutrophils are a result of a differentiation process and not simply an acute activation event.

Mechanistically, we also found that IFN-γ and GM-CSF exert their APC-promoting effects on immature neutrophils partially via the downregulation of the transcription factor Ikaros. Although Ikaros is well known as a key regulator of lymphocyte differentiation (O'Brien et al., 2014), our data suggest that Ikaros has a much broader role in hematolymphoid differentiation. Our results are consistent with previous studies in murine cells demonstrating that Ikaros controls neutrophil differentiation by silencing of genes that are necessary for macrophage-monocyte development (Papathanasiou et al., 2003).

Although the in vitro conditions used in our experiments may not necessarily reflect what actually transpires in vivo, we propose a model of human neutrophil differentiation in different lung tumor microenvironments at early stages (Figure 8). According to this model, neutrophils adapt differently to the tumor microenvironment. Mature neutrophils recruited into tumors acquire the phenotype of highly activated neutrophils, resulting in the formation of canonical TANs. However, the immature neutrophils, which circulate to varying degrees in cancer patients, are more plastic. When immature neutrophils are recruited into tumors which produce appropriate levels of IFN-γ and GM-CSF, they change their differentiation program and give rise to a subset of APC-like hybrid TANs exhibiting composite characteristics of neutrophils and APCs. However, if the level of IFN-γ and GM-CSF is not significant enough to initiate the differentiation of immature neutrophils into the hybrid neutrophils, or other inhibitory factors or conditions are present in the tumor (i.e., hypoxia), the immature neutrophils use a default pathway of differentiation and become activated canonical TANs.

The concept of neutrophil diversity and plasticity has begun to emerge in a variety of inflammatory disorders and murine tumor models; however, to date there has been no convincing evidence showing that specialized neutrophil subpopulations with different functions exist in human cancers. Our data suggest that the tumor microenvironment in some small, early-stage lung tumors can induce the formation of an immunostimulatory subset of neutrophils that have the ability to activate T cells and, in a general way, resemble the N1 neutrophil phenotype previously described in mice (Fridlender et al., 2009). By gaining a better understanding of the cellular and molecular processes in early-stage cancers that control tumor growth, it may be possible to enhance or mimic these factors and conditions to potentially boost natural or vaccine-induced anti-tumor immunity.

EXPERIMENTAL PROCEDURES

Study Design

A total of 109 patients with stage I–II lung cancer, who were scheduled for surgical resection, consented to tissue collection of a portion of their tumor and/or blood for research purposes at the Hospital of the University of Pennsylvania and The Philadelphia Veterans Affairs Medical Center, which had been approved by their respective Institutional Review Boards. Detailed characteristics of the patients can be found in the Supplemental Experimental Procedures and Table S1.

Preparation of a Single-Cell Suspension from Lung Tumor Tissue

We used our optimized disaggregation method for fresh human lung tumors that preserves the phenotype and function of the immune cells as previously described in detail (Quatromoni et al., 2015).

Neutrophil Isolation

TANs were isolated from tumor single-cell suspensions using positive selection of $CD15^{+}$ or $CD66b^{+}$ cells with microbeads as previously described (Eruslanov et al., 2014). TAN subsets were flow sorted based on the phenotype of canonical ($CD11b^{+}CD66b^{+}CD15^{hi}HLA\text{-}DR^{-}$) and hybrid ($CD11b^{+}CD66b^{+}CD15^{hi}HLA\text{-}DR^{+}$) TANs. PBNs and BMNs were isolated from EDTA anticoagulated peripheral blood and BM single-cell suspension, respectively, using positive selection of $CD15^{+}$ or $CD66b^{+}$ cells with microbeads. See Supplemental Experimental Procedures for details.

Generation of BM-Derived Macrophages, Dendritic Cells, and Hybrid and Canonical Neutrophils

To differentiate BMNs into the cells that resemble canonical and hybrid TANs, we cultured the purified BMNs with a different type of TCM for 7 days. Alternatively, hybrid neutrophils were differentiated from BMNs with low doses of IFN-γ and GM-CSF. BM-derived macrophages and dendritic cells were generated by culturing $CD15^{-}CD11b^{+}$ BM cells with M-CSF or IL-4 and GM-CSF, respectively.

Flow Cytometry

Flow cytometric analysis was performed according to standard protocols. For phenotypic and functional analysis PBNs, BMNs, and TANs were gated on live $CD11b^{+}CD15^{hi}CD66b^{+}$ cells. For more details see Supplemental Experimental Procedures.

Antigen Non-specific T Cell Response

PBMCs or purified T cells were stimulated with plate-bound anti-human CD3 and/or anti-CD28 antibodies to induce antigen non-specific T cell response. For more details see Supplemental Experimental Procedures.

Virus-Specific Memory T Cell Response

Peripheral blood autologous T cells were used as responders and co-cultured with neutrophil subsets that had been pulsed with a mixture of viral peptides with a broad array of HLA types. The T cell response was quantified by IFN-γ ELISPOT.

NY-ESO-Specific T Cell Response

To study the regulation of antigen-specific effector T cell responses by neutrophil subsets, we used Ly95 TCR transduced T cells recognizing the HLA-A2 restricted NY-ESO-1:157–165 peptide antigen (Moon et al., 2016). Generation of NY-ESO-specific Ly95 TCR T cells and details of the procedures are provided in Supplemental Experimental Procedures.

Allogeneic Mixed-Lymphocyte Reaction

Purified allogeneic T cells from healthy donor PBMCs were used as responders and reacted with canonical or hybrid neutrophils (inducers) from lung cancer patients at a ratio of 1:1. Five days later, the proliferation of CD4 and CD8 T cells was measured using a BrdU incorporation assay.

Statistics

Comparisons between two groups were assessed with a two-tailed Student's t test for paired and unpaired data if data were normally distributed. Non-parametric Wilcoxon matched-pairs test and Mann-Whitney unpaired test were used when the populations were not normally distributed. Likewise, multiple groups were analyzed by one-way ANOVA with corresponding Tukey's multiple comparison test if normally distributed, or by the Kruskal-Wallis test with Dunn's multiple comparison test if not normally distributed. All statistical analyses were performed with GraphPad Prism 6. A p value of less than 0.05 was considered statistically significant.

SUPPLEMENTAL INFORMATION

Supplemental Information includes Supplemental Experimental Procedures, five figures, and one table and can be found with this article online at http://dx.doi.org/10.1016/j.ccell.2016.06.001.

AUTHOR CONTRIBUTIONS

S.S., S.A., and E.E. conceived the study. S.S., P.B., A.R., T.S., S.B., E.M., J.Q., C.D., M.F., and E.E. performed experiments and data analysis. Reagents were contributed by E.M. S.A., S.S., A.G., W.H., and J.C.-G. Manuscript preparation was performed by S.S. and E.E. Manuscript revisions were performed by S.A., W.H., and J.C.-G. All authors read and approved the final manuscript.

ACKNOWLEDGMENTS

This work was supported by the Department of Defense (LC140199 to E.E.), NIH (RO1 CA187392-01A1 to E.E.), NIH (R01 CA193556 to S.S.), NIH (K12CA076931 to A.G.), and the Lung Cancer Translation Center of Excellence of the Abramson Cancer Center at the University of Pennsylvania.

Received: January 5, 2016
Revised: April 8, 2016
Accepted: June 1, 2016
Published: June 30, 2016

REFERENCES

Abi Abdallah, D.S., Egan, C.E., Butcher, B.A., and Denkers, E.Y. (2011). Mouse neutrophils are professional antigen-presenting cells programmed to instruct Th1 and Th17 T-cell differentiation. Int. Immunol. *5*, 317–326.

Araki, H., Katayama, N., Yamashita, Y., Mano, H., Fujieda, A., Usui, E., Mitani, H., Ohishi, K., Nishii, K., Masuya, M., et al. (2004). Reprogramming of human postmitotic neutrophils into macrophages by growth factors. Blood *8*, 2973–2980.

Ashtekar, A.R., and Saha, B. (2003). Poly's plea: membership to the club of APCs. Trends Immunol. *9*, 485–490.

Brandau, S. (2013). The dichotomy of neutrophil granulocytes in cancer. Semin. Cancer Biol. *3*, 139–140.

Carus, A., Ladekarl, M., Hager, H., Pilegaard, H., Nielsen, P.S., and Donskov, F. (2013). Tumor-associated neutrophils and macrophages in non-small cell lung cancer: no immediate impact on patient outcome. Lung Cancer *1*, 130–137.

Dai, Z.J., Gao, J., Ma, X.B., Yan, K., Liu, X.X., Kang, H.F., Ji, Z.Z., Guan, H.T., and Wang, X.J. (2012). Up-regulation of hypoxia inducible factor-1alpha by cobalt chloride correlates with proliferation and apoptosis in PC-2 cells. J. Exp. Clin. Cancer Res. *31*, 28.

Dallegri, F., and Ottonello, L. (1992). Neutrophil-mediated cytotoxicity against tumour cells: state of art. Arch. Immunol. Ther. Exp. (Warsz) *1*, 39–42.

Dumortier, A., Kirstetter, P., Kastner, P., and Chan, S. (2003). Ikaros regulates neutrophil differentiation. Blood *6*, 2219–2226.

Elghetany, M.T. (2002). Surface antigen changes during normal neutrophilic development: a critical review. Blood Cells Mol. Dis. *2*, 260–274.

Eruslanov, E.B., Bhojnagarwala, P.S., Quatromoni, J.G., Stephen, T.L., Ranganathan, A., Deshpande, C., Akimova, T., Vachani, A., Litzky, L., Hancock, W.W., et al. (2014). Tumor-associated neutrophils stimulate T cell responses in early-stage human lung cancer. J. Clin. Invest. *12*, 5466–5480.

Fridlender, Z.G., Sun, J., Kim, S., Kapoor, V., Cheng, G., Ling, L., Worthen, G.S., and Albelda, S.M. (2009). Polarization of tumor-associated neutrophil phenotype by TGF-beta: "N1" versus "N2" TAN. Cancer Cell *3*, 183–194.

Geng, S., Matsushima, H., Okamoto, T., Yao, Y., Lu, R., Page, K., Blumenthal, R.M., Ward, N.L., Miyazaki, T., and Takashima, A. (2013). Emergence, origin, and function of neutrophil-dendritic cell hybrids in experimentally induced inflammatory lesions in mice. Blood *10*, 1690–1700.

Gosselin, E.J., Wardwell, K., Rigby, W.F., and Guyre, P.M. (1993). Induction of MHC class II on human polymorphonuclear neutrophils by granulocyte/macrophage colony-stimulating factor, IFN-gamma, and IL-3. J. Immunol. *3*, 1482–1490.

Granot, Z., and Fridlender, Z.G. (2015). Plasticity beyond cancer cells and the "immunosuppressive switch". Cancer Res. *21*, 4441–4445.

Grivennikov, S.I., Greten, F.R., and Karin, M. (2010). Immunity, inflammation, and cancer. Cell *6*, 883–899.

Houghton, A.M. (2010). The paradox of tumor-associated neutrophils: fueling tumor growth with cytotoxic substances. Cell Cycle *9*, 1732–1737.

Iking-Konert, C., Cseko, C., Wagner, C., Stegmaier, S., Andrassy, K., and Hansch, G.M. (2001). Transdifferentiation of polymorphonuclear neutrophils: acquisition of CD83 and other functional characteristics of dendritic cells. J. Mol. Med. (Berl.) *8*, 464–474.

Iking-Konert, C., Ostendorf, B., Sander, O., Jost, M., Wagner, C., Joosten, L., Schneider, M., and Hansch, G.M. (2005). Transdifferentiation of polymorphonuclear neutrophils to dendritic-like cells at the site of inflammation in rheumatoid arthritis: evidence for activation by T cells. Ann. Rheum. Dis. *10*, 1436–1442.

Ilie, M., Hofman, V., Ortholan, C., Bonnetaud, C., Coelle, C., Mouroux, J., and Hofman, P. (2012). Predictive clinical outcome of the intratumoral CD66b-positive neutrophil-to-CD8-positive T-cell ratio in patients with resectable nonsmall cell lung cancer. Cancer *6*, 1726–1737.

Koffel, R., Meshcheryakova, A., Warszawska, J., Hennig, A., Wagner, K., Jorgl, A., Gubi, D., Moser, D., Hladik, A., Hoffmann, U., et al. (2014). Monocytic cell differentiation from band-stage neutrophils under inflammatory conditions via MKK6 activation. Blood *17*, 2713–2724.

Kronke, J., Hurst, S.N., and Ebert, B.L. (2014). Lenalidomide induces degradation of IKZF1 and IKZF3. Oncoimmunology *7*, e941742.

Mantovani, A., Cassatella, M.A., Costantini, C., and Jaillon, S. (2011). Neutrophils in the activation and regulation of innate and adaptive immunity. Nat. Rev. Immunol. *8*, 519–531.

Matsushima, H., Geng, S., Lu, R., Okamoto, T., Yao, Y., Mayuzumi, N., Kotol, P.F., Chojnacki, B.J., Miyazaki, T., Gallo, R.L., and Takashima, A. (2013). Neutrophil differentiation into a unique hybrid population exhibiting dual phenotype and functionality of neutrophils and dendritic cells. Blood *10*, 1677–1689.

Moon, E.K., Ranganathan, R., Eruslanov, E., Kim, S., Newick, K., O'Brien, S., Lo, A., Liu, X., Zhao, Y., and Albelda, S.M. (2016). Blockade of programmed death 1 augments the ability of human T cells engineered to target NY-ESO-1 to control tumor growth after adoptive transfer. Clin. Cancer Res. *22*, 436–447.

Nagata, Y., Ono, S., Matsuo, M., Gnjatic, S., Valmori, D., Ritter, G., Garrett, W., Old, L.J., and Mellman, I. (2002). Differential presentation of a soluble exogenous tumor antigen, NY-ESO-1, by distinct human dendritic cell populations. Proc. Natl. Acad. Sci. USA *16*, 10629–10634.

O'Brien, S., Thomas, R.M., Wertheim, G.B., Zhang, F., Shen, H., and Wells, A.D. (2014). Ikaros imposes a barrier to CD8+ T cell differentiation by restricting autocrine IL-2 production. J. Immunol. *11*, 5118–5129.

Oehler, L., Majdic, O., Pickl, W.F., Stockl, J., Riedl, E., Drach, J., Rappersberger, K., Geissler, K., and Knapp, W. (1998). Neutrophil granulocyte-committed cells can be driven to acquire dendritic cell characteristics. J. Exp. Med. *7*, 1019–1028.

Papathanasiou, P., Perkins, A.C., Cobb, B.S., Ferrini, R., Sridharan, R., Hoyne, G.F., Nelms, K.A., Smale, S.T., and Goodnow, C.C. (2003). Widespread failure of hematolymphoid differentiation caused by a recessive niche-filling allele of the Ikaros transcription factor. Immunity *1*, 131–144.

Piccard, H., Muschel, R.J., and Opdenakker, G. (2012). On the dual roles and polarized phenotypes of neutrophils in tumor development and progression. Crit. Rev. Oncol. Hematol. *3*, 296–309.

Potter, N.S., and Harding, C.V. (2001). Neutrophils process exogenous bacteria via an alternate class I MHC processing pathway for presentation of peptides to T lymphocytes. J. Immunol. *5*, 2538–2546.

Quatromoni, J.G., Singhal, S., Bhojnagarwala, P., Hancock, W.W., Albelda, S.M., and Eruslanov, E. (2015). An optimized disaggregation method for human lung tumors that preserves the phenotype and function of the immune cells. J. Leukoc. Biol. *1*, 201–209.

Radsak, M., Iking-Konert, C., Stegmaier, S., Andrassy, K., and Hansch, G.M. (2000). Polymorphonuclear neutrophils as accessory cells for T-cell activation: major histocompatibility complex class II restricted antigen-dependent induction of T-cell proliferation. Immunology *4*, 521–530.

Reinisch, W., Tillinger, W., Lichtenberger, C., Gangl, A., Willheim, M., Scheiner, O., and Steger, G. (1996). In vivo induction of HLA-DR on human neutrophils in patients treated with interferon-gamma. Blood *7*, 3068.

Schreiber, R.D., Old, L.J., and Smyth, M.J. (2011). Cancer immunoediting: integrating immunity's roles in cancer suppression and promotion. Science *6024*, 1565–1570.

Tvinnereim, A.R., Hamilton, S.E., and Harty, J.T. (2004). Neutrophil involvement in cross-priming CD8+ T cell responses to bacterial antigens. J. Immunol. *3*, 1994–2002.

van Egmond, M., and Bakema, J.E. (2013). Neutrophils as effector cells for antibody-based immunotherapy of cancer. Semin. Cancer Biol. *3*, 190–199.

Wagner, C., Iking-Konert, C., Hug, F., Stegmaier, S., Heppert, V., Wentzensen, A., and Hansch, G.M. (2006). Cellular inflammatory response to persistent localized Staphylococcus aureus infection: phenotypical and functional characterization of polymorphonuclear neutrophils (PMN). Clin. Exp. Immunol. *1*, 70–77.

Yanez, A., Ng, M.Y., Hassanzadeh-Kiabi, N., and Goodridge, H.S. (2015). IRF8 acts in lineage-committed rather than oligopotent progenitors to control neutrophil vs monocyte production. Blood *9*, 1452–1459.

RESEARCH ARTICLE The Journal of Clinical Investigation

Tumor-associated neutrophils stimulate T cell responses in early-stage human lung cancer

Evgeniy B. Eruslanov,[1] Pratik S. Bhojnagarwala,[1] Jon G. Quatromoni,[1] Tom Li Stephen,[2] Anjana Ranganathan,[3] Charuhas Deshpande,[4] Tatiana Akimova,[5] Anil Vachani,[6] Leslie Litzky,[4] Wayne W. Hancock,[5] José R. Conejo-Garcia,[2] Michael Feldman,[4] Steven M. Albelda,[6] and Sunil Singhal[1]

[1]Division of Thoracic Surgery, Department of Surgery, Perelman School of Medicine at the University of Pennsylvania, Philadelphia, Pennsylvania, USA. [2]Tumor Microenvironment and Metastasis Program, The Wistar Institute, Philadelphia, Pennsylvania, USA. [3]Division of Hematology/Oncology and [4]Department of Pathology and Laboratory Medicine, Perelman School of Medicine at the University of Pennsylvania, Philadelphia, Pennsylvania, USA. [5]Division of Transplant Immunology, Department of Pathology and Laboratory Medicine, Children's Hospital of Philadelphia and Perelman School of Medicine at the University of Pennsylvania, Abramson Research Center, Philadelphia, Pennsylvania, USA. [6]Division of Pulmonary, Allergy, and Critical Care, Department of Medicine, Perelman School of Medicine at the University of Pennsylvania, Philadelphia, Pennsylvania, USA.

Infiltrating inflammatory cells are highly prevalent within the tumor microenvironment and mediate many processes associated with tumor progression; however, the contribution of specific populations remains unclear. For example, the nature and function of tumor-associated neutrophils (TANs) in the cancer microenvironment is largely unknown. The goal of this study was to provide a phenotypic and functional characterization of TANs in surgically resected lung cancer patients. We found that TANs constituted 5%–25% of cells isolated from the digested human lung tumors. Compared with blood neutrophils, TANs displayed an activated phenotype ($CD62L^{lo}CD54^{hi}$) with a distinct repertoire of chemokine receptors that included CCR5, CCR7, CXCR3, and CXCR4. TANs produced substantial quantities of the proinflammatory factors MCP-1, IL-8, MIP-1α, and IL-6, as well as the antiinflammatory IL-1R antagonist. Functionally, both TANs and neutrophils isolated from distant nonmalignant lung tissue were able to stimulate T cell proliferation and IFN-γ release. Cross-talk between TANs and activated T cells led to substantial upregulation of CD54, CD86, OX40L, and 4-1BBL costimulatory molecules on the neutrophil surface, which bolstered T cell proliferation in a positive-feedback loop. Together our results demonstrate that in the earliest stages of lung cancer, TANs are not immunosuppressive, but rather stimulate T cell responses.

Introduction

Murine and human studies suggest that tumor initiation and progression are commonly accompanied by "smoldering" inflammation (1). Tumor-infiltrating myeloid cells represent a significant proportion of the inflammatory cell population in the tumor microenvironment, and they influence nearly every step in tumor progression, including the suppression of adaptive immunity, the promotion of neoangiogenesis and lymphangiogenesis, the remodeling of the extracellular matrix, the promotion of invasion and metastasis, and lastly, the inhibition of vaccine-induced antitumor T cell responses (2). Among the different types of myeloid cells, tumor-associated macrophages (TAMs) have been the best characterized and are generally considered protumoral in murine tumor models (3, 4). The role of tumor-associated neutrophils (TANs) in cancer progression remains unclear and has been investigated only recently in murine models. Characterization of human TANs is even less well developed.

In murine studies, TANs appear to have dichotomous protumor and antitumor effects (5–7). Similar to the classic (M1) and alternative (M2) activation pathways proposed for TAMs, the paradigm of antitumor "N1 neutrophils" versus protumoral "N2 neutrophils" has been proposed in murine models (8). Whether these paradigms translate to human tumor biology remains unanswered. Critical species-specific differences in both innate and adaptive immunity make assumptions of equivalence unwise (9), especially given recent studies that have shown that certain rodent models poorly replicate inflammatory diseases in humans (10). In humans, correlative studies using immunohistochemistry have shown that TAN infiltrates are associated with a poor prognosis for patients with head and neck cancer (11), renal cell carcinoma (12), melanoma (13), hepatocellular cancer (14), and colon cancer (15). In contrast, high tumor neutrophil counts have been associated with a favorable outcome for patients with gastric cancer (16). The results in lung cancer have been divergent (17, 18). To our knowledge, there have been no reports regarding the functional role of TANs in the progression of human cancers. Thus, one goal of this work was to determine the phenotype and function of TANs in early-stage lung cancer using fresh surgically obtained tumor.

A major challenge in TAN biology is deciphering the complex interaction of activated neutrophils with T cells in the tumor microenvironment. Understanding the role of TANs in regulating T cell responses in cancer patients is particularly important because cytotoxic T lymphocytes are the chief effector cells mediating antigen-driven antitumor immunity. There is evidence that activated neutrophils can interact with T cells in dichotomous ways. Several studies have shown that neutrophils can present antigens

Conflict of interest: The authors have declared that no conflict of interest exists.
Submitted: May 13, 2014; **Accepted:** October 2, 2014.
Reference information: *J Clin Invest.* 2014;124(12):5466–5480. doi:10.1172/JCI77053.

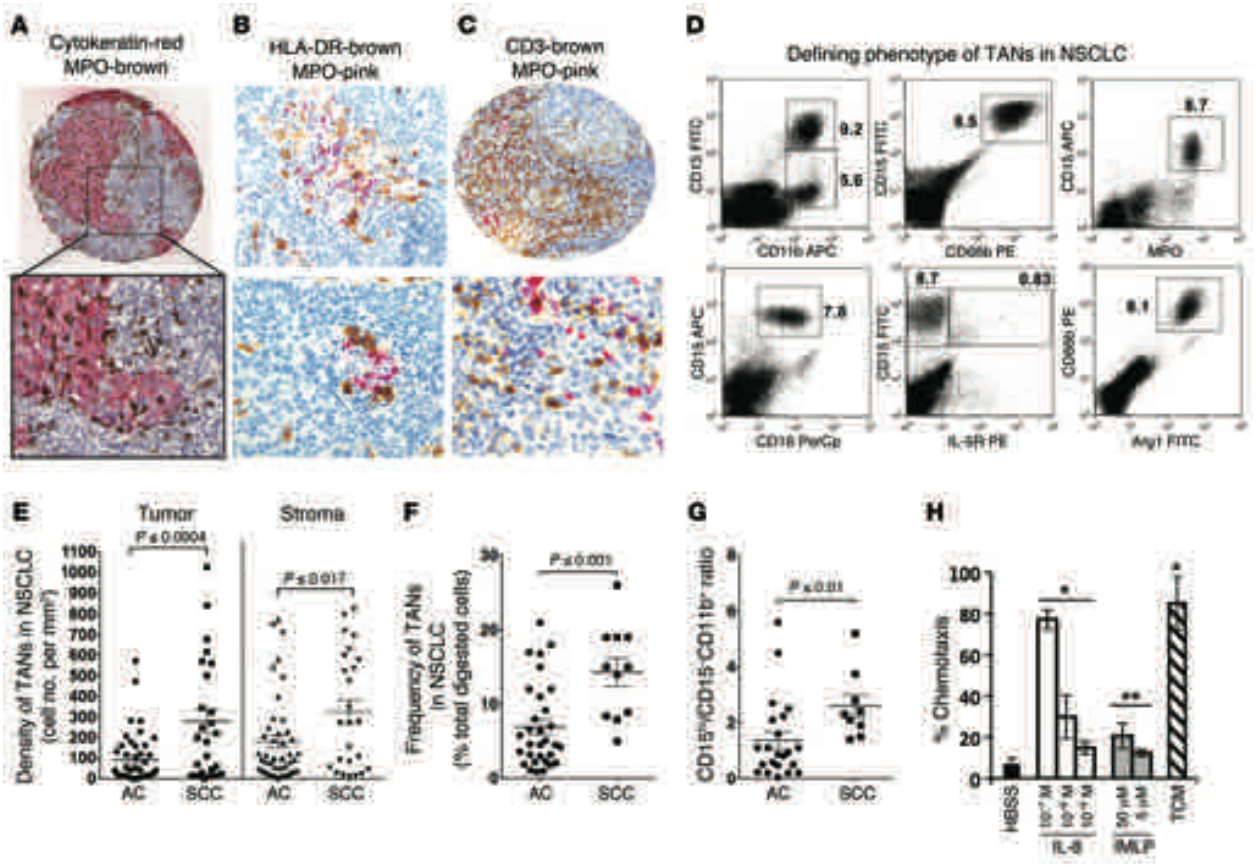

Figure 1. Neutrophils infiltrate NSCLC tissue. (**A**–**C**) Lung cancer tissue sections were stained using 2-color immunohistochemistry for MPO, HLA-DR, and CD3 to visualize neutrophils, APCs, and T lymphocytes, respectively. Representative images are shown. Original magnification, ×10 (**A** and **C**, top), ×20 (**B**, top), ×40 (bottom). (**D**) Representative dot plots of total tumor cells that define the phenotype of TANs in NSCLC. TANs were defined as $CD15^{hi}CD66b^{+}CD11b^{+}CD16^{int}Arg1^{+}MPO^{+}IL\text{-}5Ra^{-}$. Results represent 1 of 20 experiments. Numbers represent the percentage of TANs. (**E**) Comparative immunohistochemical analysis of TAN density (cells/mm²) in AC (n = 45) and SCC (n = 25) performed by counting of MPO^{+} cells in the tumor stroma and the tumor islets. Statistical analyses were performed with Student's t test for unpaired data. (**F**) The frequency of TANs in AC (n = 31) and SCC (n = 11) determined by flow cytometry as the percentage of $CD11b^{+}CD15^{hi}CD66b^{+}$ cells among all cells in tumor. Cumulative results from 42 independent experiments are shown in the scatter plot. Student's t test for unpaired data. (**G**) The ratio of TANs to other $CD15^{-}CD11b^{+}$ cells in AC (n = 22) and SCC (n = 9). Mann-Whitney test for unpaired data. For all scatter plots, error bars represent mean ± SEM. (**H**) PBNs were analyzed for migration in the Neuro Probe ChemoTx system. Each experiment was run in triplicate and repeated at least 3 times. Results of 1 representative experiment are shown. Error bars represent mean ± SEM. Statistical analysis was performed with Kruskal-Wallis and Dunn's multiple comparison tests (*$P \le 0.05$, **$P \le 0.01$). fMLP, N-formyl-methionyl-leucyl-phenylalanine.

and provide accessory signals for T cell activation (19–22). Other studies have suggested that peripheral blood neutrophils (PBNs) can suppress antigen-nonspecific T cell proliferation through the release of arginase-1 and the production of ROS (23–25). To date, the suppressive function of granulocytic cells in cancer patients has generally been attributed to a circulating low-density granulocytic myeloid-derived suppressor cell (G-MDSC) population (26–28). However, there is some uncertainty about whether G-MDSCs exist in humans and whether they are simply a sequela of disease progression. Thus, given the unclear role of neutrophils in the regulation of T cell responses, a second major goal of this study was to determine the effects of TANs on T cell activation.

Results

Intratumoral neutrophils constitute a significant portion of infiltrating cells in lung cancers. To identify and localize TANs, sections from tumor microarrays containing 45 adenocarcinomas (ACs) and 25 squamous cell carcinomas (SCCs) were double-stained for cytokeratin to identify tumor cells (red) and myeloperoxidase (MPO) to identify TANs (brown) (Figure 1A). The median numbers of MPO^{+} cells present in the tumor islets and stroma in AC (40 cells/mm² and 97 cells/mm², respectively) were significantly less ($P < 0.02$) than those seen in SCC (197 cells/mm² and 269 cells/mm², respectively) (Figure 1E).

Double staining of tumor sections with MPO and HLA-DR or CD3 revealed that neutrophils often colocalized with APCs (Figure 1B) and T cells (Figure 1C) throughout the lung tumor microenvironment. In some cases, TANs were more associated with microabscesses or coagulative necrosis (Figure 1B, top).

To perform a more detailed evaluation of TANs by multicolor flow cytometry, the generation of high-quality single-cell suspensions is required. We tested several commercially available

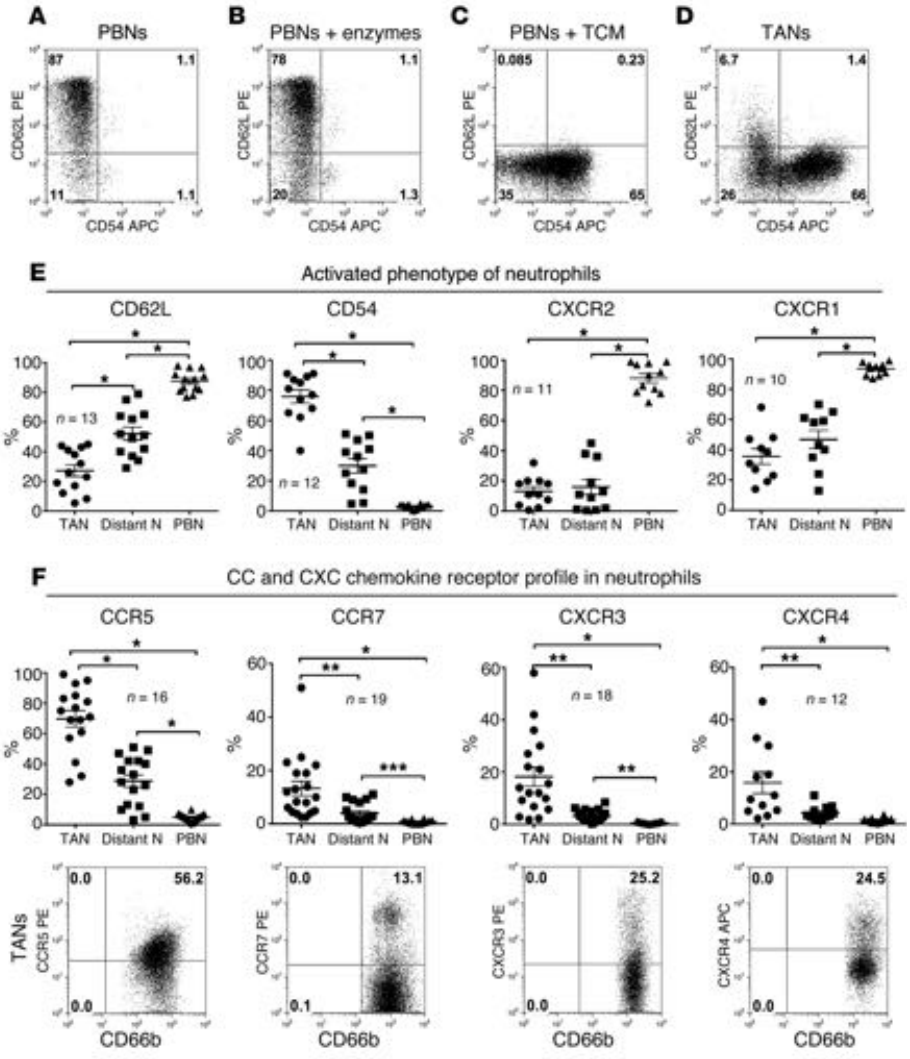

Figure 2. TANs acquire an activated phenotype and novel repertoire of chemokine receptors. (**A**) Expression of the activation markers CD62L and CD54 on CD15^{hi}CD66b^{+} PBNs. PBNs were isolated from lung cancer patients using anti-CD15 beads. Results represent 1 of 5 experiments. (**B**) Digestion protocol did not elicit premature activation of resting PBNs. Results represent 1 of 5 experiments. (**C**) PBNs acquire an activated CD62L^{lo}CD54^{+} phenotype after treatment with TCM in plates with ultralow attachment surface. Each experiment was repeated at least 5 times. (**D**) A single-cell suspension was obtained from freshly harvested tumor tissues. TANs were gated on CD11b^{+}CD15^{hi}CD66b^{+} cells and further analyzed for the expression of activation markers. TANs displayed an activated CD62L^{lo}CD54^{+} phenotype. Results represent 1 of 12 experiments. (**E**) Expression of the activation markers on gated CD11b^{+}CD15^{hi} TANs, distant lung neutrophils (Distant N), and PBNs. (**F**) Expression of CCR5, CCR7, CXCR3, and CXCR4 was analyzed on gated CD11b^{+}CD15^{hi}CD66b^{+} TANs, distant lung neutrophils, and PBNs of cancer patients. Bottom: Representative dot plots. Numbers represent the percentage of cells in each quadrant. Top: Summary of all patient data. Error bars represent mean ± SEM. Statistical analyses were performed with repeated-measures 1-way ANOVA with Tukey's multiple comparison test for CD62L, CD54, CXCR2, CXCR1, and CCR5, and Kruskal-Wallis and Dunn's multiple comparison tests for CCR7, CXCR3, and CXCR4 (*$P \le 0.001$, **$P \le 0.01$, ***$P \le 0.05$).

and individually customized enzymatic cocktails to optimize cell yield, cellular viability, myeloid cell population recovery, preservation of myeloid cell surface marker expression, and induction of neutrophil activation (Supplemental Figure 1; supplemental material available online with this article; doi:10.1172/JCI77053DS1). We selected a combination cocktail (described in Methods) that was composed of several enzymes used at low concentrations and led to a high yield of viable single cells (Supplemental Figure 1, A and B) with minimal enzyme-induced ex vivo effects on neutrophil activation (Figure 2, A and B) and cleavage of myeloid and lymphoid cell markers (Supplemental Figure 1, C–G). Once optimized, we studied tumors from 86 non–small-cell lung carcinoma patients with stage I–II SCC and AC histology. The detailed patient characteristics are shown in Supplemental Table 1.

Single-cell suspensions from these fresh human lung tumors were stained for neutrophil markers (CD15, CD66b, MPO, and arginase-1 [Arg1]), myeloid lineage markers (CD11b, CD16, and CD33), and the eosinophil marker IL-5Rα, by flow cytometry. TANs were defined as CD15^{hi}CD66b^{+}CD11b^{+}MPO^{+}Arg1^{+}CD16^{int} cells (Figure 1D). Importantly, the CD15^{hi}CD66b^{+}CD11b^{+} granulocytes had negligible expression of the eosinophil-associated surface marker IL-5Rα (Figure 1D). In multicolor tracings, we defined TANs as either CD15^{hi}CD11b^{+} or CD66b^{+}CD11b^{+}, since there was a 100% concordance between CD15 and CD66b (Figure 1D).

The CD15^{hi}CD11b^{+} TANs were found to be present in varying frequencies, ranging from 2% to 25% of live cells in the tumor microenvironment in all of the NSCLC studied (Figure 1F). In agreement with the immunohistochemical data (Figure 1E), the frequency of TANs and the CD15^{hi}CD11b^{+} to CD15^{-}CD11b^{+} ratio were significantly higher ($P = 0.001$) in patients with SCC (~15% of live cells; ratio of 2.6) compared with patients with an AC (~7% of live cells; ratio of 1.4) (Figure 1, F and G). This indicates that CD15^{hi}CD11b^{+} TANs constituted the major proportion of CD11b^{+} tumor-infiltrating myeloid cells in patients with SCC. It is noteworthy that the proportion of TANs in tumor tissue of both histological types did not correlate with tumor size (Supplemental Table 2 and Supplemental Figure 5, A–C). Importantly, the density of intratumoral neutrophils was not associ-

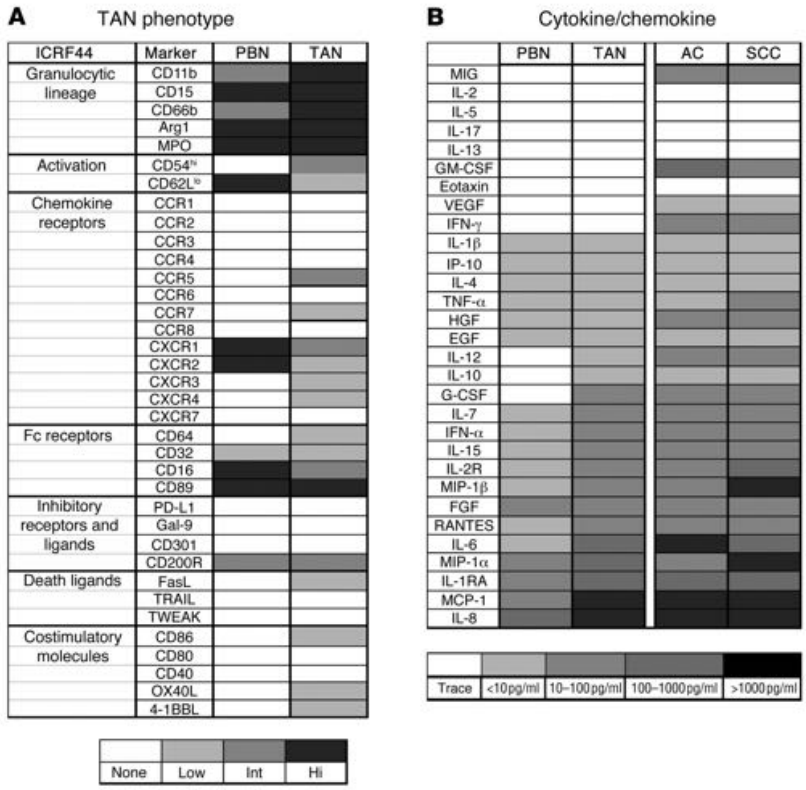

Figure 3. Characterization of TANs. (**A**) Heat map comparing the phenotypes of TANs and PBNs. A single-cell suspension was obtained from freshly harvested tumor tissues, and expression of the indicated markers was assessed using flow cytometry. TANs were gated on $CD11b^{+}CD15^{hi}$ cells and further analyzed for the expression of indicated markers. PBNs were treated similarly to TANs. Expression of each marker was analyzed in 10–18 patients. The intensity key for the heat map is shown below. (**B**) The cytokine/chemokine production by TANs, PBNs, and total tumor dissociates of AC and SCC. TANs and PBNs were isolated from tumor tissues and peripheral blood of lung cancer patients ($n = 5$) using magnetic beads. Purified neutrophils and unseparated cells from digested tumor were cultured for 24 hours in the cell culture medium, and cell-free supernatants were collected and frozen. The indicated factors were detected using the Cytokine Human 30-Plex assay. The presence of each secreted factor was heat-mapped on the basis of the concentration in tested supernatants, as indicated below.

ated with smoking use in the patients (Supplemental Table 2 and Supplemental Figure 5D).

To determine whether the tumor microenvironment stimulates trafficking of neutrophils, resting PBNs were assayed for transwell migration in the presence of tumor-conditioned medium (TCM) collected from digested tumors. In this assay, we observed that TCM induced a strong chemotactic response in blood neutrophils (Figure 1H). In fact, TCM was as efficient as high concentrations of IL-8, a known neutrophil chemotactic factor, in attracting $CD15^{+}$ granulocytes (Figure 1H).

Neutrophils are activated in the tumor microenvironment in patients with NSCLC. Since changes in cell adhesion molecules (CD62L, CD54) and CXC chemokine receptors (CXCR1, CXCR2) have been reported to correlate with leukocyte activation, augmented chemotaxis, and transendothelial migration (29, 30), these markers were measured on circulating and tumor-associated $CD11b^{+}CD15^{hi}$ neutrophils. There was no significant difference between lung cancer patients and healthy donors in the expression of these markers on PBNs; these neutrophils shared the phenotype of resting naive cells, i.e., $CD62L^{hi}CD54^{-}CXCR1^{hi}CXCR2^{hi}$ (Figure 2, A and E).

Previously, others have described a distinct subset of activated $CD11b^{+}CD14^{-}CD15^{+}CD33^{+}$ low-density granulocytes in the PBMC fraction of patients with advanced stages of NSCLC (31). This population has been referred to as granulocytic myeloid-derived suppressor cells (G-MDSCs), because of their ability to suppress T cell proliferation (32). We analyzed PBMCs from 20 healthy donors and 20 lung cancer patients at early stages of disease for the presence of G-MDSCs and found that their frequency in cancer patients was low and not significantly different from the frequency in healthy donors (0.9% ± 0.17% and 0.7% ± 0.18%, respectively).

Next, we evaluated the expression of activation markers on $CD11b^{+}CD15^{hi}$ TANs and neutrophils isolated from lung tissue adjacent to the lung cancer (Distant N; Figure 2E). Notably, the digestion protocol did not elicit premature activation of resting PBNs (Figure 2B). In contrast to PBNs, $CD11b^{+}CD15^{hi}$ TANs markedly upregulated CD54 and downregulated CD62L, CXCR1, and CXCR2 (Figure 2, D and E), acquiring the phenotype of highly activated cells ($CD62L^{lo}CD54^{+}CXCR1^{lo}CXCR2^{lo}$). However, when resting PBNs were isolated from healthy donors and cultured in the presence of primary TCM, they rapidly acquired an activated $CD62L^{lo}CD54^{hi}$ phenotype, suggesting that tumor-derived factors are sufficient to trigger these changes (Figure 2C). Similarly to TANs, neutrophils from distant noninvolved lung downregulated the expression of CXCR1 and CXCR2 when compared with PBNs. However, the analysis of the CD54 and CD62L expression demonstrated that distant neutrophils were less activated compared with TANs (Figure 2E). There were no differences in the expression of activation markers on TANs between patients with AC and SCC (Supplemental Table 2).

Phenotypic changes in tumor-infiltrating neutrophils. There is growing evidence that the inflammatory microenvironment may induce a novel chemokine receptor repertoire on infiltrating neutrophils that increases their functional responsiveness to surrounding chemokines (33). Thus, we determined whether neutrophils gained a new chemokine receptor expression profile in lung tumors.

Peripheral blood and tumor-associated $CD11b^{+}CD15^{hi}CD66b^{+}$ neutrophils from patients with lung cancer were assayed for a wide

array of CC (CCR1–CCR7) and CXC (CXCR1–CXCR7) chemokine receptors. Subpopulations of TANs expressed CCR7, CXCR3, and CXCR4, whereas these chemokine receptors were absent on PBNs (Figure 2F and summarized in Figure 3A). Virtually all TANs expressed high levels of CCR5, which was absent on PBNs (Figure 2F). Interestingly, the proportion of CCR5-positive TANs was significantly higher in patients with AC compared with SCC ($P = 0.04$) (Supplemental Table 2). In addition, CXCR1 and CXCR2 were dramatically downregulated on TANs and distant neutrophils (Figure 2E). The expression of CCR5, CCR7, and CXCR3 on the distant neutrophils was significantly higher in comparison with PBNs ($P < 0.01$) and significantly lower in comparison with TANs ($P < 0.01$). These differences in chemokine receptor expression were consistent, regardless of whether they were measured by cell surface expression (MFI) or as a percentage of chemokine receptor–positive neutrophils. Importantly, there were no differences in the expression of CC and CXC receptors on PBNs between healthy donors and patients with stages I–II NSCLC (data not shown).

The activation of neutrophils has also been suggested to lead to the upregulation of inhibitory receptors and ligands that negatively regulate T cell responses (34–37). However, the expression of PD-L1, galectin-9, CD200R, and CD301 was not increased on TANs in 10 patients with early stages of AC or SCC (Figure 3A). In addition, we found that TANs expressed low levels of FasL and the FcRI receptor CD64 (albeit higher than PBNs), whereas the expression of the FcγRIII receptor CD16 was downregulated compared with that seen on PBNs (Figure 3A).

Engagement of CD15 or CD66b molecules in the isolation of TANs. Given studies that show minimal effects of positive selection of granulocytes by anti-CD15 Ab–conjugated magnetic microbeads on ROS production or phagocytosis (38), we used a combination of our tumor digestion protocol and anti-CD15 microbeads to isolate granulocytes from digested tumors and peripheral blood for functional studies. We first treated peripheral blood of healthy donors with the enzymatic cocktail, and then isolated neutrophils using anti-CD15 microbeads. Analysis of the expression of the activation markers CD62L and CD54 on PBNs indicated that these cells were not prematurely activated or adversely affected by this process (Figure 2, A and B). Using this approach, we found that isolation of TANs with the anti-CD15 microbeads yielded high neutrophil purity, as defined by the $CD15^{hi}CD66b^{+}CD11b^{+}MPO^{+}Arg1^{+}$ phenotype (Supplemental Figure 3A). We verified the cellular purity of TANs in every patient by flow cytometry and cytomorphology. TANs isolated with purity less than 90% were discarded. Over 95% of the sorted cells expressed the neutrophilic markers CD11b, MPO, CD66b, and Arg1. Cytospins were prepared from isolated TANs, and pathological review confirmed that the cytomorphology of these cells was consistent with granulocytes (Supplemental Figure 3D). Importantly, annexin V and propidium iodide (PI) staining of isolated $CD15^{+}$ PBNs showed that only 9% ± 3% of the cells were in apoptosis, indicating that significant cell death was not occurring during the isolation procedures (Figure 4, A and B). $CD15^{hi}CD66b^{+}CD11b^{+}$ TANs isolated from the majority of patients with lung cancer were MPO and Arg1 positive (Supplemental Figure 3, B and C). However, in some patients we found that the fraction of TANs had reduced intracellular MPO and Arg1, suggesting that these enzymes had already been released in the tumor tissue before isolation. Isolation of TANs and PBNs using positive selection with engagement of CD66b demonstrated similar results (data not shown).

Cytokine/chemokine profile of TANs and total NSCLC cells. To describe the range of inflammatory factors secreted by neutrophils in lung cancer patients, 24-hour cell culture supernatants from purified TANs and PBNs were analyzed by a multiplexed fluorescent bead–based immunoassay. In addition, we analyzed these factors in the supernatants collected from total cells of digested AC or SCC. The heat map in Figure 3B shows that many chemokines and cytokines were upregulated in the TAN group. TANs isolated from patients with AC or SCC, compared with PBNs from the corresponding patients, had significantly increased ($P < 0.05$) production of the proinflammatory factors MCP-1, IL-8, MIP-1α, and IL-6 (Figure 3B). Importantly, TANs were able to simultaneously secrete considerably more of the antiinflammatory IL-1R antagonist compared with PBNs.

Interestingly, the analysis of cytokines secreted by digested tumors harvested from 5 patients with AC and 5 patients with SCC revealed a relative preponderance of the Th1 proinflammatory cytokines IFN-γ (100 ± 58 pg/ml), IL-12 (18 ± 4 pg/ml), and TNF-α (81 ± 27 pg/ml), compared with the Th2 cytokines IL-4 (2.6 ± 1.8 pg/ml), IL-5 (not detectable), IL-10 (9.8 ± 3 pg/ml), and IL-13 (not detectable) (Figure 3B). The concentration of the proangiogenic cytokine VEGF was extremely low (8 ± 2.7 pg/ml) in the supernatants from digested AC and SCC. Several prominent NSCLC-derived cytokines, such as IL-8, MCP-1, IL-1RA, GM-CSF, and MIG, were present in high quantities in the cell culture supernatants collected from total cells of AC and SCC. However, there were some significant differences ($P < 0.05$) in the cytokine production between the tumor types. Compared with AC, SCC had significantly increased secretion of MIP-1α, MIP-1β, TNF-α, and IL-2R. In contrast, AC produced significantly ($P < 0.05$) more IL-6 and GM-CSF. MIP-1α has been shown to promote neutrophil chemotaxis (39); therefore its increased production in SCC may explain the high number of TANs relative to AC (Figure 3B).

TANs exhibit high phagocytic activity, and the ability to generate ROS in vitro. To assess functionality, PBNs and TANs were isolated from the same cancer patient and evaluated for their ability to survive in culture, phagocytose bacteria, and produce ROS in vitro.

There was no significant difference in the number of apoptotic cells in freshly isolated PBNs and TANs (5% ± 2.8% and 9% ± 3% of annexin $V^{+}PI^{-}$ and annexin $V^{+}PI^{+}$ cells, $P = 0.4$, respectively) (Figure 4A, top dot plots, and Figure 4B). After 20 hours in culture, there was no survival advantage for TANs compared with PBNs (Figure 4A, center dot plots, and Figure 4B). However, when either freshly isolated PBNs or TANs were cultured in the presence of TCM, these cells had substantially increased survival time compared with PBNs and TANs that were cultured in standard medium (Figure 4, A and B). About 40% of PBNs and TANs cultured in the presence of TCM were still viable at 48 hours (Figure 4B). These data suggest that tumor-derived factors prolong neutrophil survival in the tumor microenvironment.

Next, we examined the phagocytic activity of TANs and resting PBNs by measuring the uptake of red fluorescent pHrodo *E. coli* bioparticles. The results showed that TANs phagocytosed the bioparticles as efficiently as PBNs (Figure 4D). There was no

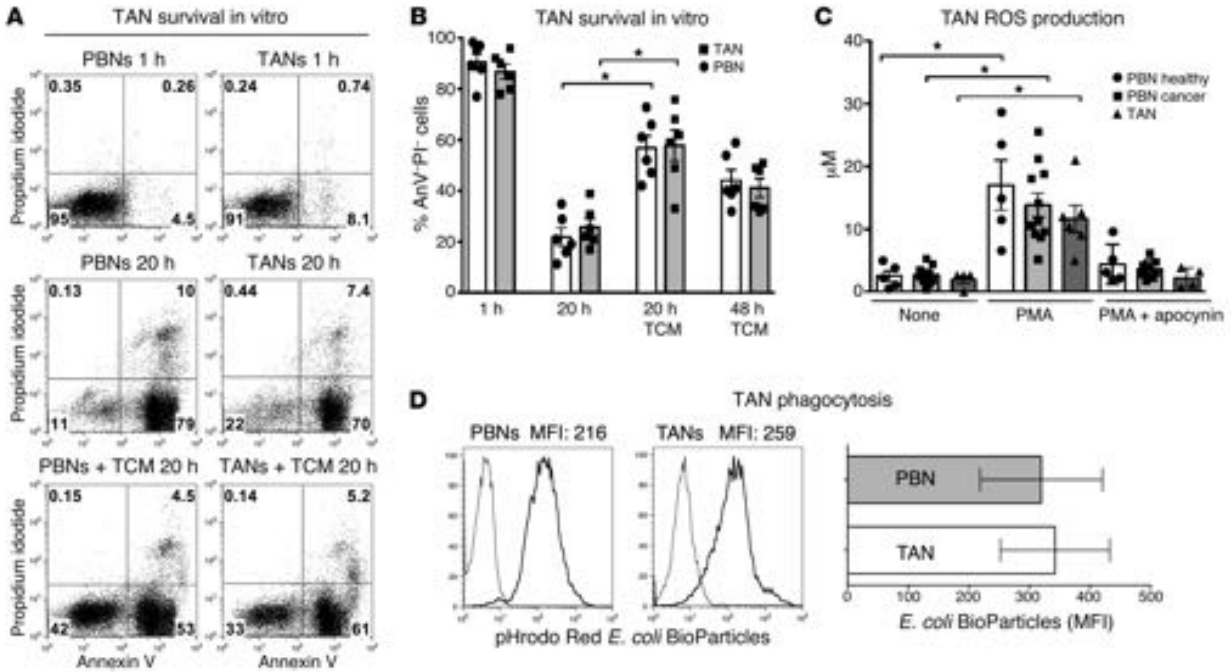

Figure 4. Characterization of neutrophils isolated from tumor tissues and peripheral blood of patients with NSCLC. (**A** and **B**) Neutrophil survival in vitro. TANs and PBNs were isolated from lung cancer patients with magnetic beads by positive selection. Cells were cultured in cell culture medium with or without TCM for 20 and 48 hours. TANs and PBNs were then assessed for apoptosis by FACS analysis of annexin V/PI staining at 1, 20, and 48 hours. Dot plots represent 1 of 6 similar experiments. Numbers represent the percentage of cells in each quadrant. Summary results from 6 lung cancer patients are also shown (*$P \leq 0.01$, Wilcoxon matched-pairs rank test). (**C**) Production of H_2O_2 in TANs and PBNs isolated from lung cancer patients and healthy donors was measured using Amplex Red with horseradish peroxidase. Error bars represent mean ± SEM from 5 independent experiments (*$P \leq 0.001$, Wilcoxon matched-pairs rank test). (**D**) Phagocytic capacity of TANs. TANs and PBNs were isolated and incubated with pHrodo Red *E. coli* BioParticles for 45 minutes to allow phagocytosis (internalized particles become fluorescent [red]). Histograms from 1 representative experiment are shown. Phagocytosis performed at 4°C and 37°C is shown by thin and thick lines, respectively; MFI values are as indicated in histograms. Summary results from 6 lung cancer patients are also shown (Wilcoxon matched-pairs rank test).

difference in the phagocytic activity between PBNs from cancer patients and healthy donors (data not shown).

We also quantified the spontaneous and PMA-stimulated ROS production by circulating and tumor-associated neutrophils using the Amplex Red assay. Despite the fact that TANs were activated, spontaneous ROS production was minimal and no different from that of resting PBNs from lung cancer patients or healthy donors (Figure 4C). However, the stimulation of PBNs and TANs with PMA resulted in a dramatic increase in H_2O_2 production, suggesting that TANs were not dysfunctional and could be stimulated further (Figure 4C). Mechanistically, ROS production in the neutrophils was mediated by the NADPH oxidase complex (NOX), since coculture of the TANs with the NOX inhibitor apocynin substantially decreased PMA-induced ROS generation (Figure 4C).

Together, our data on isolated TANs show that when appropriately triggered, they can perform major functions such as phagocytosis and ROS production, suggesting that they are not "exhausted" or hypofunctional.

Neutrophils from malignant and nonmalignant lung tissue stimulate antigen-nonspecific T cell proliferation. Multiple reports suggest that MDSCs in human and murine tumors are partially composed of granulocytic cells, and that these populations tend to negatively modulate effector T cell functions (27, 40). Accordingly, we measured the effect of TANs on lymphocyte proliferation in a CFSE-based T cell suppression assay. First, in order to validate this assay in our hands, we isolated Tregs (effectors) from the peripheral blood of lung cancer patients and cocultured them with CFSE-labeled healthy donor PBMCs (responders) that had been stimulated with plate-bound anti-CD3 Abs. As expected, after 4 days, we found that the proliferation of both $CD4^+$ and $CD8^+$ T cell populations exposed to Tregs was markedly suppressed compared with that of control cells (Supplemental Figure 2A).

Next, we performed similar experiments in which PBNs or TANs (effectors) were isolated from cancer patients and cocultured with healthy donor PBMCs (responders) that had been stimulated with plate-bound anti-CD3 Abs. We found that the proliferation of stimulated T cells after 4 days was not altered by exposure to PBNs (Figure 5A). Surprisingly, when the stimulated PBMCs were cocultured with TANs, the proliferation of $CD4^+$ and $CD8^+$ cells was markedly augmented. Specifically, whereas approximately 50% of control T cells were $CFSE^{lo}$ and underwent 1–6 rounds of cell division, the dividing T cell fraction significantly increased (to as much as 95%) in the presence of TANs (Figure 5A).

Isolation of TANs and PBNs using positive selection with engagement of the CD66b molecule demonstrated similar results (Supplemental Figure 2C). To confirm that our results were not

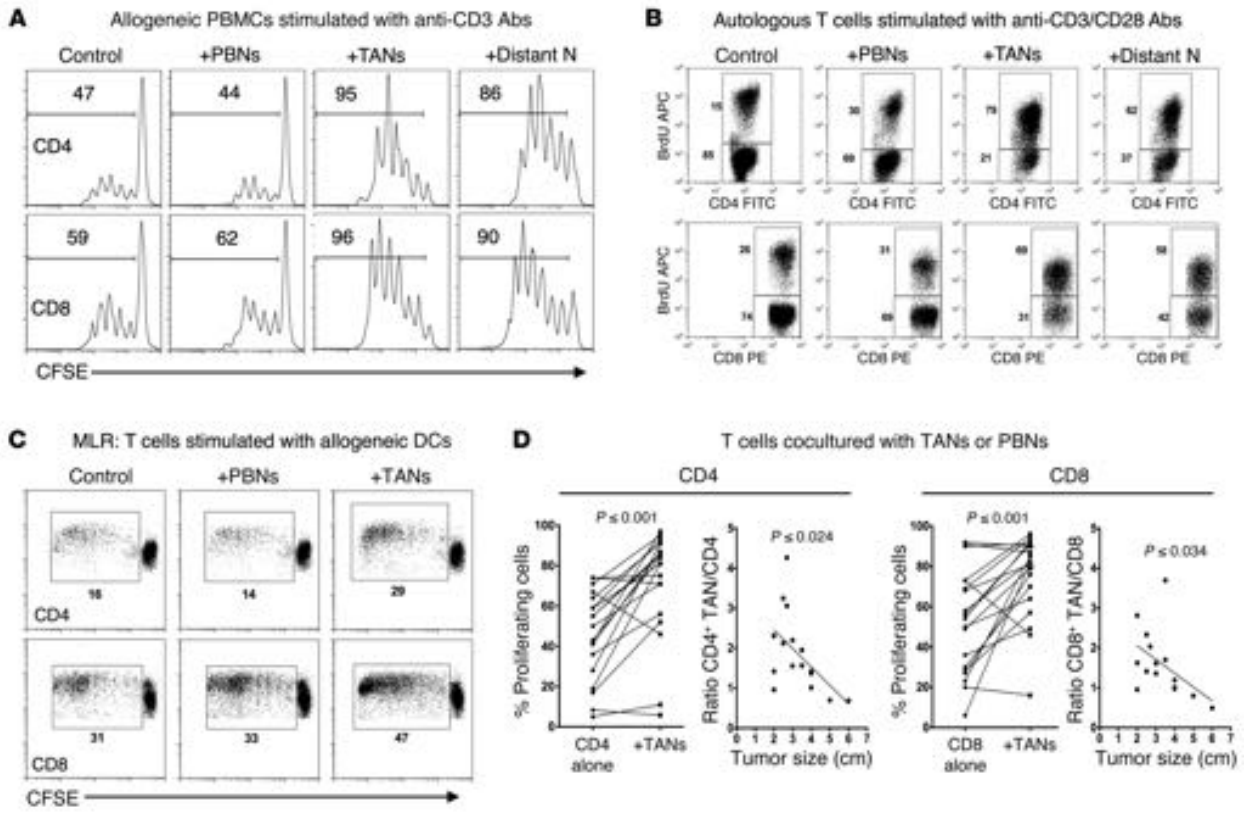

Figure 5. T cell proliferation in the presence of TANs or PBNs. (**A**) CFSE-labeled PBMCs isolated from a healthy donor were stimulated with plate-bound anti-CD3 Abs and mixed with TANs, neutrophils from distant lung tissue, or PBNs isolated from cancer patients at a 1:1 ratio for 4 days. Representative results from 1 of 12 experiments are shown. Numbers on histograms represent the percentage of proliferating T cells. (**B**) Autologous T cells were purified from PBMCs, stimulated with plate-bound anti-CD3 Abs and anti-CD28 Abs, and cultured alone or with PBNs, distant neutrophils, or TANs. 72 hours later, proliferation of T cells was assessed by incorporation of BrdU into DNA. Representative results from 1 of 5 experiments are shown. (**C**) Mixed lymphocyte reaction (MLR). CFSE-labeled T cells isolated from PBMCs of healthy donors were stimulated with allogeneic DCs in the absence or presence of PBNs or TANs for 5 days. Representative results from 1 of 5 experiments are shown. Numbers on dot plots represent the percentage of proliferating T cells. (**D**) Change in percentage of proliferating $CFSE^{lo}$ $CD4^+$ and $CD8^+$ cells cultured alone versus cells cultured in the presence of TANs (Student's *t* test, paired parametric test). Autologous PBMCs were stimulated with plate-bound anti-CD3 Abs and mixed with TANs at a 1:1 ratio for 4 days. Scatter plots show the correlation between tumor size and stimulatory activity of TANs defined as the ratio $CFSE^{lo}$ (T cells +TANs)/$CFSE^{lo}$ (T cells) (nonparametric Spearman correlation). Cumulative results from 16 independent experiments are presented.

due to contamination of our TANs by other tumor-infiltrating cells that may have escaped magnetic bead separation, we repeated the experiments using purified $CD45^+CD11b^+CD15^{hi}CD66b^+$ TANs collected by FACS. In triplicate experiments, the TANs sorted by flow cytometry again showed remarkable stimulatory effects on T cell proliferation (Supplemental Figure 2C).

To ensure that this stimulatory effect was not dependent on the allogenicity between healthy donor responders and patient TANs, or some artifact of the CFSE system, we repeated the T cell proliferation assay using T cells, PBNs, and TANs all isolated from the same patient. A BrdU incorporation assay demonstrated that the majority of T cells (79% of $CD4^+$ and 69% of $CD8^+$ cells) cocultured with TANs were in S phase of the cell cycle by 72 hours after stimulation, compared with only about 15%–30% of control T cells or T cells cocultured with PBNs (Figure 5B). This short-term assay revealed that activated T cells begin to actively synthesize DNA in the presence of TANs by 48 hours after stimulation compared with control T cells or T cells cocultured with PBNs (Supplemental Figure 2E). Interestingly, in this experiment, we found that PBNs and TANs partially liberated Arg1 in the presence of activated T cells (Supplemental Figure 3E). However, the presence of arginase did not seem to affect the rate of T cell proliferation. These data support other studies showing that the arginase, which is liberated following spontaneous polymorphonuclear neutrophil death, is not sufficient for T cell suppression (41).

Neutrophils isolated from distant nonmalignant lung tissue were also able to stimulate allogeneic and autologous T cell proliferation (Figure 5, A and B). However, there was no significant difference in stimulatory activity of distant neutrophils when compared with TANs (Supplemental Figure 2D). This suggests that stimulatory capacity of distant neutrophils is a lung tissue–specific characteristic that might be driven by adjacent early-stage lung tumor.

In order to quantify the extent to which TANs are able to increase T cell proliferation, we mixed TANs with autologous

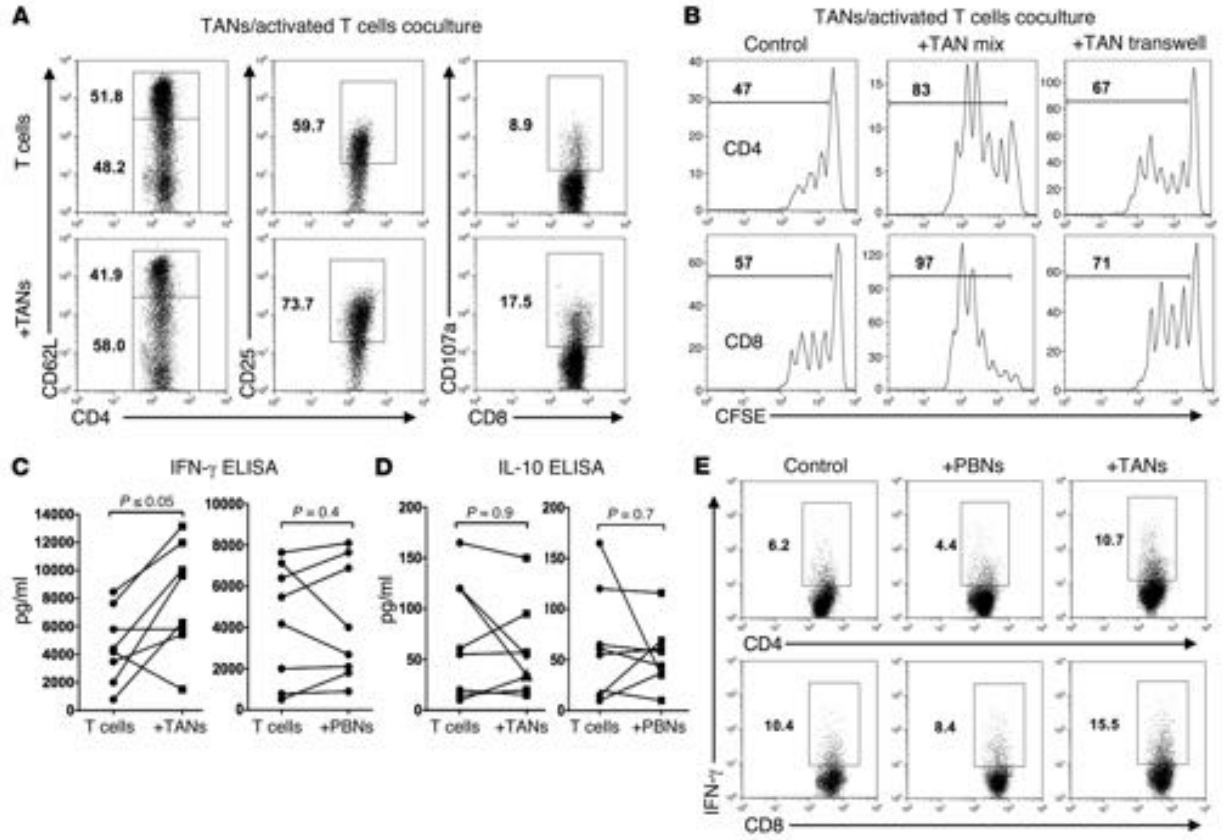

Figure 6. Effect of TANs on T cell activation, cytokine production, and proliferation. In all experiments, T cells were stimulated with plate-bound anti-CD3/CD28 Abs and incubated with TANs at a 1:1 ratio. (**A**) Expression of the CD62L, CD25, and CD107a markers on activated autologous T cells cultured with TANs for 20 hours. Representative dot plots from 1 of 3 experiments are shown. Numbers represent the percentage of $CD4^+$ and $CD8^+$ cells. (**B**) Flow cytometric analysis of autologous T cell proliferation in the presence of TANs using a transwell system. Activated CFSE-labeled T cells were mixed with TANs at a 1:1 ratio (TAN mix). To separate T cells and TANs, activated T cells were cultured in the bottom chamber and TANs were placed in the top chamber of the 24-well flat-bottom transwell culture plate (TAN transwell). Representative results from 1 of 3 experiments are shown. Numbers on histograms represent the percentage of proliferating T cells. (**C** and **D**) IFN-γ (**C**) and IL-10 (**D**) were measured by ELISA in 48- or 96-hour supernatants collected from cocultures of activated T cells with TANs or PBNs. Summary results from 8 lung cancer patients are shown in the graph (Wilcoxon matched-pairs rank test). (**E**) The percentage of IFN-γ– and IL-10–producing T cells cultured with TANs or PBNs was measured by intracellular cytokine staining at 48 hours of stimulation. The dot plots represent 1 of 3 independent experiments. Numbers represent the percentage of $CD4^+$ and $CD8^+$ cells.

PBMCs that had been stimulated with different concentrations of anti-CD3 Abs (Supplemental Figure 2B). Four days later, TANs dramatically increased the proliferation of $CD4^+$ T cells from 15% to 64% ($P < 0.01$) and that of $CD8^+$ T cells from 12% to 61% ($P < 0.01$). Moreover, the coculture of TANs with highly activated T cells (anti-CD3 Abs, 2.5 μg/ml) resulted in even more rapid division of these T cells.

Since the CD3/CD28–stimulated T cell response involves a robust polyclonal T cell proliferation, we investigated the ability of TANs and PBNs to modulate more physiological T cell responses induced by allogeneic DCs in a mixed-lymphocyte reaction. Allogeneic T cells (responders) were purified from the peripheral blood of healthy donors and cocultured with irradiated, mature, monocyte-derived DCs (MoDCs) (inducers) from unrelated donors. TANs or PBNs from patients with stage I–IIB lung cancer were added to the DCs as "third-party cells." Five days later, we found that inclusion of TANs resulted in an increased T cell proliferation that had been initiated by allogeneic MoDCs, compared with control experiments (Figure 5C). These experiments were repeated with TANs from 5 patients with early-stage lung cancer. By day 5, the addition of TANs increased the proliferation of T cells 1.7- to 2.8-fold compared with PBNs. The TANs did not appear to preferentially increase $CD4^+$ versus $CD8^+$ T cell expansion.

Next, we asked whether treatment of PBNs with TCM would recapitulate the ability of TANs to stimulate T cell proliferation. We exposed PBNs from healthy donors to a variety of TCMs collected from digested AC or SCC. The majority of these TCMs prolonged survival time of PBNs up to 48 hours (Figure 4B) and induced the expression of the activation marker CD54 on the surface of PBNs (Figure 2C). However, TCM-treated PBNs were not able to stimulate T cell proliferation to a significant level (Supplemental Figure 3H). This indicates that short-term exposure of mature PBNs to tumor-derived factors is not sufficient to convert PBNs into stimulatory cells.

In total, we analyzed the effect of TANs on the proliferation of T cells from 16 patients with lung cancer. Overall, TANs sig-

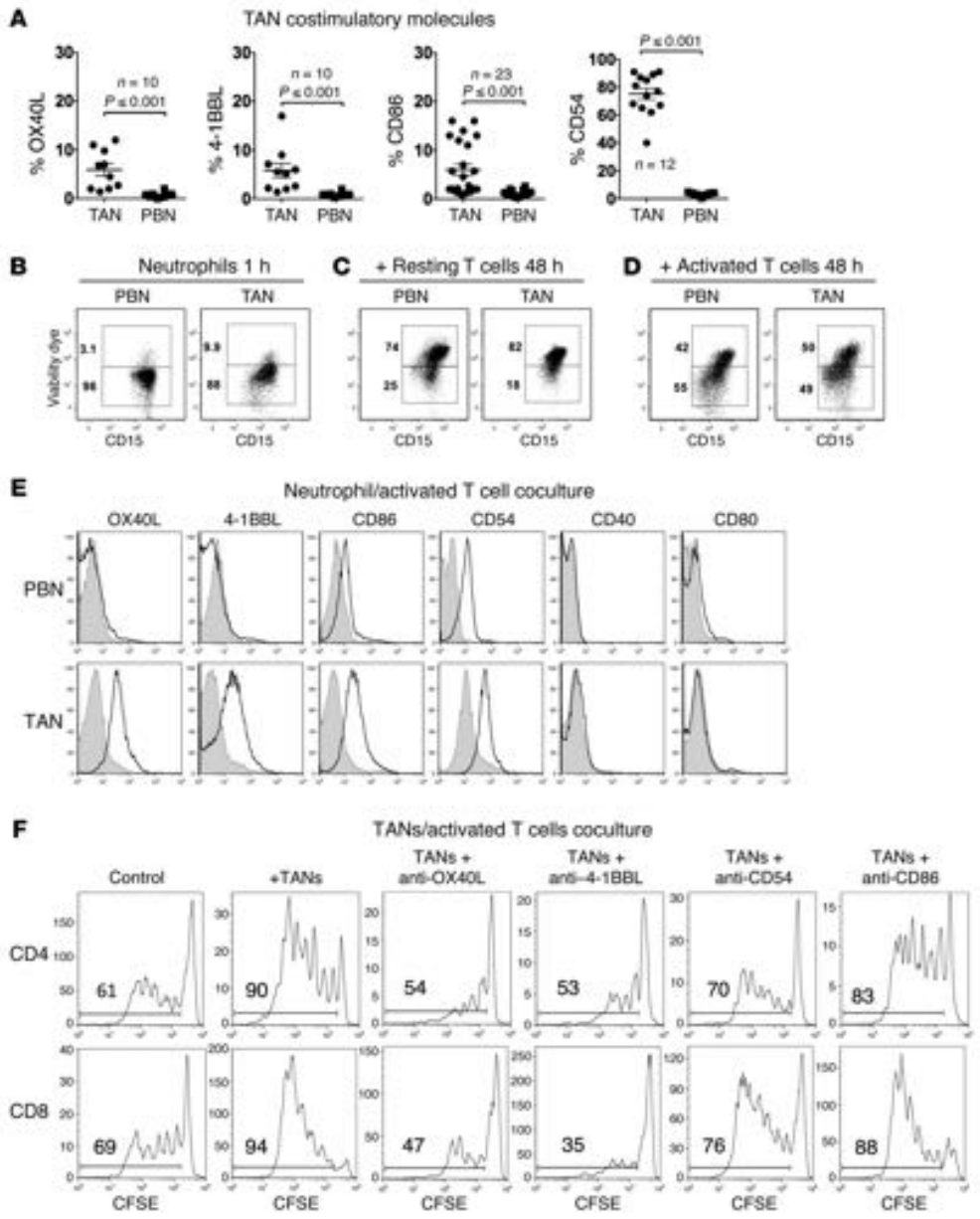

Figure 7. The expression of costimulatory molecules on TANs and their role in stimulation of T cell proliferation. (**A**) The expression of the costimulatory molecules on gated $CD11b^{+}CD15^{hi}$ TANs and PBNs was analyzed by flow cytometry. The top panel summarizes the data for all the patients. Error bars represent mean ± SEM. Statistical analyses were performed with Student's *t* test for paired data. (**B**–**D**) Neutrophil survival in the cell culture. Zombie Yellow Fixable Viability dye was used to discriminate viable CD15 neutrophils cultured alone (**B**) or in the coculture with resting T cells (**C**) and CD3/CD28–activated T cells (**D**). Representative dot plots from 1 of 5 experiments are shown. For all dot plots, numbers represent the percentage of cells in each quadrant. (**E**) The expression of costimulatory molecules was analyzed by flow cytometry on gated live $CD11b^{+}CD15^{hi}$ PBNs (top) and TANs (bottom) after 2 days of coculture with activated (black histograms) or resting autologous T cells (gray histograms). Results from 1 of 5 representative experiments are shown. (**F**) The efficacy of blocking Abs in ablating the stimulatory effect of TANs on T cell proliferation. Autologous PBMCs were stimulated with plate-bound anti-CD3 Abs and mixed with TANs at a 1:1 ratio in the presence or absence of blocking Abs against the indicated receptors for 4 days. Numbers on histograms represent the percentage of proliferating cells. Mouse IgG1 Abs were used as isotype control Abs in the control group. Results from 1 of 3 representative experiments are shown.

nificantly increased the proliferation of both $CD4^{+}$ and $CD8^{+}$ T cells an average of 2.1-fold (range 1.4- to 9-fold) compared with PBNs (Figure 5D; $P = 0.001$). Interestingly, as shown in Figure 5D and Supplemental Table 2, correlation analysis revealed that the majority of TANs from larger tumors were associated with a lower capacity to augment T cell proliferation than TANs from smaller tumors. We also divided lung cancer patients into 2 groups: patients with small tumors (<3 cm, $n = 7$) and patients with large tumors

(>3 cm, $n = 9$). The analysis of these 2 groups using a Mann-Whitney nonparametric test also revealed that stimulatory activity of TANs from small tumors was significantly higher than that of TANs from large tumors (Supplemental Table 2). Interestingly, there were no significant associations between stimulatory activity of TANs and histological type of tumor, tumor stage, and smoking history (Supplemental Table 2 and Supplemental Figure 4, A–C).

TANs enhance T cell activation. To further examine the cross-talk between activated T cells and neutrophils in lung cancer patients, we assayed T cell activation and the capacity of activated T cells to produce cytokines in the presence of TANs or PBNs. T cell activation was assessed within 24 hours of exposure to anti-CD3/anti-CD28 Abs. When T cells were cultured with TANs, they more markedly upregulated CD25 (65% ± 11% vs. 41% ± 17%, $P = 0.001$) and downregulated CD62L (39% ± 14% vs. 54% ± 11%, $P = 0.01$), compared with control T cell populations. A representative experiment depicted in Figure 6A (left and center columns) demonstrates the effect of TANs on the expression of these markers in activated T cells. TANs did not affect CD69 expression on activated T cells (data not shown). We also found that the percentage of activated $CD8^+$ cells expressing the lysosomal marker CD107a (LAMP-1) on the surface was twice as high in TAN/T cell cocultures compared with cultures of control T cells alone (Figure 6A, right column). Together, these data suggest that TANs tend to promote activation of T cells and degranulation of their cytotoxic granules.

The expression of CD25 also defines a distinct population of $CD4^+$ $FOXP3^+$ Tregs with suppressive activity in vitro and in vivo (42). However, after coculture for 4 days, analysis of FOXP3 expression showed no difference in activated $CD4^+$ cells cultured with or without TANs (4.5% ± 1.1% and 5% ± 1.5%, respectively, $P > 0.05$) (Supplemental Figure 3F).

We also determined whether TANs or PBNs modulated the production of key Th1 or Th2 cytokines in activated T cells. For these experiments, we mixed TANs or PBNs with autologous CD3/CD28–stimulated T cells purified from peripheral blood of patients with NSCLC and quantified IFN-γ and IL-10 in the supernatants 96 hours later. Figure 6C demonstrates that TANs significantly increased IFN-γ production by activated T cells, as TAN/T cell cocultures had a much higher concentration of IFN-γ compared with T cells cultured alone ($P = 0.02$). PBNs isolated from lung cancer patients did not affect the IFN-γ production by activated T cells. Intracellular staining revealed a significant increase in the frequency of IFN-γ–positive $CD4^+$ and $CD8^+$ cells in the coculture with TANs compared with activated T cells cultured alone (Figure 6E). While the percentage of IFN-γ–producing T cells was slightly changed, the stimulation of T cell proliferation by TANs resulted in a larger number of T cells and increased overall cytokine levels in the supernatant after 4 days of coculture. In addition, there was no significant difference in the production of IL-10 by activated T cells cultured with TANs or PBNs (Figure 6D). Intracellular IL-10 was not detected in activated T cells cultured in the presence or absence of TANs and PBNs (data not shown).

Direct cell contact between TANs and T cells is important for T cell stimulation. In order to understand the primary mechanism of TAN/T cell effects, we investigated whether direct cellular contact was necessary for TANs to stimulate T cell proliferation, using a transwell assay system that separated the TANs or PBNs from the T cells. The PBNs isolated from healthy donors or lung cancer patients did not induce the stimulation of T cell proliferation when the cells were mixed or separated (data not shown). When in direct contact, TANs induced a much higher level of T cell proliferation than in the transwell system, in which TANs were physically separated from activated T cells (Figure 6B). These data indicate that cellular contact is likely the chief mechanism by which TANs augment T cell proliferation. However, the TANs isolated from several patients demonstrated some stimulatory effect on T cells even when the cells were separated, suggesting that secreted factors are also involved in the stimulation of T cell proliferation, but to a lesser extent (Figure 6B, right column).

Expression of costimulatory molecules on TANs and their role in the stimulation of T cell proliferation. Given that the strong stimulatory effect of TANs on T cell proliferation was dependent on direct cell contact, we quantified the expression of costimulatory molecules (CD86, CD80, CD40, CD54 [ICAM-1], CD252 [OX40L], and CD137L [4-1BBL]) on the surface of TANs and PBNs by flow cytometry (Figure 7A). Circulating PBNs had minimal to no expression of these costimulatory molecules in all patients. The expression of CD54 was highly increased on the surface of TANs versus PBNs (75% ± 15% vs. 3% ± 1%, $P < 0.001$) (Figure 7A). In addition, we found moderate but statistically significant upregulation of CD86, OX40L, and 4-1BBL on the surface of TANs but not PBNs ($P < 0.001$). Figure 7A demonstrates that the expression of these markers varied widely from 0.5% to 20% among all cancer patients. However, the differences in the expression of these costimulatory molecules on TANs were not significantly correlated with tumor type, size, or stage (Supplemental Table 2 and Supplemental Figure 4, E–H). We were not able to detect the expression of CD80 or CD40 markers on the surface of TANs.

Given that TANs enhance the activation of T cells during cell coculture, we examined whether activated T cells, in turn, upregulate the expression of costimulatory molecules in TANs to further bolster their own proliferation. To test this hypothesis, we activated T cells with plate-bound anti–CD3/CD28 Abs and mixed them with autologous TANs or PBNs. Two days later, flow cytometry was used to characterize the viability of neutrophils cocultured with activated T cells and expression of costimulatory molecules on gated live $CD11b^+CD15^+$ TANs. Flow cytometry revealed that in the presence of activated T cells, the TANs and PBNs survived longer than neutrophils cultured with resting T cells (Figure 7, B–D). The activated T cells increased the lifespan of TANs and PBNs to 4 days (Supplemental Figure 3G). Importantly, TANs cocultured with activated T cells markedly upregulated OX40L, 4-1BBL, CD54, and CD86 costimulatory molecules, whereas PBNs increased expression of only CD86 and CD54 (Figure 7E). These data suggest that a preexisting activated state of TANs or some enhanced plasticity is required for subsequent T cell–induced upregulation of these costimulatory molecules. CD80 and CD40 continued to show low levels of expression on PBNs and TANs following exposure to activated T cells.

Next, we investigated the functional significance of these costimulatory molecules. In 3 experiments, TANs and CFSE-labeled activated autologous T cells were cocultured in the presence of blocking Abs against these upregulated costimulatory molecules. Figure 7F shows a representative experiment (all 3 showed the same results)

where the stimulatory effect of TANs was partially abrogated in the presence of anti-CD54 and -CD86 blocking Abs (right columns). The most pronounced effect was observed when anti-OX40L or anti–4-1BBL blocking Ab was added to the T cell/TAN coculture. These Abs completely blocked the strong stimulatory activity of TANs (Figure 7F, center columns). Notably, in the control groups, the proliferation of T cells without TANs was not affected by the presence of any of these blocking Abs. These data suggest that TANs enhance T cell proliferation by direct cell-cell signaling, likely due to the OX40L/OX40 and 4-1BBL/4-1BB pathways. Both pathways appear equally important for T cell proliferation.

Taken together, these results suggest that there is ongoing cross-talk between activated T cells and TANs that results in dramatic upregulation of costimulatory molecules on the surface of TANs, which enhances T cell proliferation. This interaction between the innate and adaptive sides of the immune system requires direct cell-cell interactions due to receptor engagement, although secretory cytokines may have a limited role in this relationship.

Discussion

This study provides a comprehensive phenotypic and functional characterization of tumor-infiltrating neutrophils in early-stage lung cancer patients. Our key observations were that TANs represented a significant proportion of the cellular composition of human lung tumors and that, in contrast to our expectations, early-stage lung cancer TANs were not hypofunctional or immunosuppressive, but were able to stimulate T cell responses.

Our data show that TANs express a "classic" activated phenotype characterized by upregulation of the adhesion molecule CD54 (ICAM-1) and downregulation of CD62L (L-selectin), CXCR1, CXCR2, and CD16 (29, 30). Another major change in the infiltrating neutrophils compared with systemic PBNs was in chemokine receptor expression, including upregulation of CCR5, CCR7, CXCR3, and CXCR4, and downregulation of CXCR1 and CXCR2. It has been suggested that the acquisition of new chemokine receptors by neutrophils at inflammatory sites expands their functional profile (33); however, the exact role of the chemokine receptors expressed on TANs is still unknown, and further studies are required to understand their functional significance.

In this study, we also characterized the phenotype of neutrophils from the nonmalignant lung tissue to demonstrate which characteristics of TANs are specific for the tumor microenvironment and which simply reflect the differences between blood and lung tissue neutrophils. Neutrophils from distant tissue versus TANs were more similar to each other than to blood neutrophils. However, we found that TANs exhibit an even more activated phenotype compared with neutrophils isolated from "distant" noninvolved lung tissue. The level of CCR5, CCR7, CXCR3, and CXCR4 expression on distant neutrophils was intermediate between those of PBNs and TANs. Although these data are interesting, there are some caveats associated with comparison of neutrophils from tumor and distant lung tissue. First, we believe the surrounding nonmalignant lung tissue is likely to be influenced by the adjacent tumor, so neutrophils infiltrating the adjacent lung tissue may not have exactly the same function and phenotype as those infiltrating normal lung tissue. Second, compared with tumor-infiltrating neutrophils, the majority of lung neutrophils likely represent a pool of marginated neutrophils (cells that are adherent to the endothelium of blood vessels of lung tissue) and neutrophils from alveolar space, making them difficult to define as tissue-specific.

In addition to changes in activation, we also found that the tumor microenvironment stabilizes and prolongs the survival of infiltrating neutrophils. In the presence of tumor-conditioned medium (TCM) rich in proinflammatory factors, such as IFN-γ, IL-6, IL-8, and GM-CSF (Figure 4B), TANs and naive blood neutrophils developed a significant survival advantage compared with control neutrophils. This is likely due to the ability of these proinflammatory factors to prolong the lifespan of human neutrophils by delaying apoptosis (43, 44).

Once TANs are activated in the tumor microenvironment, they appear to add to the complexity of the inflammatory milieu and are likely involved in the attraction of other leukocytes. TANs secreted large quantities of IL-8 in cell culture, which has been found to self-promote neutrophil survival and recruit more neutrophils. We also found that TANs released various immunoregulatory cytokines, chemokines, and growth factors, such as the proinflammatory mediators CCL2 (MCP-1), IL-8, CCL3 (MIP-1α), and IL-6, as well as the antiinflammatory cytokine IL-1RA. On the other hand, TANs can secrete factors that could be protumorigenic. MIP-1α may act as a growth, survival, and chemotactic factor for tumor cells (45). In our study, we did not see high levels of proangiogenic VEGF, but there were other growth factors that might support angiogenesis, such as FGF, HGF, and EGF.

Over the last decade, there has been an increasing focus on the interactions between myeloid cells and T cells in tumor-bearing mice. Most of these studies have focused on MDSCs and TAMs. The vast majority of the data suggest that these cells inhibit T cell proliferation and function (46–49). With regard to TAMs, the current paradigm is that these cells are primarily tumor-promoting (M2-type) cells but, under certain conditions, can be reprogrammed into tumor-inhibitory (M1-type) cells with therapeutic potential (50–52). Much less is known about murine TANs; however, work by our group (8) and others (5, 53–55) suggests that a similar N1 (antitumor) and N2 (protumor) polarization exists, and that most advanced tumors harbor N2-like TANs. Given this framework, we anticipated human TANs would inhibit T cell responses in human lung tumors. Unexpectedly, however, freshly isolated TANs from early-stage lung cancer patients did not suppress IFN-γ production or proliferation of T cells that had been activated with anti–CD3/CD28 Abs or allogeneic DCs. Instead, TANs increased T cell IFN-γ production and activation, and dramatically amplified T cell proliferation. Direct cell-cell contact was important for the neutrophil-mediated stimulation of T cell proliferation. One important feature of this interaction was cross-talk and mutual cell activation. With coculture, T cells further upregulated activation markers and produced more IFN-γ, whereas TANs upregulated the costimulatory molecules CD86, CD54, OX40L, and 4-1BBL. These molecules are not constitutively expressed on the surface of circulating neutrophils; however, they can be rapidly translocated from cytoplasmic granules onto the surface of neutrophils or be synthesized de novo under the appropriate circumstances (19, 56).

Follow-up experiments using blocking Abs against various costimulatory molecules showed that the OX40L/OX40 and 4-1BBL/4-1BB pathways were critical in TAN-mediated augmen-

tation of T cell proliferation. 4-1BBL/4-1BB and OX40/OX40L represent a pair of costimulatory molecules critical for T cell proliferation, survival, cytokine production, and memory cell generation, as well as reverse signaling for further activation of APCs (57, 58). Typically, the costimulatory molecules 4-1BBL and OX40L are expressed on APCs, including mature DCs, activated macrophages, and B cells (57). Our data suggest that the 4-1BBL and OX40L costimulatory molecules can also be upregulated on activated TANs as a result of the interaction with activated T cells. Thus, the OX40L/OX40 and 4-1BBL/4-1BB pathways have the potential to enhance antitumor immunity and break tumor-induced immune suppression and immunological tolerance. Furthermore, costimulation through 4-1BBL/4-1BB protects T cells from activation-induced cell death and enhances the antitumor effector functions of $CD8^+$ melanoma tumor–infiltrating lymphocytes (59, 60).

Our data are consistent with previous studies showing that granulocytes can provide accessory signals for T cell activation (19, 21, 22). For instance, Radsak et al. reported that human circulating neutrophils are accessory cells for T cell activation after treatment with IFN-γ and GM-CSF (19). They found that neutrophil-dependent T cell proliferation could be partially inhibited by blocking Abs against MHC class II, CD86, and CD54. Interestingly, our findings showed that lung tumors were able to produce IFN-γ and GM-CSF, as well as to induce expression of CD86 and CD54 costimulatory molecules in TANs. However, blocking CD86 did not substantially inhibit the stimulatory capacity of TANs compared with blocking OX40L or 4-1BBL. Inhibiting CD54 resulted in partial ablation of this effect.

Our data are consistent with some literature showing the antitumor potential of neutrophils during tumor growth in some models (61–63). For instance, Suttmann and colleagues demonstrated that polymorphonuclear neutrophils are an indispensable subset of immunoregulatory cells and orchestrate T cell chemotaxis to the bladder during bacillus Calmette-Guérin immunotherapy (64). Augmentation of T cell proliferation and/or survival by tumor-infiltrating neutrophils was found to be critical in the establishment of antitumor immunity following photodynamic therapy (65). Our group found that the blockage of TGF-β could convert N2 TANs to N1 TANs in murine models of mesothelioma and lung cancer (8).

Can human TANs exert antitumor (N1-like) activity? Although TANs isolated from early-stage lung cancers resemble murine antitumor N1 TANs, our data suggest that as tumors become larger, they become less stimulatory. It is thus possible that TANs from even more advanced tumors may become frankly protumorigenic. This concept, with regard to TANs, has recently been described in a murine tumor model. Mishalian et al. reported that TANs from early tumors were cytotoxic to tumor cells and produced higher levels of TNF-α, NO, and H_2O_2 compared with TANs in larger, established tumors (66). We are trying to test this "myeloid cell immunoediting" hypothesis with TANs from patients with advanced lung cancer (stages III and IV); however, this is logistically challenging since these individuals do not routinely undergo tumor resection and are managed with chemotherapy and radiation therapy.

Our study provides several explanations for the inconsistent data in the literature with regard to prognostic implications of TANs in cancer patients (11, 14–17). To date, most clinical studies have used immunohistochemical analyses of tumors to correlate the presence of granulocytes with prognosis. However, this approach is unable to assess the phenotype of these cells. In this study, we have demonstrated there is a heterogeneous expression of surface receptors on TANs. Thus, subpopulations of TANs likely exist in tumors at different stages of disease development and perform different functions. Also, since TANs might lose or change their antitumoral functions as the tumors progress, a simple neutrophil count in tumor tissue at any one time point (where the pro- versus antitumor status of the neutrophils is not known) may not be an accurate parameter for clinical prognosis.

In summary, our findings characterize tumor-infiltrating neutrophils in patients with lung cancer for the first time. Although the presence of a minor suppressive subpopulation of TANs cannot be excluded, our data suggest that TANs do not significantly contribute to inhibition of T cell responses in patients with early-stage lung cancer. Rather, the majority of neutrophils recruited into the tumor microenvironment undergo phenotypic and functional changes that result in the formation of cells that could potentially augment and support T cell responses. However, the in vitro conditions necessary for our experiments may not necessarily reflect what actually transpires in vivo. In addition, the ability of TANs to augment T cell responses is only one of many potential characteristics of antitumoral N1 neutrophils and does not entirely define TANs as antitumoral cells. In these studies, we were not able to assess the role of human TANs in the regulation of tumor cell proliferation, matrix remodeling, angiogenesis, and metastasis. Areas of future investigation in our laboratory are focused on deciphering subpopulations of neutrophils in human lung cancers and further characterization of the role of TANs in the regulation of tumor development using in vivo models. Ultimately, these findings may have important clinical implications, such as ways to take advantage of the T cell stimulatory activity of TANs and boost the efficacy of vaccines based on cytotoxic T lymphocyte induction.

Methods

Study design

A total of 86 patients with stage I–II lung cancer, who were scheduled for surgical resection, consented to the harvest of a portion of their tumor and blood for research purposes. All patients signed an informed consent document that was approved by the University of Pennsylvania Institutional Review Board, and met the following criteria: (a) histologically confirmed pulmonary squamous cell carcinoma (SCC) or adenocarcinoma (AC), (b) no prior chemotherapy or radiation therapy within 2 years, and (c) no other malignancy. Detailed characteristics of the patients can be found in Supplemental Table 1.

Reagents

The enzymatic cocktail for tumor digestion consisted of serum-free Hyclone Leibovitz L-15 medium supplemented with 1% penicillin-streptomycin, collagenase type I and IV (170 mg/l = 45–60 U/ml), collagenase type II (56 mg/l = 15–20 U/ml), DNase I (25 mg/l), and elastase (25 mg/l) (all from Worthington Biochemical). Cell culture reagents are described in Supplemental Methods.

Lymphocyte isolation from peripheral blood

Standard approaches were used. See Supplemental Methods.

Preparation of a single-cell suspension from lung tumor tissue

Surgically removed fresh lung tumors from patients were processed within 20 minutes of removal from the patient. In brief, the tumors were trimmed, sliced into small pieces, and digested for 1 hour at 37°C with shaking. After rbc lysis, cell viability was determined by trypan blue exclusion or Fixable Viability Dye eFluor 450 staining (Supplemental Figure 1B). If the viability of cells was less than 80%, dead cells were eliminated using a Dead Cell Removal Kit (Miltenyi Biotec Inc.). See Supplemental Methods for full details.

Tumor-conditioned medium

See Supplemental Methods.

Neutrophil isolation

Since temperature gradients can activate neutrophils, all tissues and reagents were maintained at a constant temperature during preparation. After tumor harvest, TANs and PBNs were prepared at room temperature and rapidly used.

TANs. A single-cell suspension was obtained by enzymatic digestion of tumor tissue. TANs were isolated from tumor cell suspensions using positive selection of $CD15^+$ or $CD66b^+$ cells with microbeads according to the manufacturer's instructions (Miltenyi Biotec Inc.). In some experiments, TANs were isolated by flow cytometric cell sorting based on the phenotype of TANs as $CD45^+CD11b^+CD66b^+CD15^+$. Sterile cell sorting was performed on the BD FACSAria II (BD Biosciences). For more details see Supplemental Methods.

PBNs. EDTA-anticoagulated peripheral blood was collected from lung cancer patients during surgery or from healthy donors, and density-gradient centrifugation was performed. To account for any possible effect of tissue digestion enzymes on neutrophil function, peripheral blood granulocytes were processed in a similar manner.

The purity and activation status of isolated TANs and PBNs were measured by flow cytometry for the granulocyte/myeloid markers CD66b, CD15, arginase-1 (Arg1), myeloperoxidase (MPO), and CD11b, and the activation markers CD62L and CD54. The TANs demonstrated high cell viability with minimal enzyme-induced premature cellular activation or cleavage of myeloid cell markers (Supplemental Figure 1). The purity of TANs and PBNs was typically higher than 94%. Isolates with less than 90% purity were discarded.

Flow cytometry

Flow cytometric analysis was performed according to standard protocols. Details about the Abs used are listed in Figure 3A. Matched-isotype Abs were used as controls. For more details see Supplemental Methods.

T cell proliferation assay

T cell proliferation induced by plate-bound anti–human CD3 (clone: OKT3) and/or anti-CD28 (clone: CD28.2) Abs was assessed using standard CFSE dilution methods. PBMCs or purified T cells (responders) were labeled with CFSE and cocultured in CD3/CD28–coated plates for 4 days in the complete cell culture medium. The CFSE signal was analyzed by flow cytometry on gated $CD4^+$ or $CD8^+$ lymphocytes. In several experiments, blocking Abs against CD86 (clone: IT2.2), CD80 (clone: 2D10), OX40L (clone: 11C3.1), 4-1BBL (clone: 5F4), CD54 (clone: HCD54), or CD40 (clone: 5C3) (all from Biolegend) were added to the cocultures of TANs and activated T cells at the concentration 1 μg/ml. In other experiments, the proliferation of T cells was assessed by flow cytometry using the BrdU Flow Kit (BD Pharmingen). For more details see Supplemental Methods.

Allogeneic mixed lymphocyte reaction

Purified allogeneic T cells from healthy donor PBMCs were used as responders and reacted with irradiated, mature, monocyte-derived DCs (MoDCs) (inducers) from unrelated healthy donors. Immature MoDCs were prepared by culturing of adherent peripheral blood monocytes for 7 days in DMEM supplemented with 10% FBS, recombinant human GM-CSF (50 ng/ml), and IL-4 (50 ng/ml). To mature the MoDCs, LPS (100 ng/ml) was added to the cell culture for 24 hours before harvesting. The TANs or PBNs (regulators) were added to the DC-induced mixed lymphocyte reaction as "third-party cells" at a ratio of 1:0.25:1 (regulator/inducer/responder). Five days later, the proliferation of $CD4^+$ and $CD8^+$ T cells was measured using flow cytometric analysis of CFSE dilution.

Phagocytosis

The phagocytic activity of TANs and PBNs was assayed with the pHrodo Red *E. coli* BioParticles Phagocytosis Kit for flow cytometry (Life Technologies), according to the manufacturer's instructions.

Chemotaxis

We used a previously established protocol for fluorescence-based measurement of neutrophil migration in vitro across a polycarbonate filter (67) with minor modifications. See Supplemental Methods for details.

Neutrophil survival

Freshly isolated TANs or PBNs were cultured in complete cell culture medium in the presence or absence of 50% v/v of TCM for 20 hours. Neutrophil viability, apoptosis, and necrosis were measured using the FITC-Annexin V Apoptosis Detection Kit (Biolegend) and analyzed by flow cytometry, according to the manufacturer's instructions.

Measurement of ROS

The production of H_2O_2 in TANs and PBNs isolated from lung cancer patients and healthy donors was measured using Amplex Red Hydrogen Peroxide/Peroxidase Assay Kit (Invitrogen), according to the manufacturer's instructions. See Supplemental Methods for details.

Measurement of cytokines, chemokines, and growth factors

Single-cell suspensions were obtained from lung tumors by enzymatic digestion, as described above. TANs and PBNs were isolated from lung cancer patients, as described above. Both unseparated cells and isolated neutrophils from digested tumors, and PBNs, were resuspended in DME/F-12 1:1 medium with 10% FBS at a concentration of 1×10^6 cells/ml. Twenty-four hours later, cell culture supernatants were collected, filtered, and stored at –80°C until measurement. The levels of 30 cytokines/chemokines and growth factors were measured using the Cytokine Human Magnetic 30-Plex Panel for the Luminex platform (Invitrogen). The production of IFN-γ, IL-10, and GM-CSF was measured with commercial ELISA kits purchased from BD Bioscience.

Immunohistochemistry

The tumor microarrays (TMAs) were constructed from formalin-fixed, paraffin-embedded tumor and adjacent normal specimens collected at the time of surgical resection. Sections from 45 AC and 25 SCC patients were analyzed. After standard antigen retrieval, the TMAs were double-

stained with an anti-cytokeratin Ab to label cancer cells and an Ab against human MPO to label neutrophils. Slide imaging was performed on a Vectra automated imaging robot and analyzed using Inform analysis software. Data are expressed as the intraepithelial or stromal hematopoietic cell density per square millimeter of tumor tissue. In addition, we costained for neutrophils (MPO), APCs (HLA-DR), and T cells (CD3), using their respective Abs. See Supplemental Methods for details.

Statistics

All data were tested for normal distribution of variables. Comparisons between 2 groups were assessed with a 2-tailed Student's *t* test for paired and unpaired data if data were normally distributed. Nonparametric Wilcoxon matched-pairs test and Mann-Whitney unpaired test were used when the populations were not normally distributed. Likewise, multiple groups were analyzed by 1-way ANOVA with corresponding Tukey's multiple comparison test if normally distributed, or the Kruskal-Wallis with Dunn's multiple comparison test if not. Nonparametric Spearman test was used for correlation analysis. All statistical analyses were performed with GraphPad Prism 6. A *P* value less than 0.05 was considered statistically significant.

Study approval

The study was approved by the University of Pennsylvania Institutional Review Board (IRB no. 813004). All patients signed an informed consent document.

Acknowledgments

This work was supported by the NIH (R01-CA163256 to S. Singhal), Janssen Pharmaceuticals, and the Lung Cancer Translation Center of Excellence of the Abramson Cancer Center at the University of Pennsylvania. We thank Jeffery Faust (The Wistar Institute) for assistance in flow cytometry cell sorting. We also acknowledge Timothy Baradet (Department of Pathology and Laboratory Medicine, University of Pennsylvania) for analysis of the TMA images.

Address correspondence to: Evgeniy Eruslanov, Division of Thoracic Surgery, Department of Surgery, Perelman School of Medicine at the University of Pennsylvania, 3400 Spruce Street, 6 White, Philadelphia, Pennsylvania 19104, USA. Phone: 610.772.5624; E-mail: Evgeniy.Eruslanov@uphs.upenn.edu.

1. Balkwill F, Charles KA, Mantovani A. Smoldering and polarized inflammation in the initiation and promotion of malignant disease. *Cancer Cell*. 2005;7(3):211–217.
2. Sica A, et al. Origin and functions of tumor-associated myeloid cells (TAMCs). *Cancer Microenviron*. 2012;5(2):133–149.
3. Heusinkveld M, van der Burg SH. Identification and manipulation of tumor associated macrophages in human cancers. *J Transl Med*. 2011;9:216.
4. Galdiero MR, Garlanda C, Jaillon S, Marone G, Mantovani A. Tumor associated macrophages neutrophils in tumor progression. *J Cell Physiol*. 2013;228(7):1404–1412.
5. Brandau S, Dumitru CA, Lang S. Protumor and antitumor functions of neutrophil granulocytes. *Semin Immunopathol*. 2013;35(2):163–176.
6. Houghton AM. The paradox of tumor-associated neutrophils: Fueling tumor growth with cytotoxic substances. *Cell Cycle*. 2010;9(9):1732–1737.
7. Piccard H, Muschel RJ, Opdenakker G. On the dual roles and polarized phenotypes of neutrophils in tumor development and progression. *Crit Rev Oncol Hematol*. 2012;82(3):296–309.
8. Fridlender ZG, et al. Polarization of tumor-associated neutrophil phenotype by TGF-β: "N1" versus "N2" TAN. *Cancer Cell*. 2009;16(3):183–194.
9. Mestas J, Hughes CC. Of mice and not men: differences between mouse and human immunology. *J Immunol*. 2004;172(5):2731–2738.
10. Seok J, et al. Genomic responses in mouse models poorly mimic human inflammatory diseases. *Proc Natl Acad Sci U S A*. 2013;110(9):3507–3512.
11. Trellakis S, et al. Polymorphonuclear granulocytes in human head and neck cancer: enhanced inflammatory activity, modulation by cancer cells and expansion in advanced disease. *Int J Cancer*. 2011;129(9):2183–2193.
12. Jensen HK, Donskov F, Marcussen N, Nordsmark M, Lundbeck F, von der Maase H. Presence of intratumoral neutrophils is an independent prognostic factor in localized renal cell carcinoma. *J Clin Oncol*. 2009;27(28):4709–4717.
13. Jensen TO, et al. Intratumoral neutrophils and plasmacytoid dendritic cells indicate poor prognosis and are associated with pSTAT3 expression in AJCC stage I/II melanoma. *Cancer*. 2012;118(9):2476–2485.
14. Li YW, et al. Intratumoral neutrophils: A poor prognostic factor for hepatocellular carcinoma following resection. *J Hepatol*. 2011;54(3):497–505.
15. Rao HL, et al. Increased intratumoral neutrophil in colorectal carcinomas correlates closely with malignant phenotype and predicts patients' adverse prognosis. *PLoS One*. 2012;7(1):e30806.
16. Caruso RA, Bellocco R, Pagano M, Bertoli G, Rigoli L, Inferrera C. Prognostic value of intratumoral neutrophils in advanced gastric carcinoma in a high-risk area in northern italy. *Mod Pathol*. 2002;15(8):831–837.
17. Carus A, Ladekarl M, Hager H, Pilegaard H, Nielsen PS, Donskov F. Tumor-associated neutrophils and macrophages in non-small cell lung cancer: No immediate impact on patient outcome. *Lung Cancer*. 2013;81(1):130–137.
18. Ilie M, et al. Predictive clinical outcome of the intratumoral CD66b-positive neutrophil-to-CD8-positive T-cell ratio in patients with resectable nonsmall cell lung cancer. *Cancer*. 2012;118(6):1726–1737.
19. Radsak M, Iking-Konert C, Stegmaier S, Andrassy K, Hansch GM. Polymorphonuclear neutrophils as accessory cells for T-cell activation: major histocompatibility complex class II restricted antigen-dependent induction of T-cell proliferation. *Immunology*. 2000;101(4):521–530.
20. Ashtekar AR, Saha B. Poly's plea: membership to the club of APCs. *Trends Immunol*. 2003;24(9):485–490.
21. Potter NS, Harding CV. Neutrophils process exogenous bacteria via an alternate class I MHC processing pathway for presentation of peptides to T lymphocytes. *J Immunol*. 2001;167(5):2538–2546.
22. Reali E, et al. Polymorphonuclear neutrophils pulsed with synthetic peptides efficiently activate memory cytotoxic T lymphocytes. *J Leukoc Biol*. 1996;60(2):207–213.
23. Pillay J, et al. A subset of neutrophils in human systemic inflammation inhibits T cell responses through mac-1. *J Clin Invest*. 2012;122(1):327–336.
24. Schmielau J, Finn OJ. Activated granulocytes and granulocyte-derived hydrogen peroxide are the underlying mechanism of suppression of t-cell function in advanced cancer patients. *Cancer Res*. 2001;61(12):4756–4760.
25. Munder M, et al. Suppression of T-cell functions by human granulocyte arginase. *Blood*. 2006;108(5):1627–1634.
26. Gorgun GT, et al. Tumor-promoting immune-suppressive myeloid-derived suppressor cells in the multiple myeloma microenvironment in humans. *Blood*. 2013;121(15):2975–2987.
27. Gabrilovich DI, Nagaraj S. Myeloid-derived suppressor cells as regulators of the immune system. *Nat Rev Immunol*. 2009;9(3):162–174.
28. Eruslanov E, et al. Circulating and tumor-infiltrating myeloid cell subsets in patients with bladder cancer. *Int J Cancer*. 2012;130(5):1109–1119.
29. Pignatti P, et al. Downmodulation of CXCL8/IL-8 receptors on neutrophils after recruitment in the airways. *J Allergy Clin Immunol*. 2005;115(1):88–94.
30. Fortunati E, Kazemier KM, Grutters JC, Koenderman L, Van den Bosch VJMM. Human neutrophils switch to an activated phenotype after homing to the lung irrespective of inflammatory disease. *Clin Exp Immunol*. 2009;155(3):559–566.
31. Liu CY, et al. Population alterations of L-arginase- and inducible nitric oxide synthase-expressed CD11b+/CD14(–)/CD15+/CD33+ myeloid-derived suppressor cells and CD8+ T lymphocytes in patients with advanced-stage non-small cell lung cancer. *J Cancer Res Clin Oncol*. 2010;136(1):35–45.
32. Gabrilovich DI, Ostrand-Rosenberg S, Bronte V. Coordinated regulation of myeloid cells by tumours. *Nat Rev Immunol*. 2012;12(4):253–268.

33. Hartl D, et al. Infiltrated neutrophils acquire novel chemokine receptor expression and chemokine responsiveness in chronic inflammatory lung diseases. *J Immunol*. 2008;181(11):8053–8067.
34. de Kleijn S, et al. IFN-γ-stimulated neutrophils suppress lymphocyte proliferation through expression of PD-L1. *PLoS One*. 2013;8(8):e72249.
35. Zhu C, et al. The tim-3 ligand galectin-9 negatively regulates T helper type 1 immunity. *Nat Immunol*. 2005;6(12):1245–1252.
36. van Vliet SJ, Gringhuis SI, Geijtenbeek TB, van Kooyk Y. Regulation of effector T cells by antigen-presenting cells via interaction of the C-type lectin MGL with CD45. *Nat Immunol*. 2006;7(11):1200–1208.
37. Rygiel TP, Meyaard L. CD200R signaling in tumor tolerance and inflammation: A tricky balance. *Curr Opin Immunol*. 2012;24(2):233–238.
38. Zhou L, et al. Impact of human granulocyte and monocyte isolation procedures on functional studies. *Clin Vaccine Immunol*. 2012;19(7):1065–1074.
39. Gao JL, et al. Impaired host defense, hematopoiesis, granulomatous inflammation and type 1-type 2 cytokine balance in mice lacking CC chemokine receptor 1. *J Exp Med*. 1997;185(11):1959–1968.
40. Youn JI, Collazo M, Shalova IN, Biswas SK, Gabrilovich DI. Characterization of the nature of granulocytic myeloid-derived suppressor cells in tumor-bearing mice. *J Leukoc Biol*. 2012;91(1):167–181.
41. Thewissen M, Damoiseaux J, van de Gaar J, Tervaert JW. Neutrophils and T cells: Bidirectional effects and functional interferences. *Mol Immunol*. 2011;48(15–16):2094–2101.
42. Fontenot JD, Gavin MA, Rudensky AY. Foxp3 programs the development and function of $CD4^+CD25^+$ regulatory T cells. *Nat Immunol*. 2003;4(4):330–336.
43. Kobayashi SD, Voyich JM, Whitney AR, DeLeo FR. Spontaneous neutrophil apoptosis and regulation of cell survival by granulocyte macrophage-colony stimulating factor. *J Leukoc Biol*. 2005;78(6):1408–1418.
44. Yoshimura T, Takahashi M. IFN-γ-mediated survival enables human neutrophils to produce MCP-1/CCL2 in response to activation by TLR ligands. *J Immunol*. 2007;179(3):1942–1949.
45. Lentzsch S, Gries M, Janz M, Bargou R, Dorken B, Mapara MY. Macrophage inflammatory protein 1-alpha (MIP-1α) triggers migration and signaling cascades mediating survival and proliferation in multiple myeloma (MM) cells. *Blood*. 2003;101(9):3568–3573.
46. Doedens AL, et al. Macrophage expression of hypoxia-inducible factor-1 α suppresses T-cell function and promotes tumor progression. *Cancer Res*. 2010;70(19):7465–7475.
47. Marigo I, et al. Tumor-induced tolerance and immune suppression depend on the C/EBPβ transcription factor. *Immunity*. 2010;32(6):790–802.
48. Corzo CA, et al. HIF-1α regulates function and differentiation of myeloid-derived suppressor cells in the tumor microenvironment. *J Exp Med*. 2010;207(11):2439–2453.
49. Kusmartsev S, Nefedova Y, Yoder D, Gabrilovich DI. Antigen-specific inhibition of $CD8^+$ T cell response by immature myeloid cells in cancer is mediated by reactive oxygen species. *J Immunol*. 2004;172(2):989–999.
50. Biswas SK, Mantovani A. Macrophage plasticity and interaction with lymphocyte subsets: cancer as a paradigm. *Nat Immunol*. 2010;11(10):889–896.
51. Fridlender ZG, et al. Using macrophage activation to augment immunotherapy of established tumours. *Br J Cancer*. 2013;108(6):1288–1297.
52. Guiducci C, Vicari AP, Sangaletti S, Trinchieri G, Colombo MP. Redirecting in vivo elicited tumor infiltrating macrophages and dendritic cells towards tumor rejection. *Cancer Res*. 2005;65(8):3437–3446.
53. Nozawa H, Chiu C, Hanahan D. Infiltrating neutrophils mediate the initial angiogenic switch in a mouse model of multistage carcinogenesis. *Proc Natl Acad Sci U S A*. 2006;103(33):12493–12498.
54. Jablonska J, Leschner S, Westphal K, Lienenklaus S, Weiss S. Neutrophils responsive to endogenous IFN-β regulate tumor angiogenesis and growth in a mouse tumor model. *J Clin Invest*. 2010;120(4):1151–1164.
55. Spicer JD, et al. Neutrophils promote liver metastasis via mac-1-mediated interactions with circulating tumor cells. *Cancer Res*. 2012;72(16):3919–3927.
56. Sandilands GP, McCrae J, Hill K, Perry M, Baxter D. Major histocompatibility complex class II (DR) antigen and costimulatory molecules on in vitro and in vivo activated human polymorphonuclear neutrophils. *Immunology*. 2006;119(4):562–571.
57. Watts TH. TNF/TNFR family members in costimulation of T cell responses. *Annu Rev Immunol*. 2005;23:23–68.
58. Shao Z, Schwarz H. CD137 ligand, a member of the tumor necrosis factor family, regulates immune responses via reverse signal transduction. *J Leukoc Biol*. 2011;89(1):21–29.
59. Chacon JA, et al. Co-stimulation through 4-1BB/CD137 improves the expansion and function of CD8(+) melanoma tumor-infiltrating lymphocytes for adoptive T-cell therapy. *PLoS One*. 2013;8(4):e60031.
60. Hernandez-Chacon JA, et al. Costimulation through the CD137/4-1BB pathway protects human melanoma tumor-infiltrating lymphocytes from activation-induced cell death and enhances antitumor effector function. *J Immunother*. 2011;34(3):236–250.
61. Musiani P, et al. Role of neutrophils and lymphocytes in inhibition of a mouse mammary adenocarcinoma engineered to release IL-2, IL-4, IL-7, IL-10, IFN-α, IFN-γ, and TNF-α. *Lab Invest*. 1996;74(1):146–157.
62. Giovarelli M, et al. Tumor rejection and immune memory elicited by locally released LEC chemokine are associated with an impressive recruitment of APCs, lymphocytes, and granulocytes. *J Immunol*. 2000;164(6):3200–3206.
63. Colombo MP, et al. Granulocyte colony-stimulating factor gene transfer suppresses tumorigenicity of a murine adenocarcinoma in vivo. *J Exp Med*. 1991;173(4):889–897.
64. Suttmann H, et al. Neutrophil granulocytes are required for effective bacillus calmette-guerin immunotherapy of bladder cancer and orchestrate local immune responses. *Cancer Res*. 2006;66(16):8250–8257.
65. Kousis PC, Henderson BW, Maier PG, Gollnick SO. Photodynamic therapy enhancement of antitumor immunity is regulated by neutrophils. *Cancer Res*. 2007;67(21):10501–10510.
66. Mishalian I, Bayuh R, Levy L, Zolotarov L, Michaeli J, Fridlender ZG. Tumor-associated neutrophils (TAN) develop pro-tumorigenic properties during tumor progression. *Cancer Immunol Immunother*. 2013;62(11):1745–1756.
67. Frevert CW, Wong VA, Goodman RB, Goodwin R, Martin TR. Rapid fluorescence-based measurement of neutrophil migration in vitro. *J Immunol Methods*. 1998;213(1):41–52.

CANCER

Lectin-type oxidized LDL receptor-1 distinguishes population of human polymorphonuclear myeloid-derived suppressor cells in cancer patients

Thomas Condamine,[1]* George A. Dominguez,[1] Je-In Youn,[1†] Andrew V. Kossenkov,[1] Sridevi Mony,[1] Kevin Alicea-Torres,[1] Evgenii Tcyganov,[1] Ayumi Hashimoto,[1] Yulia Nefedova,[1] Cindy Lin,[1] Simona Partlova,[1‡] Alfred Garfall,[2,3] Dan T. Vogl,[2,3] Xiaowei Xu,[2] Stella C. Knight,[4] George Malietzis,[4,5] Gui Han Lee,[4,5] Evgeniy Eruslanov,[2] Steven M. Albelda,[2,3] Xianwei Wang,[6] Jawahar L. Mehta,[6] Meenakshi Bewtra,[3] Anil Rustgi,[2,3] Neil Hockstein,[7] Robert Witt,[7] Gregory Masters,[7] Brian Nam,[7] Denis Smirnov,[8] Manuel A. Sepulveda,[8] Dmitry I. Gabrilovich[1§]

Polymorphonuclear myeloid-derived suppressor cells (PMN-MDSCs) are important regulators of immune responses in cancer and have been directly implicated in the promotion of tumor progression. However, the heterogeneity of these cells and the lack of distinct markers hamper the progress in understanding the biology and clinical importance of these cells. Using partial enrichment of PMN-MDSC with gradient centrifugation, we determined that low-density PMN-MDSC and high-density neutrophils from the same cancer patients had a distinct gene profile. The most prominent changes were observed in the expression of genes associated with endoplasmic reticulum (ER) stress. Unexpectedly, low-density lipoprotein (LDL) was one of the most increased regulators, and its receptor oxidized LDL receptor 1 (*OLR1*) was one of the most overexpressed genes in PMN-MDSC. Lectin-type oxidized LDL receptor-1 (LOX-1) encoded by *OLR1* was practically undetectable in neutrophils in peripheral blood of healthy donors, whereas 5 to 15% of total neutrophils in cancer patients and 15 to 50% of neutrophils in tumor tissues were LOX-1$^+$. In contrast to their LOX-1$^-$ counterparts, LOX-1$^+$ neutrophils had gene signature, potent immunosuppressive activity, up-regulation of ER stress, and other biochemical characteristics of PMN-MDSCs. Moreover, induction of ER stress in neutrophils from healthy donors up-regulated LOX-1 expression and converted these cells to suppressive PMN-MDSCs. Thus, we identified a specific marker of human PMN-MDSC associated with ER stress and lipid metabolism, which provides new insights into the biology and potential therapeutic targeting of these cells.

INTRODUCTION

The accumulation of relatively immature and pathologically activated myeloid-derived suppressor cells (MDSCs) with potent immunosuppressive activity is common in tumors. MDSCs have the ability to support tumor progression by promoting tumor cell survival, angiogenesis, invasion of healthy tissue by tumor cells, and metastases [reviewed in (*1*)]. There is now ample evidence of the association of accumulation of immunosuppressive MDSCs with negative clinical outcomes in various cancers (*2*). MDSCs have been implicated in resistance to anticancer therapies with kinase inhibitor (*3*), chemotherapy (*4*–*7*), and immunotherapy (*8*–*12*).

Two large populations of MDSCs are currently described: polymorphonuclear MDSCs (PMN-MDSCs) and monocytic MDSCs (M-MDSCs) (*13*). PMN-MDSC is the most abundant population of MDSC in most types of cancer, phenotypically and morphologically similar to neutrophils (PMNs) (*14*). These cells share the CD11b$^+$CD14$^-$CD15$^+$/CD66b$^+$ phenotype. At present, these cells can be separated only in peripheral blood (PB) and only by density gradient centrifugation. Distinction between PMN-MDSC and PMN in tumor tissues is not possible. Because gradient centrifugation may enrich not only for true PMN-MDSC but also for activated PMN without suppressive activity, the heterogeneity of PMN-MDSC population raised the questions of whether PMN-MDSC and PMN are truly cells with distinct features. It is not clear what defines the specific functional state of human PMN-MDSC vis-à-vis PMN in the same patient. The mechanisms responsible for the acquisition of pathological activity by human neutrophils in cancer remained unclear.

Here, we attempted to address these questions by evaluating populations of PMN-MDSC and PMN from the same patients. We identified genomic signature of PMN-MDSCs and surface markers specific for these cells. We found that induction of endoplasmic reticulum (ER) stress response was sufficient to convert neutrophils to PMN-MDSCs.

RESULTS

Human PMN-MDSCs have a distinct gene expression profile from neutrophils

To compare PMN-MDSC and PMN from PB of the same patients with non–small cell lung cancer (NSCLC) and head and neck cancer (HNC), we used dual-density Histopaque gradient, the standard method of isolation of PMN-MDSC (*15*). Low-density PMN-MDSCs are copurified

[1]Wistar Institute, Philadelphia, PA 19104, USA. [2]Abramson Cancer Center, University of Pennsylvania, Philadelphia, PA 19104, USA. [3]Department of Medicine, Perelman School of Medicine, University of Pennsylvania, Philadelphia, PA 19104, USA. [4]Antigen Presentation Research Group, Imperial College London, London HA1 3UJ, UK. [5]St. Mark's Hospital, Harrow HA1 3UJ, UK. [6]Department of Medicine, University of Arkansas for Medical Sciences, Little Rock, AR 72205, USA. [7]Helen F. Graham Cancer Center & Research Institute, Christiana Care Health System, Newark, DE 19713, USA. [8]Janssen Oncology Therapeutic Area, Janssen Research and Development LLC, Pharmaceutical Companies of Johnson & Johnson, Spring House, PA 19477, USA.
*Present address: Incyte Corporation, 1801 Augustine Cut-Off, Wilmington, DE 19803, USA.
†Present address: Wide River Institute of Immunology, Department of Biomedical Sciences, Seoul National University College of Medicine, Seoul 03080, South Korea.
‡Present address: SOTIO a.s., Prague, Czech Republic.
§Corresponding author. Email: dgabrilovich@wistar.org

with peripheral blood mononuclear cells (PBMCs), whereas high-density PMNs are collected from lower gradient (*16*). As a control, PMNs from healthy donors were used. Both low-density PMN-MDSCs and high-density PMNs were purified further with CD15 magnetic beads to achieve similar high purity of both cell populations (Fig. 1A). The immunosuppressive activity of PMN-MDSC, the main characteristic of these cells, was confirmed in allogeneic mixed leukocyte reaction (MLR) (Fig. 1B) and in autologous system with T cells activated by CD3/CD28 antibodies (Fig. 1C). As expected, PMNs were not suppressive (Fig. 1, B and C).

To study overall differences and similarities between patients' PMNs and PMN-MDSCs as well as PMNs from healthy donors, we performed whole-genome analysis using Illumina HumanHT-12 v4 bead arrays. The direct pairwise comparison identified 1870 array probes significantly differentially expressed [false discovery rate (FDR) < 5%] between PMN-MDSC and PMN in the same patients (fig. S1A), and 36 probes showed difference of at least fivefold (fig. S1B). Hierarchical clustering of the samples using expression of the 985 most differentially expressed genes (fold > 2, $P < 0.05$; Fig. 1D) revealed that PMN-MDSC samples have a unique expression profile and PMNs from cancer patients are very similar to healthy donor PMN samples, because they grouped within the same cluster for HNC and NSCLC patients (Fig. 1E). Specifically, of the 985 genes that were different between any pair of groups, most (74%) showed significant differences (FDR < 5%) between patients' PMN-MDSCs and PMNs, whereas no genes were significantly different when corrected for multiple testing (best FDR = 19%) between PMNs from healthy donors and PMNs from cancer patients, with only 12% of the genes significantly different at nominal $P < 0.05$, which indicates a high similarity of PMN samples between cancer patients and healthy donors.

Using Ingenuity Pathway Analysis (IPA), we identified 14 pathways significantly enriched in PMN-MDSCs, including eukaryotic translation initiation factor 2 (eIF2) and eIF4 pathways and mechanistic target of rapamycin signaling (table S1). The regulators of genes enriched in PMN-MDSC included regulators of ER stress response, mitogen-activated protein kinase pathway, colony-stimulating factor 1 (CSF1), interleukin-6 (IL-6), interferon-γ, and nuclear factor-κB (NF-κB). These molecules were previously directly implicated in MDSC biology, primarily PMN-MDSC [reviewed in (*17*)]. One of the most significant changes was associated with low-density lipoprotein (LDL) (Fig. 1F). Thus, PMN-MDSCs had a distinct genomic profile from PMNs isolated from the same cancer patients and PMNs from healthy donors. Genes associated with ER stress and immune responses were among the most up-regulated in PMN-MDSC.

LOX-1 is differentially expressed in PMN-MDSC and PMN

To search for potential markers of PMN-MDSCs, we evaluated differentially expressed genes, which encoded surface molecules, and compared the expression of various surface molecules between PMN-MDSCs and PMNs from the same patients and PMNs from healthy donors. More than 20 genes that encoded surface molecules were found to be differentially expressed in PMN-MDSC and PMN (Fig. 2A). In an attempt to validate these observations, we tested surface expression of some of the proteins using available antibodies and flow cytometry. Unexpectedly, the differences were found in the expression of lectin-type oxidized LDL receptor-1 (LOX-1), a 50-kDa transmembrane glycoprotein encoded by the oxidized LDL receptor 1 (*OLR1*) gene (*18*). In our analysis, *OLR1* was one of the mostly up-regulated genes in PMN-MDSCs (fig. S1B). LOX-1 is one of the main receptors for oxidized LDL (oxLDL) (*19*). It also binds other ligands including other modified lipoproteins, advanced glycation end products, aged red blood cells, apoptotic cells, and activated platelets (*20*). LOX-1 is expressed in endothelial cells, macrophages, smooth muscle cells, and some intestinal cell lines (*18*). However, it was not associated with neutrophils.

We evaluated LOX-1 expression in high-density PMNs and low-density PMN-MDSCs in cancer patients (Fig. 2B). LOX-1 was practically undetectable in PMN but expressed in about one-third of PMN-MDSC fraction (Fig. 2C). Because LOX-1 can be expressed in platelets (*21*) and platelets can adhere to activated PMN, we asked whether the increased expression of LOX-1 in PMN-MDSC fraction was the result of increased adherence of platelets. However, LOX-1$^-$ and LOX-1$^+$ cells in low-density PMN-MDSC population had the same small proportion of cells that express platelet markers CD41a and CD42b (Fig. 2D). We determined whether LOX-1 expression in PMN correlated with CD16 expression associated with neutrophil activation (*22*, *23*). Almost all PMNs in cancer patients were CD16^{hi}, and expression of LOX-1 on PMN was not associated with CD16 expression (fig. S2).

These results suggested that LOX-1 could be associated with PMN-MDSC. We asked whether LOX-1 can be a marker of PMN-MDSC. Cell density as a criterion for separation of PMN-MDSC from PMN has serious limitations. It may be changed during handling of cells. In addition, gradient centrifugation may enrich not only for PMN-MDSC but also for activated PMN without suppressive activity, which contributes to well-established heterogeneity of PMN-MDSC population. Therefore, we avoided the use of gradient centrifugation and labeled cells in PB directly with granulocyte-specific CD15 antibody and evaluated the expression of LOX-1 among all CD15$^+$ cells (Fig. 2E). In preliminary experiments, we found no differences in the results obtained with CD15 or CD66b antibodies. We referred to CD15$^+$ cells as PMNs because Siglec-8$^+$ eosinophils represented a very small proportion of CD15$^+$ cells, and no differences in the presence of eosinophils between CD15$^+$LOX-1$^+$ and CD15$^+$LOX-1$^-$ cells were seen (fig. S3). The proportion of LOX-1$^+$ cells among all PMN in healthy donors was very low (range, 0.1 to 1.5; mean, 0.7%) (Fig. 2F and fig. S4). In patients with NSCLC, it increased to 4.9% ($P < 0.001$), in patients with HNC to 6.4% ($P < 0.0001$), and in patients with colon cancer (CC) to 6.5% ($P = 0.0035$) (Fig. 2F). In all three types of cancer, >75% of patients had proportion of LOX-1$^+$ PMN higher than the range established for healthy donors. We also assessed the changes in LOX-1$^+$ PMNs in tumor-free patients with inflammatory conditions: eosinophilic esophagitis, ulcerative colitis, and Crohn's disease. Only patients with Crohn's disease had a small increase in the proportion of these cells (Fig. 2G). Thus, LOX-1 expression defined distinct population of neutrophils in cancer patients and was associated with accumulation of PMN-MDSC.

LOX-1 defines the population of PMN-MDSC among neutrophils

We addressed the question whether LOX-1 can be considered as a marker of human PMN-MDSC. LOX-1$^+$ and LOX-1$^-$ PMNs were sorted directly from PB of the same patients. LOX-1$^-$ PMN had the typical morphology of mature neutrophils, whereas LOX-1$^+$ PMN displayed more immature morphology with band-shaped nuclei (Fig. 3A). Whole-gene expression array was performed on LOX-1$^+$ and LOX-1$^-$ PMNs and compared with that of PMNs and PMN-MDSCs. Analysis of gene expression revealed 639 genes significantly different between LOX-1$^+$ and LOX-1$^-$ (FDR < 5%, fold > 2), and on the basis of the expression of those genes, LOX-1$^+$ PMNs clustered together with PMN-MDSCs, whereas LOX-1$^-$ PMNs were very similar to patients'

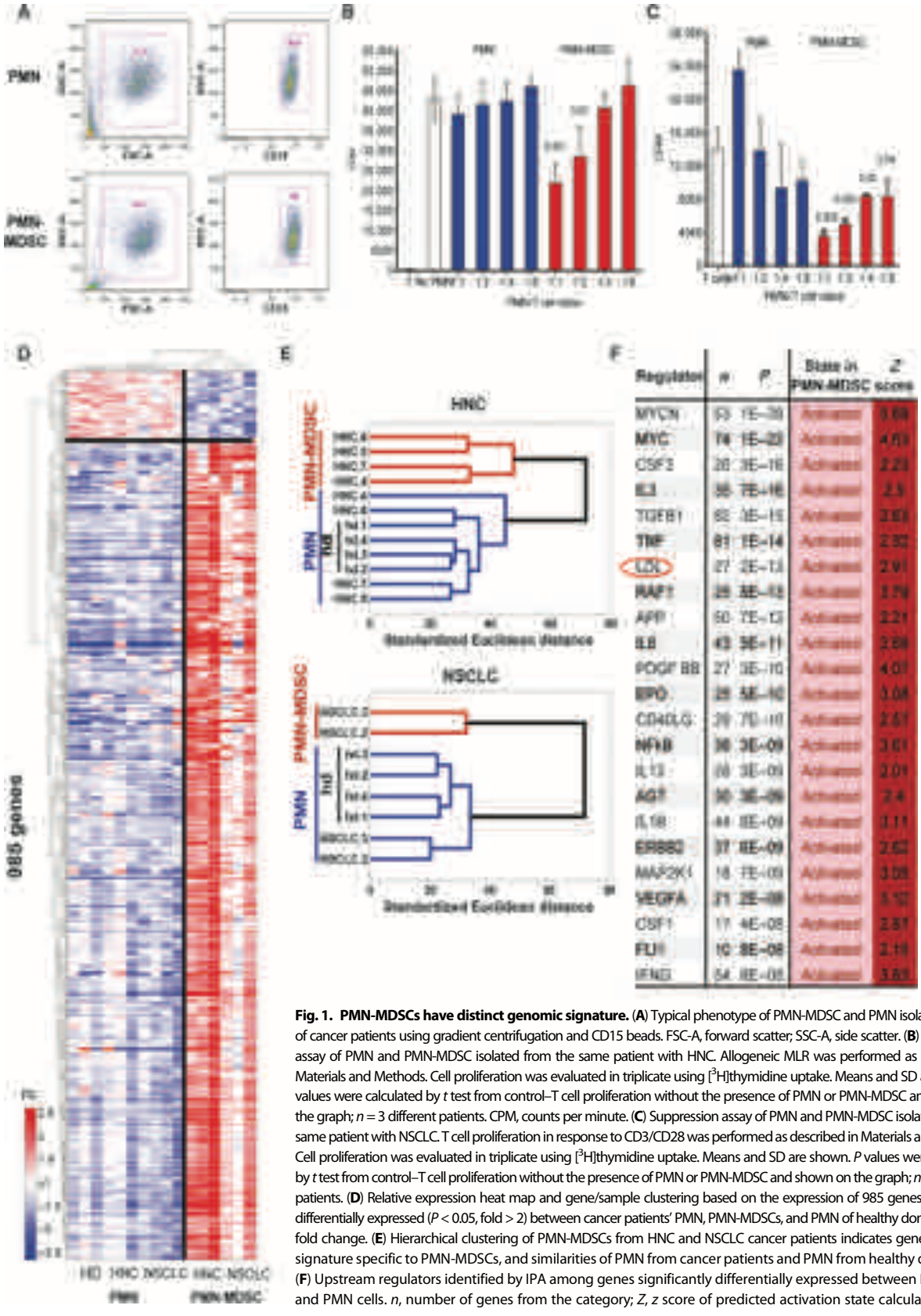

Fig. 1. PMN-MDSCs have distinct genomic signature. (**A**) Typical phenotype of PMN-MDSC and PMN isolated from PB of cancer patients using gradient centrifugation and CD15 beads. FSC-A, forward scatter; SSC-A, side scatter. (**B**) Suppression assay of PMN and PMN-MDSC isolated from the same patient with HNC. Allogeneic MLR was performed as described in Materials and Methods. Cell proliferation was evaluated in triplicate using [^{3}H]thymidine uptake. Means and SD are shown. *P* values were calculated by *t* test from control–T cell proliferation without the presence of PMN or PMN-MDSC and shown on the graph; $n = 3$ different patients. CPM, counts per minute. (**C**) Suppression assay of PMN and PMN-MDSC isolated from the same patient with NSCLC. T cell proliferation in response to CD3/CD28 was performed as described in Materials and Methods. Cell proliferation was evaluated in triplicate using [^{3}H]thymidine uptake. Means and SD are shown. *P* values were calculated by *t* test from control–T cell proliferation without the presence of PMN or PMN-MDSC and shown on the graph; $n = 3$ different patients. (**D**) Relative expression heat map and gene/sample clustering based on the expression of 985 genes significantly differentially expressed ($P < 0.05$, fold > 2) between cancer patients' PMN, PMN-MDSCs, and PMN of healthy donors (HD). FC, fold change. (**E**) Hierarchical clustering of PMN-MDSCs from HNC and NSCLC cancer patients indicates gene expression signature specific to PMN-MDSCs, and similarities of PMN from cancer patients and PMN from healthy donors (hd). (**F**) Upstream regulators identified by IPA among genes significantly differentially expressed between PMN-MDSC and PMN cells. *n*, number of genes from the category; *Z*, *z* score of predicted activation state calculated by IPA.

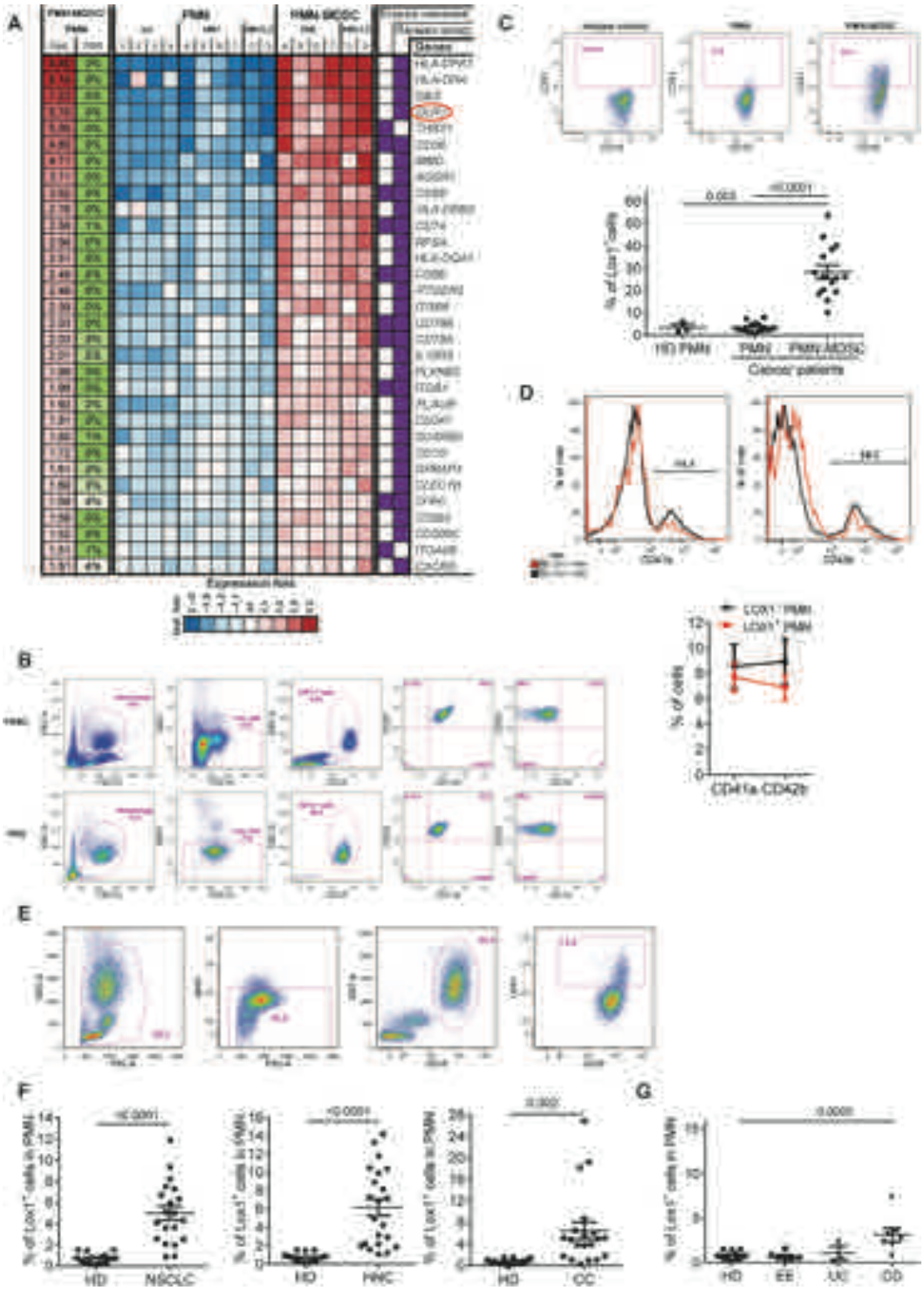

Fig. 2. LOX-1 as a marker of PMN-MDSC. (**A**) List and a heat map of relative expression of candidate surface markers specific to the PMN-MDSCs. (**B**) Typical phenotype of high-density PMN and low-density PMN-MDSC in a cancer patient. (**C**) Proportion of LOX-1$^+$ PMN and PMN-MDSC in PB of 15 cancer patients. (Top) Example of staining of PMN-MDSC and PMN with LOX-1 antibody. Cells were isolated using density gradient as described in Materials and Methods, and the proportion of LOX-1$^+$ cells was calculated among CD15$^+$ cells. (Bottom) Individual results for each patient are means and SE. *P* values (*t* test) are shown. (**D**) Example of staining with CD41a and CD42b antibody (top). Cumulative results of seven patients with NSCLC (bottom). Means and SD are shown. (**E**) Typical example of the analysis of PMN in a cancer patient. (**F**) Proportion of LOX-1$^+$ cells among PMN in unseparated PB from 16 healthy donors, 20 patients with NSCLC, 21 patients with HNC, and 19 patients with CC. *P* values calculated by *t* test are shown. (**G**) Proportion of LOX-1$^+$ cells among PMN in unseparated PB from 16 healthy donors, 6 patients with eosinophilic esophagitis (EE), 3 patients with ulcerative colitis (UC), and 7 patients with Crohn's disease (CD). *P* values calculated by *t* test are shown.

and healthy donors' PMNs (Fig. 3B). Overall, 92% of those genes had the same direction of change between LOX-1$^+$ and LOX-1$^-$ as between PMN-MDSCs and PMNs, with 93 probes significantly up-regulated (FDR < 5%) at least twofold or more in both PMN-MDSCs and LOX-1$^+$ PMNs (Fig. 3C and fig. S5). Thus, LOX-1$^+$ PMNs from cancer patients had gene expression profile similar to PMN-MDSCs.

The hallmark of PMN-MDSCs is their ability to suppress T cell function. We isolated LOX-1$^-$ and LOX-1$^+$ PMNs directly from PB of cancer patients and used them in T cell suppression assay. LOX-1$^+$ PMNs suppressed T cell proliferation, whereas LOX-1$^-$ PMNs did not (Fig. 3D). We asked whether the LOX-1 antibody used for isolation of PMN-MDSCs could directly affect the functional activity of PMN. PMNs isolated from cancer patients were cultured with T cells in the presence of LOX-1 antibody or immunoglobulin G (IgG) isotype control. LOX-1 antibody did not make PMNs to acquire immunosuppressive function (fig. S6). We determined whether LOX-1 neutralizing antibody (R&D Systems) could block the suppressive activity of LOX-1$^+$ PMNs. LOX-1$^+$ and LOX-1$^-$ PMNs were isolated from two patients with NSCLC and added to MLR in the presence of LOX-1 antibody at a concentration (10 μg/ml) that blocks more than 90% of LOX-1 binding or the same amount of mouse IgG. In both experiments, LOX-1 antibody did not abrogate the suppressive activity of LOX-1$^+$ PMNs. LOX-1$^-$ PMNs had no suppressive activity in any experiment (Fig. 3E).

We then evaluated possible mechanisms responsible for LOX-1$^+$ PMN-MDSC suppression. We tested several common mechanisms implicated in PMN-MDSC function. LOX-1$^+$ PMN-MDSCs had significantly higher production of reactive oxygen species (ROS) than LOX-1$^-$ PMN (Fig. 3F). Whole-genome array showed that LOX-1$^+$ PMN-MDSCs had higher expression of arginase 1 (*ARG1*), the gene directly associated with PMN-MDSC function, than LOX-1$^-$ PMNs. These differences were not statistically significant (FDR, 7%). However, direct evaluation of *ARG1* expression by quantitative polymerase chain reaction (qPCR) revealed significantly higher expression of this gene in LOX-1$^+$ PMN-MDSCs than in LOX-1$^-$ PMNs (Fig. 3G). The expression of *NOS2* in PMNs was much lower than that of *ARG1*. However, it was still significantly higher in LOX-1$^+$ PMN-MDSCs than in LOX-1$^-$ PMNs (Fig. 3G). We tested the contribution of ROS and ARG1 to immunosuppression mediated by LOX-1$^+$ PMN-MDSC. ROS scavenger *N*-acetylcysteine (NAC) and catalase significantly decreased the suppressive activity of LOX-1$^+$ PMNs (Fig. 4A). An inhibitor of Arg1, N^{ω}-hydroxy-nor-arginine (nor-NOHA), abrogated the suppressive activity of these cells (Fig. 4B). Together, these data thus demonstrate that LOX-1$^+$ PMNs represent a population of PMN- MDSCs. Therefore, for clarity in this study, we further refer to these cells as LOX-1$^+$ PMN-MDSCs.

We investigated the possible role of LOX-1 as a marker of mouse PMN-MDSCs. Similar to human PMNs, CD11b$^+$Ly6C^{lo}Ly6G$^+$ mouse PMNs had very low expression of LOX-1. In contrast to human PMN-MDSCs, spleen, bone marrow (BM), or tumor PMN-MDSCs from mice bearing EL-4 lymphoma or Lewis lung carcinoma (LLC) did not up-regulate LOX-1 expression (fig. S7). To evaluate the possible role of LOX-1 in PMN-MDSC function, we used BM cells from LOX-1 knockout (KO) (*olr1*$^{-/-}$) mice (*24*). Lethally irradiated wild-type (WT) recipients were reconstituted with congenic BM cells isolated from WT or *olr1*$^{-/-}$ mice. Ten weeks after reconstitution, donor's cells represented more than 95% of all myeloid cells. LLC tumor was implanted subcutaneously, and mice were evaluated 3 weeks later. No differences in the presence of PMN-MDSCs in spleens or tumors were observed between mice reconstituted with WT and LOX-1 KO BM (fig. S8A). WT and *olr1*$^{-/-}$ PMN-MDSCs suppressed T cell proliferation equally well (fig. S8B). Gene expression profile demonstrated no differences between WT and *olr1*$^{-/-}$ PMN-MDSCs. WT PMN-MDSCs had the same undetectable level of *olr1* expression as *olr1*$^{-/-}$ PMN-MDSCs. Thus, in contrast to humans, mouse LOX-1 is not associated with PMN-MDSC.

ER stress regulates LOX-1 expression in PMN-MDSC

What could induce LOX-1 up-regulation in PMN-MDSC? On the basis of the fact that in endothelial cells LOX-1 can be induced by proinflammatory cytokines (*25*), we tested the effect of several cytokines and tumor cell–conditioned medium (TCM) on LOX-1 expression in PMN isolated from healthy donors. None of the tested proinflammatory cytokines [IL-1β, TNF-α (tumor necrosis factor–α), and IL-6] or TCM-induced up-regulation of LOX-1 in PMN after 24-hour culture [granulocyte-macrophage (GM)–CSF] was added to protect PMN viability (Fig. 4C).

Our previous observations (*16*) and data obtained in this study demonstrated that PMN-MDSC in cancer patients displayed signs of ER stress response. LOX-1$^+$ and LOX-1$^-$ PMNs were isolated from PB of cancer patients, and the expression of genes associated with ER stress was evaluated. LOX-1$^+$ PMN-MDSCs had significantly higher expression of spliced X-box–binding protein 1 (*sXBP1*) and its target gene *SEC61a* than LOX-1$^-$ PMNs. The expression of *activating transcription factor 4* (*ATF4*) and its target gene *ATF3* was also higher in LOX-1$^+$ PMN-MDSCs. No changes in the expression of CCAAT/enhancer binding protein (*CHOP*) were observed (Fig. 4D). To test the effect of ER stress on the expression of LOX-1, we treated PMNs from healthy donors with ER stress inducers, thapsigargin (THG) or dithiothreitol (DTT), overnight in the presence of GM-CSF. At selected doses (1 μM THG or 1 mM DTT), cell viability remained above 95%. Both THG and DTT caused marked up-regulation of LOX-1 expression in PMN (Fig. 4E).

Overnight THG treatment of PMNs caused acquisition of potent immunosuppressive activity by the PMNs (Fig. 5A). Because LOX-1$^+$ PMN-MDSCs have increased expression preferentially of one of the ER stress sensors, sXBP1, we verified the role of ER stress using recently developed selective inhibitor of sXBP1, B-I09 (*26*). In the presence of B-I09, THG failed to induce up-regulation of LOX-1 (Fig. 5B) and immunosuppressive activity of PMN (Fig. 5C). THG treatment did not affect typical polymorphonuclear morphology of these cells (Fig. 5D). Thus, induction of ER stress in control neutrophils converted these cells to immunosuppressive PMN-MDSCs, which were associated with up-regulation of LOX-1 expression.

Up-regulation of intracellular Ca^{2+} and ROS is one of the consequences of THG treatment. We asked whether activation of neutrophils with agents that cause up-regulation of intracellular Ca^{2+} and ROS may also result to similar up-regulation of LOX-1 and suppressive activity as THG. We used two compounds: *N*-formyl-Met-Leu-Phe (*f*MLP) and phorbol 12-myristate 13-acetate (PMA). Both *f*MLP and PMA caused massive up-regulation of LOX-1 expression in control PMN within 60 min after the start of the treatment (Fig. 5E). However, in contrast to THG, the expression of LOX-1 in *f*MLP-treated PMN returned to control (untreated cells) level after overnight culture despite the presence of *f*MLP in the culture (Fig. 5E). PMNs did not survive overnight treatment with PMA. PMNs treated for 60 min with *f*MLP or PMA were washed and used in a T cell suppression assay. No suppressive activity was observed (Fig. 5F). In another set of experiments, PMNs were cultured with *f*MLP for 18 hours before they were used in the suppressive assay. However, this treatment did not result in the development of suppressive activity by PMNs (Fig. 5F). These data indicate that transient up-regulation of LOX-1 as a result of PMN activation was not associated with immunosuppressive activity.

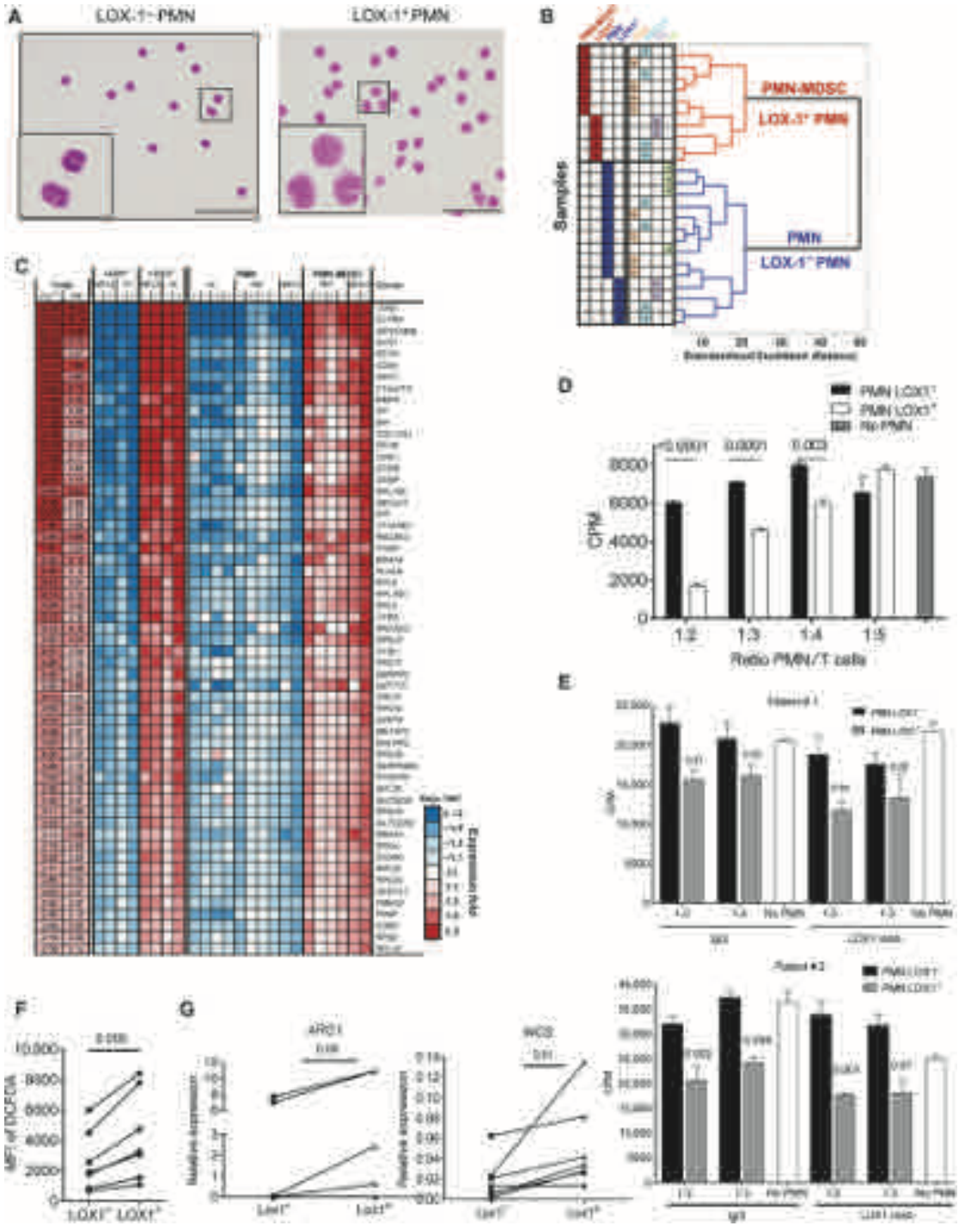

Fig. 3. LOX-1 expression defines bona fide PMN-MDSC. (**A**) Typical morphology of sorted LOX-1$^+$ and Lox-1$^-$ PMN from a patient with HNC. Scale bars, 20 μm. (**B**) Hierarchical clustering of samples based on the expression levels of genes differentially expressed between LOX-1$^+$ and LOX-1$^-$ PMN. (**C**) List and relative expression values of the most changed known genes overlapped between LOX-1$^+$ and PMN-MDSC cells. (**D**) Suppressive activity of LOX-1$^+$ and LOX-1$^-$ PMN isolated from PB of patient with HNC in allogeneic MLR. Cell proliferation was evaluated in triplicate using [^{3}H]thymidine uptake. Means and SE are shown. *P* values calculated by *t* test from T cell proliferation without the presence of PMN are shown. Experiments with similar results were performed with samples from nine patients with HNC and NSCLC. (**E**) Effect of neutralizing LOX-1 antibody on the suppressive activity of LOX-1$^+$ PMN. PMNs were isolated from two patients with NSCLC. LOX-1$^+$ and LOX-1$^-$ PMNs were isolated as described in Materials and Methods and then added to allogeneic MLR in the presence of neutralizing mouse anti-human LOX-1 antibody (10 μg/ml) or mouse IgG. Cell proliferation was evaluated in triplicate using [^{3}H]thymidine uptake. Means and SE are shown. *P* values calculated by *t* test from T cell proliferation without the presence of PMN are shown. (**F**) ROS production in LOX-1$^+$ and LOX-1$^-$ PMN from seven patients with HNC and NSCLC. ROS production was measured by staining with 2′,7′-dichlorofluorescin diacetate (DCFDA). MFI, mean fluorescence intensity. (**G**) Expression of *ARG1* and *NOS2* in LOX-1$^+$ and LOX-1$^-$ PMN from six patients with HNC and MM measured by qPCR. *P* values calculated by *t* test are shown.

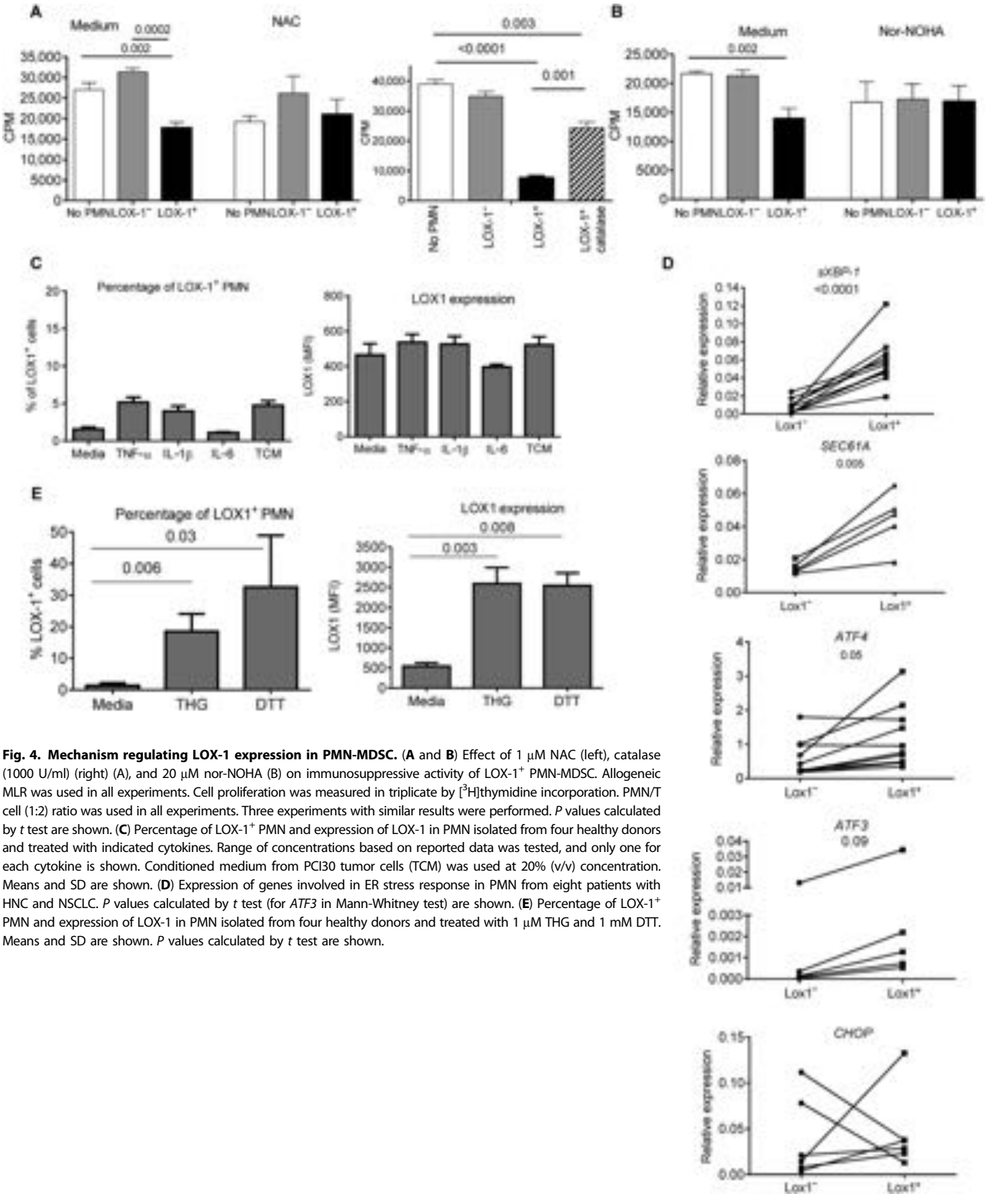

Fig. 4. Mechanism regulating LOX-1 expression in PMN-MDSC. (**A** and **B**) Effect of 1 μM NAC (left), catalase (1000 U/ml) (right) (A), and 20 μM nor-NOHA (B) on immunosuppressive activity of LOX-1$^+$ PMN-MDSC. Allogeneic MLR was used in all experiments. Cell proliferation was measured in triplicate by [^{3}H]thymidine incorporation. PMN/T cell (1:2) ratio was used in all experiments. Three experiments with similar results were performed. *P* values calculated by *t* test are shown. (**C**) Percentage of LOX-1$^+$ PMN and expression of LOX-1 in PMN isolated from four healthy donors and treated with indicated cytokines. Range of concentrations based on reported data was tested, and only one for each cytokine is shown. Conditioned medium from PCI30 tumor cells (TCM) was used at 20% (v/v) concentration. Means and SD are shown. (**D**) Expression of genes involved in ER stress response in PMN from eight patients with HNC and NSCLC. *P* values calculated by *t* test (for *ATF3* in Mann-Whitney test) are shown. (**E**) Percentage of LOX-1$^+$ PMN and expression of LOX-1 in PMN isolated from four healthy donors and treated with 1 μM THG and 1 mM DTT. Means and SD are shown. *P* values calculated by *t* test are shown.

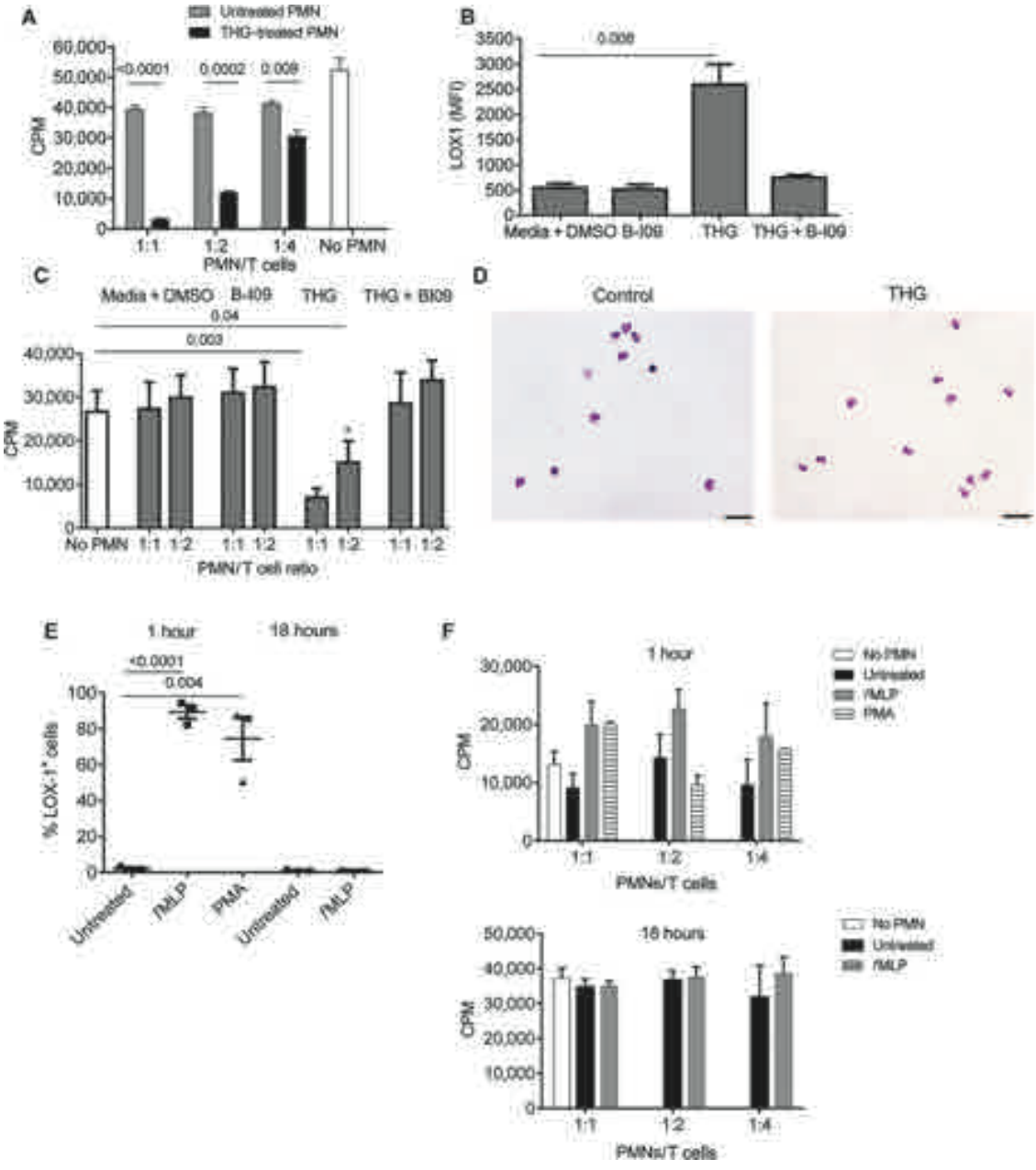

Fig. 5. ER stress induces LOX-1 expression and suppressive activity in PMN. (**A**) The ER stress inducer THG converted PMN to PMN-MDSC. PMNs isolated from healthy donors were treated overnight with 1 μM THG, extensively washed, and then used in CD3/CD28-induced T cell proliferation. T cell proliferation was measured in triplicate by [^{3}H]thymidine uptake. Three experiments with similar results were performed. *P* values calculated by *t* test are shown; *n* = 3. (**B** and **C**) The sXBP1 inhibitor B-I09 abrogated THG-inducible up-regulation of LOX-1 and T cell suppression in PMN from healthy donors. PMNs were incubated together with 20 μM B-I09 and THG overnight followed by evaluation of LOX-1 expression (B) or suppressive activity (C). PMNs from three healthy donors were used in these experiments. *P* values between treated and untreated PMNs (*t* test; *n* = 3). (**D**) Morphology of healthy donor's PMN after 18 hours of incubation with GM-CSF (10 ng/ml) and THG. Giemsa stain. Scale bars, 20 μm. (**E**) Healthy donor's PMNs were cultured for 1 or 18 hours with 10 nM *f*MLP or 20 nM PMA in the presence of GM-CSF (10 ng/ml). The proportion of LOX-1$^+$ cells was evaluated. *P* values were calculated by *t* test (*n* = 3). Analysis of PMA effect after 18 hours was not performed because of undetectable number of viable cells. (**F**) PMNs treated with *f*MLP or PMA as described in (E) were extensively washed after 1 or 18 hours (*f*MLP only) of incubation and tested in a T cell suppression assay. Each experiment was performed in triplicate. Three donors were tested.

LOX-1 defines PMN-MDSC in tumor tissues

It is known that LOX-1 is shed from the surface of the cells and can be detected in plasma (*27*). We evaluated the correlation between the presence of PMN-MDSCs in cancer patients and soluble LOX-1 in plasma. In NSCLC and CC patients, the proportion of PMN-MDSC was associated with soluble LOX-1 (Fig. 6A), suggesting that these cells may be an important source of LOX-1 in plasma of cancer patients.

There is now sufficient evidence demonstrating that tumor MDSCs are more suppressive than cells in PB [reviewed in (*28*)]. We asked whether the population of PMN-MDSCs is more prevalent among all PMNs in tumors than in PB. The proportion of LOX-1$^+$ cells in CD15$^+$ PMN isolated from tumors of patients with HNC and NSCLC was more than threefold higher than in CD15$^+$ PMN from PB of the same patients ($P < 0.001$) (Fig. 6B). Cells in blood and tumor tissues were subjected to the same digestion protocol. However, to exclude possible effect of tissue digestions and isolation on LOX-1 expression, we also evaluated patients with multiple myeloma (MM), where the tumor is located in the BM. We have previously shown a substantial increase of PMN-MDSC in both BM and PB of MM patients (*29*). Similar to solid tumors, the proportion of LOX-1$^+$ PMN-MDSC in BM was three- to fourfold higher than in PB of the same patients ($P = 0.004$) (Fig. 6C). LOX-1$^+$ PMN-MDSC isolated from BM of patients with MM had profound immunosuppressive activity, whereas LOX-1$^-$ PMN did not suppress T cells (Fig. 6D), supporting the conclusion that LOX-1$^+$ PMNs represent PMN-MDSCs at the tumor site.

To evaluate the presence of LOX-1$^+$ PMN-MDSC in tumor tissues, we have developed a method of immunofluorescence staining of paraffin-embedded tissues with the combination of LOX-1 and CD15 antibody (Fig. 6E). Control tissues from normal skin, colon, and lymph nodes had similar low numbers of LOX-1$^+$CD15$^+$ PMN-MDSCs (Fig. 6F). No statistical differences were found in the presence of these cells in melanoma samples, which is consistent with findings that M-MDSCs but not PMN-MDSCs are the predominant population of MDSCs in these patients (*2*). The number of LOX-1$^+$CD15$^+$ PMN-MDSCs in colon carcinoma increased more than 8-fold, in HNC more than 10-fold, and in NSCLC almost 8-fold (Fig. 6F). Thus, LOX-1 expression defines the population of PMN-MDSCs in tumor tissues.

OLR1 expression and the presence of LOX-1$^+$ PMN-MDSC are associated with clinical parameters

Using Oncomine and TCGA (The Cancer Genome Atlas) databases, we evaluated the association of *OLR1* expression in tumor tissues with clinical parameters in different types of cancer. Significant up-regulation of *OLR1* was observed in many types of cancer (Fig. 7A). The notable exception was lung cancer, where normal lung tissues showed markedly higher expression of *OLR1* than did other normal tissues (Fig. 7B), apparently due to cells with high expression of *OLR1* (possibly lung epithelium). *OLR1* expression positively correlated with clinical stage in patients with bladder cancer and clear cell kidney cancer. The positive correlation with tumor size was found in patients with prostate adenocarcinoma, colon adenocarcinoma, bladder cancer, and rectum adenocarcinoma (Fig. 7C). Higher expression of *OLR1* was associated with worse survival in patients with HNC (Fig. 7D). Although these results are suggestive, their interpretation as reflecting the presence of PMN-MDSC has some limitations because of the fact that *OLR1* can be expressed in different cells in the tumor microenvironment. We focused on the evaluation of LOX-1$^+$ PMN-MDSC in tumor tissues and PB.

In patients with NSCLC, we evaluated the possible link between the stage of the disease and the proportion of LOX-1$^+$ PMN-MDSC in PB. Patients with both early (I/II) and late (III/IV) stages of NSCLC had a significantly higher proportion of LOX-1$^+$ PMN-MDSC than healthy donors. There was no statistical significant difference between these two groups of patients (Fig. 7E). However, whereas 85.7% of all patients with late stages of NSCLC had an increase in LOX-1$^+$ PMN-MDSC population, only 50% of patients with early stages showed elevated level of these cells (Fig. 7E). Significant association of the presence of LOX-1$^+$ PMN-MDSC in PB of cancer patients was determined by the size of the tumors. Only patients with large tumors (T2-T3) had significantly higher proportion of LOX-1$^+$ PMN-MDSC than healthy donors, whereas patients with small tumors (T1) had a very low level of LOX-1$^+$ PMN-MDSC similar to healthy donors. Patients with large tumors had significantly more LOX-1$^+$ PMN-MDSC than those with small tumors (Fig. 7F). Using an NSCLC adenocarcinoma tissue array, we evaluated the association between the presence of LOX-1$^+$ PMN-MDSC in tumor tissues and tumor size. Similar to the data obtained in PB, no significant association was found with stage of the disease. The number of LOX-1$^+$ PMN-MDSCs was higher in larger (T2 versus T1) tumors (Fig. 7G).

DISCUSSION

The goal of this study was to address the issue of heterogeneity of human PMN-MDSCs, which limits the progress of our understanding of the biology of these cells. Currently, only partially enriched population of PMN-MDSCs isolated on Ficoll gradient can be evaluated. This population contains not only suppressive PMN-MDSCs but also nonsuppressive activated PMNs. Separation of PMN-MDSCs and PMNs in tumor tissues is not possible, which further complicates the analysis of these cells. Here, we report that PMN-MDSCs have a unique gene expression profile, which is substantially different from that of PMNs from the same patients and from healthy donors. This directly supports the notion that PMN-MDSCs represent a distinct functional state of pathological activation of neutrophils in cancer (*30*, *31*) and is consistent with the analysis of gene expression performed in mice, which demonstrated differences in transcriptome between granulocytes isolated from naïve mice and PMN-MDSCs from tumor-bearing mice (*32*).

Up-regulation of genes associated with ER stress response was a prominent feature of PMN-MDSC. The ER stress response is developed to protect cells from various stress conditions, such as hypoxia, nutrient deprivation, and low pH, and includes three major signaling cascades initiated by three protein sensors: protein kinase RNA-like ER kinase (PERK), inositol-requiring enzyme 1 (IRE1), and ATF6 (*33*). PERK phosphorylates eIF2α, which controls the initiation of mRNA translation and inhibits the flux of synthesized proteins. eIF2α induces the expression of ATF4 and its downstream targets, including the proapoptotic transcription factor CHOP. IRE1 cleaves the mRNA encoding for the transcription factor XBP1 (*34*). sXBP1 mRNA is then ligated by an RNA ligase and translated to produce sXBP1 transcription factor that regulates many target genes including *SEC61a* (*35*).

ER stress response was previously shown to be transmitted to dendritic cells and macrophages from tumor cells and was associated with up-regulation of ARG1 in macrophages (*36*–*38*). Constitutive activation of XBP1 in tumor-associated dendritic cells promoted ovarian cancer progression by blunting antitumor immunity (*39*). We have recently found activation of the ER stress response in MDSC by demonstrating that MDSCs isolated from tumor-bearing mice or cancer patients overexpress sXBP1 and CHOP and displayed an enlarged ER, one of the hallmarks of ER stress (*16*). Another study implicated CHOP in the suppressive activity of MDSC in tumor site (*40*). Consistent with these observations,

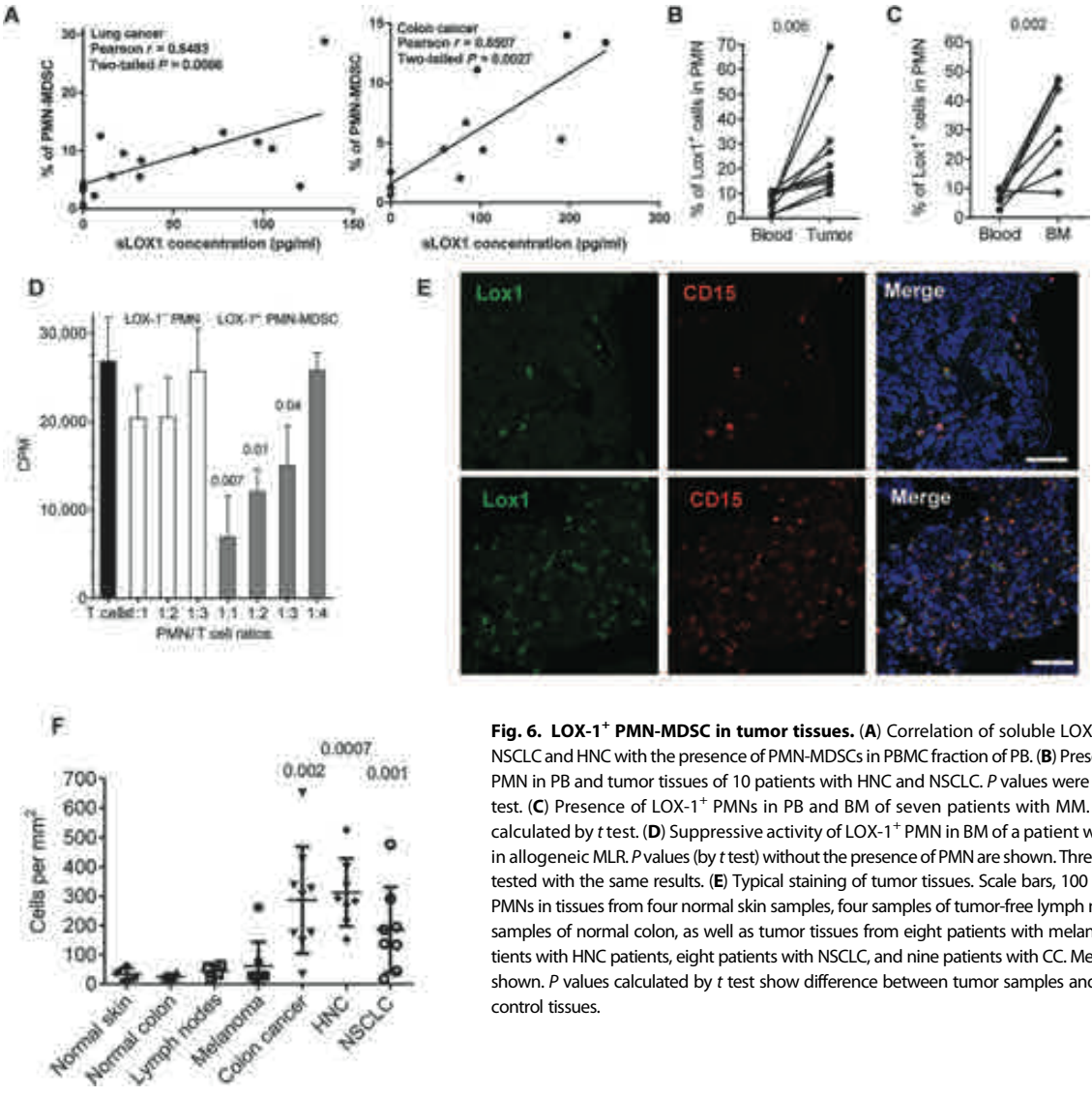

Fig. 6. LOX-1$^+$ PMN-MDSC in tumor tissues. (**A**) Correlation of soluble LOX1 in plasma of NSCLC and HNC with the presence of PMN-MDSCs in PBMC fraction of PB. (**B**) Presence of LOX-1$^+$ PMN in PB and tumor tissues of 10 patients with HNC and NSCLC. *P* values were calculated by *t* test. (**C**) Presence of LOX-1$^+$ PMNs in PB and BM of seven patients with MM. *P* values were calculated by *t* test. (**D**) Suppressive activity of LOX-1$^+$ PMN in BM of a patient with MM tested in allogeneic MLR. *P* values (by *t* test) without the presence of PMN are shown. Three patients were tested with the same results. (**E**) Typical staining of tumor tissues. Scale bars, 100 μm. (**F**) LOX-1$^+$ PMNs in tissues from four normal skin samples, four samples of tumor-free lymph nodes, and four samples of normal colon, as well as tumor tissues from eight patients with melanoma, eight patients with HNC patients, eight patients with NSCLC, and nine patients with CC. Means and SD are shown. *P* values calculated by *t* test show difference between tumor samples and samples from control tissues.

administration of an ER stress inducer to tumor-bearing mice increased the accumulation of MDSCs and their suppressive activity (*41*).

Here, we have determined that the expression of LOX-1 receptor was associated with PMN-MDSCs. LOX-1 is a class E scavenger receptor that is expressed in macrophages and chondrocytes, as well as in endothelial and smooth muscle cells (*20*). The expression of this receptor on neutrophils has not been previously described. We have found that neutrophils from healthy donors and cancer patients have practically undetectable expression of LOX-1. Our data suggested that LOX-1 expression not only is associated with but also defines the population of PMN-MDSC in cancer patients. This conclusion is supported by several lines of evidence: (i) LOX-1$^+$ PMN had gene expression profile similar to that of enriched PMN-MDSC isolated using gradient centrifugation, whereas LOX-1$^-$ PMN had profile similar to neutrophils; (ii) LOX-1$^+$, but not LOX-1$^-$, PMN potently suppressed T cell responses; (iii) LOX-1$^+$ PMN had significantly higher expression of *ARG1* and production of ROS, typical characteristics of PMN-MDSC. We also found that, in tumor tissues, only LOX-1$^+$ PMNs were immunosuppressive and could be considered as PMN-MDSCs. This opens an opportunity for a direct identification of PMN-MDSCs in PB and tumor tissues.

These observations, although unexpected, fit the overall concept of the critical role of ER stress response in MDSC biology. It was recently demonstrated that, in human endothelial cells, oxLDL induced the expression of LOX-1 through activation of the ER stress sensors IRE1 and PERK (*42*). In contrast, ER stress induced by tunicamycin in hepatic L02 cells caused down-regulation of LOX-1. Knockdown of IRE1 or XBP1 restored LOX-1 expression in these cells (*43*). In our experiment, we found that induction of ER stress in neutrophils caused marked up-regulation of LOX-1. This was associated with acquisition of immunosuppressive activity by these cells, indicating that induction of ER stress response could convert neutrophils to PMN-MDSCs. MDSCs accumulate as the result of convergences of two only partially overlapping groups of signals: the signals that promote myelopoiesis (primarily via growth factors and cytokines produced by tumors) and the signals that induce the suppressive activity in these cells (believed to be associated with proinflammatory cytokines) (*17*). ER stress emerged as an

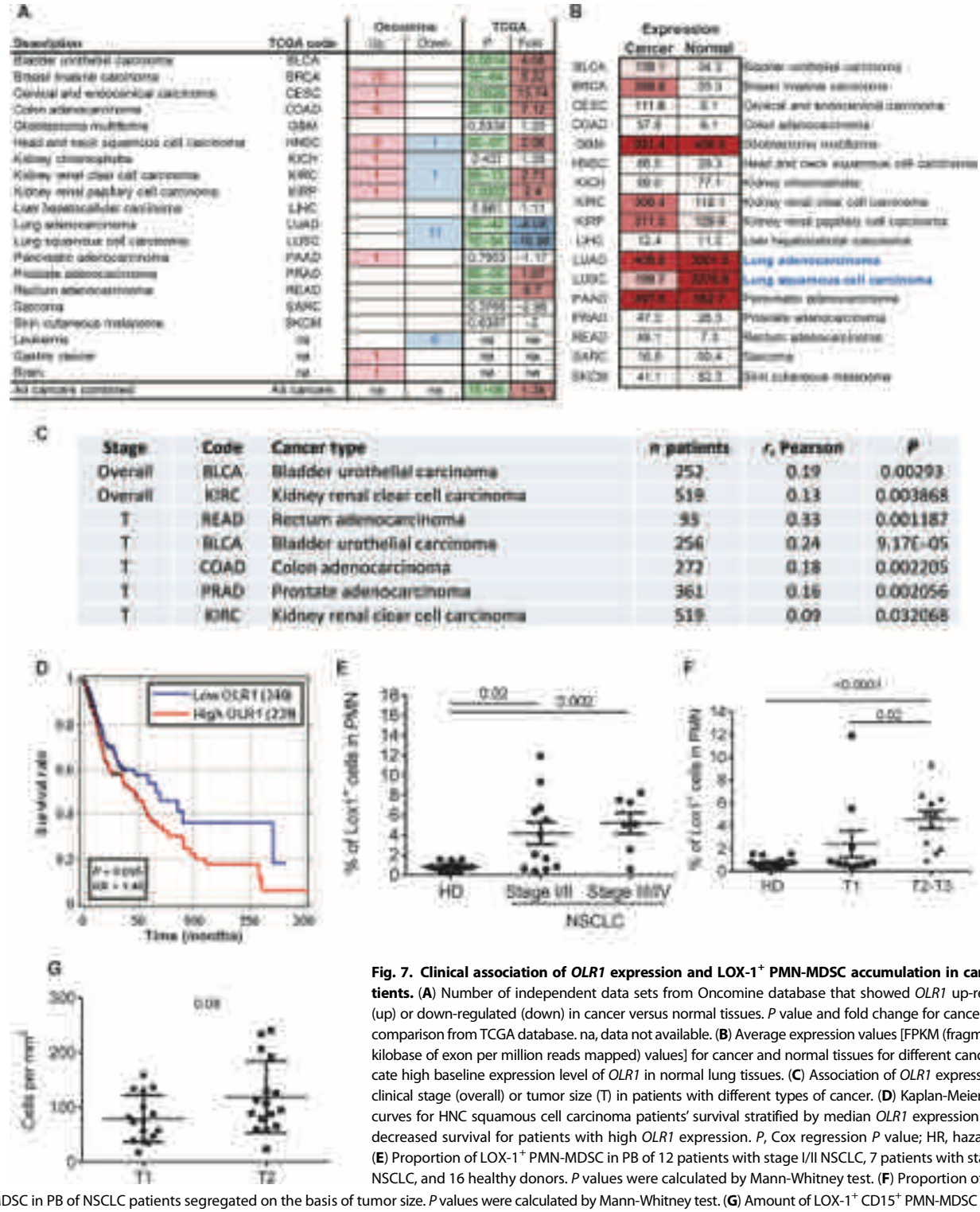

Fig. 7. Clinical association of *OLR1* expression and LOX-1$^+$ PMN-MDSC accumulation in cancer patients. (**A**) Number of independent data sets from Oncomine database that showed *OLR1* up-regulated (up) or down-regulated (down) in cancer versus normal tissues. *P* value and fold change for cancer/normal comparison from TCGA database. na, data not available. (**B**) Average expression values [FPKM (fragments per kilobase of exon per million reads mapped) values] for cancer and normal tissues for different cancers indicate high baseline expression level of *OLR1* in normal lung tissues. (**C**) Association of *OLR1* expression with clinical stage (overall) or tumor size (T) in patients with different types of cancer. (**D**) Kaplan-Meier survival curves for HNC squamous cell carcinoma patients' survival stratified by median *OLR1* expression indicate decreased survival for patients with high *OLR1* expression. *P*, Cox regression *P* value; HR, hazard ratio. (**E**) Proportion of LOX-1$^+$ PMN-MDSC in PB of 12 patients with stage I/II NSCLC, 7 patients with stage III/IV NSCLC, and 16 healthy donors. *P* values were calculated by Mann-Whitney test. (**F**) Proportion of LOX-1$^+$ PMN-MDSC in PB of NSCLC patients segregated on the basis of tumor size. *P* values were calculated by Mann-Whitney test. (**G**) Amount of LOX-1$^+$ CD15$^+$ PMN-MDSC in tumor tissues from NSCLC patients segregated on the basis of tumor size. *P* values were calculated by *t* test.

important factor in the second group. We did not find morphological evidence that PMNs dedifferentiate during the culture with THG. However, in our experiments, we targeted mature neutrophils. It is possible that ER stress may have much broader effect on precursor or progenitor cells.

In our study, we did not investigate whether signaling through LOX-1 is responsible for acquisition of immunosuppressive activity by neutrophils. However, it is likely that it contributes to this process. Engagement of LOX-1 can lead to induction of oxidative stress, apoptosis, and activation of the NF-κB pathway (*18*). These pathways are important for PMN-MDSC function. The ER stress response pathway has been shown to regulate inflammation by activating the NF-κB pathway (*35*, *44*, *45*). LOX-1 up-regulation has been observed during cellular transformation into a cancer cell and can have a pro-oncogenic effect by activating the NF-κB pathway, by increasing DNA damage through increased ROS production, and by promoting angiogenesis and cell dissemination (*46*, *47*). It is possible that LOX-1 signaling may drive pathological activation of PMN toward PMN-MDSC. Cell surface LOX-1 expression can be elevated by multiple stimuli including ROS, inflammatory cytokines [TNF-α and TGF-β (transforming growth factor–β)], and oxLDL (*48*). These factors are produced in cancer, and it is possible that they can affect differentiation of granulocytes from precursors, leading to acquisition of LOX-1 expression. The question is why only 4 to 7% of neutrophils acquire LOX-1 expression and suppressive activity to become PMN-MDSCs. This is an unresolved issue at present mainly because the nature of factors that convert neutrophils to PMN-MDSCs remains unclear. On the basis of mouse studies, it is possible that PMN-MDSCs may have different precursors than most neutrophils, and those precursors are more sensitive to ER stress–inducible factors.

Our study has obvious limitations derived from the nature of human studies and the nature of neutrophils as short-lived differentiated cells. This restrained our ability to provide deeper insight to the mechanism of the observed phenomenon of LOX-1 up-regulation. More information can be generated from the experiments studying progenitors and precursors of neutrophils. For example, we used a neutralizing LOX-1 antibody in an attempt to block signaling through this receptor. This approach may not be sufficient because of the fact that PMN-MDSCs in PB may not be amendable for such regulation. However, LOX-1 can be involved in the regulation of PMN precursors, and the antibody may have an effect. PMN progenitors could be manipulated genetically, which would allow for more precise analysis of this pathway.

We could not find an association between LOX-1 expression and PMN-MDSCs in two mouse models. These results are unexpected, because these models (EL-4 and LLC) are associated with inflammation and expansion of PMN-MDSC. It is possible that such association can be found in other tumor models. However, it is more likely that the expression of LOX-1 in mice and humans is regulated differently. The mechanism remains unclear.

Combination of neutrophil markers with LOX-1 potentially allows for detection of PMN-MDSC in tissues. We observed a marked increase in the number of PMN-MDSC in tumors of patients with HNC, CC, and NSCLC. No such increase was observed in melanoma patients. It is possible that relatively low accumulation of PMN-MDSC in melanoma patients may contribute to this observation. Our data demonstrated that patients have variable amount of LOX-1$^+$ PMN-MDSC, which, at least in patients with NSCLC, was associated with size of the tumors. Further prospective studies are needed to determine whether the presence of these cells in tumor tissues can predict clinical outcome. The expression of LOX-1 on PMN-MDSC opens an opportunity for selective targeting of these cells, because an antibody targeting LOX-1 has already been tested in cardiovascular diseases in mice (*49*, *50*).

MATERIALS AND METHODS

Study design

The aims of this study were to better characterize human PMN-MDSCs and to identify specific markers that allow distinguishing these cells from neutrophils. We performed whole-gene expression array using triplicate of samples. LOX-1 expression was measured by flow cytometry in variable number of replicates indicated in the figure legends. Experiments were performed in a controlled and nonblinded manner. No randomization was performed because of the observational nature of the study. Sample size of patient cohorts was determined on the basis of the results of initial experiments with LOX-1 expression and calculations of expected differences between mean and expected SD.

Human samples

Samples of PB and tumor tissues were collected from patients at the Helen F. Graham Cancer Center and University of Pennsylvania. The study was approved by the institutional review boards (IRBs) of the Christiana Care Health System at the Helen F. Graham Cancer Center, University of Pennsylvania, and Wistar Institute. All patients signed approved consent forms. PB was collected from (i) 26 patients with different stages of NSCLC [12 females, 18 males; ages 59 to 79 years (median, 69 years); 13 patients had squamous cell carcinoma and 13 patients had adenocarcinoma], (ii) 21 patients with HNC [8 females, 13 males; ages 32 to 82 years (median, 65 years); 19 patients had squamous cell carcinoma and 2 patients had adenocarcinoma], (iii) 38 patients with CC (adenocarcinoma) [20 females, 18 males; ages 28 to 88 years (median, 58 years)], and (iv) 6 patients with MM [1 female, 5 males; ages 58 to 81 years (median, 75 years)].

All patients were either previously untreated or received treatment (chemotherapy or radiation therapy) at least 6 months before collection of blood. In some patients, tumor tissues were collected during the surgery. In addition, six patients with eosinophilic colitis, three patients with ulcerative colitis, and eight patients with Crohn's disease were evaluated. Peripheral samples of blood from 18 healthy volunteers [12 females, 6 males; ages 35 to 56 years (median, 42 years)] were used as control. All samples were evaluated within 3 hours after collection.

Lung cancer tumor microarrays were produced from formalin-fixed, paraffin-embedded tissue. Each block was examined by a pathologist; three cores were obtained from tumor-containing areas, and three blocks were from non–tumor-involved lung regions. Samples were obtained from 32 patients with adenocarcinoma. Clinical data obtained included tumor histology, tumor size, disease stage, and time to recurrence (all patients followed for 5 years).

Deidentified samples from normal colonic biopsy colons were obtained from St. Mark's Hospital, Harrow, UK. Samples were taken from patients after obtaining informed consent and with the approval of the Outer West London Research Ethics Committee (UK). Paraffin-embedded tissue blocks of samples of normal skin, lymph nodes, and melanoma were retrieved using an approved IRB protocol for deidentified archived skin biopsies through the Department of Dermatology National Institutes of Health Skin Diseases Research Center Tissue Acquisition Core (P30-AR057217), Perelman School of Medicine, University of Pennsylvania (Philadelphia, PA).

Cell isolation and culture

PMN-MDSC and PMN were isolated by centrifugation over a double-density gradient Histopaque (Sigma) (1.077 to collect PBMCs and 1.119 to collect PMN), labeled with CD15-phycoerythrin (PE) monoclonal antibody (mAb) (BD Biosciences), and then separated using anti-PE beads and MACS column (Miltenyi).

Tissues were first digested with the Tumor Dissociation Kit, human (Miltenyi), and then red blood cells were lysed. Cells were then cultured in RPMI (BioSource International) supplemented with 10% fetal bovine serum, 5 mM glutamine, 25 mM Hepes, 50 μM β-mercaptoethanol, and 1% antibiotics (Invitrogen). In some experiments, recombinant GM-CSF (PeproTech) was added to the culture medium at a concentration of 10 ng/ml.

Isolation of Lox-1$^+$ PMN from PB and suppression assay

Whole blood was enriched for PMNs using MACSxpress Neutrophil Isolation Kit (Miltenyi) following the protocol provided by the manufacturer. Cells were then labeled with anti-Lox1–PE mAb (BioLegend) and then separated using anti-PE beads and MACS column (Miltenyi). For the three-way allogeneic MLR suppression assay, T lymphocytes from one healthy donor were purified with the Human CD3+ T Cell Enrichment Column Kit (R&D Systems) and used as responder cells. Dendritic cells were generated from adherent monocytes from another healthy donor in the presence of GM-CSF (25 ng/ml) and IL-4 (25 ng/ml) (PeproTech) for 6 days and used as stimulator cells. Responder and stimulator cells were then mixed at a 10:1 ratio followed by the addition of Lox1$^+$ or Lox1$^-$ PMNs. T lymphocyte proliferation was assessed after 5 days of culture by thymidine incorporation.

Concurrently, T lymphocytes were isolated from the PBMCs of the same patient as LOX-1$^+$ PMNs using the Human CD3+ T Cell Enrichment Column Kit. PMNs were plated at different ratios with 10^5 T lymphocytes in a 96-well plate coated with anti-CD3 (10 μg/ml) (clone UCHT1; BD Biosciences) followed by the addition of soluble anti-CD28 (1 μg/ml) (clone CD28.2; BD Biosciences). T lymphocyte proliferation was assessed after 3 days of culture by thymidine incorporation. In some experiments, 1 μM NAC (Sigma), 20 μM nor-NOHA (Cayman Chemical), or human LOX-1 mAb (10 μg/ml) (R&D Systems) was added to the culture medium to block ROS or ARG1 activity, respectively. T lymphocyte proliferation was assessed after 5 days of culture by thymidine incorporation.

In vitro PMN Lox-1 induction

PMNs from healthy donors were isolated on a Histopaque gradient. Cells (5×10^5/ml) were cultured for 12 hours with GM-CSF (10 ng/ml) in the presence of DTT (0.5, 1, and 2 mM; Sigma), tunicamycin (0.5, 1, and 2 μg/ml; Sigma-Aldrich), or THG (0.5, 1, and 2 μM; Sigma). In some instances, the XBP1 inhibitor B-I09 (20 μM) was added 3 hours before culture. Cells were then stained for flow cytometry or used for functional assays as described above. For *f*MLP and PMA stimulation, PMNs were isolated from healthy donors and cultured for 1 or 18 hours with either 10 nM *f*MLP (Sigma-Aldrich) or 20 nM PMA (Sigma-Aldrich). Cells were then washed, and LOX1 expression was measured by flow cytometry or used for functional assays as described above. For overnight cultures, GM-CSF (10 ng/ml) was added to the culture.

Flow cytometry

Flow cytometry data were acquired using a BD LSR II flow cytometer and analyzed using FlowJo software (Tree Star).

Immunofluorescence microscopy

After deparaffinization and rehydration, heat-induced antigen retrieval was performed using tris-EDTA buffer (pH 9). Tissues were stained with Lox1 antibody (Abcam, catalog no. ab126538) and CD15 antibody (BD Biosciences, catalog no. 555400) at 1:200 dilution in 5% BSA each for 1 hour at room temperature, followed by blocking with 5% bovine serum albumin (BSA). The following secondary antibodies were used: Alexa Fluor anti-rabbit A647 (1:200 dilution in 5% BSA, Life Technologies) for Lox1 and anti-mouse A514 (1:400 dilution in 5% BSA, Life Technologies) for CD15 staining. CD15 staining was pseudocolored red, and Lox1 staining was pseudocolored green. The nucleus was stained with 4′,6-diamidino-2-phenylindole (1:5000 dilution in phosphate-buffered saline, Life Technologies). Images were obtained using Leica TCS SP5 confocal microscope. Cell counts from 16 frames were used to calculate counts per square millimeter.

Microarray analysis

For sample preparation and hybridization, total RNA from purified cells was isolated with TRIzol reagent according to the manufacturer's recommendations. RNA quality was assessed with the Bioanalyzer (Agilent). Only samples with RNA integrity numbers >8 were used. Equal amount (400 ng) of total RNA was amplified as recommended by Illumina and was hybridized to the Illumina HumanHT-12 v4 human whole-genome bead arrays.

For data preprocessing, the Illumina GenomeStudio software was used to export expression values and calculated detection *P* values for each probe of each sample. Signal intensity data were $\log_2$-transformed and quantile-normalized. Only probes with a significant detection *P* value ($P < 0.05$) in at least one of the samples were considered. The data were submitted to Gene Expression Omnibus (GEO) and are accessible using accession number GSE79404.

Differential expression for probes was tested using "significance analysis of microarrays" method (*51*). Multiple groups were compared using "multiclass" option, and matched patient sample groups were compared using "two-sample paired" option. FDR was estimated using the procedure of Storey and Tibshirani (*52*). Genes with an FDR of <5% were considered significant unless stated otherwise. Hierarchical cluster was performed using standardized Euclidean distance with average linkage. Genes that had Gene Ontology (GO) annotation GO:0005886 (plasma membrane) and either GO:0004872 (receptor activity) or GO:0009897 (external side of plasma membrane) were considered as candidates for surface molecular markers. For expression heat maps, samples from the same patient were additionally normalized to the average between them, and samples from healthy donors were normalized to average between all patient samples. Enrichment analyses were done using IPA (Qiagen, Redwood City; www.qiagen.com/ingenuity). Pathway results with FDR < 5% and $P < 10^{-5}$ were considered significant. Only regulators that passed $P < 10^{-8}$ threshold with significantly predicted ($Z > 2$) activation state in PMN-MDSCs were reported. For OLR1 gene expression associated with cancer, Oncomine (https://www.oncomine.org) was used with "cancer versus normal" gene report without any additional filters. Additionally, TCGA RNA-seqV2 level 3 data (https://tcga-data.nci.nih.gov) were used, and RPKM (reads per kilobase of transcript per million mapped reads) expression values were compared between cancer and normal tissues (where available) using *t* test. Association with survival was done using univariate Cox regression, and Kaplan-Meier curves were plotted for patients split into two groups using median expression. Results with $P < 0.05$ were considered significant.

Quantitative reverse transcription polymerase chain reaction

Total RNA was prepared with E.Z.N.A. Total RNA isolation Kit I (Omega Bio-tek), and complementary DNA (cDNA) was synthesized with High-Capacity cDNA Reverse Transcription Kit (Applied Biosystems). Quantitative reverse transcription PCR was performed with Power SYBR Green PCR Master Mix (Applied Biosystems). The relative amount of mRNA was estimated by the comparative threshold cycle method, with *gapdh* as the reference gene. For the analysis of gene expression, the following primers were used: *sXBP1*, 5′-CTGAGTCCGCAGCAGGTG-3′ and 5′-AGTTGTCCAGAATGCCCAACA-3′; *DDIT3* (*CHOP*), 5′-GCACCTCCCAGAGCCCTCACTCTCC-3′ and 5′-GTCTACTCCAAGCCTTCCCCCTGCG-3′; *ATF4*, 5′-TTCCTGAGCAGCGAGGTGTTG-3′ and 5′-TCCAATCTGTCCCGGAGAAGG-3′; *ATF3*, 5′-TGCCTCGGAAGTGAGTGCTT-3′ and 5′-GCAAAATCCTCAAACACCAGTG-3′; *SEC61a*, 5′-GGATGTATGGGGACCCTTCT-3′ and 5′-CTCGGCCAGTGTTGACAGTA-3′; *ARGI*, 5′-CTTGTTTCGGACTTGCTCGG-3′ and 5′-CACTCTATGTATGGGGGCTTA-3′; *NOS2*, 5′-CAGCGGGATGACTTTCCAA-3′ and 5′-AGGCAAGATTTGGACCTGCA-3′; *GAPDH*, 5′-GGAGTCAACGGATTTGGTCGTA-3′ and 5′-GGCAACAATATCCACTTTACCAGAGT-3′.

Statistics

Statistical analysis was performed using a two-tailed Student's *t* test or Mann-Whitney test after the analysis of distribution of variables. Significance was determined at $P < 0.05$ with normal-based 95% confidence interval means ± 2 SDs. Analysis of gene expression was adjusted for multiple variables, and FDR was estimated as described in (*52*). All calculations were made using GraphPad Prism 5 software (GraphPad Software Inc.).

SUPPLEMENTARY MATERIALS

immunology.sciencemag.org/cgi/content/full/1/2/aaf8943/DC1

Fig. S1. Gene expression differences between PMN-MDSCs and PMNs cells from cancer patients and healthy donors.

Fig. S2. CD16 and LOX-1 staining in PMN.

Fig. S3. Siglec-8 staining of $CD15^+$ PMN.

Fig. S4. LOX1 staining of healthy donor neutrophils.

Fig. S5. List of genes and their relative expression targeted by 93 microarray probes shown to be highly differentially expressed (FDR < 5%, fold > 2) for both $LOX\text{-}1^+/LOX\text{-}1^-$ and PMN-MDSC/PMN comparisons.

Fig. S6. LOX-1 antibody does not induce immunosuppressive activity of PMN.

Fig. S7. LOX-1 expression in mouse PMN-MDSC.

Fig. S8. LOX-1 expression is not associated with mouse PMN-MDSC.

Table S1. Canonical pathways identified by IPA among genes significantly differentially expressed between PMN-MDSC and PMN cells.

Source data (Excel)

REFERENCES AND NOTES

1. T. Condamine, I. Ramachandran, J.-I. Youn, D. I. Gabrilovich, Regulation of tumor metastasis by myeloid-derived suppressor cells. *Annu. Rev. Med.* **66**, 97–110 (2015).
2. M. N. Messmer, C. S. Netherby, D. Banik, S. I. Abrams, Tumor-induced myeloid dysfunction and its implications for cancer immunotherapy. *Cancer Immunol. Immunother.* **64**, 1–13 (2015).
3. J. Finke, J. Ko, B. Rini, P. Rayman, J. Ireland, P. Cohen, MDSC as a mechanism of tumor escape from sunitinib mediated anti-angiogenic therapy. *Int. Immunopharmacol.* **11**, 856–861 (2011).
4. P.-H. Feng, K.-Y. Lee, Y.-L. Chang, Y.-F. Chan, L.-W. Kuo, T.-Y. Lin, F.-T. Chung, C.-S. Kuo, C.-T. Yu, S.-M. Lin, C.-H. Wang, C.-L. Chou, C.-D. Huang, H.-P. Kuo, $CD14^+S100A9^+$ monocytic myeloid-derived suppressor cells and their clinical relevance in non–small cell lung cancer. *Am. J. Respir. Crit. Care Med.* **186**, 1025–1036 (2012).
5. E.-K. Vetsika, F. Koinis, M. Gioulbasani, D. Aggouraki, A. Koutoulaki, E. Skalidaki, D. Mavroudis, V. Georgoulias, A. Kotsakis, A circulating subpopulation of monocytic myeloid-derived suppressor cells as an independent prognostic/predictive factor in untreated non-small lung cancer patients. *J. Immunol. Res.* **2014**, 659294 (2014).
6. C.-Y. Liu, Y.-M. Wang, C.-L. Wang, P.-H. Feng, H.-W. Ko, Y.-H. Liu, Y.-C. Wu, Y. Chu, F.-T. Chung, C.-H. Kuo, K.-Y. Lee, S.-M. Lin, H.-C. Lin, C.-H. Wang, C.-T. Yu, H.-P. Kuo, Population alterations of L-arginase- and inducible nitric oxide synthase-expressed $CD11b^+/CD14^-/CD15^+/CD33^+$ myeloid-derived suppressor cells and $CD8^+$ T lymphocytes in patients with advanced-stage non-small cell lung cancer. *J. Cancer Res. Clin. Oncol.* **136**, 35–45 (2010).
7. C. M. Diaz-Montero, M. L. Salem, M. I. Nishimura, E. Garrett-Mayer, D. J. Cole, A. J. Montero, Increased circulating myeloid-derived suppressor cells correlate with clinical cancer stage, metastatic tumor burden, and doxorubicin–cyclophosphamide chemotherapy. *Cancer Immunol. Immunother.* **58**, 49–59 (2009).
8. C. Meyer, L. Cagnon, C. M. Costa-Nunes, P. Baumgaertner, N. Montandon, L. Leyvraz, O. Michielin, E. Romano, D. E. Speiser, Frequencies of circulating MDSC correlate with clinical outcome of melanoma patients treated with ipilimumab. *Cancer Immunol. Immunother.* **63**, 247–257 (2014).
9. A. A. Tarhini, H. Edington, L. H. Butterfield, Y. Lin, Y. Shuai, H. Tawbi, C. Sander, Y. Yin, M. Holtzman, J. Johnson, U. N. M. Rao, J. M. Kirkwood, Immune monitoring of the circulation and the tumor microenvironment in patients with regionally advanced melanoma receiving neoadjuvant ipilimumab. *PLOS One* **9**, e87705 (2014).
10. Z. Wang, Y. Zhang, Y. Liu, L. Wang, L. Zhao, T. Yang, C. He, Y. Song, Q. Gao, Association of myeloid-derived suppressor cells and efficacy of cytokine-induced killer cell immunotherapy in metastatic renal cell carcinoma patients. *J. Immunother.* **37**, 43–50 (2014).
11. S. E. Finkelstein, T. Carey, I. Fricke, D. Yu, D. Goetz, M. Gratz, M. Dunn, P. Urbas, A. Daud, R. DeConti, S. Antonia, D. Gabrilovich, M. Fishman, Changes in dendritic cell phenotype after a new high-dose weekly schedule of interleukin-2 therapy for kidney cancer and melanoma. *J. Immunother.* **33**, 817–827 (2010).
12. T. Kimura, J. R. McKolanis, L. A. Dzubinski, K. Islam, D. M. Potter, A. M. Salazar, R. E. Schoen, O. J. Finn, MUC1 vaccine for individuals with advanced adenoma of the colon: A cancer immunoprevention feasibility study. *Cancer Prev. Res.* **6**, 18–26 (2013).
13. J.-I. Youn, S. Nagaraj, M. Collazo, D. I. Gabrilovich, Subsets of myeloid-derived suppressor cells in tumor-bearing mice. *J. Immunol.* **181**, 5791–5802 (2008).
14. I. Poschke, R. Kiessling, On the armament and appearances of human myeloid-derived suppressor cells. *Clin. Immunol.* **144**, 250–268 (2012).
15. S. Mandruzzato, S. Brandau, C. M. Britten, V. Bronte, V. Damuzzo, C. Gouttefangeas, D. Maurer, C. Ottensmeier, S. H. van der Burg, M. J. P. Welters, S. Walter, Toward harmonized phenotyping of human myeloid-derived suppressor cells by flow cytometry: Results from an interim study. *Cancer Immunol. Immunother.* **65**, 161–169 (2016).
16. T. Condamine, V. Kumar, I. R. Ramachandran, J.-I. Youn, E. Celis, N. Finnberg, W. S. El-Deiry, R. Winograd, R. H. Vonderheide, N. R. English, S. C. Knight, H. Yagita, J. C. McCaffrey, S. Antonia, N. Hockstein, R. Witt, G. Masters, T. Bauer, D. I. Gabrilovich, ER stress regulates myeloid-derived suppressor cell fate through TRAIL-R–mediated apoptosis. *J. Clin. Invest.* **124**, 2626–2639 (2014).
17. T. Condamine, J. Mastio, D. I. Gabrilovich, Transcriptional regulation of myeloid-derived suppressor cells. *J. Leukoc. Biol.* **98**, 913–922 (2015).
18. N. Al-Banna, C. Lehmann, Oxidized LDL and LOX-1 in experimental sepsis. *Mediators Inflamm.* 2013, 761789 (**2013**).
19. T. Sawamura, N. Kume, T. Aoyama, H. Moriwaki, H. Hoshikawa, Y. Aiba, T. Tanaka, S. Miwa, Y. Katsura, T. Kita, T. Masaki, An endothelial receptor for oxidized low-density lipoprotein. *Nature* **386**, 73–77 (1997).
20. A. Taye, A. A. K. El-Sheikh, Lectin-like oxidized low-density lipoprotein receptor 1 pathways. *Eur. J. Clin. Invest.* **43**, 740–745 (2013).
21. R. Yoshimoto, Y. Fujita, A. Kakino, S. Iwamoto, T. Takaya, T. Sawamura, The discovery of LOX-1, its ligands and clinical significance. *Cardiovasc. Drugs Ther.* **25**, 379–391 (2011).
22. I. Moldovan, J. Galon, I. Maridonneau-Parini, S. Roman Roman, C. Mathiot, W.-H. Fridman, C. Sautès-Fridman, Regulation of production of soluble Fcγ receptors type III in normal and pathological conditions. *Immunol. Lett.* **68**, 125–134 (1999).
23. A. Banerjee, N. K. Mondal, D. Das, M. R. Ray, Neutrophilic inflammatory response and oxidative stress in premenopausal women chronically exposed to indoor air pollution from biomass burning. *Inflammation* **35**, 671–683 (2012).
24. J. L. Mehta, N. Sanada, C. P. Hu, J. Chen, A. Dandapat, F. Sugawara, H. Satoh, K. Inoue, Y. Kawase, K.-i. Jishage, H. Suzuki, M. Takeya, L. Schnackenberg, R. Beger, P. L. Hermonat, M. Thomas, T. Sawamura, Deletion of LOX-1 reduces atherogenesis in LDLR knockout mice fed high cholesterol diet. *Circ. Res.* **100**, 1634–1642 (2007).
25. A. Pirillo, G. D. Norata, A. L. Catapano, LOX-1, OxLDL, and atherosclerosis. *Mediators Inflamm.* **2013**, 152786 (2013).
26. C.-H. A. Tang, S. Ranatunga, C. L. Kriss, C. L. Cubitt, J. Tao, J. A. Pinilla-Ibarz, J. R. Del Valle, C.-C. Hu, Inhibition of ER stress-associated IRE-1/XBP-1 pathway reduces leukemic cell survival. *J. Clin. Invest.* **124**, 2585–2598 (2014).
27. T. Sawamura, A. Kakino, Y. Fujita, LOX-1: A multiligand receptor at the crossroads of response to danger signals. *Curr. Opin. Lipidol.* **23**, 439–445 (2012).

28. V. Kumar, S. Patel, E. Tcyganov, D. Gabrilovich, The nature of myeloid-derived suppressor cells in the tumor microenvironment. *Trends Immunol.* **37**, 208–220 (2016).
29. I. R. Ramachandran, A. Martner, A. Pisklakova, T. Condamine, T. Chase, T. Vogl, J. Roth, D. Gabrilovich, Y. Nefedova, Myeloid-derived suppressor cells regulate growth of multiple myeloma by inhibiting T cells in bone marrow. *J. Immunol.* **190**, 3815–3823 (2013).
30. D. I. Gabrilovich, S. Ostrand-Rosenberg, V. Bronte, Coordinated regulation of myeloid cells by tumours. *Nat. Rev. Immunol.* **12**, 253–268 (2012).
31. D. Marvel, D. I. Gabrilovich, Myeloid-derived suppressor cells in the tumor microenvironment: Expect the unexpected. *J. Clin. Invest.* **125**, 3356–3364 (2015).
32. Z. G. Fridlender, J. Sun, I. Mishalian, S. Singhal, G. Cheng, V. Kapoor, W. Horng, G. Fridlender, R. Bayuh, G. S. Worthen, S. M. Albelda, Transcriptomic analysis comparing tumor-associated neutrophils with granulocytic myeloid-derived suppressor cells and normal neutrophils. *PLOS One* **7**, e31524 (2012).
33. M. Holcik, N. Sonenberg, Translational control in stress and apoptosis. *Nat. Rev. Mol. Cell Biol.* **6**, 318–327 (2005).
34. D. Ron, P. Walter, Signal integration in the endoplasmic reticulum unfolded protein response. *Nat. Rev. Mol. Cell Biol.* **8**, 519–529 (2007).
35. N. Cláudio, A. Dalet, E. Gatti, P. Pierre, Mapping the crossroads of immune activation and cellular stress response pathways. *EMBO J.* **32**, 1214–1224 (2013).
36. N. R. Mahadevan, V. Anufreichik, J. J. Rodvold, K. T. Chiu, H. Sepulveda, M. Zanetti, Cell-extrinsic effects of tumor ER stress imprint myeloid dendritic cells and impair $CD8^+$ T cell priming. *PLOS One* **7**, e51845 (2012).
37. N. R. Mahadevan, J. Rodvold, H. Sepulveda, S. Rossi, A. F. Drew, M. Zanetti, Transmission of endoplasmic reticulum stress and pro-inflammation from tumor cells to myeloid cells. *Proc. Natl. Acad. Sci. U.S.A.* **108**, 6561–6566 (2011).
38. N. R. Mahadevan, M. Zanetti, Tumor stress inside out: Cell-extrinsic effects of the unfolded protein response in tumor cells modulate the immunological landscape of the tumor microenvironment. *J. Immunol.* **187**, 4403–4409 (2011).
39. P. Walter, D. Ron, The unfolded protein response: From stress pathway to homeostatic regulation. *Science* **334**, 1081–1086 (2011).
40. P. T. Thevenot, R. A. Sierra, P. L. Raber, A. A. Al-Khami, J. Trillo-Tinoco, P. Zarreii, A. C. Ochoa, Y. Cui, L. Del Valle, P. C. Rodriguez, The stress-response sensor chop regulates the function and accumulation of myeloid-derived suppressor cells in tumors. *Immunity* **41**, 389–401 (2014).
41. B. R. Lee, S. Y. Chang, E. H. Hong, B. E. Kwon, H. M. Kim, Y. J. Kim, J. Lee, H. J. Cho, J. H. Cheon, H. J. Ko, Elevated endoplasmic reticulum stress reinforced immunosuppression in the tumor microenvironment via myeloid-derived suppressor cells. *Oncotarget* **5**, 12331–12345 (2014).
42. D. Hong, Y. P. Bai, H. C. Gao, X. Wang, L. F. Li, G. G. Zhang, C. P. Hu, Ox-LDL induces endothelial cell apoptosis via the LOX-1-dependent endoplasmic reticulum stress pathway. *Atherosclerosis* **235**, 310–317 (2014).
43. D. Hong, L. F. Li, H. C. Gao, X. Wang, C. C. Li, Y. Luo, Y. P. Bai, G. G. Zhang, High-density lipoprotein prevents endoplasmic reticulum stress-induced downregulation of liver LOX-1 expression. *PLOS One* **10**, e0124285 (2015).
44. S. E. Bettigole, L. H. Glimcher, Endoplasmic reticulum stress in immunity. *Annu. Rev. Immunol.* **33**, 107–138 (2014).
45. K. Zhang, R. J. Kaufman, From endoplasmic-reticulum stress to the inflammatory response. *Nature* **454**, 455–462 (2008).
46. H. A. Hirsch, D. Iliopoulos, A. Joshi, Y. Zhang, S. A. Jaeger, M. Bulyk, P. N. Tsichlis, X. Shirley Liu, K. Struhl, A transcriptional signature and common gene networks link cancer with lipid metabolism and diverse human diseases. *Cancer Cell* **17**, 348–361 (2010).
47. J. Lu, S. Mitra, X. Wang, M. Khaidakov, J. L. Mehta, Oxidative stress and lectin-like ox-LDL-receptor LOX-1 in atherogenesis and tumorigenesis. *Antioxid. Redox Signal.* **15**, 2301–2333 (2011).
48. X. Wang, M. I. Phillips, J. L. Mehta, LOX-1 and angiotensin receptors, and their interplay. *Cardiovasc. Drugs Ther.* **25**, 401–417 (2011).
49. J. De Siqueira, I. Abdul Zani, D. A. Russell, S. B. Wheatcroft, S. Ponnambalam, S. Homer-Vanniasinkam, Clinical and preclinical use of LOX-1-specific antibodies in diagnostics and therapeutics. *J. Cardiovasc. Transl. Res.* **8**, 458–465 (2015).
50. J. L. Mehta, M. Khaidakov, P. L. Hermonat, S. Mitra, X. Wang, G. Novelli, T. Sawamura, LOX-1: A new target for therapy for cardiovascular diseases. *Cardiovasc. Drugs Ther.* **25**, 495–500 (2011).
51. S. Zhang, A comprehensive evaluation of SAM, the SAM R-package and a simple modification to improve its performance. *BMC Bioinformatics* **8**, 230 (2007).
52. J. D. Storey, R. Tibshirani, Statistical significance for genomewide studies. *Proc. Natl. Acad. Sci. U.S.A.* **100**, 9440–9445 (2003).

Acknowledgments: We thank Q. Liu for help with statistical analysis and C. C. Hu and J. R. Del Valle for providing us with B-I09 inhibitor. **Funding:** This work was supported in part by the NIH (grants CA084488 and CA100062) and Janssen Pharmaceutical to D.I.G., the National Cancer Institute (grant P01 CA 098101) and American Cancer Society (grant RP-10-033-01-CCE) to A.R., and the flow cytometry and bioinformatics core facilities at the Wistar Institute. **Author contributions:** T.C. designed and performed most of the experiments and analyzed data; G.A.D. performed experiments, analyzed data, and wrote the manuscript; J.-I.Y., S.M., K.A.-T., E.T., A.H., C.L., and S.P. performed experiments; A.V.K. performed bioinformatics analysis; Y.N. analyzed data and wrote the manuscript; A.G., D.T.V., X.X., S.C.K., G. Malietzis, G.H.L., E.E., S.M.A., M.B., A.R., N.H., R.W., G. Masters, and B.N. provided clinical material and analyzed clinical correlates; X.W. and J.L.M. provided LOX-$1^{-/-}$ BM for the experiment; D.S. and M.A.S. designed experiments and analyzed data; D.I.G. designed the concept of the study and experiments, analyzed data, and wrote the manuscript. **Competing interests:** The authors declare that they have no competing interests. **Data and materials availability:** The data for this study have been deposited to GEO database and are accessible using accession number GSE79404.

Submitted 20 April 2016
Accepted 12 July 2016
Published 5 August 2016
10.1126/sciimmunol.aaf8943

Citation: T. Condamine, G. A. Dominguez, J.-I. Youn, A. V. Kossenkov, S. Mony, K. Alicea-Torres, E. Tcyganov, A. Hashimoto, Y. Nefedova, C. Lin, S. Partlova, A. Garfall, D. T. Vogl, X. Xu, S. C. Knight, G. Malietzis, G. H. Lee, E. Eruslanov, S. M. Albelda, X. Wang, J. L. Mehta, M. Bewtra, A. Rustgi, N. Hockstein, R. Witt, G. Masters, B. Nam, D. Smirnov, M. A. Sepulveda, D. I. Gabrilovich, Lectin-type oxidized LDL receptor-1 distinguishes population of human polymorphonuclear myeloid-derived suppressor cells in cancer patients. *Sci. Immunol.* **1**, aaf8943 (2016).

AACR American Association for Cancer Research

CANCER DISCOVERY

Tumor Cell-Independent Estrogen Signaling Drives Disease Progression through Mobilization of Myeloid-Derived Supressor Cells

Nikolaos Svoronos, Alfredo Perales-Puchalt, Michael J Allegrezza, et al.

Cancer Discov Published OnlineFirst September 30, 2016.

Author Manuscript Published OnlineFirst on September 30, 2016; DOI: 10.1158/2159-8290.CD-16-0502
Author manuscripts have been peer reviewed and accepted for publication but have not yet been edited.

TUMOR CELL-INDEPENDENT ESTROGEN SIGNALING DRIVES DISEASE PROGRESSION THROUGH MOBILIZATION OF MYELOID-DERIVED SUPPRESSOR CELLS

Nikolaos Svoronos[1], Alfredo Perales-Puchalt[1], Michael J. Allegrezza[1], Melanie R. Rutkowski[1], Kyle K. Payne[1], Amelia J. Tesone[1], Jenny M. Nguyen[1], Tyler J. Curiel[2, 3, 4], Mark G. Cadungog[5], Sunil Singhal[6] Evgeniy B. Eruslanov[6], Paul Zhang[7], Julia Tchou[8], Rugang Zhang[9] and Jose R. Conejo-Garcia[1#]

[1]Tumor Microenvironment and Metastasis Program and [9]Gene Expression and Regulation Program, The Wistar Institute, Philadelphia, PA 19104, USA. [2]The Graduate School of Biomedical Sciences, University of Texas Health Science Center, San Antonio, TX 78229. [3]Department of Medicine, University of Texas Health Science Center, San Antonio, TX 78229. [4]Cancer Therapy & Research Center, University of Texas Health Science Center, San Antonio, TX 78229. [5]Helen F. Graham Cancer Center, Christiana Care Health System, 4701 Ogletown-Stanton Road, Newark, DE 19713, USA. [6]Divisions of Thoracic Surgery and [8]Endocrine and Oncologic Surgery, Department of Surgery, and [7]Department of Pathology and Laboratory Medicine, University of Pennsylvania, Philadelphia, PA 19104.

#CORRESPONDENCE: Jose R Conejo-Garcia, MD, PhD
The Wistar Institute
3601 Spruce St
Philadelphia, PA 19104
Phone: (215) 495-6825
Fax: (215) 898-0847
Email: jrconejo@Wistar.org

Running title: Estrogens mobilize MDSCs

Keywords: MDSC, tumor immunology, tumor microenvironment

COI: The authors declare no conflict of interest

Financial support: This study was supported by grants to Jose R. Conejo-Garcia (R01CA157664, R01CA124515, R01CA178687, The Jayne Koskinas&Ted Giovanis Breast Cancer Research Consortium at Wistar and Ovarian Cancer Research Fund (OCRF) Program Project Development awards); Tyler J. Curiel (R01CA164122, CDMRP CA140355, P3054174, The Owens Foundation, The Skinner Endowment and OCRF Program Project Development award); Evgeniy B. Eruslanov: RO1CA187392. Michael J Allegrezza and Nikolaos Svoronos (T32CA009171); Kyle K Payne (5T32CA009140-39); and Alfredo Perales-Puchalt (Ann Schreiber Mentored Investigator Award (OCRF)). Support for Shared Resources was provided by Cancer Center Support Grant (CCSG) CA010815 (Dario Altieri).

Author Manuscript Published OnlineFirst on September 30, 2016; DOI: 10.1158/2159-8290.CD-16-0502
Author manuscripts have been peer reviewed and accepted for publication but have not yet been edited.

ABSTRACT

The role of estrogens in anti-tumor immunity remains poorly understood. Here we show that estrogen signaling accelerates the progression of different estrogen insensitive tumor models by contributing to deregulated myelopoiesis by both driving the mobilization of myeloid-derived suppressor cells (MDSCs) and enhancing their intrinsic immunosuppressive activity *in vivo*. Differences in tumor growth are dependent on blunted anti-tumor immunity and, correspondingly, disappear in immunodeficient hosts and upon MDSC depletion. Mechanistically, estrogen receptor alpha activates the STAT3 pathway in human and mouse bone marrow myeloid precursors by enhancing JAK2 and SRC activity. Therefore, estrogen signaling is a crucial mechanism underlying pathological myelopoiesis in cancer. Our work suggests that new anti-estrogen drugs that have no agonistic effects may have benefits in a wide range of cancers, independently of the expression of estrogen receptors in tumor cells, and may synergize with immunotherapies to significantly extend survival.

STATEMENT OF SIGNIFICANCE

Ablating estrogenic activity delays malignant progression independently of the tumor cell responsiveness, owing to a decrease in the mobilization and immunosuppressive activity of MDSCs, which boosts T-cell-dependent anti-tumor immunity. Our results provide a mechanistic rationale to block estrogen signaling with newer antagonists to boost the effectiveness of novel anti-cancer immunotherapies.

INTRODUCTION

Estrogens are pleiotropic steroid hormones known to influence many biological processes that ultimately affect homeostasis, such as development and metabolism. Estrogens bind to two high-affinity receptors (ERs; α and β) that activate similar but not identical response elements and are differentially expressed in multiple tissues. Due to their pathogenic role in accelerated malignant progression, ER^+ breast cancers have been commonly treated with tamoxifen. Tamoxifen, however, has mixed antagonist/agonist effect on on ERs, depending on cell type (1). Correspondingly, alternative interventions are currently evolving as results from clinical testing emerge (2). In contrast to breast cancer, anti-estrogen therapies have proven to be effective in only some ovarian cancer patients (3-7). However, these studies were exclusively focused on ER^+ cancer patients, which represent only 31% of ovarian cancer patients for ERα and 60% of patients for ERβ and did not provide any insight into the effects of estrogen activity on non-tumor cells.

Besides tumor cells, the tumor microenvironment plays a critical role in determining malignant progression as well as response to various therapies. In particular, it is becoming evident that tumors elicit immune responses that ultimately impact survival. In ovarian cancer, for instance, the presence of tumor-infiltrating lymphocytes is a major positive prognostic indicator of tumor survival (8), and multiple T-cell inhibitory pathways have been identified (9-11).

In addition to tumor cells, both ERs are expressed by most immune cell types, including T-cells, B-cells and NK cells, in which ERα46 is the predominant isoform (12). Correspondingly, estrogens influence helper CD4 T cell differentiation favoring humoral Th2

over cell-mediated Th1 responses (13). Pre-menopausal women have higher levels of estrogen than men, which may contribute to differences in the incidence of certain autoimmune diseases. Notably, various cancers exhibit sex biases that are at least partly explained by hormonal differences. Obesity, which is associated with increased adipocyte production of estrogens, is also a risk factor for a number of cancers. Changes in estrogen levels in women caused by menstruation, menopause, and pregnancy are associated with changes in the immune system, which could ultimately affect disease susceptibility. Despite growing evidence implicating estrogen as a fundamental mediator of inflammation, currently little is known about its potential role in antitumor immune responses, and particularly in patients without direct estrogen signaling on tumor cells but with a strongly responsive immune-environment.

Among suppressors of anti-tumor immune responses, factors driving tumor-associated inflammation universally induce aberrant myelopoiesis in solid tumors, which fuels malignant progression in part by generating immunosuppressive myeloid cell populations (14). In ovarian cancer, deregulated myelopoiesis results in the mobilization of myeloid-derived suppressor cells (MDSCs) from the bone marrow (15) and, eventually, the accumulation of tumor-promoting inflammatory Dendritic Cells (DCs) with immunosuppressive activity in solid tumors (16, 17), while canonical macrophages buildup in tumor ascites (16, 18). Although all these cell types express at least ERα and are influenced by estrogen signaling (19-21), how estrogens impact the orchestration and maintenance of protective anti-tumor immunity remains elusive. Here, we show that estrogens, independently of the sensitivity of tumor cells to estrogen signaling, are a crucial mechanism underlying pathological myelopoiesis in ovarian cancer. We report that estrogens drive MDSC mobilization and augment their immunosuppressive activity, which directly facilitates malignant progression. Our data provide mechanistic insight into how

augmented estrogenic activity could contribute to tumor initiation (e.g., in BRCA1-mutation carriers (22)), and provide a rationale for blocking estrogen signals to boost the effectiveness of anti-cancer immunotherapies.

RESULTS

Estrogen signaling impairs protective immunity against ovarian cancer independent of tumor cell signaling

Nuclear expression of ERs specifically in neoplastic cells has been identified in human ovarian carcinomas of all histological subtypes, with positive signal in ~60% of high-grade serous tumors (23). ERα is the predominant estrogen receptor in mouse hematopoietic cells (12). To define the expression of ERα in human ovarian cancer-infiltrating leukocytes, we performed immunohistochemical analysis in 54 serous ovarian carcinomas. Supporting previous reports, we found specific nuclear staining in tumor cells in ~35% of tumors (**Figure 1A, left**). In addition, we identified weaker signals in individual cells in the stroma with leukocyte morphology (different from tumor cell nuclei) in ~20% of ovarian tumors, independent of the ERα status of tumor cells (**Figure 1A, center**). We finally identified 2 specimens that showed specific signals restricted to stromal fibroblasts (**Figure 1A, right**). To confirm that hematopoietic cells at tumor beds express ERα, we sorted ($CD45^+$) cells from 7 different dissociated human ovarian tumors. As shown in **Figure 1B** and **Supplemental Figure 1A**, both tumor-infiltrating ($CD11b^+$) myeloid cells and ($CD11b^-$) non-myeloid leukocytes express variable levels of ERα. In addition, both myeloid and lymphoid cells sorted from either the bone marrow of a cancer patient or the

Author Manuscript Published OnlineFirst on September 30, 2016; DOI: 10.1158/2159-8290.CD-16-0502
Author manuscripts have been peer reviewed and accepted for publication but have not yet been edited.

peripheral blood of 5 ovarian cancer patients were also ERα$^+$ (**Figures 1B&C,** and **Supplemental Figures 1A&B**), suggesting that in addition to potentially having tumor cell-intrinsic effects, estrogens may also play wider a role in shaping the tumor immune-environment. To determine the role of estrogen signaling in tumor-promoting inflammation or anti-tumor immunity, we used a preclinical model of aggressive ovarian cancer in which syngeneic epithelial ovarian tumor cells (ID8-*Defb29/Vegf-a*) develop intraperitoneal tumors and ascites that recapitulate the inflammatory microenvironment of human ovarian tumors (9, 15, 17, 24). Importantly, no ERα was detected in these tumor cells, unlike tumor-associated myeloid cells (**Figure 1D**). Of note, ID8-*Defb29/Vegf-a* cells fail to respond to E2 (E2) treatment or the ER antagonist fulvestrant *in vitro*, unlike established estrogen-responsive MCF-7 cells (**Figure 1E**). Supporting a tumor cell-independent role of estrogen signaling in malignant progression, oöphorectomized (estrogen-depleted) wild-type mice survived significantly longer than non-oöphorectomized, aged-matched controls after orthotopic tumor challenge in multiple independent experiments (**Figure 1F**), while estrogen supplementation further accelerated malignant progression and reversed the protective effects of oöphorectomy (**Figure 1F** and **Supplemental Figure 1C**). Strikingly, the survival benefit imparted by oöphorectomy disappeared in tumor-bearing immunodeficient RAG1-deficient KO mice (**Figure 1G**), indicating that an adaptive immune response is required for the protective effects of estrogen depletion.

Interestingly, *ad libitum* E2 supplementation resulted in augmented T-cell inflammation at tumor (peritoneal) beds (**Figure 2A**). However, the proportions of antigen experienced (CD44$^+$), recently activated (CD69$^+$) tumor-associated CD4 and CD8 T-cells were significantly higher in oöphorectomized tumor-bearing hosts, with corresponding decreases in E2-

supplemented animals (**Figure 2B**). Accordingly, the frequencies of T cells isolated from the peritoneal cavity of oöphorectomized tumor-bearing mice producing interferon (IFN)-γ in response to cognate tumor antigens were significantly higher than those generated by control (non-oöphorectomized) mice in conventional ELISpot analysis (**Figure 2C**), indicative of superior T cell-dependent anti-tumor immunity in the former. Consistently, tumor-associated T cells from E2-treated mice responded significantly worse than either group (**Figure 2C**). Taken together, these results demonstrate that human ovarian cancer microenvironmental hematopoietic cells express ERα, and that, independent of a direct effect on tumor cells, estrogens accelerate ovarian cancer progression through a mechanism that blunts protective anti-tumor immunity.

ERα signaling in hematopoietic cells enhances ovarian cancer-induced myelopoietic expansion

The benefits of estrogen depletion were not restricted to ID8-*Defb29/Vegf-a* tumors, because the progression of estrogen-insensitive (**Supplemental Figure 1D**), intraperitoneal Lewis Lung Carcinomas (LLC) was also significantly delayed in oöphorectomized mice, ultimately resulting in decreased survival (**Figure 3A, left**), while E2 supplementation accelerated flank tumor growth (**Figure 3A, right**). Further supporting the general applicability of this mechanism, E2 supplementation also accelerated the growth of estrogen-insensitive (**Supplemental Figure 1E**) syngeneic A7C11 mammary tumor cells, derived from autochthonous p53/Kras-dependent mammary tumors (15) (**Figure 3B**). Finally, E2 treatment also increased the number of lung metastases in a model of I.V. injected (estrogen-insensitive) B16 melanoma cells (**Figure 3C** and **Supplemental Figure 1F**).

Author Manuscript Published OnlineFirst on September 30, 2016; DOI: 10.1158/2159-8290.CD-16-0502
Author manuscripts have been peer reviewed and accepted for publication but have not yet been edited.

To determine the mechanism by which estrogen signaling accelerates malignant progression, we next investigated differences in the mobilization of immunosuppressive cells. We identified strong estrogen-dependent differences only in the accumulation of MDSCs, both in the spleen (**Figure 3D&E**) and at tumor beds (**Figure 3F&G**), which persisted in tumors of similar size (**Supplemental Figure 1G**). Hence, estrogen treatment increased the percentage and total numbers of both $Ly6C^{high}Ly6G^{-}$ myelomonocytic (M-MDSC) and $Ly6C^{+}Ly6G^{+}$ granulocytic MDSCs (G-MDSC) in tumor-bearing mice, while estrogen depletion through oöphorectomy significantly decreased their percentage and total numbers both in the spleen and at tumor beds (**Figure 3D-G**).

To define whether estrogen-driven MDSC mobilization is sufficient to explain accelerated tumor growth, we depleted MDSCs with anti-Gr1 antibodies in A7C11 breast tumor-bearing mice. As expected, oöphorectomized mice injected with an irrelevant IgG again showed accelerated tumor progression when E2 was supplemented *ad libitum* throughout disease progression (**Figure 3H**). However, differences in tumor growth were completely abrogated when MDSCs were depleted with anti-Gr1 antibodies (**Figure 3H**).

Estrogens primarily signal through the nuclear receptors ERα and ERβ, the former being expressed in virtually all murine hematopoietic cells (20). Further supporting that differences in the ovarian cancer immuno-environment are independent of estrogen signaling on tumor cells, we identified ERα expression in MDSCs derived from tumor-bearing mice (**Figure 1D**). Importantly, myeloid cells sorted from tumor-bearing mice were also highly effective at suppressing T-cell proliferative responses and therefore are true immunosuppressive MDSCs and not merely immature myeloid cells (**Figure 3I** and **Supplemental Figure 2A**), supporting their role in estrogen-dependent abrogation of anti-tumor immunity. Interestingly, G-MDSCs from

E2-depleted (oöphorectomized) mice exhibit weaker immunosuppressive potential compared to vehicle or E2-treated mice.

To confirm that ERα signaling is sufficient to mediate accelerated malignant progression, we then challenged ERα$^{-/-}$ and wild-type control mice with orthotopic ID8-*Defb29/Vegf-a* tumors. As shown in **Figure 4A**, E2 supplementation failed to accelerate tumor progression in ERα KO hosts but again had significant effects in wild-type controls, indicative that estrogen's tumor-promoting responses are attributable to ERα signaling. In addition, accelerated tumor growth depends on ERα signaling specifically on hematopoietic cells because in response to E2 treatment, tumors progress significantly faster in lethally irradiated mice reconstituted with wild-type bone marrow, compared to identically treated mice reconstituted with ERα-deficient bone marrow (**Figure 4B**). Together, these results indicate that ERα signaling on hematopoietic cells accelerates malignant progression independently of the stimulation of neoplastic cells, through a mechanism that results in the mobilization of (ERα^{+}) immunosuppressive MDSCs.

Estrogens signal through ERα on human and mouse myeloid progenitors to boost the proliferation of regulatory myeloid cells and enhance their immunosuppressive activity

To rule out that estrogen-dependent myeloid expansion in tumor-bearing mice was the result of subtle differences in tumor burden or inflammation, we reconstituted lethally irradiated mice with a 1:1 mixture of CD45.2^{+}ERα$^{-/-}$ and (congenic) CD45.1^{+}ERα^{+} bone marrow and challenged them with orthotopic ovarian tumors. As shown in **Figure 4C&D**, a significantly higher percentage (3.6-fold) of total (CD11b^{+}Gr-1^{+}) MDSCs arose from ERα^{+} hematopoietic progenitors, compared to ERα-deficient cells. Because reconstitution of total hematopoietic cells

occurred at a similar ratio (**Figure 4C**) and MDSCs mobilization took place in the same host under an identical milieu, dissimilar ERα-dependent MDSC accumulation can only be attributed to cell-intrinsic ERα^{+} signaling on myeloid precursors (**Figure 4E**).

To understand how estrogen signaling promotes MDSC expansion, we next differentiated MDSCs *in vitro* by treating naïve wild-type (ERα^{+}) BM with GM-CSF and IL-6. As reported (25), these inflammatory cytokines induced the generation of immature myeloid cells that express Ly6G and Ly6C similar to MDSCs seen *in vivo* (**Figure 5A left**).

Normal cell culture medium drives estrogen signaling due to the presence of various estrogens in FBS (26) in addition to the estrogenic properties of phenol red. Blocking the estrogen activity of cell culture medium with MPP, a selective antagonist of ERα, severely inhibited the expansion of both M-MDSCs and G-MDSCs (**Figure 5A, left & Figure 5B**), similar to *in vivo* in tumor-bearing mice (**Figure 4E**) and, to an even greater extent, bone marrow-MDSCs expanded with ID8-*Defb29/Vegf-a*-tumor conditioned medium (**Supplemental Figure 2B**). In addition, the presence ERα antagonists allowed spontaneous differentiation of more mature CD11c^{+}MHC-II^{+} myelo-monocytic cells (**Figure 5A, right**). Corresponding to *in vivo* observations (**Figure 3F**), further addition of E2 resulted in G-MDSCs that were more potently immunosuppressive while abrogation of ERα signaling prevented the acquisition of stronger immunosuppressive activity by G-MDSCs (**Figure 5C, top**). In contrast, E2 did not affect the inhibitory activity of M-MDSCs (**Figure 5C, bottom**) suggesting that the role of estrogens in the accumulation of M-MDSCs is primarily to drive their expansion, although the low yields of BM-MDSCs obtained in the presence of estrogen antagonists precludes testing their suppressive activity.

Author Manuscript Published OnlineFirst on September 30, 2016; DOI: 10.1158/2159-8290.CD-16-0502
Author manuscripts have been peer reviewed and accepted for publication but have not yet been edited.

To support the relevance of ERα signaling in boosting pathological expansion of MDSCs, we finally procured bone marrow from 5 different lung cancer patients, and expanded myeloid cells with GM-CSF and IL-6 (25), in the presence of different concentrations of the ERα-selective antagonist MPP. As shown in **Figure 5D**, this system results in reproducible expansion of $CD11b^{+}CD33^{+}CD15^{+}CD14^{-}MHC\text{-}II^{-}$ granulocytes and $CD11b^{+}CD33^{+}CD15^{-/low}CD14^{+}MHC\text{-}II^{-}$ monocytic cells, corresponding to the human counterparts of granulocytic and monocytic MDSCs, along with more mature myeloid cells (**Supplemental Figure 2C**). Notably, blockade of ERα signaling resulted in a dramatic dose-dependent reduction in the expansion of both MDSC lineages, both at the level of proportions (**Figure 5D**) and, especially, absolute numbers (**Figure 5E**). Equally important, analysis of 266 serous ovarian cancer patients in TCGA datasets confirmed that patients with expression levels of the aromatase gene CYP19A1 (the enzyme responsible for a key step in the biosynthesis of estrogens) above the median also exhibit lower expression of CD3e and perforin, indicators of cytotoxic activity and total T cell infiltration, respectively (**Figure 5F**).

Together, these data show that estrogen signaling through ERα influences myelopoiesis in both mice and humans to boost the expansion of highly immunosuppressive MDSCs in response to inflammatory signals and block their differentiation into $MHC\text{-}II^{+}$ myeloid cells. These combined functions of ERα signaling in myeloid cells promote malignant progression through MDSC-mediated immune-suppression.

Estrogen signaling enhances pSTAT3 activity through transcriptional up-regulation of Janus kinase 2 (JAK2) and increased total STAT3 expression in myeloid progenitors

To determine the mechanism by which estrogen signaling promotes MDSC mobilization, we focused on the effect of estrogen signaling on STAT3 signaling, which plays a major role in regulating myeloid lineage cells and MDSC expansion (14). As shown in **Figure 6A**, levels of $pSTAT3^{Y705}$ were significantly increased in both monocytic and granulocytic MDSCs immunopurified from the peritoneal cavity of oöphorectomized ovarian cancer-bearing mice supplemented with E2, compared to control oöphorectomized mice receiving vehicle. Accordingly, anti-estrogen treatment of *in vitro* BM-MDSC cultures also inhibited STAT3 signaling resulting in lower phospho-STAT3 in both M-MDSCs and G-MDSCs (**Figure 6B**), confirming that pSTAT3 signaling is enhanced by estrogen activity.

Because STAT3 activation is triggered by IL-6, which was used for *in vitro* MDSC expansion, we next investigated the role of estrogen signaling on IL6R. Treating BM-MDSCs with E2 or anti-estrogens did not elicit changes in surface expression of the IL6Rα chain (**Figure 6C, left**), while gp130 was paradoxically up-regulated by MPP (**Figure 6C, right**). We therefore focused on downstream JAK and SRC kinases, both of which mediate STAT3 phosphorylation, subsequent dimerization, and nuclear translocation following cytokine receptor engagement (27, 28). As shown in **Figure 6D**, E2 supplementation induced transcriptional up-regulation of Jak2 in cytokine-induced bone marrow MDSCs of both lineages, while no detectable expression or changes were identified for other Jak members (not shown). Accordingly, E2 also induced a reproducible Jak2 up-regulation at the protein level, including higher levels of active (phosphorylated) Jak2 after a short pulse (**Figure 6E&F**). Notably, estrogen antagonists also reduced the levels of (active) phospho-Src in both M-MDSCs and G-MDSCs, while E2 supplementation also increased Src activity in the former (**Figure 6G**).

Author Manuscript Published OnlineFirst on September 30, 2016; DOI: 10.1158/2159-8290.CD-16-0502
Author manuscripts have been peer reviewed and accepted for publication but have not yet been edited.

To define which kinase (Jak2 *versus* Src) plays a predominant role in estrogen-dependent MDSC expansion, we expanded BM-MDSCs in the presence of specific Src (Dasatinib), Jak1/2 (Ruxolitinib), or ERα (MPP) inhibitors. As shown in **Figure 6H&I**, Jak1/2 inhibition had a dramatic negative effect in the differentiation of M-MDSCs. G-MDSC expansion was also heavily decreased upon Jak1/2 inhibition, but concurrent use of ERα antagonists significantly potentiated these suppressive effects (**Figure 6H&I**). On the other hand, Src inhibition had no effect on preventing G-MDSC differentiation, but resulted in a significant decrease in M-MDSC mobilization, which was further enhanced by additional ERα inhibition (**Figure 6I&J**). Therefore, concomitant inhibition of ERα signaling and STAT3-activating kinases has stronger negative effects on the expansion of both monocytic and granulocytic MDSC mobilization than inhibition of either pathway individually. Taken together, these data indicate that ERα signaling on myeloid precursors promotes MDSC expansion by driving STAT3 phosphorylation. In M-MDSCs, this occurs through both enhanced (phosphorylated) Src activity and the necessary function of Jak2, while only Jak2 activity is relevant in G-MDSCs.

Taken together, these data indicate that ERα signaling on myeloid precursors promotes MDSC expansion both through driving STAT3 phosphorylation and through a STAT3 independent mechanism. In M-MDSCs, this occurs through both enhanced (phosphorylated) Src activity and the necessary function of Jak2, while only Jak2 activity is relevant in G-MDSCs.

Estrogen also affects other components of the tumor immune-environment

Finally, to rule out that differences in malignant progression due to the direct effect of estrogens on effector T cells, we performed mixed BM chimera experiments in which mice

received a 1:1 mixture of ERα$^{-/-}$ and congenic wild-type BM. Compared to ERα$^{-/-}$ T cells, E2-responsive wild-type CD4 and CD8 T cells display a less activated phenotype characterized by lower expression of CD44 (**Figure 7A**). Correspondingly, the frequencies of wild-type T cells responding to tumor antigens in IFNγ ELISpot re-challenge assays were lower than those of their counterpart ERα$^{-/-}$ T cells, sorted from the same microenvironment (**Figure 7B**).

To determine the relative importance of these differences in direct ERα signaling in T cells, independent of estrogen-dependent MDSC activity, wild-type and ERα$^{-/-}$ T cell splenocytes were identically enriched for tumor-reactive populations by *ex vivo* priming against tumor lysate-pulsed BMDCs (29, 30), and then adoptively transferred into ovarian cancer-bearing mice. Confirming previous reports (29, 30), both wild-type and ERα$^{-/-}$ T cells significantly extended survival. However, there was no difference between wild-type and ERα KO T cells regardless of whether mice were treated with E2 (**Figure 7C**). Therefore, while E2 has measurable T cell-intrinsic effects, these are not sufficient to drive differences in malignant progression, and, therefore, E2 effects on immunosuppressive cells, namely MDSCs, are the main driver underlying estrogen-driven tumor acceleration.

DISCUSSION

Here we show that ERα signaling on myeloid precursors is a major contributor to pathological myelopoiesis in cancer, resulting in MDSC expansion and augmented immunosuppressive activity. Accordingly, oöphorectomized mice exhibit delayed malignant progression upon challenge with different estrogen insensitive tumor models, while E2

Author Manuscript Published OnlineFirst on September 30, 2016; DOI: 10.1158/2159-8290.CD-16-0502
Author manuscripts have been peer reviewed and accepted for publication but have not yet been edited.

supplementation has the opposite effects. Supporting the crucial role of spontaneous anti-tumor immunity in this mechanism, differences in tumor growth disappear in T-cell-deficient mice.

Although the role of estrogen signaling in the progression of breast tumors and a subset of ovarian cancer patients has been underscored by the clinical use of ER antagonists, our results demonstrate that estrogens have a profound effect on anti-tumor immunity and tumor-promoting inflammation, independent of their direct activity on tumor cells. Our data therefore provide novel mechanistic insight into how enhanced estrogenic activity contributes to malignant progression in established tumors. Furthermore, our data support that novel anti-estrogen drugs that, unlike tamoxifen (1), have no agonistic effects on non-breast cell types, may have benefits in a wide range of cancers in pre-menopausal women, independently of the expression of ERs in tumor cells. Therefore, anti-estrogens, especially when used as an adjuvant therapy, could synergize with immunotherapies such as checkpoint inhibitors to extend survival significantly. Thus, while bilateral oöphorectomy is standard in ovarian cancer treatment, our data suggest that ER^- breast tumors and other malignancies in at least pre-menopausal female cancer patients could be delayed by specifically blocking ERα in a systemic manner, especially if complementary immunotherapies are implemented as adjuvant therapy.

Our results also have implications to understand gender-dependent differences in tumor initiation and malignant progression in different malignancies. For example, we showed that responses to αPD-L1 immunotherapy was sex-dependent in hormone-independent melanoma (31). This could be particularly relevant in BRCA1-mutation carriers, where augmented estrogenic signals has been recently demonstrated (22, 32). Furthermore, ERα expression is regulated by BRCA1-dependent ubiquitination (33), so that cancer-predisposing heterozygous BRCA1 mutations could result in increased ER expression, and therefore increase estrogen

activity. Whether mobilization of MDSCs in the context of additional inflammatory signals contributes to tumor initiation in BRCA1 mutation carriers demands further experimental proof, but our study suggests this as a likely pathogenic mechanism.

This study contributes to the understanding of the complexity of factors deregulating myelopoiesis (and therefore antigen presentation) in virtually all solid tumor-bearing hosts. Our data indicate that ERα signaling has a triple effect on myeloid bone marrow progenitors by altering pSTAT3 signaling, which drives both expansion and increased survival in these cells (14): on the one hand, estrogens up-regulate JAK2, which mediates STAT3 phosphorylation, as well as total STAT3 itself. Therefore, estrogenic activity prepares the bone marrow for acute expansion of myeloid precursors, but estrogen-dependent mobilization of MDSCs only occurs in the presence of direct inflammatory signals that activate JAK kinases, which may not necessarily be present during the high estrogen phase of the menstrual cycle. These mechanisms appear to be important during pregnancy though, where E2 also drives the expansion and activation of MDSCs (21), but our study demonstrates their relevance in the pathogenesis of women's malignancies.

In summary, our study unveils the role of estrogen signaling in pathological myelopoiesis, and supports that more specific anti-estrogen drugs could complement emerging immunotherapies to significantly extend the survival of cancer patients, independently of the expression of ERs in tumor cells.

Acknowledgments: We than the Gabrilovich lab at Wistar for outstanding technical insight.

METHODS

Mice and cell lines

Female 5-8 week old wild-type (WT) C57BL/6 and congenic Ly5.1 mice were purchased from the Charles River Frederick facility. Esr1 knockout (ERα KO) were purchased from The Jackson Laboratory. Oöphorectomies were performed by Charles River staff at 5 weeks of age. Mice were treated with vehicle (0.1% ethanol) or 10 μM E2 (USP grade, Sigma) in drinking water refreshed every 3-4 days. All mice were maintained in specific pathogen-free barrier facilities. All experiments were conducted according to the approval of the Wistar Institute Institutional Animal Care and Use Committee.

ID8 cells were provided by K. Roby (Department of Anatomy and Cell Biology, University of Kansas; in 2011) (34) and retrovirally transduced to express *Defb29* and *Vegf-a* (24). Clones were passaged less than 4 times. MCF-7, B16.F10 and LLC1 cells were obtained from American Type Culture Collection in 2009, 2013 and 2009, respectively, and passaged less than 4 times. Cell lines used in this article were not authenticated by us.

Peritoneal tumors were initiated in mice by injecting $3X10^6$ ID8-*Defb29/Vegf-a* cells intraperitoneal (i.p.). Intraperitoneal cells were harvested from tumor-bearing mice by flushing the peritoneal cavity with PBS. Cells were maintained in vitro at 37° C, 5% CO2 by culturing in RPMI+10% FBS or steroid free medium (SFR10), which was comprised of phenol red-free RPMI+10% charcoal-stripped FBS. Cells were treated *in vitro* with vehicle (0.1% DMSO) or varying concentrations of E2, fulvestrant, or methylpiperidino pyrazole (MPP) purchased from Cayman Chemical. Cell line proliferation was determined by MTS assay (Promega), and increased/decreased proliferation relative to vehicle was calculated.

The A7C11 mammary tumor cell line was generated by passaging sorted tumor cells from a mechanically disassociated p53/Kras mammary tumor (35). Flank tumors were initiated by injecting $2x10^4$ cells into the axillary flank. Tumor volume was calculated as: 0.5 x (L x W^2), where L is length, and W is width.

For generating mixed BM chimeras, mononuclear BM cells were collected from adult age-matched CD45.1 (congenic) WT or CD45.2 *Esr1*$^{-/-}$ donor mice, and 1–2 × 10^6 cells were mixed in a 1:1 ratio and retro-orbitally injected into lethally irradiated (~950 rad) adult recipients. Mixed chimeras were analyzed after 7–8 weeks as indicated.

Human Samples

Human ovarian carcinoma tissues were procured under a protocol approved by the Committee for the Protection of Human Subjects at Dartmouth-Hitchcock Medical Center (#17702) and under a protocol approved by the Institutional Review Board at Christiana Care Health System (#32214) and the Institutional Review Board of The Wistar Institute (#21212263). Bone marrow (BM) was obtained from Stage I-II lung cancer patients scheduled for surgical resection at the Hospital of the University of Pennsylvania and The Philadelphia Veterans Affairs Medical Center with approval from respective Institutional Review Boards. All patients selected for entry into the study met the following criteria: (i) histologically confirmed pulmonary squamous cell carcinoma (SCC) or adenocarcinoma (AC), (ii) no prior chemotherapy or radiation therapy within two years, and (iii) no other active malignancy. BM cell suspension was obtained from rib fragments that were removed from patients as part of their lung cancer surgery. Informed consent was obtained from all subjects.

Flow Cytometry

Flow cytometry was performed by staining cells with Zombie Yellow viability dye, blocking with anti-CD16/32 (2.4G2), and staining for 30 min at 4°C with the following anti-mouse antibodies: CD45 (30-F11), CD45.1 (A20), CD45.2 (104), CD11c (N418), I-A/I-E (M5/114.15.2), CD3 (145-2C11), Ly6G (1A8), Ly6C (HK1.4), gp130 (4H1B35), IL6R (D7715A7), Gr1 (RB6-4C5) CD4 (RM4-5), CD8b (YTS156.7.7), CD44 (IM7), CD69 (H1.2F3), CD11b (M1/70); or anti-human antibodies: CD45 (HI30), CD11c (Bu15), HLA-DR-APC/Cy7 (L243), CD15 (HI98), CD14 (HCD14), CD11b (ICRF44), CD33 (WM53), CD19 (HIB19). Samples were subsequently run using an LSRII and analyzed using FlowJo.

ELISpot

Dendritic cells (BMDCs) were differentiated by culturing WT mouse bone marrow for 7 days with 20 ng/mL GM-CSF (Peprotech 315-03), added on day 0 and 3, and 10 ng/mL GM-CSF added on day 6. BMDCs were subsequently primed with tumor antigen by pulsing for 24 hours with irradiated (100 Gy+30 minutes UV) ID8-*Defb29/Vegf-a* cells at a ratio of 10:1. ELISPOT assay was performed by stimulating $1x10^5$ cells obtained from peritoneal wash with $1x10^4$ antigen-primed BMDCs in a 96-well filter plate (Millipore MSIPS4510) coated with IFNγ capture antibody according to manufacturer's guidelines (eBioscience 88-3784-88). Following incubation at 37° C, 5% CO2 for 48 hours, positive spots were developed using Avidin-AP and BCIP-NBT substrate (R&D Systems SEL002).

Adoptive T-Cell Transfer

Naïve T cells were harvested from spleens of WT or ERα KO mice via RBC lysis followed by magnetic bead negative selection to remove non-T cell $B220^+$, $CD16/32^+$,$CD11b^+$

and MHC-II$^+$ cells and primed for 5 days with BMDCs pulsed with tumor antigen as reported (30). A total of 1x10^6 T cells was injected i.p. 7 and 14 days post tumor injection.

Bone Marrow-Derived MDSC Cultures

Mouse MDSCs were expanded from mouse bone marrow harvested by flushing tibias and femurs with media. Following red blood cell lysis, 2.5X10^6 cells were cultured in 10 mL of RPMI+10% FBS augmented with recombinant mouse 40 ng/mL GM-CSF+40 ng/mL IL6 (Peprotech) and incubated at 37°C, 5% CO2 3 or 6 days. Vehicle, estradiol, or MPP treatments were added as described above. For 6 day cultures, cytokines and estrogen treatments were refreshed on day 3. Following red blood cell lysis, 2.5x10^6 cells were cultured in 10 mL of RPMI+10% FBS augmented with recombinant mouse 40 ng/mL GM-CSF+40 ng/mL IL6 (Peprotech) and incubated at 37°C, 5% CO2 3 or 6 days. Vehicle, E2, or MPP treatments were added as described above. For 6 day cultures, cytokines and E2 were refreshed on day 3. Following incubation, floating and adherent cells were collected, and M-MDSCs and G-MDSCs were isolated via Miltenyi MDSC purification kit according to manufacturer's protocol. Human MDSCs were expanded from human lung cancer patient bone marrow acquired as single cell suspensions (see above). Briefly, 2x10^6 cells were cultured in 3 mL of IMDM+15% FBS supplemented with recombinant human 40 ng/mL GM-CSF+40 ng/mL IL6 (Peprotech) and treated with vehicle, 2μM, or 10μM MPP (see above) for 4 days. Cells were subsequently harvested and analyzed by flow cytometry.

MDSC Suppression Assay

Naïve WT T cells were purified from spleens as described and labeled with the proliferation tracker Cell Trace Violet according to manufacturer protocol. T cell proliferation was stimulated by adding anti-CD3/CD28 mouse T-activator beads (Thermo) at a 1:1 T cell to bead ratio according to manufacturer protocol. T cells ($2x10^5$) were subsequently co-cultured with MDSC at 1:4, 1:8, or 1:16 MDSC to T cell ratios and incubated for 3 days prior to flow cytometric analysis.

Western Blot and IHC

Cells were lysed in RIPA buffer supplemented with protease inhibitors, phosphatase inhibitors, and Na3VO4 (Thermo) according to manufacturer protocol. Protein quantification was determined via BCA assay, and protein was run on TGX 4-15% gradient gels. . Following transfer, PVDF membranes were blocked with 5% BSA in TBS + 0.05% Tween-20. The following primary antibodies were added to membranes, as indicated, and incubated overnight: Jak2 (rabbit clone#D2E12), Stat3 (clone#124H6) and pStat3 (Tyr705, rabbit clone#D3A7), from Cell Signaling; and ERα (Thermo, clone#TE111.5D11) and beta-actin (Sigma, clone#AC-15). Following secondary staining with HRP-conjugated anti-mouse or rabbit IgG, membranes were developed using ECL prime (GE Healthcare).

ERα staining was initially performed in frozen sections from 54 ovarian cancer specimens with clone #TE111.5D11 as primary antibody (Thermo), followed by a biotinylated goat anti-mouse and completion of immunohistochemical procedure according to manufacturer instructions (Vector Labs). Positive staining was confirmed in 19 paraffin-embedded ovarian cancer sections using FDA-approved ER tests (DAKO) in the Laboratory of the Diagnostic

Author Manuscript Published OnlineFirst on September 30, 2016; DOI: 10.1158/2159-8290.CD-16-0502
Author manuscripts have been peer reviewed and accepted for publication but have not yet been edited.

Immunohistochemistry at the Hospital of the University of Pennsylvania, following the FDA approved manufacture guidelines.

Quantitative Real Time PCR

Cells were lysed in Trizol buffer and RNA was subsequently purified using RNEasy kit (Qiagen). Reverse transcription was carried out using High-Capacity Reverse Transcription kit (Applied Biosystems). SYBR Green PCR Master Mix (Applied Biosystems) was used with an ABI 7500 Fast Sequence Detection Software (Applied Biosystems). The following primer sequences were used (5'→3'): *Stat3* <F: GACTGATGAAGAGCTGGCTGACT, R: GGGTCTGAAGTTGAGATTCTGCT>; *Jak2* <F: GTGTCGCCGGCCAATGTTC, R: CACAGGCGTAATACCACAAGC>; and *Tbp* (mRNA normalization) <F: CACCCCCTTGTACCCTTCAC, R: CAGTTGTCCGTGGCTCTCTT>.

Expression of human ESR1 was quantified with primers: *ESR1* <F: CCACTCAACAGCGTGTCTC, and R: GGCAGATTCCATAGCCATAC>, and normalized with primers: *GAPDH* <F: CCTGCACCACCAACTGCTTA, R: AGTGATGGCATGGACTGTGGT>.

Expression of mouse ERα was determined with primers: *ERα* <F:GTGCAGCACCTTGAAGTCTCT, R: TGTTGTAGAGATGCTCCATGCC>.

Analysis of TCGA data

Aligned Sequence files related to solid ovarian cancer samples including whole exon sequencing and outcome data were downloaded from TCGA data portal (2015). Scores (number

of tags in each transcript) were obtained from each sample, normalized with respect to total tags in the sample as well as total tags in the chromosome, and expressed as FPKM (fragments/Kb of transcript/million mapped reads).

REFERENCES

1. Gallo MA, Kaufman D. Antagonistic and agonistic effects of tamoxifen: significance in human cancer. Semin Oncol. 1997;24:S1-71-S1-80.
2. Sini V, Cinieri S, Conte P, De Laurentiis M, Leo AD, Tondini C, et al. Endocrine therapy in post-menopausal women with metastatic breast cancer: From literature and guidelines to clinical practice. Crit Rev Oncol Hematol. 2016;100:57-68.
3. Hasan J, Ton N, Mullamitha S, Clamp A, McNeilly A, Marshall E, et al. Phase II trial of tamoxifen and goserelin in recurrent epithelial ovarian cancer. Br J Cancer. 2005;93:647-51.
4. del Carmen MG, Fuller AF, Matulonis U, Horick NK, Goodman A, Duska LR, et al. Phase II trial of anastrozole in women with asymptomatic mullerian cancer. Gynecol Oncol. 2003;91:596-602.
5. Smyth JF, Gourley C, Walker G, MacKean MJ, Stevenson A, Williams AR, et al. Antiestrogen therapy is active in selected ovarian cancer cases: the use of letrozole in estrogen receptor-positive patients. Clin Cancer Res. 2007;13:3617-22.

6. Argenta PA, Thomas SG, Judson PL, Downs LS, Jr., Geller MA, Carson LF, et al. A phase II study of fulvestrant in the treatment of multiply-recurrent epithelial ovarian cancer. Gynecol Oncol. 2009;113:205-9.

7. Bowman A, Gabra H, Langdon SP, Lessells A, Stewart M, Young A, et al. CA125 response is associated with estrogen receptor expression in a phase II trial of letrozole in ovarian cancer: identification of an endocrine-sensitive subgroup. Clin Cancer Res. 2002;8:2233-9.

8. Zhang L, Conejo-Garcia JR, Katsaros D, Gimotty PA, Massobrio M, Regnani G, et al. Intratumoral T cells, recurrence, and survival in epithelial ovarian cancer. N Engl J Med. 2003;348:203-13.

9. Stephen TL, Rutkowski MR, Allegrezza MJ, Perales-Puchalt A, Tesone AJ, Svoronos N, et al. Transforming Growth Factor beta-Mediated Suppression of Antitumor T Cells Requires FoxP1 Transcription Factor Expression. Immunity. 2014;41:427-39.

10. Cubillos-Ruiz JR, Engle X, Scarlett UK, Martinez D, Barber A, Elgueta R, et al. Polyethylenimine-based siRNA nanocomplexes reprogram tumor-associated dendritic cells via TLR5 to elicit therapeutic antitumor immunity. J Clin Invest. 2009;119:2231-44.

11. Cubillos-Ruiz JR, Martinez D, Scarlett UK, Rutkowski MR, Nesbeth YC, Camposeco-Jacobs AL, et al. CD277 is a Negative Co-stimulatory Molecule Universally Expressed by Ovarian Cancer Microenvironmental Cells. Oncotarget. 2010;1:329-8.

12. Pierdominici M, Maselli A, Colasanti T, Giammarioli AM, Delunardo F, Vacirca D, et al. Estrogen receptor profiles in human peripheral blood lymphocytes. Immunol Lett. 2010;132:79-85.

13. Salem ML. Estrogen, a double-edged sword: modulation of TH1- and TH2-mediated inflammations by differential regulation of TH1/TH2 cytokine production. Curr Drug Targets Inflamm Allergy. 2004;3:97-104.

14. Gabrilovich DI, Ostrand-Rosenberg S, Bronte V. Coordinated regulation of myeloid cells by tumours. Nat Rev Immunol. 2012;12:253-68.

15. Rutkowski MR, Stephen TL, Svoronos N, Allegrezza MJ, Tesone AJ, Perales-Puchalt A, et al. Microbially driven TLR5-dependent signaling governs distal malignant progression through tumor-promoting inflammation. Cancer Cell. 2015;27:27-40.

16. Scarlett UK, Rutkowski MR, Rauwerdink AM, Fields J, Escovar-Fadul X, Baird J, et al. Ovarian cancer progression is controlled by phenotypic changes in dendritic cells. J Exp Med. 2012;209:495-506.

17. Tesone AJ, Rutkowski MR, Brencicova E, Svoronos N, Perales-Puchalt A, Stephen TL, et al. Satb1 Overexpression Drives Tumor-Promoting Activities in Cancer-Associated Dendritic Cells. Cell Rep. 2016;14:1774-86.

18. Huarte E, Cubillos-Ruiz JR, Nesbeth YC, Scarlett UK, Martinez DG, Buckanovich RJ, et al. Depletion of dendritic cells delays ovarian cancer progression by boosting antitumor immunity. Cancer Res. 2008;68:7684-91.

19. Kovats S. Estrogen receptors regulate an inflammatory pathway of dendritic cell differentiation: mechanisms and implications for immunity. Horm Behav. 2012;62:254-62.

20. Kovats S. Estrogen receptors regulate innate immune cells and signaling pathways. Cell Immunol. 2015;294:63-9.

21. Pan T, Zhong L, Wu S, Cao Y, Yang Q, Cai Z, et al. 17beta-Oestradiol enhances the expansion and activation of myeloid-derived suppressor cells via signal transducer and activator of transcription (STAT)-3 signalling in human pregnancy. Clin Exp Immunol. 2016;185:86-97.

22. Widschwendter M, Rosenthal AN, Philpott S, Rizzuto I, Fraser L, Hayward J, et al. The sex hormone system in carriers of BRCA1/2 mutations: a case-control study. Lancet Oncol. 2013;14:1226-32.

23. Sieh W, Kobel M, Longacre TA, Bowtell DD, deFazio A, Goodman MT, et al. Hormone-receptor expression and ovarian cancer survival: an Ovarian Tumor Tissue Analysis consortium study. Lancet Oncol. 2013;14:853-62.

24. Conejo-Garcia JR, Benencia F, Courreges MC, Kang E, Mohamed-Hadley A, Buckanovich RJ, et al. Tumor-infiltrating dendritic cell precursors recruited by a beta-defensin contribute to vasculogenesis under the influence of Vegf-A. Nat Med. 2004;10:950-8.

25. Marigo I, Bosio E, Solito S, Mesa C, Fernandez A, Dolcetti L, et al. Tumor-induced tolerance and immune suppression depend on the C/EBPbeta transcription factor. Immunity. 2010;32:790-802.

26. Briand P, Lykkesfeldt AE. Effect of estrogen and antiestrogen on the human breast cancer cell line MCF-7 adapted to growth at low serum concentration. Cancer Res. 1984;44:1114-9.

27. Murray PJ. The JAK-STAT signaling pathway: input and output integration. J Immunol. 2007;178:2623-9.

28. Rebe C, Vegran F, Berger H, Ghiringhelli F. STAT3 activation: A key factor in tumor immunoescape. JAKSTAT. 2013;2:e23010.

29. Nesbeth Y, Scarlett U, Cubillos-Ruiz J, Martinez D, Engle X, Turk MJ, et al. CCL5-mediated endogenous antitumor immunity elicited by adoptively transferred lymphocytes and dendritic cell depletion. Cancer Res. 2009;69:6331-8.

30. Nesbeth YC, Martinez DG, Toraya S, Scarlett UK, Cubillos-Ruiz JR, Rutkowski MR, et al. CD4+ T cells elicit host immune responses to MHC class II- ovarian cancer through CCL5 secretion and CD40-mediated licensing of dendritic cells. J Immunol. 2010;184:5654-62.

31. Lin PY, Sun L, Thibodeaux SR, Ludwig SM, Vadlamudi RK, Hurez VJ, et al. B7-H1-dependent sex-related differences in tumor immunity and immunotherapy responses. J Immunol. 2010;185:2747-53.

32. Hu Y, Ghosh S, Amleh A, Yue W, Lu Y, Katz A, et al. Modulation of aromatase expression by BRCA1: a possible link to tissue-specific tumor suppression. Oncogene. 2005;24:8343-8.

33. Eakin CM, Maccoss MJ, Finney GL, Klevit RE. Estrogen receptor alpha is a putative substrate for the BRCA1 ubiquitin ligase. Proc Natl Acad Sci U S A. 2007;104:5794-9.

34. Roby KF, Taylor CC, Sweetwood JP, Cheng Y, Pace JL, Tawfik O, et al. Development of a syngeneic mouse model for events related to ovarian cancer. Carcinogenesis. 2000;21:585-91.

35. Rutkowski MR, Allegrezza MJ, Svoronos N, Tesone AJ, Stephen TL, Perales-Puchalt A, et al. Initiation of metastatic breast carcinoma by targeting of the ductal epithelium with adenovirus-cre: a novel transgenic mouse model of breast cancer. J Vis Exp. 2014:51171.

Author Manuscript Published OnlineFirst on September 30, 2016; DOI: 10.1158/2159-8290.CD-16-0502
Author manuscripts have been peer reviewed and accepted for publication but have not yet been edited.

FIGURE LEGENDS

Figure 1. Estrogen-depletion impairment of ovarian tumor progression is independent of tumor cell signaling and is immune dependent. (**A**) Frozen human ovarian tumor sections stained for ERα. Scale bar indicates 1 μm. (**B-C**) Reverse transcription qPCR for *ESR1* expression in myeloid ($CD45^+CD11b^+$) and non-myeloid ($CD45^+CD11b^-$) cells isolated from dissociated ovarian tumor or bone marrow (**B**) or the peripheral blood (**C**) of 5 ovarian cancer patients. (**D**) Western-blot for ERα (66 kDa) expression by ID8-*Defb29/Vegf-a* tumor cells and myeloid-derived suppressor cells isolated from mouse tumors. (**E**) Proliferation relative to vehicle of ID8-*Defb29/Vegf-a* and MCF-7 (positive control) cells in response increasing doses of E2 (in steroid-free media) and the ER antagonist fulvestrant as determined by MTS assay. (**F**) Survival of WT oöphorectomized (OVX) or sham-operated mice challenged with intraperitoneal ID8-*Defb29/Vegf-a* tumors and supplemented or not with E2. Pooled from 3 independent experiments. Total number of mice per group is depicted. (**G**) Survival of OVX or sham-operated *Rag1* KO mice challenged with i.p. ID8-*Defb29/Vegf-a*. pooled from 6 independents Total number of mice per group is depicted. *$p < 0.05$.

Figure 2. Estrogen suppresses anti-tumor T cell responses. (**A**) Proportion of $CD45^+$ cells isolated from ID8-*Defb29/Vegf-a* peritoneal tumors that are T cells ($CD45^+CD3^+\gamma\delta\text{-}TCR^-$). (**B**) Proportion of activated $CD44^+CD69^+$ double positive cells among $CD4^+$ and $CD8^+$ T cells. (**C**) ELISpot analysis of T cells isolated from ID8-*Defb29/Vegf-a* peritoneal tumors stimulated with

tumor lysate-pulsed BM-derived dendritic cells. Results shown are representative of multiple independent experiments. *$p < 0.05$.

Figure 3. Estrogen drives accumulation of myelomonocytic (M-MDSC) and granulocytic (G-MDSC) myeloid-derived suppressor cells and increases the immunosuppressive potential of G-MDSCs. (**A**) Intraperitoneal LLC lung tumor progression in oöphorectomized *vs.* sham-treated WT mice (**left**) or subcutaneous LLC growth in WT mice treated with vehicle (Vh) *vs.* E2 (**right**) (5 mice/group in both cases). (**B**) Flank A7C11 breast tumor growth in oöphorectomized WT mice treated with vehicle (Vh) *vs.* E2 (5 mice/group). (**C**) $5X10^5$ B16.F10 cells (ATCC) were injected I.V. into mice (n=5/group). Upon injection, mice were treated with vehicle (0.1% EtOH) or E2 (10 uM) in drinking water. After 15 days, mice were euthanized and the number of lung metastases per mm^2 was determined by H&E staining. Representative images of lung metastases are also shown. (**D**, **E**) Expression and quantification of M-MDSCs ($Ly6C^{high}Ly6G^-$) and G-MDSCs ($Ly6C^+Ly6G^+$) in the spleen of ID8-*Defb29/Vegf-a* peritoneal tumor-bearing mice. (**F**, **G**) Expression and quantification of M-MDSCs ($Ly6C^{high}Ly6G^-$) and G-MDSCs ($Ly6C^+Ly6G^+$) in the peritoneal cavity of ID8-*Defb29/Vegf-a* peritoneal tumor-bearing mice. (**H**) Flank A7C11 breast tumor growth in oöphorectomized mice treated with vehicle (Vh) *vs.* E2 and receiving 250 μg of anti-Gr1 (RB6-8C5; BioXCell) *vs.* control isotype antibodies every other day, starting at day 2 after tumor challenge (5 mice/group). (**I**) Dilution of Cell Trace Violet in labeled T cells activated with anti-CD3/CD28 beads co-cultured with varying ratios of M- and G-MDSCs isolated from ID8-*Defb29/Vegf-a* tumors. *$p < 0.05$; **$p < 0.01$.

Figure 4. Host estrogen receptor α (ERα) activity is required for E2-driven tumor acceleration and optimal MDSC accumulation. (**A**) Survival of WT and ERα KO mice treated with Vh or E2 and challenged with i.p. ID8-*Defb29/Vegf-a* tumors (n=5 mice/group). (**B**) Survival of WT mice lethally irradiated (10 Gy) and reconstituted with WT or ERα KO bone marrow treated with Vh or E2 and challenged with i.p. ID8-*Defb29/Vegf-a* tumors. Pooled from 3 independent experiments (n≥9 mice/group). (**C**, **D**) Expression and quantification of WT and ERα KO MDSCs ($CD45^+CD11b^+Gr\text{-}1^+$) in the spleens of tumor bearing mice lethally irradiated and reconstituted with a 1:1 mix of WT $CD45.1^+$ and ERα KO $CD45.2^+$ bone marrow. (**E**) Expression of Ly6C and Ly6G by WT and ERα KO $CD11b^+$MHC-II^- cells in the spleens of mixed BM reconstituted mice. *$p < 0.05$.

Figure 5. Optimal MDSC expansion and suppressive activity is dependent on estrogen signaling. (**A**) Expression of Ly6C and Ly6G (left) or MHC-II and CD11c (right) by naïve mouse WT bone marrow cultured with GM-CSF+IL6 and treated with Vh or 2 μM anti-estrogen MPP for 3 and 6 days. (**B**) Total number of M-MDSCs and G-MDSCs after culturing naïve WT mouse BM with GM-CSF+IL6 and treating with 2μM MPP for 6 days. Cumulative results of 3 independent experiments. (**C**) Dilution of Cell Trace Violet by labeled T cells activated with anti-CD3/CD28 beads co-cultured with varying ratios of G- or M-MDSCs isolated from 6-day bone marrow cultures treated with Vh, 100 ng/mL E2, or 2 μM MPP. (**D**) Expansion of human M-MDSCs ($CD45^+$HLA-$DR^-CD11b^+CD33^+CD14^+$) and G-MDSCs ($CD45^+$HLA-DR^- $CD11b^+CD33^+CD15^+$) from lung cancer patient bone marrow cultured in GM-CSF+IL6 and treated with Vh, 2 μM, or 10 μM MPP. (**E**) Total number of human M- and G-MDSCs derived from lung cancer patient bone marrow. *$p < 0.05$. (**F**) Scatter plot of the level of CD3E and

PRF1 mRNA (measured as FKPM) in 266 serous ovarian cancers from TCGA datasets, separated by CYP19A1 expression above or below the median.

Figure 6. Estrogen increases cytokine-induced STAT3 activation during MDSC expansion. (**A**) Phosphorylated and total STAT3 protein expression in M- and G-MDSCs sorted from the peritoneal cavity of i.p. ID8-*Defb29/Vegf-a* tumor-bearing oöphorectomized mice, supplemented or not with E2 during malignant progression (pooled from 5 animals/group). (**B**) pSTAT3 and total STAT3 protein expression in *in vitro* BM-derived MDSC cultures treated with Vh, 100 ng/mL E2, or 2 μM MPP. (**C**) *In vitro* BM-derived MDSC surface expression of IL6Rα and GP-130 in response to Vh, E2, or MPP treatment. (**D**) *Jak2* RNA expression of *in vitro* BM-derived MDSC in response to estrogen agonists and antagonists. (**E**) Expression of total Jak2 protein under the same conditions. (**F**) Active (phosphorylated) Jak2 protein expression in day 6 *in vitro* BM-derived MDSCs in response to a 5 h. pulse of 100 ng/mL E2. (**G**) pSrc protein expression in *in vitro* BM-derived MDSC cultures treated with Vh, E2, or MPP as in B. (**H**) Live cell counts in day 6. BM-derived MDSC cultures treated with Vh, 2 μM MPP and/or 1μM of Ruxolitinib. Fresh inhibitors were replaced at day 3. (**I**) Ly6C/Ly6G differentiation in BM-MDSC cultures in the presence of Vh, 10 nM of Dasatinib or 1μM of Ruxolitinib. (**J**) Same as in F using Dasatinib instead of Ruxolitinib. *$p < 0.05$.

Figure 7. T cell-intrinsic ERα activity suppresses anti-tumor response, but is insufficient to abrogate the effectiveness of tumor-primed T cells. (**A**) Intratumoral T cell expression of CD44 and CD69 in mice lethally irradiated and reconstituted with a 1:1 mix of WT $CD45.1^+$ and ERα KO $CD45.2^+$ bone marrow. (**B**) ELISpot analysis of intratumoral WT and ERα KO T cells

FACS-isolated from tumor-bearing mice stimulated with tumor antigen loaded BMDCs. (**C**) Survival of tumor-bearing Vh or E2 treated mice following adoptive transfer of tumor antigen-primed WT or ERα KO T cells. Representative survival curves shown for multiple independent experiments. *$p < 0.05$.

Author Manuscript Published OnlineFirst on September 30, 2016; DOI: 10.1158/2159-8290.CD-16-0502
Author manuscripts have been peer reviewed and accepted for publication but have not yet been edited.

FIGURE 1

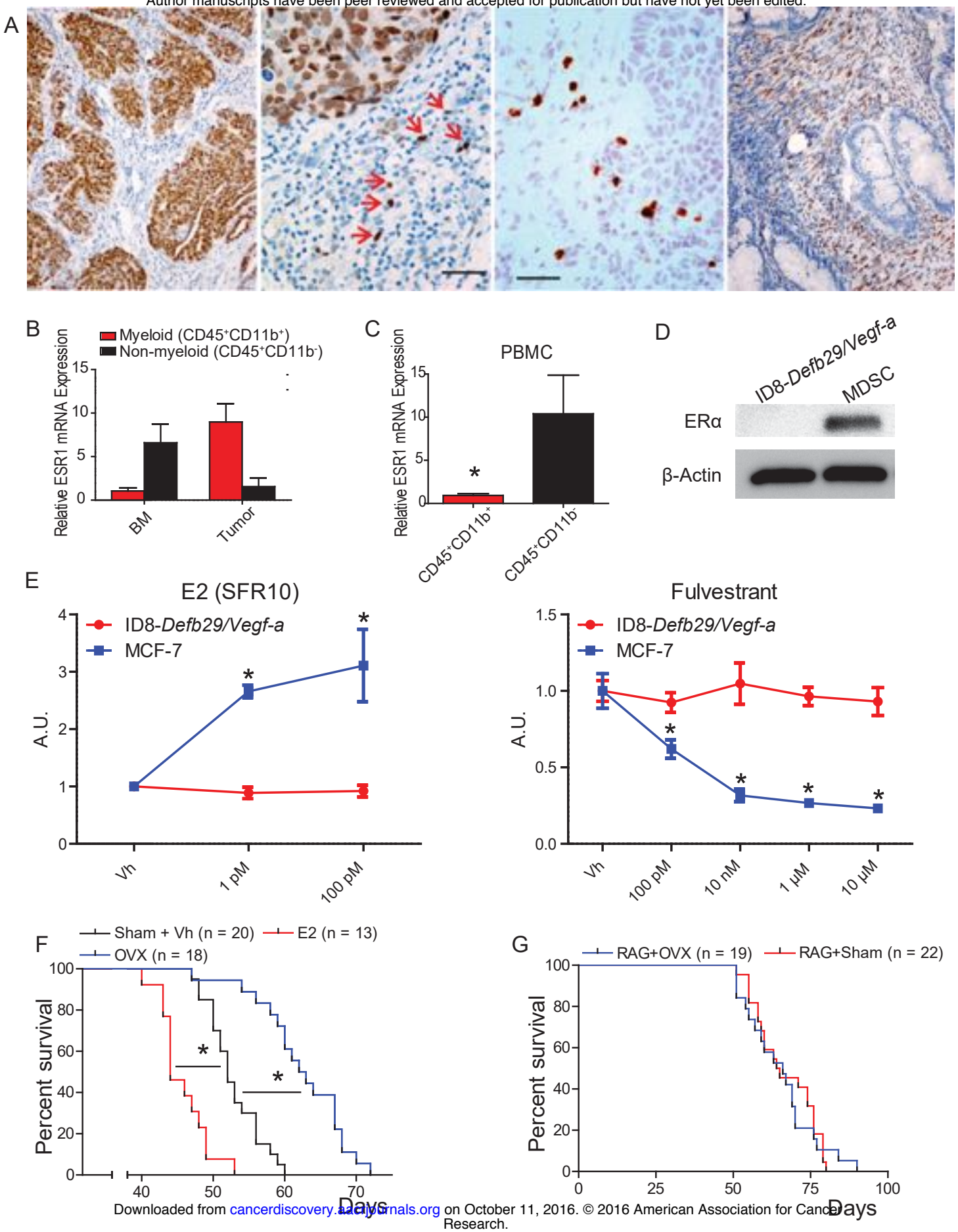

Author Manuscript Published OnlineFirst on September 30, 2016; DOI: 10.1158/2159-8290.CD-16-0502
Author manuscripts have been peer reviewed and accepted for publication but have not yet been edited.

FIGURE 2

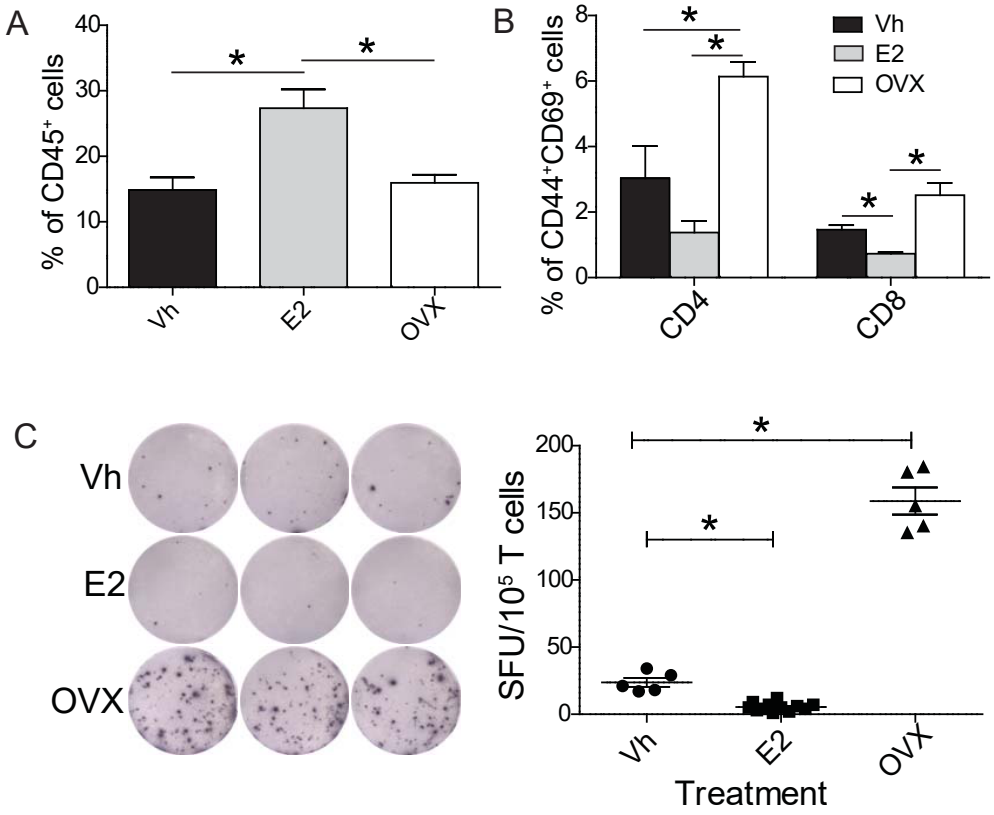

Author Manuscript Published OnlineFirst on September 30, 2016; DOI: 10.1158/2159-8290.CD-16-0502
Author manuscripts have been peer reviewed and accepted for publication but have not yet been edited.

FIGURE 3

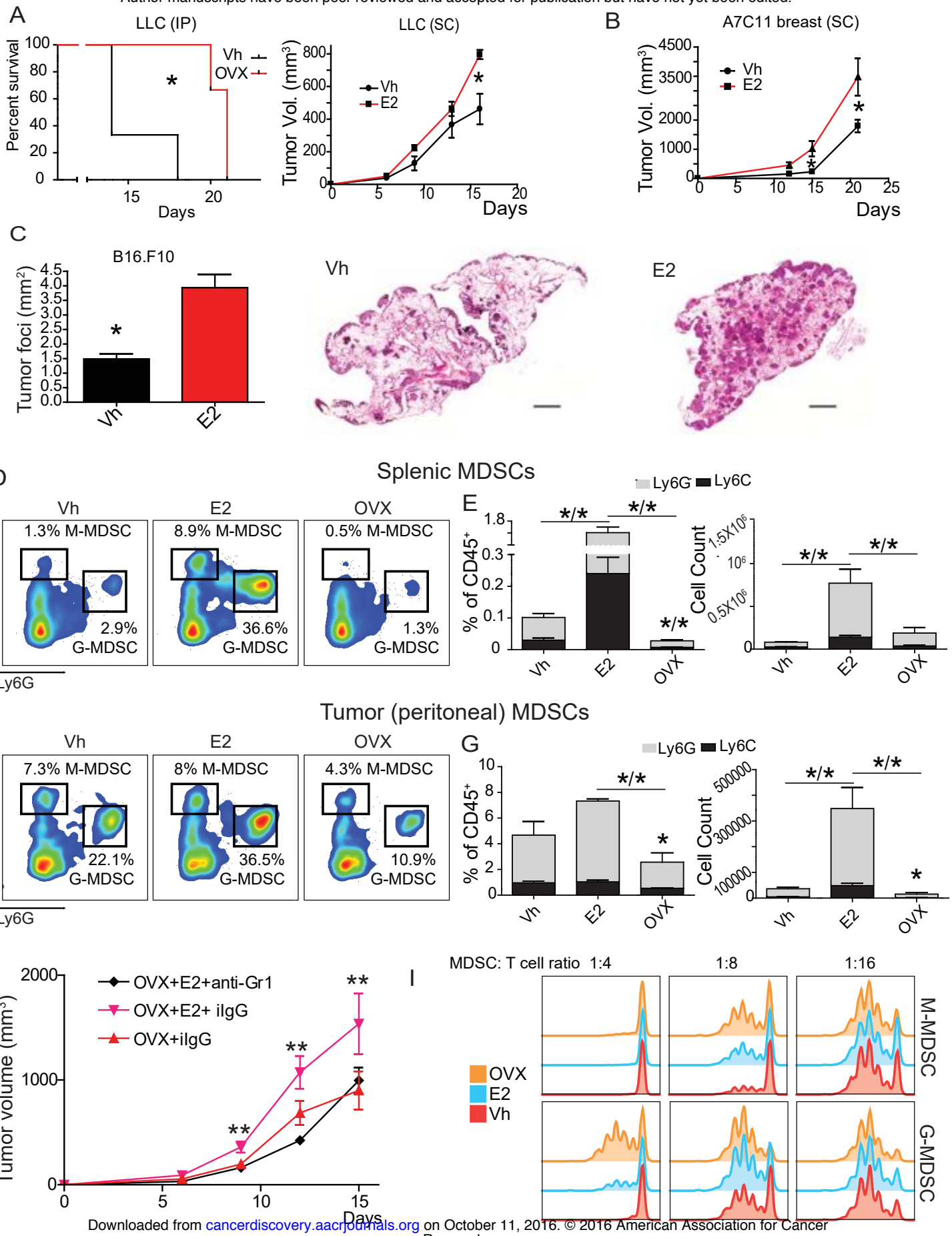

Author Manuscript Published OnlineFirst on September 30, 2016; DOI: 10.1158/2159-8290.CD-16-0502
Author manuscripts have been peer reviewed and accepted for publication but have not yet been edited.

FIGURE 4

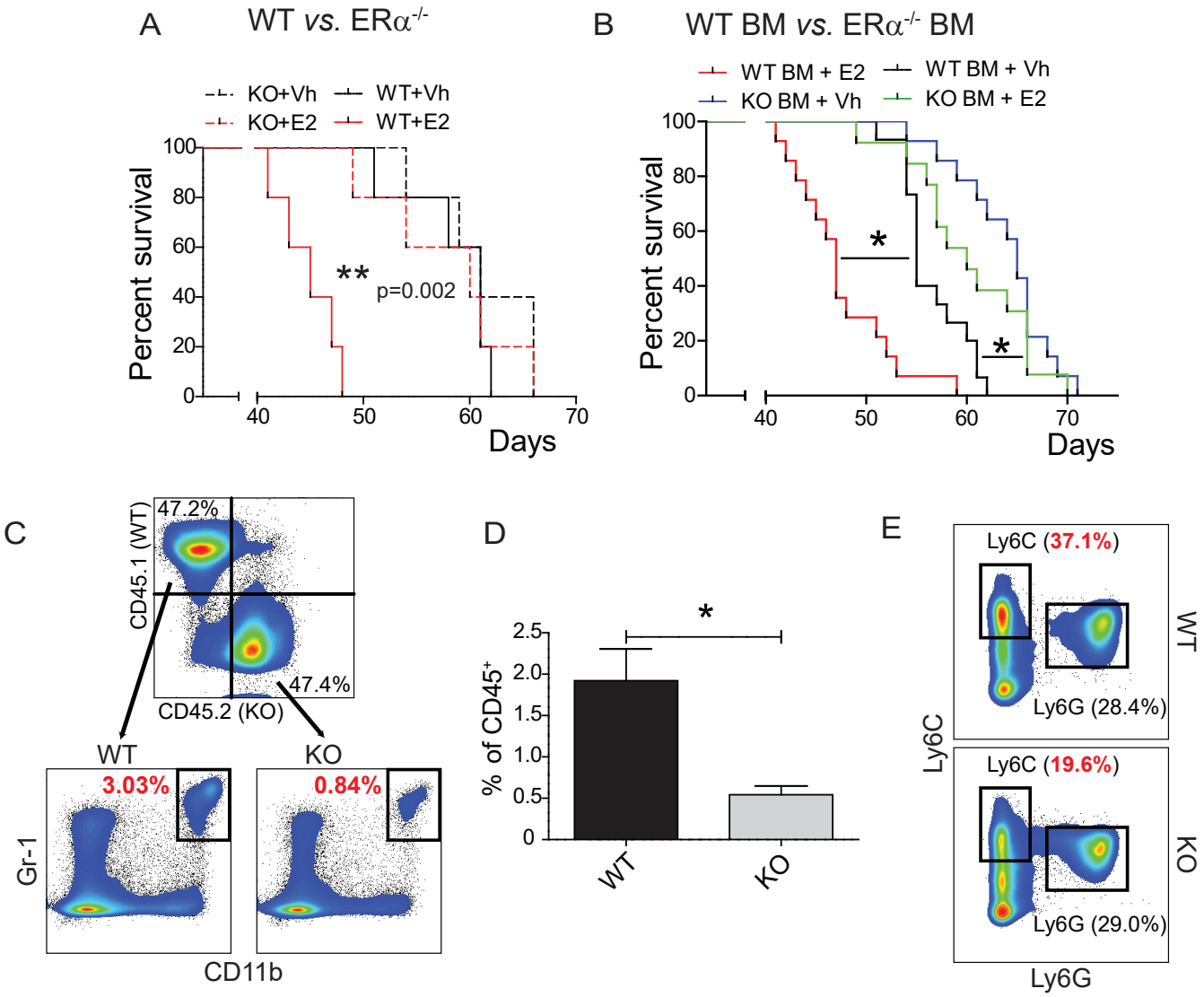

Author Manuscript Published OnlineFirst on September 30, 2016; DOI: 10.1158/2159-8290.CD-16-0502
Author manuscripts have been peer reviewed and accepted for publication but have not yet been edited.

FIGURE 3

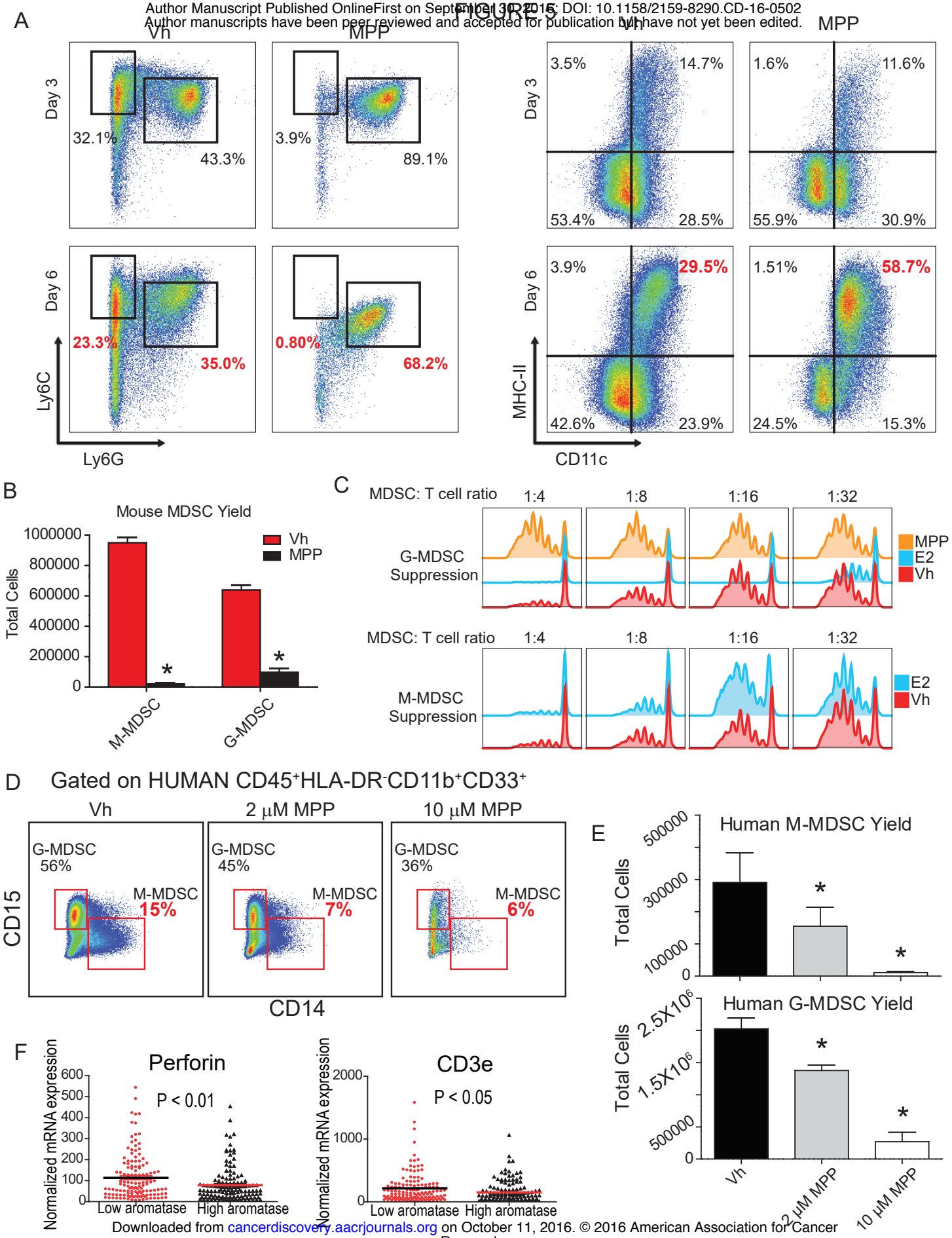

Author Manuscript Published OnlineFirst on September 30, 2016; DOI: 10.1158/2159-8290.CD-16-0502
Author manuscripts have been peer reviewed and accepted for publication but have not yet been edited.

FIGURE 6

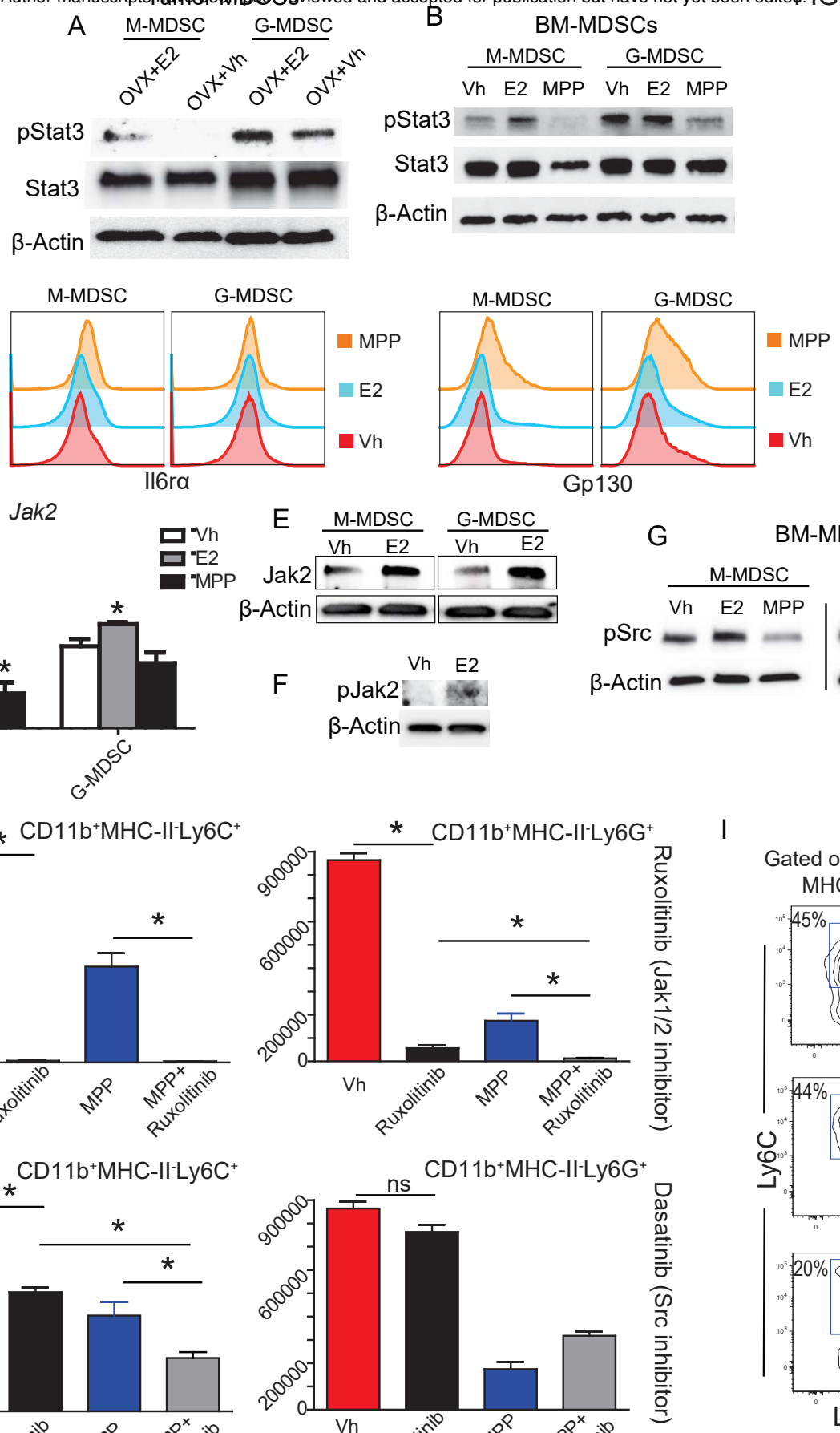

Author Manuscript Published OnlineFirst on September 30, 2016; DOI: 10.1158/2159-8290.CD-16-0502
Author manuscripts have been peer reviewed and accepted for publication but have not yet been edited.

FIGURE 7

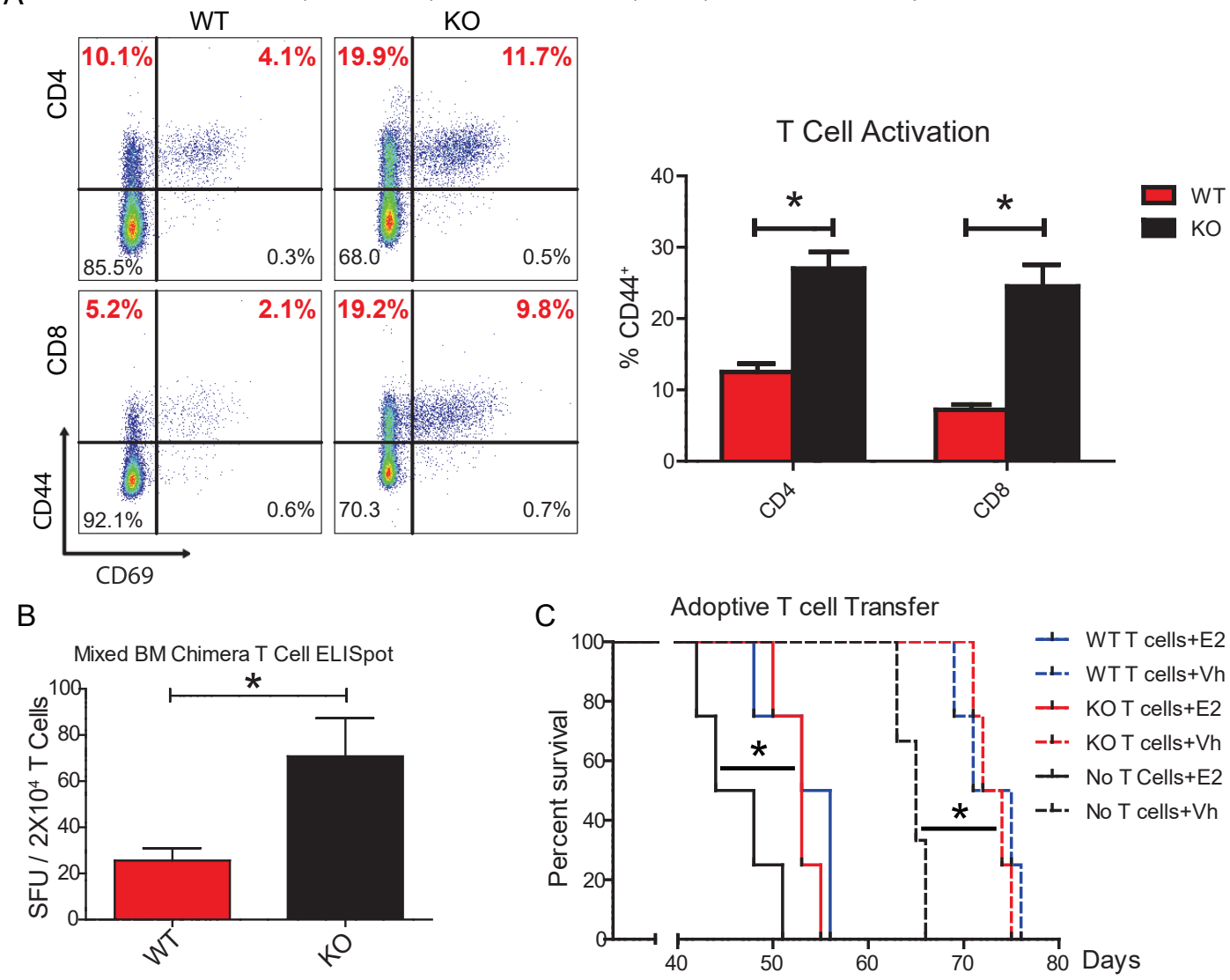

THE WISTAR INSTITUTE

August 26, 2015

Dear Evgeniy,

Thank you for accepting our invitation to speak at the Regulatory Myeloid Suppressor Cells conference – June 16-19, 2016. We are delighted that you will participate! This communication comes to advise that we will register you for the conference, and to provide you with pertinent details. At your earliest convenience, please visit the conference website at www.myeloidsuppressors.com. There you will find the overview, preliminary program, speakers' list, details related to abstract submission, and information about lodging.

Given that we will register you for the conference, it is important that you be conscientious of the abstract submission deadline (March 31, 2016) and the manner in which abstracts should be submitted (via email to myeloidposters@wistar.org). Details related to formatting, presentation, and publication of abstracts are available by clicking the Abstract tab on the website.

The closest hotel to the conference is the Sheraton University City Hotel, which is located 0.3 miles (a short walk through the University of Pennsylvania campus) from The Wistar Institute. A block of rooms has been reserved at a reduced rate of $189.00/night and reservations can be made by calling 1-888-627-7071 (please reference the Wistar Myeloid Conference) or by visiting this special link: https://www.starwoodmeeting.com/Book/WistarMyeloidConference. Please let me know (via email to alston@wistar.org) the length of your planned stay in Philadelphia (Thursday, June 16 – Sunday, June 19). **Be encouraged to secure lodging early.**

To express our appreciation for your participation in this program, the pleasure of your company is requested at a speakers' dinner on Saturday evening, June 18 (Please contact me at alston@wistar.org to provide any dietary restrictions.) More information about the dinner will be included in the registration materials you will receive upon arrival.

Again, we are delighted that you will participate in this conference and welcome any questions or concerns that you might have. Please direct inquiries to my attention at alston@wistar.org.

Best,

William E. Alston
Sr. Coordinator, Research Development and Pre-Award Administration
Manager, Wistar Seminar Series

Evgeniy Eruslanov
University of Pennsylvania
Evgeniy.Eruslanov@uphs.upenn.edu

October 15, 2015

Dear Dr. Eruslanov,

The Scientific Organizing Committee of the 2016 Annual Meeting of the *Society for Leukocyte Biology (SLB) and Neutro2016* is delighted to have you confirmed as an invited speaker at the meeting entitled "*Inflammation, Immunity and Cancer: Neutrophils and Other Leukocytes*." The meeting is to be held September 15-17, 2016, in Verona, Italy, at the *Polo Didattico Giorgio Zanotto, Congress Center*, University of Verona. Once the definitive program is confirmed, you will be notified about the schedule of your talk.

TRAVEL and LOGISTICS: To help defray the cost of your expenses, SLB will pay invited speakers a stipend of $700 *US dollars* if traveling within Europe and $1000 *US dollars* if traveling from the US or Canada. Travel and accommodation arrangements will be the responsibility of each individual, although hotel links and special rates will be provided on the meeting website. **Please make your own hotel reservations early! The deadline to book your hotel is April 15th. Verona will be very busy during our congress dates and if you do not book early, there may not be available housing.** Details of your session and talk time along with the complete conference program will be forthcoming.

REGISTRATION: Your registration for the meeting is complimentary and will be completed for you. We will notify you of your registration confirmation number in the spring.

ABSTRACTS: You are welcome, but not required, to submit an abstract in relation to this talk during the online submission period.

For any questions or assistance please contact SLB Meeting Manager, Kendra LaDuca (kladuca@faseb.org) or the SLB Executive Director, Jen Holland (jholland@faseb.org). Thank you and we are glad you'll be joining us in Verona next fall!

Sincerely,
The Scientific Organizing Committee:

Marco A. Cassatella Patrick P. McDonald

ФЕДЕРАЛЬНОЕ ГОСУДАРСТВЕННОЕ
БЮДЖЕТНОЕ НАУЧНОЕ УЧРЕЖДЕНИЕ
«ЦЕНТРАЛЬНЫЙ НАУЧНО-
ИССЛЕДОВАТЕЛЬСКИЙ ИНСТИТУТ
ТУБЕРКУЛЕЗА»
(ФГБНУ «ЦНИИТ»)
www.cniitramn.ru
Российская Федерация, Москва, 107564
Яузская аллея, 2
Тел.: +7 499 785 90 19, +7 499 785 91 36
Факс: +7 499 785 91 08
E-mail: cniit@ramn.ru; office_cniit@mail.ru

Federal State Budgetary Scientific Institution
"Central Tuberculosis Research Institute»
(CTRI)
www.cniitramn.ru
2 Yauzskaya alley, 107564 Moscow,
Russian Federation
Tel.: +7 499 785 90 19, +7 499 785 91 36
Fax: +7 499 785 91 08
E-mail: cniit@ramn.ru;
office_cniit@mail.ru

№ 89-4220 «24» 12 2015 г.

Eugeniy Eruslanov

Research Assistant Professor
Department of Surgery
Perelman School of Medicine
University of Pennsilvania
3615 Civic Center Blvd
Abramson Research Center, Office#916D
Philadelphia, PA 19104

USA

Dear Prof. Eruslanov,

It is our pleasure to invite you to participate in the School "Regulation of Lung Inflammation" and to deliver a lecture on a subject linked to this title.

The School for young scientists and physicians is scheduled for May 11-13, 2016, and will be organized in the Central Institute for Tuberculosis, Moscow. The event is financially supported by the Russian Scientific Foundation, and we are pleased to inform you that we will be able to cover your travel and hotel expenses on a reimbursement basis. We will book hotel rooms for the foreign participants with the Cosmos Hotel, Prospect Mira, 150, Moscow, which is located not far from the Institute, which allows comfortable transportation. The working languages of the School will be Russian and English. For those who are not bilingual, we will organize translation of key slides either way, and provide other translational help.

The primary purpose of this first official letter of invitation is to let you to apply for Russian visa, and to arrange the trip with your Department. We expect to form provisional program in January and distribute it among lecturers and other participants.

Looking very much forward to seeing you in Moscow in May.

Sincerely,

Director of CTRI,
Professor

A. Ergeshov

Tatiana Kondratieva

Chair, School "Regulation of Lung Inflammation"

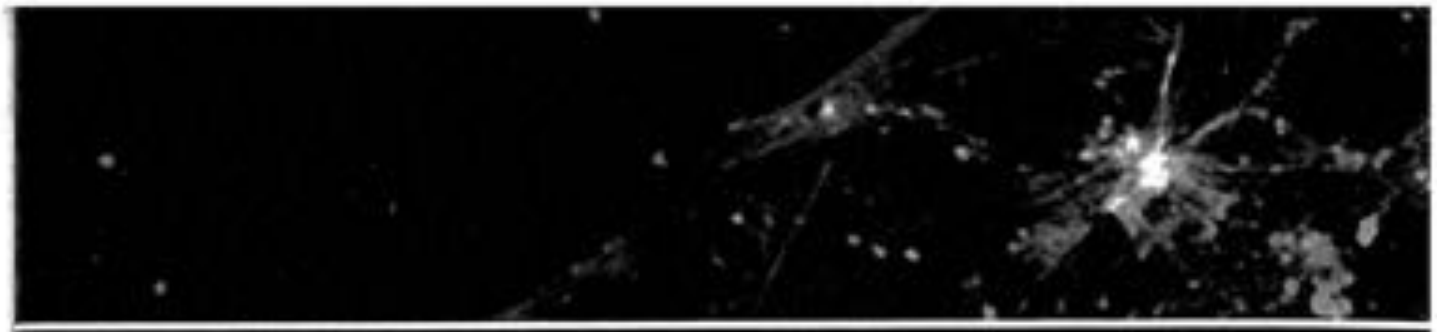

An AACR Special Conference on

THE FUNCTION OF TUMOR MICROENVIRONMENT IN CANCER PROGRESSION

January 7-10, 2016
Hard Rock Hotel
San Diego, CA

CONFERENCE CO-CHAIRPERSONS

Raghu Kalluri
The University of Texas MD Anderson Cancer Center, Houston, TX

Robert A. Weinberg
MIT Whitehead Institute for Biomedical Research, Cambridge, MA

Douglas Hanahan
Swiss Institute for Experimental Cancer Research (ISREC), Lausanne, Switzerland

Morag Park
McGill University, Montréal, QC, Canada

Program and Proceedings

AACR American Association for Cancer Research
FINDING CURES TOGETHER™

www.AACR.org/Calendar

Continuing Medical Education (CME) Activity–*AMA PRA Category 1 Credits™ available*

Tumor Immune Response

A01 Inflammatory responses within the lung tumor microenvironment correlate with oncogenic mutation and histologic subtype. Stephanie E. Busch, Julia Kargl, Mark L. Hanke, Heather E. Metz, Kyoung-Hee Kim, A. McGarry Houghton. Fred Hutchinson Cancer Research Center, Seattle, WA.

This abstract is being presented as a short talk in the scientific program. A full abstract is printed in the Proffered Abstracts section (PR04) of the Conference Proceedings.

A02 The origin and role of APC-like hybrid tumor-associated neutrophils in early-stage human lung cancer. Evgeniy Eruslanov[1], Pratik Bhojnagarwala[1], Jon Quatromoni[1], Shaun O'Brien[1], Edmund Moon[1], Tom Stephen[1,2], Abhishek Rao[1], Alfred Garfall[1], Wayne Hancock[1], Jose Conejo-Garcia[2], Charuhas Deshpande[1], Michael Feldman[1], Sunil Singhal[1], Steven Albelda[1]. [1]University of Pennsylvania, Philadelphia, PA, [2]The Wistar Institute, Philadelphia, PA.

To date there has been an increasing focus on the interactions between inflammatory myeloid cells and T cells in the tumor microenvironment because cytotoxic anti-tumoral T cells represent the chief effector mechanism of anti-tumoral immunity. Tumor-associated neutrophils (TANs) represent a significant portion of inflammatory cells in lung tumors; however, whether specialized neutrophil subpopulations capable of regulating T cell responses exist in human cancers is unknown. Our goal was to identify subsets of TANs and determine their specific roles in the regulation of T cell responses in patients with early stage lung cancer.

To address this question, freshly isolated tumors from Non-Small Cell Lung Cancer (NSCLC) patients with Stage I-II squamous cell and adenocarcinoma histology were studied. An extensive phenotypic analysis of 55 early-stage human lung tumors revealed that TANs, defined as $CD11b^+Arg1^+MPO^+CD66b^+CD15^+$ cells, contained two major sub-populations. One subset of canonical TANs expressed classic neutrophil markers. A second subset of TANs displayed a combination of neutrophil markers plus markers ($CD14^+HLA\text{-}DR^+CCR7^+CD86^+$) normally expressed on antigen-presenting cells (APC). This subset of TANs was found in lung tumor tissue but not in adjacent uninvolved lung. We termed this unique neutrophil population "APC-like hybrid TANs". The frequency of these hybrid TANs varied widely within lung cancers and ranged from 0.5-25% of all TANs. Interestingly, the frequency of this hybrid population declined as tumors enlarged, and they were almost completely absent in tumors greater than 5 cm in diameter.

Mechanistically, we determined that low doses of IFN-γ and GM-CSF in the tumors were required for the development of APC-like hybrid neutrophils. The high proportion of hybrid TANs (>10% of all TANs) directly correlated with the presence of IFN-γ and GM-CSF in the autologous tumor tissue. Using bone marrow-derived immature granulocytes, which were found to have prolonged survival in vitro, we discovered that these APC-like hybrid neutrophils originate from $CD11b^+CD15^+CD10^+CD16^{-/low/int}$ neutrophil progenitors in the presence of IFN-γ and GM-CSF or in tumor-conditioned media. By contrast, mature $CD11b^+CD15^+CD10^+CD16^{hi}$ neutrophils did not acquire the phenotype of hybrid TANs, when cultured under these conditions. In addition, we determined that IFN-γ and GM-CSF synergistically exerted APC promoting effects on immature neutrophils via the downregulation of the transcription factor, Ikaros. However, the development of APC-like hybrid neutrophils was profoundly inhibited under hypoxic conditions.

Functionally, the APC-like hybrid neutrophils are superior to canonical neutrophils in their ability to: 1) produce APC cytokines such as TNF and IL-12 after stimulation, 2) stimulate antigen non-specific autologous T cell responses induced by plate-bound anti-CD3 antibodies 3) directly stimulate antigen-specific autologous memory T cell responses to virus-derived antigens, 4) augment NY-ESO-1 specific effector T cell responses by providing a co-stimulatory signals through the OX40L, 4-1BBL CD86, CD54 molecules, and 5) cross present tumor-associated antigen as IgG-immune complex.

In summary, we provide the first evidence of two subsets of TANs in lung cancer. All TANs had an activated phenotype and could support (rather than inhibit) T cell functions to some degree. However, we identified a subset of TAN in early-stage lung tumors that can undergo a unique differentiation process resulting in formation of specialized subset of APC-like hybrid neutrophils. These hybrid TANs had enhanced ability to trigger and support T cell responses in direct cell-cell interactions. This property of hybrid neutrophils may provide new opportunities to boost the efficacy of vaccines based on cytotoxic T lymphocyte induction.